

# ADVANCING SNOW ACCUMULATION MODELS IN NEEDLELEAF FORESTS

A dissertation submitted to the  
College of Graduate and Postdoctoral Studies  
in partial fulfillment of the requirements  
for the degree of Doctor of Philosophy  
in the Department of Geography and Planning  
(Centre for Hydrology)  
University of Saskatchewan  
Saskatoon

By  
Alex C. Cebulski

©Alex C. Cebulski, November 2025. All rights reserved.  
Unless otherwise noted, copyright of the material in this thesis belongs to  
the author.

## Permission to Use

In presenting this dissertation in partial fulfillment of the requirements for a Postgraduate degree from the University of Saskatchewan, I agree that the Libraries of this University may make it freely available for inspection. I further agree that permission for copying of this dissertation in any manner, in whole or in part, for scholarly purposes may be granted by the professor or professors who supervised my dissertation work or, in their absence, by the Head of the Department or the Dean of the College in which my dissertation work was done. It is understood that any copying or publication or use of this dissertation or parts thereof for financial gain shall not be allowed without my written permission. It is also understood that due recognition shall be given to me and to the University of Saskatchewan in any scholarly use which may be made of any material in my dissertation.

## Disclaimer

Reference in this dissertation to any specific commercial products, process, or service by trade name, trademark, manufacturer, or otherwise, does not constitute or imply its endorsement, recommendation, or favoring by the University of Saskatchewan. The views and opinions of the author expressed herein do not state or reflect those of the University of Saskatchewan, and shall not be used for advertising or product endorsement purposes.

Requests for permission to copy or to make other uses of materials in this dissertation in whole or part should be addressed to:

Head of the Department of Geography and Planning  
117 Science Place  
University of Saskatchewan  
Saskatoon, Saskatchewan, S7N 5C8  
Canada

OR

Dean  
College of Graduate and Postdoctoral Studies  
University of Saskatchewan  
116 Thorvaldson Building, 110 Science Place  
Saskatoon, Saskatchewan S7N 5C9 Canada

## Abstract

Interception and ablation of snow in needleleaf canopies regulates the quantity, timing, and phase of precipitation that reaches the ground in cold region forests. Sparse observations have limited understanding of these processes and hindered their representation in hydrological and land-surface models. Consequently, simulations of subcanopy snow accumulation have shown variable accuracy across different climates and canopy structures, and diagnosing the causative processes that partition snowfall in needleleaf forests remains difficult. This study aims to better understand snow interception and canopy snow ablation processes, which act collectively to govern subcanopy snow accumulation in forested environments. To achieve this goal a comprehensive review of the literature was conducted, along with in-situ observations of forest-snow processes and subcanopy snow accumulation to evaluate the theories underlying existing parameterisations, derive new relationships, and validate a newly proposed model.

The results from the literature review showed that existing parameterisations for snow interception and canopy snow ablation have incomplete and potentially duplicated process representation. For example, existing studies show that existing snow interception parameterisations may overemphasize the role of increasing canopy snow load increasing throughfall of snow in the initial interception process. This association between snow load and throughfall has been attributed to either reduced canopy coverage due to branch bending [Schmidt1990; Schmidt1991] and/or increased rates of unloading. Staines2023 showed using novel aerial lidar based observations of canopy density and throughfall found limited influence of snow load on canopy coverage due to branch bending. Therefore, if the relationship of initial interception with snow load is not resulting from canopy density changes, perhaps it may be better represented using the unloading parameterisation alone to avoid double counting this process. Moreover, the methodologies used to parameterise non-melt induced canopy snow unloading routines rely on indirect measurements and should be assessed using more direct measurements. While many canopy snow ablation processes occur simultaneously using a hybrid modelled-observed processes to help isolate individual canopy snow processes has not been utilised to help understand canopy snow processes.

New observations of initial snow interception, collected when ablation processes were minimal, showed that canopy density is the primary factor influencing subcanopy snow throughfall. Contrary to existing theories, no relationships were found with canopy snow load or air temperature. Canopy density was best represented by a snow-leaf contact area metric, which accounts for increasing contact area with more horizontal snowfall trajectories. This metric was highly sensitive to wind speed in sparse canopies, increasing by up to an order of magnitude with a  $1 \text{ m s}^{-1}$  wind speed. A new parameterisation was developed that calculates throughfall as a function of snowfall and snow-leaf contact area based on these observations. This approach is consistent with some rainfall interception studies, which also separate canopy loading and ablation processes, and

calculate interception as a function of canopy cover.

Observations showed that canopy snow unloading was strongly associated with snow load, wind shear stress, and canopy snowmelt, but not with air temperature or sublimation. A new canopy snow ablation model was developed based on these associations and their impact on the canopy snow energy and mass balance. The model improved simulation of canopy snow load relative to previous approaches, especially for melt- and wind-dominated ablation events. The improved performance in representing canopy snow load compared to existing models results from including energy balance-based melt and dry snow unloading relationships with snow load and wind shear stress. The inclusion of both melt and dry snow unloading processes in the new model also led to more accurate partitioning of snowfall to the atmosphere versus the ground compared to existing approaches across a wide range of meteorologies.

Validation of the revised canopy snow mass and energy balance was conducted at four needleleaf forests characterised by differing tree species, canopy structure, and meteorological conditions. The new physically based approach reduced error in simulating subcanopy snow water equivalent (SWE) compared to an existing model. Improved process representation also enabled clearer process diagnosis on the influence of vegetation on snow accumulation. At two cold, low-snowfall sites, roughly half of annual snowfall was lost to the atmosphere via sublimation of intercepted snow. A cold wind-exposed site with higher annual snowfall had increased unloading rates and reduced atmospheric losses. In contrast, at a temperate-maritime site, nearly half of annual snowfall melted within the canopy, and combined with melt-induced unloading led to the lowest fraction of snowfall lost through canopy snow sublimation.

This research identified key limitations in existing models using in-situ process-level observations of snow interception and ablation. New parameterisations of the canopy snow mass and energy balance are introduced to more explicitly represent the processes that govern snowfall partitioning in needleleaf canopies. This new approach led to more accurate simulations of canopy snow load and subcanopy SWE across a broad range of meteorologies and forest types and also improved process diagnosis, though further validation is required across a diverse range of sites.

## Acknowledgements

I am incredibly thankful for random text Fuerint certius dormire duratio exiprat mea has agendis. Sequeretur et praecipuus recensenda du gi pensitatis ei intelligam. Est externarum sit scripturas praemissae. Nulla demus has rebus timet sui mecum certe. Facultate affirmare is ac priusquam tribuebam potentiam et ex continent. Unam pati suae vice hos luce addi dem. Meos ipsa atra vi unam in tale. Reges istam mundo spero ad at ha nolle.

”Human nature is like water. It takes the shape of its container.”

## TABLE OF CONTENTS

<b>Permission to Use . . . . .</b>	<b>i</b>
<b>Abstract . . . . .</b>	<b>ii</b>
<b>Acknowledgements . . . . .</b>	<b>iv</b>
<b>Contents . . . . .</b>	<b>vi</b>
<b>List of Tables . . . . .</b>	<b>vii</b>
<b>List of Figures . . . . .</b>	<b>viii</b>
<b>1 Introduction . . . . .</b>	<b>1</b>
1.1 Research Objectives . . . . .	4
1.1.1 Objective 1: Evaluate the suitability of existing snow interception and ablation parameterisations for application in needleleaf forests with differing canopy structure and meteorology . . . . .	4
1.1.2 Objective 2: Determine how new snow interception and ablation parameterisations could enhance the representation of processes important for subcanopy snow accumulation. . . . .	4
1.2 Organization of Chapters . . . . .	4
<b>2 The Theoretical Underpinnings of Existing Snow Interception and Ablation parameterisations . . . . .</b>	<b>6</b>
2.1 Abstract . . . . .	6
2.2 Introduction . . . . .	7
2.3 The Mass and Energy Balance of Snow in the Canopy . . . . .	9
2.3.1 Mass Balance . . . . .	9
2.3.2 Energy Balance . . . . .	11
2.4 Measurement Techniques . . . . .	13
2.4.1 Weighed Tree . . . . .	13
2.4.2 Mass Balance Methods . . . . .	13
2.4.3 Remote Sensing . . . . .	17
2.4.4 Tree Sway Frequency . . . . .	20
2.4.5 Trunk Compression . . . . .	20
2.4.6 Eddy Covariance . . . . .	20
2.4.7 Snow Isotopes . . . . .	21
2.5 Parameterisations . . . . .	21
2.5.1 Snow Interception Parameterisations . . . . .	21
2.5.2 Canopy Snow Ablation Parameterisations . . . . .	31
2.6 Discussion . . . . .	35
2.6.1 Differences in Snow Interception Parameterisations . . . . .	35
2.6.2 Forest Structure and Snow Interception . . . . .	36
2.6.3 In Search of a Canopy Snow Storage Capacity . . . . .	37
2.6.4 Differences in Canopy Snow Ablation Parameterisations . . . . .	37
2.6.5 Contribution of Measurement Uncertainty on Canopy Snow Ablation Parameterisations . . . . .	38
2.6.6 The Applicability of Parameterisations in Diverse Forest Structures and Species . . . . .	39
2.6.7 The Potential of Hybrid Parameterisations . . . . .	40
2.7 Conclusions . . . . .	40
2.8 Acknowledgments . . . . .	41

2.9	Appendix . . . . .	41
2.9.1	Snow Interception Parameterization Derivations . . . . .	41
2.9.2	Snow Unloading Parameterization Derivations . . . . .	43
<b>3</b>	<b>Snow Interception Relationships with Meteorology and Canopy Density . . . . .</b>	<b>44</b>
3.1	Abstract . . . . .	44
3.2	Introduction . . . . .	45
3.3	Theory . . . . .	46
3.3.1	Canopy snow mass balance . . . . .	46
3.3.2	Hydrometeor trajectory angle . . . . .	47
3.3.3	Within-canopy wind flow . . . . .	47
3.4	Data and methods . . . . .	48
3.4.1	Study site . . . . .	48
3.4.2	Meteorological measurements . . . . .	48
3.4.3	Lysimeter measurements . . . . .	50
3.4.4	UAV-Lidar data collection and processing . . . . .	51
3.4.5	Snow surveys . . . . .	53
3.4.6	UAV-Lidar canopy metrics . . . . .	54
3.5	Results . . . . .	55
3.5.1	The influence of meteorology on snow interception . . . . .	55
3.5.2	The influence of canopy density on snow interception . . . . .	61
3.5.3	The combined influence of trajectory angle and canopy density on snow interception . . . . .	67
3.5.4	Throughfall model performance . . . . .	69
3.6	Discussion . . . . .	71
3.7	Conclusions . . . . .	74
3.8	Acknowledgments . . . . .	75
3.9	Data Availability . . . . .	75
<b>4</b>	<b>Processes Governing the Ablation of Intercepted Snow . . . . .</b>	<b>76</b>
4.1	Abstract . . . . .	76
4.2	Introduction . . . . .	77
4.3	Methods . . . . .	80
4.3.1	Study Site . . . . .	80
4.3.2	The Cold Regions Hydrological Model Platform . . . . .	81
4.3.3	Canopy Snow Mass Balance . . . . .	83
4.3.4	Mass Balance Parameterisations . . . . .	83
4.3.5	Canopy Snow Energy Balance . . . . .	84
4.3.6	Energy Balance Parameterisations . . . . .	84
4.3.7	Influence of Predictive Variables on Unloading . . . . .	86
4.4	Results . . . . .	88
4.4.1	Unloading Relationships . . . . .	88
4.4.2	New Canopy Snow Model . . . . .	93
4.4.3	Event-based Evaluation of Canopy Snow Ablation Models . . . . .	95
4.4.4	Canopy Snow Partitioning . . . . .	97
4.5	Discussion . . . . .	100
4.5.1	Processes Governing Canopy Snow Unloading . . . . .	100
4.5.2	Performance Comparison of Ablation Models . . . . .	102
4.5.3	Canopy Snow Partitioning . . . . .	103
4.5.4	Future Directions . . . . .	104
4.6	Conclusions . . . . .	104
4.7	Acknowledgements . . . . .	105
4.8	Data & Software Availability Statement . . . . .	106
<b>5</b>	<b>Evaluation of a New Needleleaf Forest Snowpack Model for Diagnosing Snow Accumulation Regimes in Western and Northern Canada . . . . .</b>	<b>107</b>

5.1	Abstract . . . . .	107
5.2	Introduction . . . . .	107
5.3	Methods . . . . .	109
5.3.1	Study Sites . . . . .	109
5.3.2	Simulation of Subcanopy Snowpack . . . . .	110
5.3.3	Model Evaluation . . . . .	113
5.4	Results . . . . .	114
5.4.1	Snowpack Observations . . . . .	114
5.4.2	Evaluation of Snowpack Models . . . . .	114
5.4.3	Snowfall Partitioning . . . . .	119
5.4.4	Simulated Canopy Snow Load . . . . .	120
5.5	Discussion . . . . .	124
5.5.1	Model Performance in Simulating Subcanopy Snow Accumulation . . . . .	124
5.5.2	Influence of Climate on Snowfall Partitioning . . . . .	125
5.5.3	Influence of Tree Species on Snowfall Partitioning . . . . .	126
5.6	Conclusions . . . . .	126
5.7	Acknowledgements . . . . .	127
5.8	Data and Software Availability Statement . . . . .	128
	<b>References . . . . .</b>	<b>129</b>

## LIST OF TABLES

2.1 Summary of canopy interception/precipitation (I/P) model behaviour and measurement techniques. . . . .	22
3.1 Leaf area index (LAI) and canopy closure of the three subcanopy lysimeters located proximal to the FT Station. . . . .	51
3.2 Meteorology of the 26 snowfall events. Air temperature and wind speed were measured at FT station. Interception efficiency is estimated from cumulative snowfall measured at PWL station and the average cumulative throughfall of all three subcanopy lysimeters located within the FT forest plot. . . . .	57
3.3 Statistics corresponding to the ordinary least squares linear regression test between hourly interval measurements of independent variables: mean air temperature, mean wind speed, and initial canopy snow load and the dependent variable mean interception efficiency. The test was run separately for three levels of canopy coverage ( $C_c$ ) corresponding to each subcanopy lysimeter (SCL). . . . .	58
3.4 Results of the Wilcoxon signed-rank tests comparing the distributions of hourly interception efficiency (IP) measured by the subcanopy lysimeters for differing groups of air temperatures (Ta), wind speeds (u), and initial canopy snow loads (L). The table reports the canopy corresponding to the subcanopy lysimeter (Canopy), null hypothesis ( $H_0$ ), p-value, and sample size (n) and median IP for the ‘low’ group (e.g., Ta < -5°C) and ‘high’ group (e.g., Ta > -5°C). . . . .	60
3.5 Summary of error statistics for the linear regression models relating leaf contact area to interception efficiency, presented in Figure 3.9. The Mean bias is the difference in the model and observed values, MAE is the mean of the absolute error, RMS Error is the root mean squared error, $R^2$ is the coefficient of determination adjusted using Equation 10 in Kozak & Kozak (1995). . . . .	67
3.6 Model error statistics calculated for the prediction of leaf contact area from trajectory angle using Equation 3.11 and Equation 10 from Hedstrom & Pomeroy (1998) (HP98) for the PWL and FT forest plots. Mean bias is the difference in the model and observed values, MAE is the mean of the absolute error, RMS Error is the root mean squared error and $R^2$ is the coefficient of determination. The units for all metrics are dimensionless. A forested downwind distance of 100 m was used for the HP98 calculation. . . . .	69
3.7 Model error statistics for model estimates of snow interception efficiency (I/P) and throughfall (TF) compared to measurements of I/P and TF using UAV-lidar averaged over the FT and PWL forest plots. Units for I/P are (-) and TF are (mm). The vector-based model utilized Equation 3.9 with $C_p$ adjusted for trajectory angle. The nadir model also utilized Equation 3.9 but was not adjusted for trajectory angle and thus $C_c$ was used instead of $C_p$ . The ‘Obs. Value’ column contains measurements from UAV-lidar while the ‘Mod. Value’ column contains the modelled values. The mean bias was calculated as observed minus modelled and percent error is the percent error between predicted and observed values. . . . .	71
4.1 Summary of multivariate linear regression results evaluating all combinations of predictor variables for canopy snow unloading including: canopy load (L), wind speed (u), canopy snowmelt rate ( $q_{melt}$ ), canopy snow sublimation rate ( $q_{subl}$ ), and air temperature ( $T_a$ ). Columns L to $T_a$ show the coefficient estimate for each respective term, and the significance of each term is shown in brackets. Significance codes: * = p < 0.05; ns = not significant (p > 0.05). The models are ranked by their corresponding AIC value. . . . .	89
4.2 Summary of regression error statistics and coefficients for the relationship between canopy snow unloading with wind speed (Equation 4.12) and shear stress (Equation 4.13), as shown in Figure 4.5. Coefficients are shown for hourly unloading. . . . .	91

4.2	Summary of regression error statistics and coefficients for the relationship between canopy snow unloading with wind speed (Equation 4.12) and shear stress (Equation 4.13), as shown in Figure 4.5. Coefficients are shown for hourly unloading. . . . .	92
4.3	Fraction of canopy-intercepted snow returned to the atmosphere as sublimation and evaporation of melted snow or input to the ground as unloading or drip of melted snow for each parameterisation over the 17 select ablation events. . . . .	99
5.1	Simulation period (Years), location, and vegetation characteristics, including canopy cover ( $C_c$ ), leaf area index (LAI), and mean tree height ( $\bar{h}_t$ ), for the four study sites. . . . .	110
5.2	Mean bias (MB) and root mean squared error (RMSE) determined from time-series simulations of snow water equivalent for the two canopy snow models at each of the four sites. . . . .	118

## LIST OF FIGURES

<p>2.1 The mass balance of intercepted snow in a needleleaf forest canopy and the subcanopy snowpack. The colours of the arrows correspond to the water phase: solid (purple), liquid (blue) and vapour (light green). The head of the arrow indicates a positive flux either into the canopy (positive) or away from the canopy (negative). Fluxes may transition between positive and negative. In the case of sublimation from the canopy or snowpack, the flux may be positive (sublimation) or negative (deposition). This figure was adapted from Pomeroy and Gray (1995). . . . .</p> <p>2.2 Conceptual representation of the physical processes important in the energy balance of the forest canopy and surface snowpack. Where <math>Q_{sw}</math> and <math>Q_{lw}</math> (<math>\text{W m}^{-2}</math>) are shortwave and longwave fluxes, <math>Q_l</math> and <math>Q_h</math> (<math>\text{W m}^{-2}</math>) are the turbulent fluxes of latent heat and sensible heat, <math>Q_p</math> (<math>\text{W m}^{-2}</math>) is the advective energy rate, and <math>Q_g</math> (<math>\text{W m}^{-2}</math>) is the ground heat flux. A superscript specifies which control volume the flux refers to: the vegetation control volume (veg), the snow-atmosphere interface (sai), and the top of the canopy between the upper atmosphere and canopy air space (total). The dashed lines represent radiation extinguished, reflected or re-emitted by the canopy, intercepted snow or surface snowpack. This figure was adapted from Clark et al. (2015a). . . . .</p> <p>2.3 Weighed tree lysimeters, (a) Subalpine fir tree lysimeter loaded with snow, Fortress Mountain Research Basin, Alberta, Canada and (b) Black spruce tree lysimeter relatively free of snow, Havikpak Creek Research Basin, Inuvik, Northwest Territories, Canada. . . . .</p> <p>2.4 Gravimetric fresh snow density sample collection, Fortress Mountain Research Basin, Alberta, Canada. A 1000 cm<sup>3</sup> snow density wedge sampler (RIP Cutter, <a href="https://snowmetrics.com/shop/rip-1-cutter-1000-cc/">https://snowmetrics.com/shop/rip-1-cutter-1000-cc/</a>) is shown being pushed into the surface of the snowpack. The scale used to measure the weight of the sample is shown on the bottom right. . . . .</p> <p>2.5 An example of a suspended subcanopy lysimeter installed at Fortress Mountain Research Basin, Alberta, Canada to measure rates of throughfall, unloading, and drip. . . . .</p> <p>2.6 Panel (a) Comparison of the Hedstrom &amp; Pomeroy (1998) (HP98) and Andreadis et al. (2009) (SA09) canopy snow storage capacity parameterisations. Panel (b) shows interception efficiency for event totals as the change in event canopy snow load divided by the corresponding change in event snowfall in the open for parameterisations: HP98, Katsushima et al., (2023) (KA23), SA09, and Moeser et al., (2009) (M15). Initial canopy load is held at 0, air temperature is -5°C, LAI of 3.5 and the HP98 species coefficient for spruce (5.9 kg m<sup>-2</sup>). . . . .</p> <p>2.7 The state of canopy snow load (solid lines) for a cold and warm event using the parameterisations by Hedstrom and Pomeroy (1998) (HP98), Katsushima et al., (2023), combined Storck et al. (2002) and Andreadis et al., (2009) (SA09). The interception storage capacity is shown for the HP98 (purple) and SA09 (orange) parameterisations using a horizontal dashed line. The KA23 parameterisation does not include a canopy snow storage capacity. To isolate the influence of snow interception parameterisations ablative processes have not been computed. Constants for these two plots include a wind speed of 1 m s<sup>-1</sup>, LAI of 3.5 (-) and the HP98 species coefficient for spruce (5.9 kg m<sup>-2</sup>). . . . .</p> <p>2.8 Plots showing the leaf contact area (top) and increase in leaf contact area (bottom) with increasing wind speed calculated using the method from Hedstrom &amp; Pomeroy (1998). The colour of each line represents the leaf contact area at nadir which is equal to the canopy coverage. Here the canopy height is held constant at 10 m, the forested downwind distance is 100 m, and the fall velocity is 0.8 m s<sup>-1</sup>. . . . .</p> <p>3.1 Map showing the location of forest plots, flux towers, subcanopy lysimeter instruments, and survey transects. The inset map on the lower right shows the regional location of Fortress Mountain Research basin. . . . .</p>	<p>10</p> <p>12</p> <p>14</p> <p>16</p> <p>18</p> <p>22</p> <p>24</p> <p>27</p> <p>49</p>
--	---

3.2	Images of the three subcanopy lysimeter instruments and surrounding canopy located in sparse (a), mixed (b), and dense (c) canopy. The top row presents a side view of each instrument and the bottom row shows hemispherical photographs. These hemispherical images are oriented with north at the top and have been mirrored to provide a view from above (e.g., east is on the right side of each image). See Table 3.1 for the corresponding canopy density measurement.	52
3.3	Plot showing the cumulative event snowfall versus canopy snow load calculated using the mean of the three subcanopy lysimeters (left) and weighed tree lysimeter (right) for each of the 26 snowfall events. Both datasets represent canopy snow load for a canopy closure of 0.73 corresponding to the mean of the three subcanopy lysimeter canopies.	55
3.4	Wind rose showing the frequency of wind speed and direction over the 26 snowfall periods for the ultrasonic anemometer 4.3 m above ground at FT station.	56
3.5	Scatter plots showing the interception efficiency calculated from accumulated snowfall (Pluvio) and throughfall (subcanopy lysimeter) measurements for bins of air temperature, wind speed, and initial canopy snow load (the snow load observed by the weighed tree at the beginning of the timestep) over the 26 snowfall events. The error bars represent the estimated combined instrument error of the snowfall gauge and subcanopy lysimeters.	59
3.6	UAV-lidar measurements of the change in snow water equivalent, SWE (mm) and interception efficiency, I/P (-), over the March 13–14 <sup>th</sup> 24-hour snowfall event for the FT and PWL forest plots at a 0.25 m resolution. See the location of the two forest plots in Figure 4.3.	62
3.7	The Pearson Correlation Coefficient between rasters (0.25 m resolution) of interception efficiency and leaf contact area (measured on March 13th) for each grid cell across the study site for each azimuth angles (0°, 1°, ..., 359°) and zenith angles (0°, 1°, ..., 90°) for the FT (left) and PWL (right) forest plots.	63
3.8	UAV-lidar VoxRS measurements of leaf contact area measured on March 13 <sup>th</sup> for the PWL and FT forest plots for zenith angles (PWL = 22°, FT = 21°) and azimuth angles (PWL = 167°, 178°, ... 217°; FT = 171°, 172°, ... 223°).	64
3.9	Scatter plots showing the relationship between leaf contact area and interception efficiency rasters resampled to a 5 m grid cell resolution. The left plot (nadir) shows canopy coverage and the right plot (Vector Based) shows the leaf contact area averaged over rasters with zenith angles (PWL = 22°, FT = 21°) and azimuth angles (PWL = 167°, 178°, ... 217°; FT = 171°, 172°, ... 223°). The solid lines (Model fit) show an ordinary least squares linear regression forced through the origin and fitted to the PWL (red) and FT (black) data and the light grey dotted line shows a 1:1 line. The $R^2$ values for the four different models are shown in the upper left of each panel calculated following the methods outlined in Kozak & Kozak (1995).	65
3.10	Plots showing the relationship between hydrometeor trajectory angle (left column) and wind speed (right column) with mean plot-wide snow-leaf contact area, $C_p$ (top row) and the increase in mean plot-wide $C_p$ , i.e., $C_p - C_c$ (bottom row). The simulated hydrometeor trajectory angle is measured as degrees from zenith. Simulated wind speed was calculated as a function of hydrometeor trajectory angle by rearranging Equation 3.4 and an observed event hydrometeor fall velocity of 0.9 m s <sup>-1</sup> . The solid lines (VoxRS) represent the mean $C_p$ (top row) or increase in mean $C_p$ (bottom row) for a single zenith angle observed from VoxRS across all grid cells for each forest plot and across all azimuth angles. The shaded area represents one standard deviation above and below the observed VoxRS mean. The dashed lines (Fitted) represent predictions from Equation 3.10 (top row) and Equation 3.11 (bottom row). The dotted lines (HP98) represent the predictions from Equation 10 in Hedstrom & Pomeroy (1998). A forested downwind distance of 100 m was assumed for the HP98 calculation.	68
3.11	Bar chart comparing the observed and modelled mean change in throughfall ( $\Delta$ SWE, mm) over the March 13–14 <sup>th</sup> snowfall event averaged over forest plots FT and PWL. The ‘Nadir-model’ calculated interception efficiency as a function of canopy coverage and the Vector-based ‘VB-model’ used Equation 3.9 with $C_p$ adjusted for trajectory angle. ‘UAV-lidar’ corresponds to throughfall calculated using Equation 3.6 incorporating UAV-lidar snow depth and snow density from in-situ snow pits. The black horizontal dashed line shows the accumulated SWE (mm) over the snowfall event to the PWL station open clearing.	70

4.1	The Roesch et al. (2001) model of unloading rate with increasing wind speed and canopy snow load (left, R01) and the Hedstrom & Pomeroy (1998) model of unloading rate with increasing snow load (right, E10). Both examples have a constant air temperature of -10°C to disable the influence of warming on unloading and drip. . . . .	80
4.2	The Ellis et al. (2010) and Floyd (2012) (E10) model of unloading and drip rate (left) and the Roesch et al. (2001) (R01) model of unloading rate (right) with increasing air temperature. Wind speed for the R01 parameterisation was set to zero. . . . .	81
4.3	Map showing the location of flux towers and lysimeter instruments. The inset map on the upper left shows the regional location of Fortress Mountain Research basin. Flux towers are denoted by a circle, lysimeters by a square, and tipping bucket rain gauges (TB) by diamonds. . . . .	82
4.4	Scatter plots showing the mean unloading rate ( $\text{mm hr}^{-1}$ ) for differing bins of air temperature ( $^{\circ}\text{C}$ ), ice-bulb temperature depression ( $^{\circ}\text{C}$ ), shear stress ( $\text{N m}^{-2}$ ), canopy snowmelt ( $\text{mm hr}^{-1}$ ), canopy snow sublimation ( $\text{mm hr}^{-1}$ ), and wind speed ( $\text{m s}^{-1}$ ). Note: unloading was measured by the subcanopy lysimeters, air temperature and wind speed were measured at FT station, canopy snowmelt and sublimation were calculated using CRHM. . . . .	90
4.5	Canopy snow unloading rate measured by the subcanopy lysimeters versus shear stress (left) and wind speed (right) during periods without canopy snowmelt. The dots represent mean unloading rates within bins of shear stress and wind speed for three canopy snow load levels; error bars indicate +/- 1 standard deviation. The fitted lines show predictions from Equation 4.12 (left) and Equation 4.13 (right). . . . .	91
4.6	The ratio of canopy snow unloading (weighed tree residual) to snowmelt across different canopy snow load bins and events. Black dots represent the observed cumulative unloading divided by the cumulative simulated snowmelt from the updated CP25 canopy snow routine in CRHM for each of the five warm & humid events. Red dots show the cumulative observed unloading divided by snowmelt measured by the rain gauges. Multiple dots within a bin correspond to different events. The blue line represents the best-fit line derived from ordinary least squares regression. . . . .	93
4.7	Cumulative canopy snow drip measured by the average of four subcanopy tipping bucket rain gauges (TB) and simulated using the CRHM CP25 model (Equation 4.3). Yellow shading indicates the range of $\pm 1$ standard deviation amongst the individual rain gauge measurements. . . . .	94
4.8	Boxplots showing the distribution of meteorological measurements of air temperature, relative humidity, and wind speed over each of the seventeen select ablation events. Air temperature, relative humidity, and wind speed were measured at FT station. Note: the rectangle vertical extent represents the interquartile range (25 <sup>th</sup> to 75 <sup>th</sup> percentile), the horizontal line within each box indicates the median, and the whiskers extend to 1.5 times the interquartile range. Circular points beyond the whiskers represent outliers. . . . .	96
4.9	Time series of canopy snow load for individual events measured by the weighed tree (observed) and simulated using the four canopy snow models. . . . .	98
4.10	Boxplots illustrating the distribution of event mean biases calculated between simulations of canopy snowload and observations from the weighed tree. The vertical extent of each rectangle represents the interquartile range (25 <sup>th</sup> to 75 <sup>th</sup> percentile), the horizontal line within each box indicates the median, and the whiskers extend to 1.5 times the interquartile range. Circular points beyond the whiskers represent outliers. The diamonds represent the mean of the event biases. . . . .	99
4.11	Bar chart illustrating the proportion of intercepted snow that was either lost to the atmosphere as sublimation and/or evaporation of melted snow or transferred to the ground through unloading or drip of melted snow by each event type for all 17 events. . . . .	100
5.1	Map showing the regional scale location of the four research basins and land cover data from the Canada Centre for Remote Sensing et al. (2020) North American Land Change Monitoring 30-meter dataset. . . . .	111

5.2	Graph showing mean monthly relative humidity, air temperature, total precipitation, and wind speed over the simulation period for each station. See Table 5.1 for the corresponding date ranges of each site. Observations were not available during the snow free period for Russell Creek (Jun—Sept). . . . .	112
5.3	Time series showing seasonal cumulative snowfall (black lines) and subcanopy snow water equivalent from in situ snow surveys (red dots). Note: snowfall was determined from observed total precipitation for each site using the snowfall fraction simulated in CRHM following Harder & Pomeroy (2013). . . . .	115
5.4	Bar chart comparing mean water year snow water equivalent between snow survey observations (OBS) and the two models (CP25 and E10). . . . .	116
5.5	Bar chart comparing peak water year snow water equivalent between snow survey observations (OBS) and the two models (CP25 and E10). . . . .	117
5.6	Timeseries of observed and simulated (CP25 and E10) forest snow water equivalent at each station. . . . .	119
5.7	Boxplots showing the distribution of the fraction of total atmospheric snowfall that was sublimated out of the canopy at each station. Note: the rectangle vertical extent represents the interquartile range (25 <sup>th</sup> to 75 <sup>th</sup> percentile), the horizontal line within each box indicates the median, and the whiskers extend to 1.5 times the interquartile range. Circular points beyond the whiskers represent outliers. . . . .	120
5.8	Boxplots showing the distribution of the fraction of total atmospheric snowfall that reached the subcanopy via unloading and/or throughfall. Note: the rectangle vertical extent represents the interquartile range (25 <sup>th</sup> to 75 <sup>th</sup> percentile), the horizontal line within each box indicates the median, and the whiskers extend to 1.5 times the interquartile range. Circular points beyond the whiskers represent outliers. . . . .	121
5.9	Boxplots showing the distribution of the fraction of total atmospheric snowfall that was melted out of the canopy at each station. Note: the rectangle vertical extent represents the interquartile range (25 <sup>th</sup> to 75 <sup>th</sup> percentile), the horizontal line within each box indicates the median, and the whiskers extend to 1.5 times the interquartile range. Circular points beyond the whiskers represent outliers. . . . .	121
5.10	Timeseries of simulated canopy load for CP25 and E10 at each station for the full simulation period. . . . .	122
5.11	Timeseries of simulated canopy load for CP25 and E10 at each station for select water years. The water year 2017 was selected for Fortress, Marmot, and Wolf Creek, while 2007 was selected for Russell. . . . .	123
5.12	Boxplots showing the annual fraction of time where simulated canopy snow load is greater than 2 kg m <sup>-2</sup> by the CP25 and E10 models. . . . .	123

# 1 INTRODUCTION

Melt of the seasonal snowpack directly supports over two billion people worldwide—crucial for downstream ecosystems, energy production, and agricultural irrigation (Immerzeel et al., 2020; Vivioli et al., 2020). The high albedo and energy required to melt snow also provides a large-scale cooling effect for our planet by reflecting most of the incoming solar radiation and dissipating energy during spring melt (Henderson et al., 2018; Leach & Moore, 2014). Snowfall in forested areas occurs over 50% of the northern hemisphere (Kim et al., 2017), and over 20% of the global landmass (Deschamps-Berger et al., 2025). Intercepted snow in the canopy is subjected to higher rates of sublimation and melt compared to the subcanopy snowpack due to greater surface area, turbulent energy exchange, and solar exposure (Floyd, 2012; Pomeroy et al., 1998b; Storck et al., 2002). In cold-dry continental climates, researchers estimate that 25 to 45% of annual snowfall may be lost to the sublimation of intercepted snow from the canopy (Essery et al., 2003; Sanmiguel-Vallelado et al., 2017). In warm-humid maritime climates the majority of snowfall melts in the canopy (Floyd, 2012; Storck et al., 2002), limiting atmospheric losses from sublimation, and contributes to changes in the phase and timing of precipitation reaching the subcanopy. The strong hydrological influence of forest canopies leads to high variability of snowpack accumulation in forested basins. Observations of this variability is not well represented due to a sparse and unrepresentative network of in situ observations, which are mostly located in clearings (Vionnet et al., 2021). Moreover, observing snow accumulation under forest canopies at large extents remains uncertain with current remote sensing technologies (Rittger et al., 2020). Thus, there is a need for reliable models of snow redistribution by forest to estimate snow accumulation (Clark et al., 2015a; Pomeroy et al., 2022) and to diagnose the impact of changing climate and vegetation cover on snowpack accumulation (Immerzeel et al., 2020; López-Moreno et al., 2014; Vivioli et al., 2020).

Limited observations of forest-snow processes including throughfall, unloading, sublimation, drip, and melt of canopy snow have limited process understanding and led to uncertainties in representing these processes in hydrological models (Lundquist et al., 2021). Existing snow interception parameterisations have been developed for both warm maritime (Andreadis et al., 2009; Storck et al., 2002) and cold continental (Ellis et al., 2010; Hedstrom & Pomeroy, 1998; Roesch et al., 2001) climates characterized by dense forest canopy. The strong dependence of snowfall partitioning by vegetation on meteorology and canopy density has challenged earlier parameterisations that were developed and tested in distinct climates in dense forest canopies. As a result these parameterisations often need to be calibrated when applied to new sites to better represent canopy snow interception (e.g., Lumbrazo et al., 2022). Although accurate performance in simulating subcanopy snow

water equivalent (SWE) has been achieved across different climates in some studies (Essery & Pomeroy, 2004; Gelfan et al., 2004), other snow model comparisons (Krinner et al., 2018; Rutter et al., 2009) have shown limited performance. The omission or simplified representation of processes and reliance on empirically derived coefficients likely contribute to model uncertainty when applied in climates and forests other than where they were developed (Krinner et al., 2018; Lumbrazo et al., 2022; Lundquist et al., 2021; Roth & Nolin, 2019; Rutter et al., 2009).

In hydrological models, the partitioning of snowfall in forest canopies is typically handled by first calculating the fraction of snowfall that is intercepted in the canopy (initial interception) and also parameterisations for ablation processes including unloading, melt/drip, and sublimation (Clark et al., 2015a; Pomeroy et al., 2022). Lundquist et al. (2021) and Staines & Pomeroy (2023) show that parameterisations developed by Hedstrom & Pomeroy (1998) and Storck et al. (2002) typically used in hydrological and land surface models (Clark et al., 2015a; Pomeroy et al., 2022; Verseghy, 2017) may overemphasize the role of increasing canopy snow load increasing throughfall of snow in the initial interception process. However, the snow loads observed by Staines & Pomeroy (2023) were relatively small, and thus their observations should be confirmed using additional observations over larger snowfall events and variable canopy densities and also over longer timescales. Several studies emphasize the importance of representing both dry/cold- and melt-induced unloading of snow in the canopy (Ellis et al., 2010; Essery & Pomeroy, 2004; Gelfan et al., 2004; Roesch et al., 2001). These processes are supported through physical mechanisms such as loss of structural integrity, particle bond weakening, and lubrication of intercepted snow during the melt process (Floyd, 2012; Storck et al., 2002). Sublimation promotes unloading via structural degradation and bond weakening of intercepted snow (MacDonald, 2010). Wind drag promotes unloading through shear stress applied to intercepted snow, wind erosion through direct entrainment in the atmosphere of intercepted snow, and branch movement (Bartlett & Verseghy, 2015; Lumbrazo et al., 2022; Roesch et al., 2001). Increasing air temperature promotes unloading by increasing the elasticity of branches and its association with melt and/or sublimation (Schmidt & Gluns, 1991; Schmidt & Pomeroy, 1990). While direct measurements of canopy snow unloading associated with melt were provided using detailed process-level lysimetry by Storck et al. (2002) dry-snow unloading parameterisation have been developed using indirect measurements from above canopy albedo (Bartlett & Verseghy, 2015; Roesch et al., 2001). Therefore, validation of the theories underlying dry-snow unloading parameterisations would benefit from additional direct observations of canopy snow unloading. Moreover, the canopy snowmelt induced unloading association proposed by Storck et al. (2002) was based on a single event and thus should be validated using additional observations. Additional processes currently not encoded in snow interception models include wind redistribution of snow, rain on intercepted snow, hoarfrost, rime ice and the cohesion and adhesion of snow in the canopy which will also be investigated.

Future climate change is expected to change the dominant hydrological processes in mountain forests largely as a result of the dependence of many snow processes on temperature (Dettinger, 2014; Fang & Pomeroy,

2020; He et al., 2021; Vivioli et al., 2011). A report by Environment and Climate Change Canada (Bush & Lemmen, 2019), suggest an increase in air temperature of 2 °C from the 1986-2005 reference period by 2050 for the low emission scenario and 6 °C for the high emission scenario by the late 21<sup>st</sup> century. Bush & Lemmen (2019) project an increase in annual mean precipitation over all of Canada during the second half of the 21<sup>st</sup> century, with a larger increase in northern Canada. As the climate warms, regions such as continental climates in Canada may shift from a dry-snow unloading and sublimation dominated regime to more influences from canopy snowmelt and drip processes. Thus, additional investigations on both melt- and dry-snow unloading are warranted to better understand both processes that are expected to become more prevalent in Canada with climate change.

In addition to shifting snow processes as a result of climate change, vegetation cover has already started experiencing changes resulting from drought (Dai, 2013), disease (Ruess et al., 2021), insects (Kurz et al., 2008), fire (Kasischke et al., 2010; Kasischke & Turetsky, 2006), changing land use (López-Moreno et al., 2014), and changing species (Gottfried et al., 2012). These changes in temperature, precipitation, along with the changing forest species, structure, and density are expected to have strong impacts on snowpack accumulation worldwide. However, to better understand these impacts, greater confidence in the application of forest-snow process parameterisations is needed. Since snow interception and ablation parameterisation were developed in distinct cold or warm climates with dense canopy structure there is a need to ensure these parameterisations are transferable across diverse climate and forest canopies.

To assess the performance of existing parameterisations, a modular and flexible model platform will be used to simulate the individual mass and energy balance fluxes and states of the canopy and snowpack. The advantage of modular and flexible model platforms is that it is possible to adjust process parameterisations while holding the remaining model parameters and mass and energy conservation equations constant (Clark et al., 2015a; Pomeroy et al., 2022). The Cold Regions Hydrological Model platform (CRHM, Pomeroy et al., 2022) will be used in this study as its mass and energy balance parameterisations have been successfully used in previous studies (Ellis et al., 2010; Pomeroy et al., 2012; Rasouli et al., 2019b; Sanmiguel-Vallelado et al., 2022a) to assess forest-snow interactions in Spain, USA, and Canada. Since CRHM is a process-based model agnostic platform, individual state and flux variables including subcanopy snow accumulation, snow interception, sublimation, unloading, drip, and wind redistribution can be evaluated using differing parameterisations. To evaluate existing parameterisations of snow interception (Andreadis et al., 2009; Hedstrom & Pomeroy, 1998; Storck et al., 2002), and ablation of canopy snow by unloading (Andreadis et al., 2009; Ellis et al., 2010; Roesch et al., 2001), drip (Andreadis et al., 2009; Ellis et al., 2010; Storck et al., 2002) and sublimation (Pomeroy et al., 1998b) CRHM will be run at four mountain forest research basins in western and northern Canada and compared to in-situ observations of subcanopy SWE. Modifications to the existing parameterisations to better represent snow interception processes will be validated on the associated change in error in simulated and observed forest snow accumulation.

## **1.1 Research Objectives**

The overarching goal of this thesis is to better understand the dominant processes that govern snow accumulation in forested environments and to determine how these processes can be accurately represented in hydrological models. To achieve this goal, two specific research objectives were formulated each with underlying research question(s):

### **1.1.1 Objective 1: Evaluate the suitability of existing snow interception and ablation parameterisations for application in needleleaf forests with differing canopy structure and meteorology.**

1. What are the theoretical underpinnings and assumptions behind existing snow interception and ablation parameterisations?
2. Are the theories and assumptions of existing snow interception parameterisations supported by field measurements collected across diverse canopy structures and meteorological conditions?
3. Are the theories and assumptions of existing canopy snow ablation parameterisations supported by field measurements collected across varying meteorological conditions?

### **1.1.2 Objective 2: Determine how new snow interception and ablation parameterisations could enhance the representation of processes important for subcanopy snow accumulation.**

4. How can the use of novel snow interception parameterisations enhance simulations of snow accumulation in forests with differing tree species, canopy structures, and meteorological conditions?

## **1.2 Organization of Chapters**

Following the Introduction of the thesis (Chapter 1), four manuscripts are presented as thesis chapters designed for submission to peer-reviewed journals and correspond to the aforementioned four research questions. Chapter 2 addresses Research Question 1 by providing a comprehensive review of the literature on snow interception and ablation parameterisations. This review identified the theories and assumptions underlying existing parameterisations and highlights the primary research gaps that this thesis seeks to address. The outcomes of Chapter 2 provide the foundation for evaluating parameterisations using field observations in the subsequent chapters.

Chapter 3 addresses Research Question 2 by presenting an evaluation of snow interception relationships based on novel observations of throughfall and canopy density. The results demonstrate theories underlying

existing snow interception parameterisations are not supported and show improved representation of the initial interception process with a new parameterisation across diverse meteorology, snow loads, and canopy densities.

Chapter 4 addresses Research Question 3 through an evaluation of theories regarding canopy snow ablation processes using a hybrid diagnostic mass balance approach which combined both direct observations of individual canopy snow ablation processes with simulations—where some process observations were not available (i.e., canopy snow sublimation). The results reveal that canopy snow load, wind shear stress, and snowmelt were most strongly associated with unloading and differed from existing theories. These findings highlight the need for revised parameterisations to accurately represent canopy snow ablation. Collectively, Chapters 2 through 4 demonstrate the successful completion of Objective 1.

Chapter 5 addresses Objective 2 (and Research Question 4) and describes the development of a new canopy snow model that incorporates the relationships identified in Chapters 3 and 4. The model is implemented in the Cold Regions Hydrological Modelling Platform across four research sites in western and northern Canada. Results demonstrate improved simulations of subcanopy SWE, especially under warm-humid climates dominated by canopy snow melt, validating the new parameterisations.

The thesis concludes with Chapter 6 which provides a synthesis of the results and conclusions from the previous chapters.

## 2 THE THEORETICAL UNDERPINNINGS OF EXISTING SNOW INTERCEPTION AND ABLATION PARAMETERISATIONS

Manuscript Status: The contents of this chapter have been compiled from a advanced review article published in the journal *WIREs Water*.

Citation: Cebulski, A. C., & Pomeroy, J. W. (2025). Theoretical Underpinnings of Snow Interception and Canopy Snow Ablation Parameterisations. *WIREs Water*, 12, e70010. <https://doi.org/10.1002/wat2.70010>

Role in thesis: This paper is an advanced review article and corresponds to objective 1, research question 1.1 of the thesis. This advanced review will provide the context necessary for interpreting whether the theories and assumptions of existing parameterisations are true for the field observations collected in this study in the second part of objective 1.

Author Contribution:

A. Cebulski: Conceptualization (lead), investigation (equal), software (lead), visualization (lead), writing – original draft (lead), writing review and editing (equal) J. Pomeroy: Conceptualization (supporting), funding acquisition (lead), investigation (equal), project administration (lead), resources (lead), supervision (lead), writing review and editing (equal).

### 2.1 Abstract

In needleleaf forests, up to half of annual snowfall may be returned to the atmosphere through sublimation of snow intercepted in the canopy. However, limited and sparse observations of snow interception and ablation processes have hindered the development of fundamental theories underpinning current estimates of snow accumulation in forests. Existing parameterisations for snow interception and ablation have been developed in locations with distinctive climate, tree species and forest structures, resulting in inconsistent and non-comprehensive process representations. This variability limits the transferability of these parameterisations across diverse landscapes and climates. Moreover, difficulties in isolating individual processes in field-based measurements has led to parameterisations that inadvertently coupled multiple processes, adding to uncertainty. Many studies have also simplified original parameterisations and do not include recent advances from observational studies. This review article aims to elucidate the theoretical foundations and assumptions

underlying the current snow interception and ablation parameterisations to provide a better understanding of uncertainties in existing methods and identify priorities for future field-based observational studies. The methods behind snow interception and ablation studies are also reviewed to provide necessary context for examining current parameterisations. Specific gaps in the literature include determining the canopy snow storage capacity, challenges in distinguishing snow throughfall measurements from canopy snow ablation, partitioning unloading rates and canopy snowmelt drainage, the assumption of vertical falling hydrometeor trajectories, the absence of wind resuspension parameterisations, and the limited testing of parameterisations in varied forests and climates.

## 2.2 Introduction

The melt of seasonal snowpacks is an important source of streamflow around the world, crucial for downstream ecosystems, energy production, drinking water supply and agricultural irrigation that directly support over 2 billion people (Viviroli et al., 2007, 2020). Despite this importance, there is uncertainty in estimates of snow accumulation due to redistribution of snow by wind and forest canopy (Ellis et al., 2010; Krinner et al., 2018; Rutter et al., 2009). In the Northern Hemisphere, over 50% of snowmelt-dominated basins are covered by needleleaf forest (Kim et al., 2017). This extensive canopy coverage reduces the amount of snow that is available for streamflow through interception of snowfall and subsequent canopy snow sublimation (Ellis et al., 2010; Essery et al., 2003; Hedstrom & Pomeroy, 1998). Intercepted snow in the canopy is subjected to higher rates of sublimation and melt compared to subcanopy snow due to greater surface area, warmer temperatures, turbulent energy exchange and solar exposure (Lundberg & Halldin, 1994; Pomeroy et al., 1998b). Across the Northern Hemisphere, researchers have estimated that 25–45% of annual snowfall may be lost to the sublimation of intercepted snow from the canopy (Essery et al., 2003). However, the magnitude of sublimation losses depends on the amount of snowfall that is intercepted in the canopy and the competing ablation processes including unloading, melt, drip, and resuspension of snow that control the duration that snow resides in the canopy. These processes contribute to spatial and temporal variability in the accumulation of snowpacks both between and within forested and non-forested landscapes (Krinner et al., 2018; Rutter et al., 2009). This snowpack variability is not well represented due to a sparse and unrepresentative network of in-situ observations, which are mostly located in forest clearings (e.g., Canada, Vionnet et al., 2021). Moreover, while high spatial resolution snow depth measurements from aerial lidar are useful for canopy-snow process investigations at the plot scale (e.g., Staines & Pomeroy, 2023), observing snow accumulation under forest canopies at large extents remains uncertain with current remote sensing technologies (Rittger et al., 2020; Stillinger et al., 2023). Therefore, there is a need for robust models of snow redistribution by vegetation to estimate snow accumulation in forests and generate predictions of how water resources will change with future climates (Clark et al., 2015a; Pomeroy et al., 2007; Rutter et al., 2009). Such models require a comprehensive understanding of snow redistribution processes.

Existing theories of snow interception and ablation have primarily been developed for dense forest canopies in either warm maritime (Andreadis et al., 2009; Katsushima et al., 2023; Storck et al., 2002) or cold continental (Ellis et al., 2010; Hedstrom & Pomeroy, 1998; Roesch et al., 2001) climates. These isolated observations have resulted in distinctive theories of the key snow interception and ablation processes. Whilst parameterisations founded on these theories can yield accurate simulations of the timing and magnitude of forest snow accumulation when applied in similar climates to where they were developed (Lundquist et al., 2021; Rasouli et al., 2019a; Roth & Nolin, 2019) or when combined into a hybrid parameterisation and assessed at global and regional scales in a wide range of climates (Essery et al., 2003; Gelfan et al., 2004), large discrepancies in simulated subcanopy snow accumulation have been demonstrated in inter-model comparisons by (Krinner et al., 2018) and (Rutter et al., 2009). Some of the uncertainty in subcanopy snowpack simulations observed by (Krinner et al., 2018) and (Rutter et al., 2009) was attributed to differing snow interception and ablation process representation, in addition to model platform differences (Clark & Kavetski, 2010). One example of differing process behaviour is the increase in canopy snow storage capacity with warmer temperatures shown by (Storck et al., 2002) and an opposing relationship suggested by (Hedstrom & Pomeroy, 1998). The difficulty in isolating individual processes such as throughfall, unloading, and drip in field measurements may have also contributed to unintentional coupling of processes in existing parameterisations. Issues arise when combining coupled parameterisations, such as snow interception parameterisations that also include ablation, with additional ablation parameterisations. Unless models have been calibrated to account for this (e.g., Hedstrom & Pomeroy, 1998), this combination can potentially result in some double-counting of the ablation process.

This review builds on recent work by Friesen et al. (2015), Van Stan et al. (2020), and Lundquist et al. (2021), who examined data collection methods and theories of snow interception and canopy snow ablation. While Friesen et al. (2015) and Van Stan et al. (2020) provide broad overviews of the methodologies for measuring and modelling liquid water and snow intercepted in the canopy, they lack the detail necessary to interpret snow interception studies. Lundquist et al. (2021) trace the development of two widely-used snow interception models, Hedstrom & Pomeroy (1998) and the combined Storck et al. (2002) and Andreadis et al. (2009), and provide a model experiment that showed the maximum canopy snow load capacity may be unnecessary for modelling snow interception if a comprehensive canopy snow ablation routine is included. However, these reviews do not provide a complete description of the canopy snow mass and energy balance, include recent updates to parameterisations, or discuss the parameterisations required to represent canopy snow ablation. Additionally, they do not connect measurement uncertainties with inconsistencies in process understanding. This review addresses these gaps by first detailing the theoretical mass and energy balance of canopy snow, along with the methods used to measure these processes. Additionally, a comprehensive synthesis of the literature on snow interception and canopy snow ablation process representations is provided, incorporating recent advancements in the field. The review then connects uncertainties in measurement techniques, such as challenges in partitioning throughfall rates from canopy snow ablation and distinguishing

unloading from canopy snowmelt drainage, to issues within current parameterisations of snow interception and ablation. The article will also explore processes often overlooked in existing parameterisations, including non-vertical hydrometeor trajectories, wind redistribution of snow in forests, and rime accretion. Lastly, it examines how the limited research on snow interception and ablation in forests with diverse species and structure has impacted process understanding and restricts transferability across differing environments.

## 2.3 The Mass and Energy Balance of Snow in the Canopy

The accumulation of snow under vegetation can be described using coupled mass and energy balance equations applied to control volumes representing the canopy and the snowpack. These control volumes are shown in Figures 1 and 2, where the canopy control volume includes snow, liquid water (stored within canopy snow), ice, and vegetation components, while the snowpack control volume represents snow accumulated on the surface. The mass and energy terms are represented as follows: the symbol  $q$  in lowercase signifies mass flux, while the uppercase  $Q$  signifies energy flux. The state of snow water equivalent (SWE,  $\text{kg m}^{-2}$ ) is denoted by  $L$  for snow intercepted in the canopy and  $S$  for the subcanopy snowpack. Fluxes that are repeated between the canopy and snowpack control volume have a superscript to specify what control volume they refer to (i.e.,  $q^{veg}$  refers to the vegetation control volume and  $q^{\wedge}$  refers to the surface snowpack control volume).

### 2.3.1 Mass Balance

The change in canopy snow load over time,  $\frac{dL}{dt}$  ( $\text{kg m}^{-2}$ ), may be represented as:

$$\frac{dL}{dt} = [q_{sf} - q_{tf}(L) + q_{ros}(L)] - q_{unld}(L) - q_{drip}(L) - q_{wind}^{veg}(L) - q_{sub}^{veg}(L) \quad (2.1)$$

where  $q_{sf}$  ( $\text{kg m}^{-2} \text{ s}^{-1}$ ) is the above canopy snowfall rate,  $q_{ros}$  ( $\text{kg m}^{-2} \text{ s}^{-1}$ ) is the rate of rainfall falling on snow intercepted in the canopy (does not include rainfall falling directly on canopy elements),  $q_{tf}$  ( $\text{kg m}^{-2} \text{ s}^{-1}$ ) is the throughfall rate, which is snowfall that passes through gaps in the canopy,  $q_{unld}$  ( $\text{kg m}^{-2} \text{ s}^{-1}$ ) is the canopy snow unloading rate,  $q_{drip}$  ( $\text{kg m}^{-2} \text{ s}^{-1}$ ) is the canopy snow drip rate due to canopy snowmelt and/or transmission of rainfall through snow intercepted in the canopy,  $q_{wind}^{veg}$  ( $\text{kg m}^{-2} \text{ s}^{-1}$ ) is the wind transport rate of snow by suspension in or out of the control volume, and  $q_{sub}^{veg}$  ( $\text{kg m}^{-2} \text{ s}^{-1}$ ) is the intercepted snow sublimation rate. In the treatment of rainfall interception,  $q_{unld}$  and  $q_{drip}$  are typically incorporated within the throughfall rate (i.e, Dingman, 2015; Van Stan et al., 2020). The rates in Equation 4.1, except for  $q_{sf}$ , are a function of the snow load present in the canopy ( $L$ ). Methods to estimate  $q_{tf}$ ,  $q_{unld}$ ,  $q_{drip}$  and  $q_{sub}^{veg}$  are described in detail in Section 2.5.

The rate of snow in the canopy undergoing phase change,  $q_{melt}^{veg}$  ( $\text{kg m}^{-2} \text{ s}^{-1}$ ), may be calculated as:

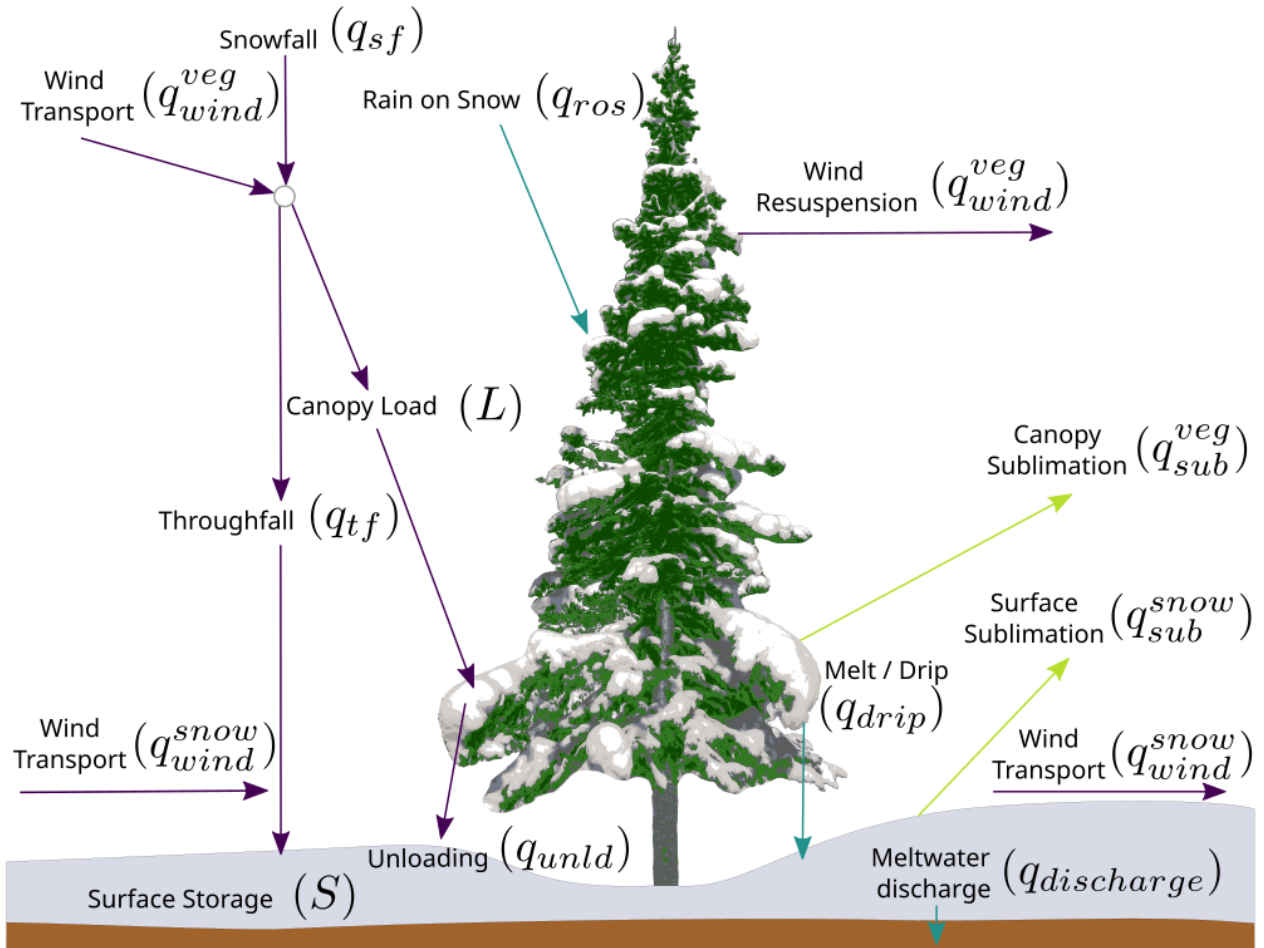


**Figure 2.1:** The mass balance of intercepted snow in a needleleaf forest canopy and the subcanopy snowpack. The colours of the arrows correspond to the water phase: solid (purple), liquid (blue) and vapour (light green). The head of the arrow indicates a positive flux either into the canopy (positive) or away from the canopy (negative). Fluxes may transition between positive and negative. In the case of sublimation from the canopy or snowpack, the flux may be positive (sublimation) or negative (deposition). This figure was adapted from Pomeroy and Gray (1995).

$$q_{drip} \approx q_{melt}^{veg} = \frac{Q_{melt}^{veg}}{\lambda_{fus} B} \quad (2.2)$$

where  $\lambda_{fus}$  ( $\text{J kg}^{-1}$ ) is the latent heat of fusion,  $B$  is the fraction of ice in a unit mass of wet snow (usually taken as 0.95-0.97, Gray & Landine (1988)).

The liquid meltwater output from snow intercepted in the canopy,  $q_{drip}$  ( $\text{kg m}^{-2} \text{s}^{-1}$ ) may be assumed to be approximately equal to  $q_{melt}^{veg}$  once the snow has reached its water holding capacity.  $Q_{melt}^{veg}(L)$  ( $\text{W m}^{-2}$ ) is the rate of energy available to melt canopy snow which is a function of  $L$ . The processes influencing  $Q_{melt}^{veg}(L)$  are shown in Equation 2.4.

The rate of sublimation from snow intercepted in the canopy,  $q_{sub}^{veg}$  ( $\text{kg m}^{-2} \text{s}^{-1}$ ) is determined by the latent heat flux,  $Q_l^{veg}$  ( $\text{W m}^{-2}$ ). Thus, the sublimation rate of snow intercepted in the canopy may be calculated as (Stull, 2017, eq. 4.45):

$$q_{sub}^{veg}(L) = \frac{Q_l^{veg}}{\lambda_{sub}} \quad (2.3)$$

where  $\lambda_{sub}$  ( $\text{J kg}^{-1}$ ), is the latent heat required for sublimation.

### 2.3.2 Energy Balance

The processes providing energy available for,  $Q_{melt}^{veg}(L)$ , or the rate of change of the bulk temperature of all constituents of vegetation, liquid water and snow,  $\frac{\partial T^{veg}}{\partial t}$  ( $\text{K s}^{-1}$ ) are shown in Figure 2.2. The notation in Figure 2.2 and in Equation 2.4 uses superscripts to specify which control volume the flux refers to: the vegetation control volume (veg), the snow-atmosphere interface (sai), and the top of the canopy between the upper atmosphere and canopy air space (total). Figure 2.2 shows the canopy air space which is a control volume used by some models (e.g., Clark et al. (2015a)) to differentiate the atmospheric conditions within and above the forest canopy.

The energy balance of the canopy is typically solved using a bulk approach in hydrological models which treats the canopy as a mixture of air, water, snow, ice, stems, and leaves (Clark et al. (2015b); Ellis et al. (2010); Parviaainen & Pomeroy (2000)):

$$Q_{melt}^{veg}(L) = Q_{sw}^{veg} + Q_{lw}^{veg} + Q_p^{veg} + Q_h^{veg} - Q_l^{veg} - C_p^{veg} \frac{\partial T^{veg}}{\partial t} D_{can} \quad (2.4)$$

where  $C_p^{veg}$  ( $\text{J m}^{-3} \text{K}^{-1}$ ) is the volumetric bulk storage capacity for heat of all constituents of vegetation, liquid water and snow,  $D_{can}$  (m) is the depth of the vegetation canopy,  $Q_{sw}^{veg}$  and  $Q_{lw}^{veg}$  ( $\text{W m}^{-2}$ ) are the net

shortwave and longwave radiation heat fluxes to the canopy,  $Q_p$  ( $\text{W m}^{-2}$ ) is the advective energy rate, which may include energy added to the canopy by  $q_{ros}$ , and  $Q_l^{veg}$  and  $Q_h^{veg}$  ( $\text{W m}^{-2}$ ) are the turbulent fluxes of latent heat and sensible heat, respectively, from the vegetation elements to the canopy air space. A negative value corresponds to a transfer of energy away from the vegetation elements.

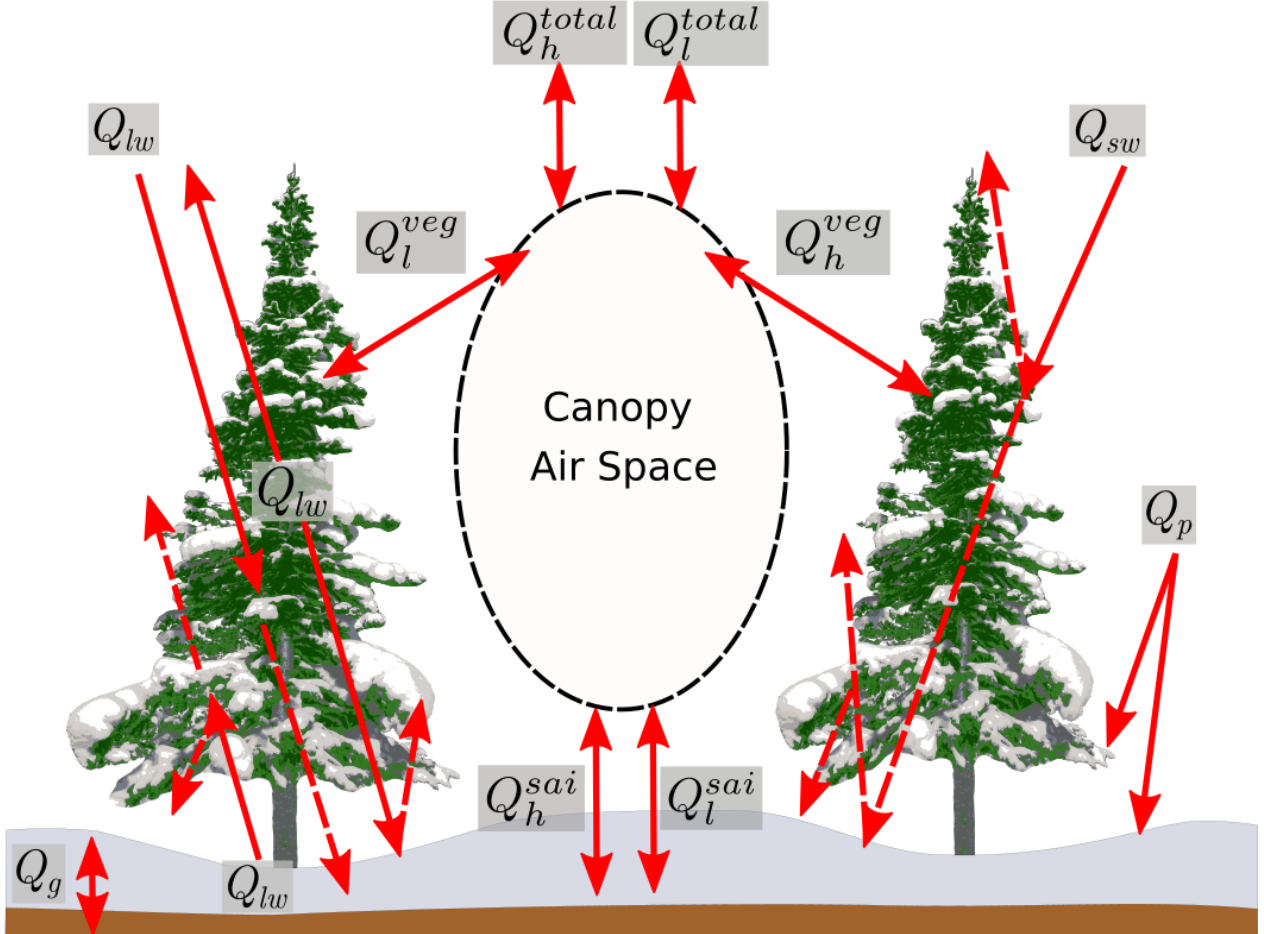


**Figure 2.2:** Conceptual representation of the physical processes important in the energy balance of the forest canopy and surface snowpack. Where  $Q_{sw}$  and  $Q_{lw}$  ( $\text{W m}^{-2}$ ) are shortwave and longwave fluxes,  $Q_l$  and  $Q_h$  ( $\text{W m}^{-2}$ ) are the turbulent fluxes of latent heat and sensible heat,  $Q_p$  ( $\text{W m}^{-2}$ ) is the advective energy rate, and  $Q_g$  ( $\text{W m}^{-2}$ ) is the ground heat flux. A superscript specifies which control volume the flux refers to: the vegetation control volume (veg), the snow-atmosphere interface (sai), and the top of the canopy between the upper atmosphere and canopy air space (total). The dashed lines represent radiation extinguished, reflected or re-emitted by the canopy, intercepted snow or surface snowpack. This figure was adapted from Clark et al. (2015a).

With Equation 2.4, for a cold canopy snowpack ( $T^{veg} < 0^\circ\text{C}$ ), all energy goes into warming the control volume (increasing  $\frac{\partial T^{veg}}{\partial t}$ ) and no melt of canopy snow occurs (warming phase,  $T^{veg} = 0$ ). Once  $T^{veg}$  reaches  $0^\circ\text{C}$ ,  $Q_{melt}^{veg}(L)$  increases as more energy becomes available for melt and  $\frac{\partial T^{veg}}{\partial t}$  equals zero (ripening and output phase) assuming the temperature of canopy snow is equal to that of the canopy when  $T^{veg} \leq 0^\circ\text{C}$ .

## 2.4 Measurement Techniques

### 2.4.1 Weighed Tree

Weighed tree lysimetry is one of the few direct methods to quantify the amount of snow intercepted in and ablated from the canopy. A cut tree is either weighed from a load cell on the ground (Lundberg & Halldin, 1994; e.g., Schmidt et al., 1988; Storck et al., 2002; Watanabe & Ozeki, 1964) or an inline strain gauge suspended from the crown of the tree as shown in Figure 3 (Hedstrom & Pomeroy, 1998; e.g., Pomeroy et al., 1993). To scale the weight of snow in the canopy (kg) to per unit area ( $\text{kg m}^{-2}$ ), there are two methods described in the literature. Katsushima et al. (2023), Satterlund & Haupt (1967), and Watanabe & Ozeki (1964) estimated the projected crown area ( $\text{m}^2$ ) of the weighed tree to convert weighed tree measurements in weight (kg) to snow load per unit area ( $\text{kg m}^{-2}$ ). Pomeroy et al. (1993) and Hedstrom & Pomeroy (1998), calculated areal estimates of  $\frac{dL}{dt}$ , using the mass balance method described in Section 2.4.2 along with fresh snow survey measurements of throughfall and point measurements of  $q_{sf}$ , to relate the weight change measured by the weighed tree to a per-unit-area measurement of  $\frac{dL}{dt}$ . Although the weighed tree method offers a direct measurement of  $\frac{dL}{dt}$ , it is limited to a point scale and can be impracticable for very tall trees due to challenges in constructing a tree mounting system. During periods of snowfall,  $\frac{dL}{dt}$  measured by the weighed tree is attributed to intercepted snowfall and ablation (Equation 4.1). In the absence of  $q_{sf}$  and hence  $q_{tf}$  and  $q_{ros}$ , the change in canopy snow load can be attributed to the remaining processes in Equation 4.1.

### 2.4.2 Mass Balance Methods

Since  $L$  is difficult to measure over spatial and temporal time scales, throughfall measurements can be used to infer canopy snow load as a residual based on Equation 4.1. If the assumption is made during snowfall periods with calm winds and cool air temperatures that ablative processes are negligible, Equation 4.1 can be simplified to:

$$\frac{dL}{dt} = q_{sf} - q_{tf}(L) \quad (2.5)$$

Over a discrete time interval,  $\Delta t$ , the change in canopy snow load,  $\Delta L$  ( $\text{kg m}^{-2}$ ) may be calculated as:

$$\frac{\Delta L}{\Delta t} = \overline{q_{sf}} - \overline{q_{tf}(L)} = \frac{\Delta sf}{\Delta t} - \frac{\Delta tf}{\Delta t} \quad (2.6)$$

where  $\overline{q_{sf}}$  and  $\overline{q_{tf}(L)}$  are the average snowfall and throughfall rate over  $\Delta t$ .  $\Delta sf$  and  $\Delta tf$  is the accumulated above canopy snowfall ( $\text{kg m}^{-2}$ ) and throughfall respectively.

Throughfall measurements of snow differ from rainfall measurements of throughfall which typically include

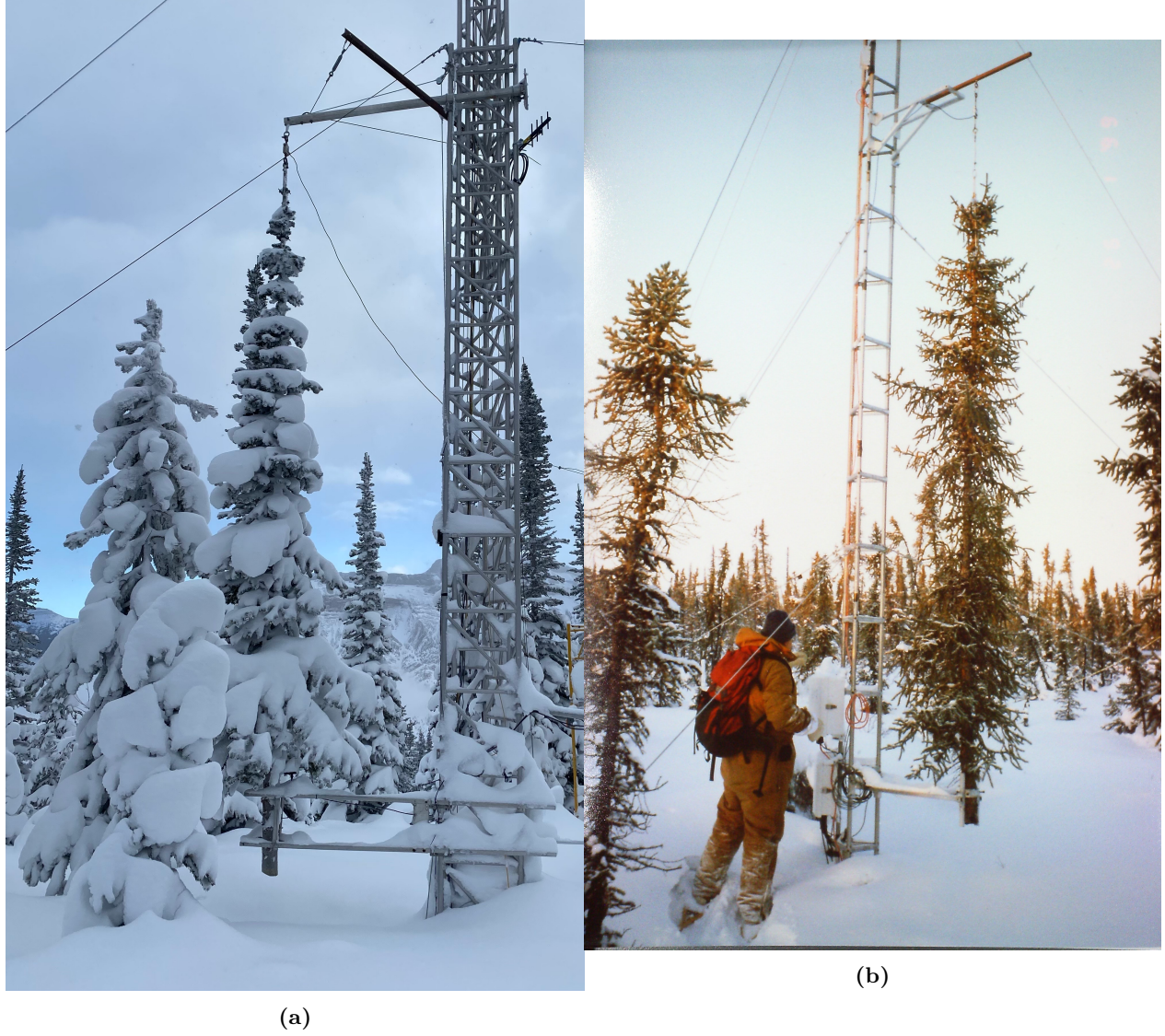


**Figure 2.3:** Weighed tree lysimeters, (a) Subalpine fir tree lysimeter loaded with snow, Fortress Mountain Research Basin, Alberta, Canada and (b) Black spruce tree lysimeter relatively free of snow, Havikpak Creek Research Basin, Inuvik, Northwest Territories, Canada.

$q_{drip}$  (Van Stan et al., 2020). However, even for snowfall events with cold temperatures and calm winds, ablative processes are likely non-zero and thus true measurements of throughfall are difficult to ascertain.

#### 2.4.2.1 Snow Surveys

Snow surveys conducted below the canopy are one method to provide areal estimates of  $\frac{\Delta t_f}{\Delta t}$ . Combined with measurements of  $\frac{\Delta s_f}{\Delta t}$ , Equation 2.6 can be used to estimate  $\frac{\Delta L}{\Delta t}$ . Throughfall depths may be converted to SWE using observed relationships between snow depth and snow density (e.g., Staines & Pomeroy, 2023) or modelled using empirical equations (e.g., Lv & Pomeroy, 2020). If the covariance between snow depth and density is found to be insignificant, Pomeroy & Gray (1995) recommend calculating SWE as:

$$\frac{\Delta t_f}{\Delta t} = \bar{\rho}_s \cdot \frac{d_{tf}}{\Delta t} \quad (2.7)$$

where  $\bar{\rho}_s$  is the average snow density over the snow survey and  $d_{tf}$  is the depth of throughfall (m).  $d_{tf}$  may be determined using the difference in post-event and pre-event snow depth using rulers (e.g., Hedstrom & Pomeroy, 1998), or using aerial lidar derived surface models (e.g., Staines & Pomeroy, 2023). Uncertainties with these two methods include penetration of the ruler into the soil which falsely increases the snow depth, and errors associated with lidar methods of 5—20 cm (RMSE) described in Harder et al. (2020) and Staines & Pomeroy (2023). If a defined layer (i.e., natural ice crust or measurement plate) is present prior to a snowfall event, depths of snow above this layer may be taken as  $d_{tf}$  as in Moeser et al. (2015b). Automated acoustic snow depth sensors have also been used to measure  $d_{tf}$  as the difference in the change in snow depth to an open area and subcanopy (Lv & Pomeroy, 2020; Roth & Nolin, 2019). Regardless of the method chosen, care must be taken to ensure ablation of snow in the canopy and on the ground is minimal over the snowfall period to ensure Equation 2.6 is valid.

$\rho_s$  may be measured using gravimetric fresh snow density sampling. With this method a pit is dug to below the bottom of the new throughfall layer and a snow density sampler of a known volume is pushed horizontally into the new snow layer (e.g., Figure 2.4) and the resulting sample is weighed. Additional methods are available for the calculation of snow density including snow tubes, microwave radar, gamma ray, snow pillow, and snow scale. However, these methods have constraints in providing a density of a new snow layer and are more commonly applied to measure density of the entire snowpack to the ground.

#### 2.4.2.2 Subcanopy Lysimeters

Subcanopy lysimeters may provide measurements of  $\bar{q}_{tf}$  and/or the downward ablation of snow in the canopy,  $\bar{q}_{unld}$  and  $\bar{q}_{drip}$ . When paired with an automated data logger, measurements can be taken over relatively shorter discrete time intervals compared to manual snow surveys. With this method, a trough or bucket is suspended from a load cell (e.g., Figure 2.5) or installed on the ground (e.g., Storck et al., 2002) and



**Figure 2.4:** Gravimetric fresh snow density sample collection, Fortress Mountain Research Basin, Alberta, Canada. A 1000 cm<sup>3</sup> snow density wedge sampler (RIP Cutter, <https://snowmetrics.com/shop/rip-1-cutter-1000-cc/>) is shown being pushed into the surface of the snowpack. The scale used to measure the weight of the sample is shown on the bottom right.

measures the accumulated weight (kg) of snow entering the lysimeter. The surface area of the opening of the trough is used to convert the weight to a per unit area measurement in ( $\text{kg m}^{-2}$ ). For periods where,  $q_{unld}$  and  $q_{drip}$  can be considered negligible, the subcanopy lysimeters provide measurements of  $\overline{q}_{tf}\Delta t$  and using Equation 2.6 along with  $\overline{q}_{sf}\Delta t$  can be used to estimate  $\frac{dL}{dt}$ . For periods without snowfall, the subcanopy lysimeters provide measurement of  $q_{unld} + q_{drip}$ .

Measurements of  $q_{drip}$  are difficult to ascertain due to its simultaneous occurrence with  $q_{unld}$  especially in warm temperatures. To isolate,  $q_{drip}$ , researchers(e.g., Floyd, 2012; Storck et al., 2002) have utilized tipping bucket rainfall gauges positioned beneath the canopy to quantify the drainage rate of liquid water from snow intercepted in the canopy. However, employing tipping buckets in temperatures close to 0°C presents difficulties as the mechanical apparatus can freeze, resulting in missed measurements. The simultaneous occurrence of  $q_{unld}$  during the melt process may provide an additional source of liquid water as ripe clumps of snow continue to melt into the tipping bucket device. The difficulty in isolating the multiple processes, as outlined in Equation 4.1 and Figure 2.1, that contribute snow beneath the canopy is the main limitation of using subcanopy lysimeters to measure snow interception and canopy snow ablation. Therefore, use of this methodology should be paired with other observations such as meteorological measurements, timelapse imagery or a weighed tree to help determine if unloading and drip are likely.

### 2.4.3 Remote Sensing

Remote sensing methodologies have proven effective in acquiring measurements of throughfall, canopy snow load, and ablation over larger spatial extents and more frequent temporal scales compared to the measurements discussed above (Bartlett & Verseghy, 2015; Calder, 1990; Floyd & Weiler, 2008; Russell et al., 2020). For example, Calder (1990) used a gamma ray attenuation system to continuously measure canopy snow load within a forest plot. However, the gamma ray technique has not been repeated in canopy-scale snow interception studies due to the danger of emissions from the radioactive source. Aside from the study conducted by Calder (1990), remote sensing methods generally do not directly measure canopy snow load in units of  $\text{kg m}^{-3}$ . Instead, they provide a volumetric measurement of canopy load, a measurement of throughfall, an index based on above canopy albedo, or an areal fraction of canopy covered by snow.

One volumetric approach, as demonstrated by Russell et al. (2020), utilized autonomous terrestrial laser scanning (ATLS) to measure the volume of snow intercepted in the canopy. This method involves collecting ATLS point clouds for an individual tree during snow-free and snow-on conditions. The 3D approximations created from these point clouds are used to calculate the canopy volume for both conditions, while also accounting for branch bending and lidar beam occlusion. By subtracting the snow-on volume from the snow-free volume, an estimate of the snow intercepted in the canopy is obtained. Limitations with the ATLS method include challenges such as changes in tree geometry under snow loading and lidar beam occlusion which were only partially addressed by the Russell et al. (2020) method, and the difficulty of estimating the density of



**Figure 2.5:** An example of a suspended subcanopy lysimeter installed at Fortress Mountain Research Basin, Alberta, Canada to measure rates of throughfall, unloading, and drip.

intercepted snow in the canopy. These challenges contributed to the weak correlation observed by Russell et al. (2020) when comparing results with measurements of canopy snow load obtained through weighed tree assessments. Indirect measurements of canopy snow load using aerial lidar throughfall measurements are discussed in Section 2.4.2.1.

The studies conducted by Roesch et al. (2001) and Bartlett & Verseghy (2015) utilized measurements of above canopy albedo, which is hypothesised to increase as snow is intercepted in the canopy and reduce light transmittance through the canopy. However, given the potential for fresh snowfall to cover the upward-facing radiometer and lead to erroneous albedo measurements, cleaning radiometers following snowfall events is crucial. A study using radiometer measurements that were cleaned after each snowfall event, by Nakai et al. (1999) highlights that very large canopy snow loads show an increase in above canopy albedo. For small snow loads ( $< 1.6 \text{ kg m}^{-2}$ ) Pomeroy & Dion (1996) show that no relationship was found between canopy snow load and above canopy albedo over a mature pine canopy using a frequently cleaned radiometer. More recent work by Lv & Pomeroy (2019) shows that the normalised snow difference index calculated using Landsat satellite imagery dramatically increased with canopy snow load. Lv & Pomeroy (2019) also show a small, but detectable increase in albedo was found when the canopy was covered with snow. This method has limitations for smaller snowfall events in some tree species and canopy structures Pomeroy & Dion (1996) or when radiometer measurements are erroneous.

Time-lapse photography has been an important component of understanding canopy snow processes at the plot or individual tree scale since early work by Berndt & Fowler (1969) to quantify rime accretion on needleleaf canopy. Pomeroy et al. (1993) developed perimeter-area relationships to quantify the sublimation rate of intercepted snow, using photographs and fractal geometry, but found no unique relationship between oblique snow-covered canopy fraction, measured using digital images and Java image analysis software, and the mass of snow weighed on a suspended tree. A method to determine the snow-covered fraction of the canopy was developed by Floyd & Weiler (2008) using automated image analysis who noted limitations of this method due to condensation/frost build up on the camera lens and lighting conditions. Similar methodologies have also been utilized by several other studies to understand canopy-snow processes (Dong & Menzel, 2017; Garvelmann et al., 2013; Parajka et al., 2012). Recent work by Lumbrago et al. (2022) involved citizen scientists to classify time-lapse images of snow in the canopy into an index of canopy snow-covered fraction to diagnose canopy snow ablation process models. Additionally, Harvey et al. (2025) show that a deep learning convolutional neural network model provided estimates of canopy snow presence from time-lapse imagery that had very close agreement to images analyzed by humans and also much better accuracy than the automated thresholding methods used by previous studies.

#### 2.4.4 Tree Sway Frequency

The sway frequency of trees has been shown to decrease proportionally with increasing mass stored in the canopy (Papesch, 1984; Raleigh et al., 2022). A study by Raleigh et al. (2022) utilized a three-dimensional accelerator attached to the upper section of a tree to quantify wind induced movements and provide an index of canopy snow load. Raleigh et al. (2022) showed that the influence of thermal effects on tree rigidity must be considered when analyzing sway frequency in cold climates. Raleigh et al. (2022) notes additional challenges with this method including difficulties in isolating a separate relationship for tree sway frequency and thermal effects and relating changes in sway frequency to changes in snow load. Schmidt & Pomeroy (1990) show that the modulus of elasticity of tree branches varies with temperature below 0°C, indicating this technique is strongly impacted by freezing and thawing of trunks. Measurements of canopy snow load are also limited to periods of heightened wind where canopy snow is also likely to ablate.

#### 2.4.5 Trunk Compression

Measurement of trunk compression, initially utilized for monitoring the mass of intercepted rain in the canopy (Friesen et al., 2008), has been adapted for measurement of canopy snow load by Martin et al. (2013). This method is based on Hooke's law of elasticity to infer a change in mass through the trunk's compression and expansion. However, uncertainties with this method include the need for individual tree-specific calibration for determining the modulus of elasticity. Additionally, factors such as transpiration, sap flow, wind, and temperature contribute to noise in the instrumentation, primarily through thermal expansion and wind induced compression of the trunk. The expansion and compression of trees with freezing and thawing discussed by Gutmann et al. (2017) suggests further research is required to apply this method to freezing trunks. Sensors with extremely high precision ( $\pm 1\text{--}2 \mu\text{m}$ ) are also required for this method leading to high cost.

#### 2.4.6 Eddy Covariance

The rate of canopy snow sublimation,  $q_{sub}^{veg}$  ( $\text{kg m}^{-2} \text{s}^{-1}$ ), can be measured using the eddy covariance technique (e.g., Harding & Pomeroy, 1996; Lundberg & Halldin, 2001; Molotch et al., 2007; Parviainen & Pomeroy, 2000). With this method, an eddy covariance system measures the latent heat flux above the canopy resulting from evapotranspiration, evaporation, and sublimation of snow on the surface and in the canopy. During cool periods where evapotranspiration and evaporation rates are assumed negligible, the latent heat flux can be attributed to  $Q_l^{sai} + Q_l^{veg}$  and can be converted to  $q_{sub}^{snow} + q_{sub}^{veg}$  using Equation 2.3. A second eddy covariance system installed beneath the canopy above the surface snowpack to measure  $Q_l^{sai}$ , which can be used to isolate  $Q_l^{veg}$  in the above canopy latent heat measurements (Molotch et al., 2007). Alternatively, the subcanopy snowpack sublimation rate may be assumed negligible, and a single eddy covariance system is used (Lundberg & Halldin, 2001; Parviainen & Pomeroy, 2000). Uncertainties in this measurement technique

stem from assumptions such as negligible transpiration rates from surrounding vegetation, the requirements of a homogeneous surface, and slow variations in airflow properties. Many studies show a failure to close the above canopy energy balance when the canopy is snow-covered (e.g., Harding & Pomeroy, 1996). Harvey et al. (2025) also demonstrated that this method incorrectly identified  $q_{sub}^{veg}$  for several days when the canopy was observed to be without snow in time-lapse images. They attributed this to differing flux footprints of the above and below-canopy eddy covariance measurements and/or sublimation of wind-suspended snow.

### 2.4.7 Snow Isotopes

Investigating the isotopic composition of water and snow has proven valuable for understanding hydrological (e.g., Galewsky et al., 2016) and snow (Beria et al., 2018) processes. During phase changes, snow undergoes isotopic fractionation, altering the relative abundance of heavier and lighter isotopes of hydrogen and oxygen among the different phases. While sublimation of snow intercepted in the canopy is known to enrich heavier isotopes in the remaining snow (Beria et al., 2018), relatively few studies have utilized snow isotopes to explore canopy snow processes (Claassen & Downey, 1995; Koeniger et al., 2008). Interpreting isotopic fractionation in canopy snow is challenging, as fractionation from cold, sublimating snow can be minimal (Schlaepfer et al., 2014), whilst wet snow undergoing sublimation, deposition, and melt shows varying degrees of fractionation (Beria et al., 2018). Additionally, some clumps of snow may completely sublimate while others partially sublimate or melt, complicating the link between isotope enrichment and a specific process. Chemical changes in intercepted snow have been shown by Pomeroy et al. (1999) to present similar complications on linking chemical changes to individual processes, limiting its usefulness for quantifying canopy snow mass exchange processes. Subsequent fractionation also can occur in the subcanopy snowpack as meltwater percolates and refreezes or the surface snow sublimates (Beria et al., 2018), which further complicates isolating specific processes.

## 2.5 Parameterisations

### 2.5.1 Snow Interception Parameterisations

Snow interception parameterisations differ in their approximation of the maximum canopy snow storage capacity (Figure 2.6, a) and the fraction of snowfall intercepted (Figure 2.6, b), due to differences in the relationships and variables included in each parameterisation (Table 2.1). This leads to large discrepancies in the predicted canopy snow load shown in Figure 2.7 and thus the amount of snow available for sublimation losses. The factors contributing to these model discrepancies can be grouped into intrinsic factors of the vegetative structure (e.g., canopy coverage, leaf area and surface temperature) and extrinsic factors (e.g., snowfall event meteorology, methodologies). Parameterisations for snowfall interception have all been derived for evergreen needleleaf forests and thus constrain the scope of this section (Hedstrom & Pomeroy, 1998;

Satterlund & Haupt, 1967; Storck et al., 2002).

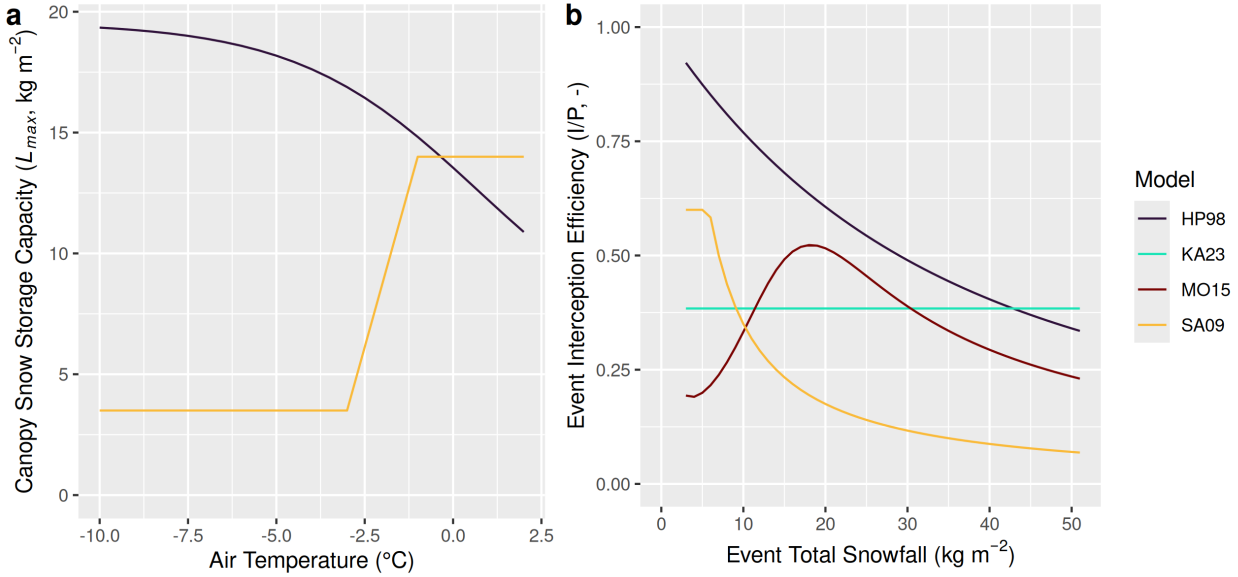


**Figure 2.6:** Panel (a) Comparison of the Hedstrom & Pomeroy (1998) (HP98) and Andreadis et al. (2009) (SA09) canopy snow storage capacity parameterisations. Panel (b) shows interception efficiency for event totals as the change in event canopy snow load divided by the corresponding change in event snowfall in the open for parameterisations: HP98, Katsushima et al., (2023) (KA23), SA09, and Moeser et al., (2009) (M15). Initial canopy load is held at 0, air temperature is  $-5^{\circ}\text{C}$ , LAI of 3.5 and the HP98 species coefficient for spruce ( $5.9 \text{ kg m}^{-2}$ ).

**Table 2.1:** Summary of canopy interception/precipitation (I/P) model behaviour and measurement techniques.

Model	Variables	General Description	Measurement Technique
Satterlund & Haupt (1967)	$L_{max}$ , $K$ , $q_{sf}$ , $P_{sf}^e$	I/P initially rises due to rising $L$ which bridges gaps and increases $C_p$ . I/P later declines when $L$ approaches $L_{max}$ due to branch bending which reduces $C_p$ and increases unloading.	Weighed tree lysimeter

Model	Variables	General Description	Measurement Technique
Hedstrom & Pomeroy (1998)	$C_p(C_c, u, w, H, J), L, L_0, q_{sf}, L_{max}(S, \bar{S}, LAI, \rho_s, T_a)$	I/P starts high and then declines as $L$ approaches $L_{max}$ which reduces $C_p$ and increases unloading. This decline is stronger for warmer $T_a$ as branches bend more easily.	Snow survey mass balance
Storck et al. (2002)	$L_{max}(L_r, T_a, m, LAI)$	I/P is constant over time and space. $L_{max}$ increases with $LAI$ and increases as a step function of $T_a$ due to higher cohesion and adhesion. When $L > L_{max}$ new snow is unloaded to the surface snowpack.	Weighed tree lysimeter with subcanopy lysimeter
Roth & Nolin (2019)	$q_{sf}, T_a, G_z$	I/P increases with increasing $T_a$ and a lidar derived canopy structure metric $G_z$ .	Paired open and forested acoustic snow depth sensors and aerial lidar canopy metrics
Katsushima et al. (2023)	$L, T_a, u_{1/3}$	I/P decreases with increasing $u_{13}$ when $T_a < 0^\circ\text{C}$ , I/P increases with $T_a$ when $-4^\circ\text{C} \leq T_a < 0^\circ\text{C}$ , and I/P decreases with $T_a$ and $L$ when $T_a > 0^\circ\text{C}$ .	Weighed tree lysimeter

### 2.5.1.1 Hedstrom & Pomeroy (1998)

In the observations collected by Hedstrom & Pomeroy (1998) in the southern boreal forest from a Jack Pine and Black Spruce stand, snow interception efficiency starts high and then declines and was represented using an inverse exponential function (Figure 2.6, b). Hedstrom & Pomeroy (1998) describe a relationship to relate

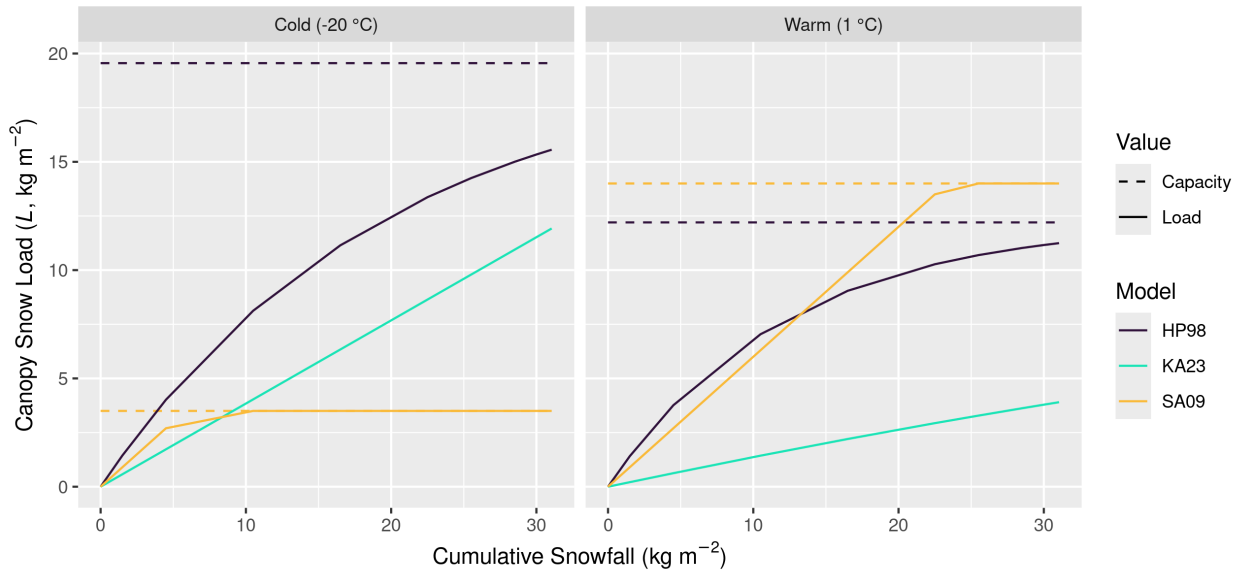


**Figure 2.7:** The state of canopy snow load (solid lines) for a cold and warm event using the parameterisations by Hedstrom and Pomeroy (1998) (HP98), Katsushima et al., (2023), combined Storck et al. (2002) and Andreadis et al., (2009) (SA09). The interception storage capacity is shown for the HP98 (purple) and SA09 (orange) parameterisations using a horizontal dashed line. The KA23 parameterisation does not include a canopy snow storage capacity. To isolate the influence of snow interception parameterisations ablative processes have not been computed. Constants for these two plots include a wind speed of  $1 \text{ m s}^{-1}$ , LAI of 3.5 (-) and the HP98 species coefficient for spruce ( $5.9 \text{ kg m}^{-2}$ ).

$q_{tf}(L)$  to interception efficiency,  $\frac{I}{P}(L)$ , the fraction of snow intercepted over a snowfall period, both of which are proposed to be a function of  $L$ . The mass balance method (i.e., Equation 2.5) was used to estimate  $\frac{I}{P}$  which incorporated fresh snow survey measurements of  $\Delta_{tf}$  at the plot scale and  $\Delta_{sf}$  to an open clearing over events with  $\Delta t$  ranging from days to weeks. Average cumulative snowfall over these events was  $4 \text{ kg m}^{-2}$  with event temperatures ranging from  $-40^\circ\text{C}$  to near  $0^\circ\text{C}$  and very low wind speeds (exact values not reported). These measurements, in addition to those collected by Schmidt & Gluns (1991) were used to formulate the Hedstrom & Pomeroy (1998) snow interception parameterisation. Hedstrom & Pomeroy (1998) calculate  $q_{tf}$  as:

$$q_{tf}(L) = \begin{cases} (1 - \frac{I}{P}(L)) q_{sf}, & \text{if } L < L_{max} \\ q_{sf}, & \text{otherwise} \end{cases} \quad (2.8)$$

$\frac{I}{P}(L)$  is calculated as:

$$\frac{I}{P}(L) = \frac{\Delta L}{\bar{q}_{sf}\Delta t} \quad (2.9)$$

where  $\bar{q}_{sf}$  ( $\text{kg m}^{-2}$ ), is the average snowfall rate over the discrete time interval  $\Delta t$ . For a given snowfall event, Hedstrom & Pomeroy (1998) propose a function to calculate  $\frac{I}{P}(L)$  as:

$$\frac{I}{P}(L) = C_p \frac{L_{max} - L}{L_{max}} \quad (2.10)$$

where  $C_p$  (-) is the fraction of snow-leaf contact area per unit area of ground. Equation 2.10 has been simplified slightly from the original formula presented in Hedstrom & Pomeroy (1998). See Equation 2.35 in Section 2.9 for the steps to simplify.

The calculation of  $C_p$  in Hedstrom & Pomeroy (1998) is:

$$C_{lca} = \frac{C_c}{1 - \frac{C_c u H}{w J}} \quad (2.11)$$

where  $C_c$  (-) is the canopy closure,  $u$  ( $\text{m s}^{-1}$ ) is the horizontal velocity of the snow particle (approximated by wind speed),  $w$  ( $\text{m s}^{-1}$ ) is the snow particle vertical fall velocity,  $H$  (m) is the height of the canopy,  $J$  (m) is the forested downwind distance. Since  $w$  is not a commonly available meteorological forcing variable Hedstrom & Pomeroy (1998) assume a constant of  $0.8 \text{ m s}^{-1}$ . In the absence of detailed canopy structure metrics  $J$  is difficult to determine in practice. An example of how  $C_p$  varies with wind speed and canopy

coverage is shown in Figure 2.8. A limit in the increase in  $C_p$  is shown in Figure 2.8 as  $C_p$  reaches 1.0 and does not increase further at a wind speed of 2 m s<sup>-1</sup> and  $C_c$  of 0.8.

Hedstrom & Pomeroy (1998) integrate Equation 2.35 to provide an analytical solution to calculate the change in intercepted snow load,  $\Delta L$  (kg m<sup>-2</sup>) over a discrete time interval:

$$\Delta L = (L_{max} - L_0) \left( 1 - \exp \left( -\frac{C_{lca}}{L_{max}} \bar{q}_{sf} \Delta t \right) \right) \quad (2.12)$$

where  $L_0$  (kg m<sup>-2</sup>) is the canopy snow load before snowfall is added to the canopy and  $L_{max}$  (kg m<sup>-2</sup>) is the canopy snow storage capacity. The steps of the derivation of Equation 2.12 from Equation 2.10 are shown in Equation 2.37 of Section 2.9. Equation 2.12 has similar form to the rainfall interception parameterisations developed by (Aston, 1979; Merriam, 1960):

$$\Delta L = (L_{max}) (1 - \exp(-\gamma \bar{q}_{sf} \Delta t)) \quad (2.13)$$

with  $\gamma$  being an exponential fitting parameter.

Hedstrom & Pomeroy (1998) calculate  $L_{max}$  as:

$$L_{max} = S \cdot LAI \quad (2.14)$$

where  $LAI$  (dimensionless) is the leaf area index, and  $S$  (kg m<sup>-2</sup>) is a species maximum snow load correction factor that is a function of snow density:

$$S = \bar{S} \left( 0.27 + \frac{46}{\rho_s} \right) \quad (2.15)$$

where  $\rho_s$  (kg m<sup>-3</sup>) is the fresh snow density (kg m<sup>-3</sup>) and Schmidt & Gluns (1991) observed  $\bar{S} = 6.6$  and 5.9 kg m<sup>-2</sup> for pine and spruce, respectively.

Fresh snow density  $\rho_s$  was estimated by Hedstrom & Pomeroy (1998) based on a regression through observations from sites in Saskatchewan and Yukon (Hedstrom & Pomeroy, 1998), the Fraser Experimental Forest, Colorado (1989) and Nelson, British Columbia (1990) (Schmidt & Gluns, 1991), and the Central Sierra Snow Laboratory, California (of Engineers, 1956) as:

$$\rho_s = 67.92 + 51.25e^{(T_a)/2.59} \quad (2.16)$$

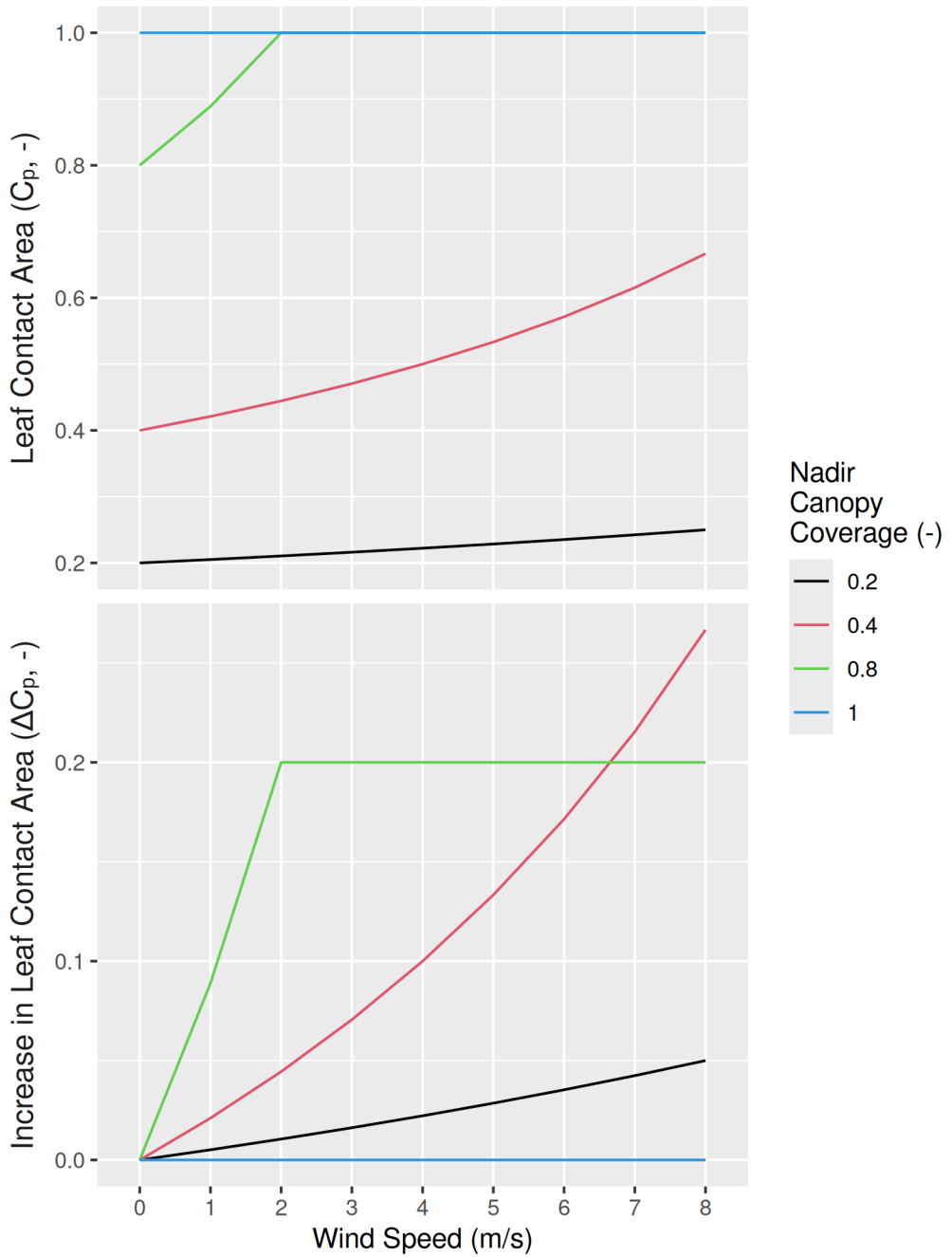


**Figure 2.8:** Plots showing the leaf contact area (top) and increase in leaf contact area (bottom) with increasing wind speed calculated using the method from Hedstrom & Pomeroy (1998). The colour of each line represents the leaf contact area at nadir which is equal to the canopy coverage. Here the canopy height is held constant at 10 m, the forested downwind distance is 100 m, and the fall velocity is  $0.8 \text{ m s}^{-1}$ .

where  $T_a$  is the ambient air temperature ( $^{\circ}\text{C}$ ). According to this equation,  $\rho_s$  increases with higher temperatures which will result in lower  $S$  and subsequently lower  $L_{max}$  (Figure 2.6, a), resulting in the lower canopy snow loads for warm temperatures compared to cold temperatures shown in Figure 2.7). There are other factors not directly accounted for by this equation such as solar radiation, humidity, hydrometeor type and size, wind speed, and compression of snow which may contribute to the melt and/or metamorphism of fresh snowfall.

### 2.5.1.2 Storck et al. (2002) and Andreadis et al. (2009)

Andreadis et al. (2009) developed a snow interception parameterisation using data collected by Storck et al. (2002) in dense old growth forest in the maritime climate of southwestern Oregon, USA. Storck et al. (2002) used a weighed tree lysimeter (Douglas fir, Ponderosa pine, White fir, and Lodgepole pine) to measure  $\frac{dL}{dt}$ , a subcanopy lysimeter (installed beneath the subcanopy snowpack) measured  $q_{tf} + q_{unld} + q_{drip} + q_{discharge}$ , and  $q_{sf}$  was measured in an open clearing. Using these point scale measurements Storck et al. (2002) attempted to isolate the individual processes in Equation 4.1 to develop their process understanding. The opposing relationship and increased sensitivity of the Storck et al. (2002) calculation of canopy snow storage capacity to air temperature compared to Hedstrom & Pomeroy (1998) is shown in Figure 2.6. The observations from Storck et al. (2002) found  $\frac{I}{P}$  was equal to a constant of 0.6 up to canopy snow loads of  $40 \text{ kg m}^{-2}$ . This results in the positive linear relationship of  $L$  with increasing snowfall until  $L_{max}$  is reached (Figure 2.7). This is similar to the observations by Calder (1990) who also observed a constant value of  $\frac{I}{P}(L)$  for canopy snow loads up to 30 mm in the uplands of Scotland (see Fig. 2 in Lundberg & Halldin, 2001). Storck et al. (2002) limit,  $L$  as being less than or equal to  $L_{max}$  using a step function of temperature.

Storck et al. (2002) calculate  $L_{max}$  as:

$$L_{max} = L_r \cdot m \cdot LAI \quad (2.17)$$

where  $m$  ( $\text{kg m}^{-2}$ ) is an empirical parameter determined based on their observations of the canopy snow storage capacity (default value =  $5 \cdot e^{-6}$ ),  $L_r$  (dimensionless) is a step function of temperature based on observations by Kobayashi (1987) of snow cohesion on a plank of wood and Pfister & Schneebeli (1999) and Storck et al. (2002) who observed that snow interception decreases with decreasing temperatures. Based on these observations  $L_r$  is calculated as:

$$L_r = \begin{cases} 4, & \text{if } T_a > -1^{\circ}\text{C} \\ 1.5T_a + 5.5, & \text{if } -1^{\circ}\text{C} \geq T_a > -3^{\circ}\text{C} \\ 1.0, & \text{if } T_a \leq -3^{\circ}\text{C} \end{cases} \quad (2.18)$$

The Storck et al. (2002) dataset was derived from observed snowfall events of 5—80 kg m<sup>-2</sup> with an average of  $\sim 15$  kg m<sup>-2</sup>, winds less than 2 m s<sup>-1</sup> and relatively warm air temperatures above -5°C.

### 2.5.1.3 Katsushima et al. (2023)

More recent work by Katsushima et al. (2023) collected measurements of snow interception using a weighed Japanese cedar tree (*Cryptomeria japonica*) in a warm-humid coastal environment. To isolate periods of interception without unloading they selected weighed tree observations at night with precipitation rate  $\geq 1$  kg m<sup>-2</sup> hr<sup>-1</sup>, wind speed  $\leq 1$  m s<sup>-1</sup>, and an air temperature of  $\leq 1.5$  °C. Katsushima et al. (2023) observed a decline in interception efficiency with increasing wind speed, which they attributed to increased hydrometeor velocity and bouncing on impact. They did not observe a maximum interception capacity within their canopy snow load measurement range of 0-25 kg m<sup>-2</sup>. Katsushima et al. (2023) propose a new step-based equation based on their observations in Japan for the calculation of  $\frac{I}{P}(L, T_a, v)$  as a function of  $L$ , wind speed and air temperature:

$$\frac{I}{P}(L) = \begin{cases} 0.73 - 0.59T_a - 0.0082L, & \text{if } T_a \geq 0^\circ C \\ 0.86 + 0.064T_a - 0.22v_{1/3}, & \text{if } -4^\circ C \leq T_a < 0^\circ C \\ 0.86 + 0.064 \cdot (-4) - 0.22v_{1/3}, & \text{if } T_a < -4^\circ C \end{cases} \quad (2.19)$$

where  $T_a$  is the air temperature (°C) 4 m above the ground and  $v_{1/3}$  is the wind speed (m s<sup>-1</sup>) at one-third of the canopy height.

### 2.5.1.4 Event Based Snow Interception Parameterisations

Additional snow interception parameterisations are available in the literature that approximate the increase in canopy load over a snowfall accumulation period. However, since these parameterisations were developed over events with varying time intervals, they cannot directly be included in hydrological models that run on regular time intervals. Still, the work by Satterlund & Haupt (1967), Moeser et al. (2015b) and Roth & Nolin (2019) has been important to develop theory on the influence of forest structure on snow interception.

Satterlund & Haupt (1967) derived a snow interception function by fitting a curve to observations of snow accumulation on a weighing tree over two storms in Idaho. The two storms had accumulated snowfall ranging from 0.5—7 kg m<sup>-2</sup> and temperatures close to 0°C with little wind. These observations showed an initial increase in the rate of intercepted snow, as snowflakes bridge gaps between needles. The initial low interception efficiency was followed by an increase and then flattening off of the interception rate as branches bent due to the weight of snow which Satterlund & Haupt (1967) represented by a numerical analytical sigmoidal function fitted to their observed data:

$$\Delta L = \frac{L_{max}}{1 + \exp^{-K(\bar{q}_{sf}\Delta t - P_{sf}^e)}} \quad (2.20)$$

where  $K$  is a constant expressing the rate of interception ( $\text{kg m}^{-2} \text{ s}^{-1}$ ), and  $P_{sf}^e$  ( $\text{kg m}^{-2}$ ), is the amount of snowfall accumulated at the point of most rapid loading.

The Moeser et al. (2015b) parameterisation is based on the Satterlund & Haupt (1967) sigmoidal growth curve, Equation 2.20, and a modification to the Hedstrom & Pomeroy (1998)  $L_{max}$  function (Figure 2.6, b). Their modifications to  $L_{max}$  were informed by detailed measurements of canopy structure derived from aerial LiDAR and manual snow depth measurements within a dense forest with a temperate climate in Switzerland. The observations in the Moeser et al. (2015b) study are based on snowfall events of 13 to 27 cm in a temperate climate with observed air temperatures ranging from -12 °C to -1.9 °C. Since Moeser et al. (2015b) did not observe snowfall storm events below 10 mm, their decision to use a sigmoidal function with initially low snow interception efficiency is based observations from Satterlund & Haupt (1967).

The Moeser et al. (2015b) formulation of  $L_{max}$  also differs from the previous studies in that it does not include a parameter for air temperature. To calculate  $L_{max}$ , Moeser et al. (2015b) use the natural logarithm of mean distance to canopy ( $\bar{D}_c$ , m), and total open area ( $A_o$ ,  $\text{m}^2$ ):

$$L_{max} = 2.167(\bar{D}_c) + -3.410(\bar{D}_c)^2 + \\ 55.761(C_c) + 181.858(C_c)^2 + -2.493(A_o) + 0.499(A_o)^2 + 20.819 \quad (2.21)$$

The use of additional forest structure metrics in the Moeser et al. (2015b) snow interception equation allows for application to highly heterogeneous forests, something that LAI-based algorithms such as Hedstrom & Pomeroy (1998) were not designed for. While lidar-derived canopy metrics like those in Equation 2.21 are beneficial for capturing plot-scale variability in subcanopy snow accumulation, these metrics are currently not feasible to obtain for larger scale hydrological models.

A more recent study by Roth & Nolin (2019) presents another event-based snow interception algorithm based on point-scale measurements of snow depth between paired open and forested sites. The Roth & Nolin (2019) study was conducted over 6 years at stations located in Oregon with air temperatures ranging from -14 to 6 °C. The wind speed observed over their study period is not provided. They make use of a new forest structure metric, median gap length  $G_z$  which can be derived by aerial LiDAR observations. Like Andreadis et al. (2009), the Roth & Nolin (2019) formulation includes air temperature but rather than using a step function they use a continuous representation. This new algorithm is derived using a power law relationship,

based on an empirical relationship with event size, temperature, and forest structure, which deviates from the exponential function used in Hedstrom & Pomeroy (1998) or Moeser et al. (2015b). The Roth & Nolin (2019) algorithm does not include a maximum canopy snow capacity, such as used in Hedstrom & Pomeroy (1998) and Moeser et al. (2015b), but rather calculates the change in canopy snow load,  $\Delta L$  ( $\text{kg m}^{-2}$ ) as:

$$\Delta L = \overline{q_{sf}} \Delta t^{0.04 \cdot T_{air} - 0.75 \cdot G_z + 1.56} \quad (2.22)$$

where  $\overline{q_{sf}}$  is the average event snowfall rate ( $\text{kg m}^{-2}$ ),  $T_a$  is the within canopy air temperature ( $^{\circ}\text{C}$ ), and  $G_z$  is the median gap length versus change in height (dimensionless).

## 2.5.2 Canopy Snow Ablation Parameterisations

Current canopy snow ablation parameterisations are based on measurements collected in Saskatchewan (Hedstrom & Pomeroy, 1998), British Columbia (Floyd, 2012; Schmidt & Gluns, 1991), Oregon (Storck et al., 2002), Colorado (Sexstone et al., 2018), Japan (Katsushima et al., 2023; Yamazaki et al., 1996), and Russia (Gelfan et al., 2004). The following section will discuss the various processes that ablate snow intercepted in the canopy.

### 2.5.2.1 Sublimation

To estimate canopy snow sublimation, Pomeroy et al. (1998b) builds on earlier laboratory experiments by Thorpe & Mason (1966), applied to blowing snow by Schmidt (1972) and modified for forested environments by Schmidt & Gluns (1991), Pomeroy & Schmidt (1993), and Pomeroy et al. (1998b). Since snow intercepted in the canopy is not as well exposed to the atmosphere as a single ice sphere, Pomeroy & Schmidt (1993) derived an exposure coefficient to reduce the rate of sublimation allowing the calculation to be scaled from particle to the canopy scale. The sublimation rate for snow in the canopy,  $q_{sub}^{veg}(L)$  ( $\text{kg m}^{-2} \text{ s}^{-1}$ ) can be calculated as:

$$q_{sub}^{veg}(L) = \kappa_{sub}^{sphere} C_e L \quad (2.23)$$

where  $C_e$  is a dimensionless exposure coefficient. Methods to estimate  $C_e$  are described in Pomeroy et al. (1998b).

The sublimation rate coefficient for single ice spheres,  $\kappa_{sub}^{sphere}$  ( $\text{s}^{-1}$ ), is represented as a function of the mass  $m$  (kg) of the ice sphere:

$$\kappa_{sub}^{sphere} = \frac{dm}{m dt} = \frac{\frac{2\pi r}{m} (\frac{\rho_{wa}}{\rho_s} - 1) - KJ}{\lambda_{sub} J + \frac{1}{D\rho_s Sh}} \quad (2.24)$$

with a radius  $r$  (m) where  $\rho_{wa}$  ( $\text{kg m}^{-3}$ ), is the water vapour density of the remote environment,  $\rho_s$  ( $\text{kg m}^{-3}$ ) is the saturation water vapour density at temperature  $T_a$  (K) for the particle surface,  $D$  is the diffusivity of water vapour in still air ( $\text{m}^2 \text{s}^{-1}$ ),  $Sh$  is the Sherwood number indexing the turbulent transfer of water vapour (-), and  $K$  is the net shortwave radiation flux ( $\text{W m}^{-2}$ ) to the particle found as:

$$K = \pi r^2 (1 - \alpha) S \downarrow \quad (2.25)$$

where  $\alpha$  (dimensionless) is the particle shortwave albedo and  $S \downarrow$  ( $\text{W m}^{-2}$ ) is the incoming shortwave radiation.

$J$  is found as:

$$J = \frac{1}{\lambda_T T_a Nu} \left[ \frac{\lambda_{sub} M}{RT_a} - 1 \right] \quad (2.26)$$

where  $R$  is the universal gas constant ( $8313 \text{ J kmole}^{-1} \text{ K}^{-1}$ ),  $M$  ( $\text{kg kmole}^{-1}$ ) is the molecular weight of water,  $\lambda_T$  is the thermal conductivity of the atmosphere ( $\text{W m}^{-1} \text{ K}^{-1}$ ), and  $Nu$  is the Nusselt number (-). Values of acceptable constants and coefficients for the above equations are given in Pomeroy & Gray (1995).

### 2.5.2.2 Unloading and Drip

Hedstrom & Pomeroy (1998) did not find any association between canopy snow unloading and meteorological factors such as wind speed and air temperature in the cold dense canopy of the Saskatchewan boreal forest. As a result, the rate of canopy snow unloading,  $q_{unld}(L)$ , attributed to snow metamorphism and wind gusts is represented in Hedstrom & Pomeroy (1998) as a function of time and  $L$ :

$$q_{unld}(L) = \kappa_{unld} L \quad (2.27)$$

where  $\kappa_{unld}$  ( $\text{s}^{-1}$ ), is a time constant.

Integrating Equation 2.27 provides an analytical solution for  $L^{t+\Delta t}$ , the canopy snow load following unloading over a discrete time interval,  $\Delta t$  ( $\text{s}^{-1}$ ):

$$L^{t+\Delta t} = L^t \exp^{-\kappa_{unld} \Delta t} \quad (2.28)$$

The steps to derive to Equation 2.28 from Equation 2.27 are shown in Section 2.9.

Later modifications to the Hedstrom & Pomeroy (1998) algorithm were provided in Gelfan et al. (2004) who found that all snow was unloaded from the canopy as liquid meltwater (drip) within 6 hours when ice-bulb temperatures remained above freezing for 3 hours with observed wind speed greater than  $0.5 \text{ m s}^{-1}$ . Using this concept, Ellis et al. (2010) built on additional observations by Floyd (2012) to modify the value of  $\kappa_{unld}$  based on ice-bulb temperature thresholds to unload canopy snow as either wet clumps ( $q_{unld}$ ) or meltwater drip ( $q_{drip}$ ). When the ice-bulb temperature exceeds the snow threshold, snow is unloaded as  $q_{unld}$ ; if it exceeds the drip threshold, all canopy snow is unloaded as  $q_{drip}$  within 6 hours. The threshold values from Floyd (2012) were found to be  $2^\circ\text{C}$  and  $4^\circ\text{C}$  for wet snow and drip unloading respectively.

Storck et al. (2002) found unloading to occur in maritime environments when air temperature rose above  $0^\circ\text{C}$ . The amount of solid snow unloading from the canopy was found to be linearly proportional to the amount of meltwater drip from canopy snow. For their field experiment in Oregon, Storck et al. (2002) provide a ratio of mass release to meltwater drip found during a two-week snowfall event. During this unloading event they measured  $33 \text{ kg m}^{-2}$  to have reached the ground as snow and  $84 \text{ kg m}^{-2}$  as meltwater drip resulting in a mass release to meltwater drip ratio of 0.4. Storck et al. (2002) suggested wind speed may influence canopy snow unloading; however, this was not observed due to the low wind speeds observed during their study. Using the observations from Storck et al. (2002), Andreadis et al. (2009) created a parameterisation to calculate unloading proportional to the rate of meltwater drip leaving the canopy  $q_{drip}(L)$ .

$$q_{unld}(L) = \begin{cases} 0, & \text{if } L \leq L_{res} \\ X_u q_{drip}, & \text{if } L > L_{res} \end{cases} \quad (2.29)$$

where  $L_{res}$  ( $\text{kg m}^{-2}$ ) is the residual intercepted snow that can only be melted or sublimated (taken as  $5 \text{ kg m}^{-2}$  based on observations from Storck et al. (2002)),  $X_u$  (-) is the ratio of mass release to meltwater drip (taken as 0.4 from Storck et al., 2002). In Andreadis et al. (2009),  $q_{drip}(L)$  is calculated by solving an energy balance equation to produce meltwater drip if sufficient energy is available.

Roesch et al. (2001) proposed a third approach to address unloading and drip, where the mass release of canopy snow is proportional to a temperature function,  $f(T)$  ( $\text{s}^{-1}$ ) and a wind-induced unloading function,  $f(u)$  ( $\text{s}^{-1}$ ):

$$q_{unld}(L) = L \cdot [f(T) + f(u)] \quad (2.30)$$

The theory behind the Roesch et al. (2001) parameterisation is based on the Yamazaki et al. (1996) study who found an exponential decrease of interception efficiency with time, temperature and wind speed, with a

response time of 0.5 day when temperature is below 0°C and 1–5 h with a temperature above 0°C. The Roesch et al. (2001) parameterisation was also informed by the Miller (1962) study that observed a decline in snow interception with wind speed greater than 2 m s<sup>-1</sup>. Roesch et al. (2001) show that boreal forest observations by Betts & Ball (1997), who noted a weak relationship (no R<sup>2</sup> given) between low wind speeds (< 3 m s<sup>-1</sup>) and occurrence of high above-canopy albedos, also supported their theory, though no such association was observed in the same environment by Pomeroy & Dion (1996) who carefully cleaned their upward facing radiometers after snowstorms. The outcome of this wind speed denominator is that 50% of intercepted snow is unloaded within 6 hours for a wind speed of 5 m s<sup>-1</sup>. The Roesch et al. (2001) temperature induced unloading function,  $f(T)$  (s<sup>-1</sup>), is:

$$f(T) = \begin{cases} 0, & \text{if } T_c < T_m \\ \frac{T_c - T_m}{C_1}, & \text{if } T_c \geq T_m \end{cases} \quad (2.31)$$

$T_c$  is the air temperature of the canopy (K),  $T_m$  is a user defined threshold temperature (270.15 K is suggested by Roesch et al., 2001) and  $C_1$  is a constant of 1.87 x 10<sup>5</sup> (K s<sup>-1</sup>). The result of Equation 2.31 is that once  $T_c$  reaches  $T_m$  canopy snow is unloaded at a rate proportional to  $T_c$ . The Roesch et al. (2001) wind induced unloading function,  $f(v)$  (s<sup>-1</sup>), is:

$$f(u) = \begin{cases} 0, & \text{if } u_{top} < u_m \\ \frac{u_{top}}{C_2}, & \text{if } u_{top} \geq u_m \end{cases} \quad (2.32)$$

where  $u_{top}$  (m s<sup>-1</sup>) is the wind speed at a height above ground corresponding to the mean canopy height,  $u_m$  is a threshold wind speed (m s<sup>-1</sup>) and  $C_2$  is a constant of 1.56 x 10<sup>5</sup> m.

Another approach to estimate  $f(u)$  is provided by Bartlett & Verseghy (2015):

$$f(u) = 0.38u_{top} - 0.13 \quad (2.33)$$

where  $u_{top}$  is the wind speed at the canopy top (m s<sup>-1</sup>). Bartlett & Verseghy (2015) also experimented with calculating  $f(u)$  based on air temperature and solar radiation in addition to wind speed but found the addition of three meteorological variables did not provide consistent improvement across all three sites.

The observations by Katsushima et al. (2023) provide additional insights on canopy snow unloading from a warm and humid region. To isolate periods of unloading due to melt, Katsushima et al. (2023) filtered their weighed tree measurements to daytime periods with a canopy snow load > 5 kg m<sup>-2</sup>, a wind speed of < 1 m s<sup>-1</sup> and no precipitation. Using these periods of unloading due to melt, Katsushima et al. (2023)

found a statistically significant relationship between air temperature, solar radiation and the unloading rate coefficient due to snowmelt,  $f(T)$  for a range of temperatures from -3.7–3.5 °C. To isolate periods of unloading due to wind, weighed tree observations were obtained at night with a canopy snow load > 5 kg m<sup>-2</sup>, an air temperature < 0°C, and no precipitation. Katsushima et al. (2023) calculated unloading due to snowmelt,  $f(T)$  as:

$$f(T) = 0.039T_a + 0.097Q_{sw} + 0.0049L \quad (2.34)$$

and wind-induced unloading,  $f(u)$  as:

$$f(u) = 0.020u_{1/3}$$

where  $u_{1/3}$  is the wind speed at one-third the canopy height.

## 2.6 Discussion

### 2.6.1 Differences in Snow Interception Parameterisations

Various theories have been formulated to describe the mechanisms underlying the loading of snow into and ablation of snow from the canopy, offering insights for how to describe these processes in hydrological models. However, the decision of choosing an appropriate snow interception parameterisation remains uncertain across different climates and forests. For maritime climates, Storck et al. (2002) suggest the increase in cohesive forces amongst snow particles and adhesive forces between snow clumps to the branch leads to a higher canopy storage capacity during mild air temperatures (-2 to 0.2 °C) as shown in Figure 2.7. While Storck et al. (2002) presents the most comprehensive study to measure the individual processes in Equation 4.1, many of the snowfall events they observed transitioned between snow and rain which presented difficulties in isolating snow interception from canopy snow ablation processes and rainfall interception. The small snowfall events (2–5 kg m<sup>-2</sup>) observed by Satterlund & Haupt (1967) at temperatures close to 0 °C had very low interception efficiencies. However, it is unclear how much of an influence canopy snowmelt and unloading attributed to the warm temperatures contributed to the low interception efficiency observed by Satterlund & Haupt (1967). Pomeroy & Gray (1995), Hedstrom & Pomeroy (1998) and Schmidt & Gluns (1991) observed a slight decline in interception with above zero air temperatures as frozen branches thaw and bend, thereby reducing the effective canopy contact area and increasing the angle of repose of snow intercepted in the canopy (Figure 2.7). These observations were used to develop an equation for interception efficiency presented by Hedstrom & Pomeroy (1998). However, the duration (days to weeks) between snow surveys conducted by Hedstrom & Pomeroy (1998) likely contributed to increased ablation of canopy snow, potentially reducing

interception efficiency at higher canopy snow loads. For temperatures above 0°C, Katsushima et al. (2023) also found a decline in interception efficiency above 10 kg m<sup>-2</sup> which support the findings by Hedstrom & Pomeroy (1998), although these weighed tree measurements are also influenced by ablation and may explain the very low snow loads predicted by this parameterisation for warm events in Figure 2.7.

## 2.6.2 Forest Structure and Snow Interception

Two of the most commonly used snow interception parameterisations, Hedstrom & Pomeroy (1998) and Storck et al. (2002), both use LAI as a primary variable. However, methods for measuring LAI are highly variable and may (e.g., plant area index) or may not include both leaf and non-photosynthetic material, both of which can intercept snow. Additionally, research by López-Moreno & Latron (2007) and Staines & Pomeroy (2023) has shown variability in the zenith angle of the canopy hemisphere important for snow interception. These findings challenge the use of broadband LAI or nadir canopy cover metrics currently employed in snow interception models. Using novel lidar based snow accumulation and canopy metrics methods, Staines & Pomeroy (2023) investigated whether leaf contact area is influenced by canopy snow load. In a closed canopy, they found that the number of lidar beam contacts with the canopy increased with canopy snow load as a result of new snow covering small canopy gaps. However, in partially open canopy, a decrease in canopy contacts with increased snow load was observed due to branch bending. These two processes partially compensated for each other, with an overall increase in canopy contacts with snow load observed by at the plot scale (Staines & Pomeroy, 2023).

Snowflake trajectories are frequently non-vertical (e.g., Thériault et al., 2012), which can also significantly affect the fraction of leaf contact area per unit of ground (Herwitz & Slye, 1995; Staines & Pomeroy, 2023; Van Stan et al., 2011). Previous research on rainfall interception by Herwitz & Slye (1995) and Van Stan et al. (2011) have shown rainfall trajectory angle to have an important influence on leaf contact area, which dramatically altered observed throughfall rates at the forest plot scale. Moreover, Katsushima et al. (2023) found that air temperature and wind speed were insufficient to describe interception efficiency and hypothesize that hydrometeor diameter may be a key factor to consider. Estimates of the hydrometeor trajectory angle can be made primarily as a function of wind speed (Herwitz & Slye, 1995) if assumptions are made about the hydrometeor vertical velocity, which is less variability than wind speed. Using this theory, Hedstrom & Pomeroy (1998) provide a model, shown in Figure 2.8, of increasing C<sub>p</sub> with wind speed. However, insufficient observations from wind-driven snowfall have been made to test this theory or Equation 2.11. As a result, Equation 2.11 is typically not included in hydrological model application of snow interception parameterisations. An assessment of the Hedstrom & Pomeroy (1998) theory could be facilitated through new aerial lidar measurements of snow accumulation and forest structure metrics similar to those described in Staines & Pomeroy (2023).

### **2.6.3 In Search of a Canopy Snow Storage Capacity**

Recent work by Roth & Nolin (2019), Lundquist et al. (2021), and Lumbrazo et al. (2022) have observed higher canopy storage capacities than those observed by Storck et al. (2002) and Hedstrom & Pomeroy (1998). This suggests that the sensitivity of interception efficiency to the state of canopy snow load (Hedstrom & Pomeroy, 1998) or air temperature (Storck et al., 2002) may be less than previously thought. Measurement uncertainty of throughfall, which may have included some downward ablation of snow intercepted in the canopy and/or melt of subcanopy snow, may have contributed to an oversensitivity of the theory developed by Satterlund & Haupt (1967) and Hedstrom & Pomeroy (1998) to branch bending and bridging. As a result of these measurement uncertainties, parameterisations derived from empirical observations are unlikely to be truly isolated from other processes which may contribute to the underestimate of canopy storage capacities. For example, snow interception parameterisations that include some degree of ablation, could lead to potential double counting of ablative processes, such as unloading or drip, when interception parameterisations are combined with subsequent unloading and drip routines, unless these were calibrated to include any early ablation (e.g. Hedstrom & Pomeroy, 1998).

The deposition of water vapour as rime-ice in the forest canopy has also been shown to accumulate large amounts of snow and ice in the canopy (Berndt & Fowler, 1969; Lumbrazo et al., 2022), which are greater than the Hedstrom & Pomeroy's (1998) and Storck et al. (2002)'s canopy storage capacities and exhibit ablation rates much lower than existing models (Lumbrazo et al., 2022). For example, observations from Berndt & Fowler (1969) found 50 kg m<sup>-2</sup> of rime-ice accumulated on the canopy during precipitation free days over a winter season. Lehtonen et al. (2016) also note the potential for rime-ice accretion to contribute to forest damage due to heavy canopy loads causing stem breakage. Under projected future climate in eastern and northern Finland, Lehtonen et al. (2016) found that heavy snow loads from rime and wet snow were expected to increase due a more humid and warmer climate. Aside from the Lehtonen et al. (2016) study in Finland, rime-ice accumulation is not typically included in snow interception parameterisations and may contribute to an underestimation of snow loads in coastal-temperate climates under certain conditions.

### **2.6.4 Differences in Canopy Snow Ablation Parameterisations**

Parameterisations that ablate snow intercepted in the canopy are generally consistent regarding their relationships with different processes but vary in their rate and complexity. Recent work by Lundquist et al. (2021) demonstrated the importance of calculating melt of snow intercepted in the canopy to better represent canopy snow unloading. They also found that by using this method, while also omitting the canopy snow storage capacity in their snow loading parameterisation, they improved subcanopy snow accumulation estimates. However, aside from a few models, JULES (Best et al., 2011), CLASS (Verseghy, 2017) and SUMMA (Clark et al., 2020), meltwater drip of canopy snow is typically calculated using an empirical time-based, temperature and humidity approach (Ellis et al., 2010; Pomeroy et al., 2007). If a physically based canopy

snow melt routine is implemented, it is often simplified. For example, Best et al. (2011), Clark et al. (2020), Parviainen & Pomeroy (2000) and Verseghy (2017) assume the air temperature and surface temperature of the canopy are in equilibrium with that of the snow in the canopy (Equation 2.4). However, the energy balance of the snow and vegetative components are different due to differing heat capacities, albedo and energy transfer processes (Musselman & Pomeroy, 2017; Pomeroy et al., 2009). As a result, the surface temperature of the vegetative elements is nearly always greater than clumps of snow intercepted in the canopy (Musselman & Pomeroy, 2017; Pomeroy et al., 2009). This simplification likely results in an underestimation in the melt rate of snow intercepted in the canopy. An alternative to the bulk temperature approach used by Clark et al. (2015b), would be to solve for the energy balance of snow in the canopy separately from the canopy element energy balance. To better represent the vertical heterogeneity that exists within the forest canopy or snowpack, Clark et al. (2015b) suggest that partial differential equations (PDEs) can be used to discretize the canopy into multiple vertical layers. Separating the canopy into multiple discretized units which would be more exposed to the atmosphere, compared to a single snowpack layer used by many models, may also yield a better representation of the melt of snow intercepted in the canopy. However, the benefit of the additional model complexity in separating the snow and vegetative component energy balances has not yet been directly assessed. Limited research has been conducted on the density and water holding capacity of snow intercepted in the canopy and therefore the value of B is estimated from surface snowpack studies (Dingman, 2015; Gray & Landine, 1988). With more snowfall events falling at warmer temperatures because of climate change (Bush & Lemmen, 2019; Hu & Nolin, 2020), melt and drip process of canopy snow will become more apparent and will warrant better representation in models.

### 2.6.5 Contribution of Measurement Uncertainty on Canopy Snow Ablation Parameterisations

A comparison of snow process models by Rutter et al. (2009), noted that some of the model uncertainty in estimating subcanopy snow accumulation can be attributed to the misrepresentation of canopy snow ablative processes. Unloading parameterisations (Andreadis et al., 2009; Hedstrom & Pomeroy, 1998; Roesch et al., 2001) have been shown to have poor transferability when applied at new locations with the default calibration (Bartlett & Verseghy, 2015; Lumbrazo et al., 2022). While physically based models exist for the calculation of  $q_{drip}$ , the associated increase in  $q_{unld}$  due to the decline in cohesion and adhesion as snow melts is still empirically based in Storck et al. (2002) and Ellis et al. (2010) and has uncertain transferability to new environments. However, collecting measurements of  $q_{drip}$  separate from  $q_{unld}$  is challenging as in the case of the Storck et al. (2002) and Floyd (2012) methodology and thus methods to estimate  $q_{unld}$  are highly uncertain. The lowest performance in canopy snow unloading parameterisations assessed by Lumbrazo et al. (2022) was observed for locations characterized with sparse wind-exposed forest which led to wind-induced unloading, and warm and humid conditions which led to rime-ice formation. During the rime-ice events canopy snow was unloaded by the model but was observed to stay attached to the canopy due to

the adhesion of rime-ice to the canopy which is not easily removed by wind. Under more typical snowfall conditions, the poor transferability of existing parameterisations to new locations shown in Lumbrazo et al. (2022) may be attributed to the weak statistical relationships of some parameterisations and misrepresentation of canopy snow loading. For example, the relationships identified by both Betts & Ball (1997) and Bartlett & Verseghy (2015) were found to be relatively weak. The association of canopy snow interception and albedo measurements are complicated as fresh snowfall events typically cover the upward-facing radiometer causing biased readings. Neither Betts & Ball (1997) nor Bartlett & Verseghy (2015) discuss the frequency of cleaning snow-covered radiometers. Since the Roesch et al. (2001) and Bartlett & Verseghy (2015) parameterisations are used widely across hydrological models and land surface schemes (Clark et al., 2020; Verseghy, 2017; Wheater et al., 2022), they would benefit from additional testing using direct measurements of canopy snow unloading.

If canopy snow sublimation is included in the ablation parameterisation, the Pomeroy et al. (1998b) method is often used and has shown relatively good performance across differing landscapes and climates from maritime to continental in North America and Europe (Essery et al., 2003; Gelfan et al., 2004; Parviainen & Pomeroy, 2000). This method was first validated using weighed trees in Saskatchewan over 23 cold winter days, where the cumulative error in simulated sublimation rates were  $0.06 \text{ kg m}^{-2}$  (Pomeroy et al., 1998b). Additional validations were provided by Parviainen & Pomeroy (2000) in Saskatchewan using a combination of parameterisations from the Canadian Land Surface Scheme model (CLASS) in Verseghy et al. (1993) and from Pomeroy et al. (1998a). Parviainen & Pomeroy (2000) compared simulated sublimation rates to observations from eddy covariance which resulted in a mean bias of  $0.103 \text{ kg m}^{-2}$  over an eight-day period. The low bias reported was attributed to the diurnal fluctuation of over-estimation at night and under-estimation during the day which balanced out; maximum and minimum errors were not reported but can be observed to be much higher depending on the part of the day (Fig. 3, Parviainen & Pomeroy, 2000). More recent model testing of winter sublimation rates has been conducted in the north-central Rocky Mountains by Sexstone et al. (2018), who simulated cumulative snow sublimation above the forest canopy over four seasons and reported errors between  $15$  to  $57 \text{ kg m}^{-2} \text{ year}^{-1}$  (percent bias from -37% to 29%), or  $0.04$  to  $0.16 \text{ kg m}^{-2} \text{ day}^{-1}$ . Uncertainties in estimating sublimation rates are related to the difficulty in making direct observations (Sexstone et al., 2016), the influence of atmospheric stability and turbulence within canopies (LeMone et al., 2019), and the canopy snow-covered duration (Rutter et al., 2009).

## 2.6.6 The Applicability of Parameterisations in Diverse Forest Structures and Species

Theories of snow interception and ablation included in existing parameterisations were based on observations collected within dense forest canopies (Betts & Ball, 1997; Hedstrom & Pomeroy, 1998; Storck et al., 2002). Aside from Lumbrazo et al. (2022), the theory behind snow interception and ablation parameterisations has

not been tested for sparse or discontinuous forest canopies. Moreover, Gouttevin et al. (2015) and Musselman & Pomeroy (2017) have shown forest gaps allow for additional input of energy from solar irradiance, which creates variations in the canopy temperature which is important for melting or sublimating intercepted snow in the canopy. Furthermore, sparse forests exhibit higher wind speeds which has important implications for hydrometeor trajectory angles, wind induced unloading, and wind transport to surrounding sites (Dickerson-Lange et al., 2017; King et al., 2008). The added complexity of these processes within sparse forests lead to additional challenges when understanding snow interception and interception losses. While needleleaf canopies have been the main focus of this review and existing interception and ablation studies, process investigation in more diverse tree species remain a notable research gap. For example, Huerta et al. (2019) observed significant canopy snow loads in a deciduous forest canopy in the Andes Cordillera in the Southern Hemisphere. Coefficients from existing snow interception parameterisations, derived in needleleaf canopies, were not transferable to this location. Therefore, the theory included in existing snow interception and ablation parameterisations, derived in dense needleleaf forests, also need to be tested in discontinuous forest environments of differing tree species.

### 2.6.7 The Potential of Hybrid Parameterisations

While the existing parameterisations have shown good performance in some studies (Ellis et al., 2010; Essery et al., 2003; Krinner et al., 2018; Pomeroy et al., 2022; Rasouli et al., 2019a), combining parameterisations has been shown to provide increased transferability across diverse environments (Essery et al., 2003; Gelfan et al., 2004). For example, in Essery et al. (2003) and Gelfan et al. (2004), a step function was used to apply the Storck et al. (2002) snow interception parameterisation during warm events and the Hedstrom & Pomeroy (1998) parameterisation for cold events (Essery & Pomeroy (2004); Gelfan et al. (2004)). While this method of combining different parameterisations based on a step function of air temperature was successful in Essery et al. (2003) and Gelfan et al. (2004), this technique remains infrequently used in current hydrological models with a few exceptions (Ellis et al., 2010). There is also an opportunity to develop and assess other methods to combine different parameterisations to better model transitional climates.

## 2.7 Conclusions

Numerous conceptual models of snow interception and ablation have been developed, reflecting differences in the climate, canopy structure, and methodological approaches across previous studies. The choice of parameterisation can significantly influence simulated outcomes, underscoring the importance of informed model decision-making. However, acquiring the necessary knowledge from the literature to facilitate such decisions has proven challenging, with notable knowledge gaps persisting in process understanding. Previous difficulties in isolating snow interception processes in in-situ measurements may have resulted in parameterisations that are not isolated to a single process. Future work to isolate initial canopy snow interception

and ablation processes could help revise parameterisations to better represent the intended physical process. Previous attempts to model snow accumulation and ablation in transitional climates had success by combining parameterisations derived from diverse climates. However, using combined parameterisations remains underutilized in contemporary models, and has the potential to better model transitional climates. Recent advances in lidar-based methods to measure subcanopy snow accumulation and canopy metrics has enhanced the understanding of how leaf contact area is influenced by snowfall trajectory angle and canopy snow load. However, further work is required to integrate these novel results into snow interception parameterisations. Parameterisations that ablate snow intercepted in the canopy differ in the level of detail in canopy snowmelt models and number of processes included snow such as wind-induced unloading and resuspension, rime-ice accretion, and time-based unloading. Future research is necessary to establish the appropriate level of process inclusion in canopy snowmelt models, to better represent rates of canopy snow unloading and meltwater drip resulting from canopy snowmelt, and to evaluate whether the relationships used in existing ablation parameterisations can apply to other locations.

Additional field-based investigations of canopy snow interception and ablation processes are needed to address remaining research gaps, including whether existing theories of snow interception are applicable for measurements of initial snow interception before ablation, if non-vertical snowfall trajectories significantly impact throughfall, determining the fraction of melting canopy snow that is unloaded as mass clumps compared to meltwater, evaluating the importance of wind resuspension and transport of canopy snow, and testing parameterisations in varied forests and climates. Observations of initial snow interception and canopy snow ablation collected at high-temporal and fine-scale resolutions across diverse forests and climates will help isolate individual processes, improve assessments of theoretical applicability, and help address these research gaps. This approach will enhance the understanding of where existing parameterisations fail, what processes drive model uncertainty, and how parameterisations can be modified to better represent forest snow accumulation.

## 2.8 Acknowledgments

We wish to acknowledge financial support from the University of Saskatchewan, Natural Sciences and Engineering Research Council of Canada, Global Water Futures Programme, Alberta Innovates and the Canada Research Chairs Programme. We thank Martyn Clark for his advice in outlining the steps to derive analytical solutions from the ordinary difference equation representation of the parameterisations.

## 2.9 Appendix

### 2.9.1 Snow Interception Parameterization Derivations

The original formulation of the Hedstrom & Pomeroy (1998) snow interception parameterisation is:

$$\frac{I}{P}(L) = C_{lca} \frac{L_{max} - L_0 - \Delta L}{L_{max}} \quad (2.35)$$

where  $L_0$  ( $\text{kg m}^{-2}$ ), is the canopy snow load before snowfall is added to the canopy,  $\Delta L$  ( $\text{kg m}^{-2}$ ), is the change in canopy snow load due to snowfall. Equation 2.35 is written in this way in Hedstrom & Pomeroy (1998) since they had measurements of  $L_0$  at the beginning of the storm. However, this equation further simplified here since:

$$L = L_0 + \Delta L$$

and therefore:

$$\frac{I}{P}(L) = C_{lca} \frac{L_{max} - L}{L_{max}}$$

The derivation of the Hedstrom & Pomeroy (1998) analytical snow interception solution, Equation 2.12, from Equation 2.10 is provided by first combining Equation 3.2 and Equation 2.10:

$$\frac{dL}{q_{sf}dt} = C_{lca} \frac{L_{max} - L}{L_{max}} \quad (2.36)$$

$$\begin{aligned} \frac{1}{L_{max} - L} dL &= \frac{C_{lca}}{L_{max}} q_{sf} dt \\ \int_{L_0}^{L_1} \left[ \frac{1}{L_{max} - L} \right] dL &= \frac{C_{lca}}{L_{max}} \overline{q_{sf}} \int_{t_0}^{t_1} dt \\ -\ln \left( \frac{L_{max} - L_1}{L_{max} - L_0} \right) &= \frac{C_{lca}}{L_{max}} \overline{q_{sf}} \Delta t \\ \frac{L_{max} - L_1}{L_{max} - L_0} &= \exp \left( -\frac{C_{lca}}{L_{max}} \overline{q_{sf}} \Delta t \right) \\ 1 - \frac{L_{max} - L_1}{L_{max} - L_0} &= 1 - \exp \left( -\frac{C_{lca}}{L_{max}} \overline{q_{sf}} \Delta t \right) \\ (L_{max} - L_0) - (L_{max} - L_1) &= (L_{max} - L_0) \left( 1 - \exp \left( -\frac{C_{lca}}{L_{max}} \overline{q_{sf}} \Delta t \right) \right) \end{aligned}$$

$$\Delta L = (L_{max} - L_0) \left( 1 - \exp \left( -\frac{C_{lca}}{L_{max}} \overline{q_{sf}} \Delta t \right) \right) \quad (2.37)$$

here, it is assumed that  $\overline{q_{sf}}$  is the average snowfall rate over the discrete time interval  $\Delta t$ . Since  $\overline{q_{sf}}$ ,  $C_{lca}$  and  $L_{max}$  are temporally constant over the discrete time interval  $\Delta t$  they can be moved outside the integral. The analytical solution in Equation 2.12 is only possible because the snowfall and throughfall rate are treated in isolation from the other processes in Equation 4.1.

### 2.9.2 Snow Unloading Parameterization Derivations

If the change in canopy snow load due to unloading alone is:

$$\frac{dL}{dt} = -q_{unld}(L)$$

then:

Then the steps to get from Equation 2.27 to Equation 2.28 when  $L \geq 0$  are:

$$\begin{aligned} \frac{1}{L} dL &= -\kappa_{unld} \Delta t \\ \int_{L(t)}^{L(t+\Delta t)} \frac{1}{L} dL &= -\kappa_{unld} \int_t^{t+\Delta t} dt \\ \ln(L^{t+\Delta t}) - \ln(L^t) &= -\kappa_{unld} \Delta t \\ \ln\left(\frac{L^{t+\Delta t}}{L^t}\right) &= -\kappa_{unld} \Delta t \\ L^{t+\Delta t} &= L^t \exp^{-\kappa_{unld} \Delta t} \end{aligned} \tag{2.38}$$

note since  $\kappa_{unld}$  is temporally constant it can be moved outside the integral. The analytical solution in Equation 2.28 is only possible because unloading is treated in isolation from the other processes in Equation 4.1.

### 3 SNOW INTERCEPTION RELATIONSHIPS WITH METEOROLOGY AND CANOPY DENSITY

Manuscript status: The contents of this chapter have been compiled from a research article published in the journal *Hydrological Processes*.

Citation: Cebulski, A. C., & Pomeroy, J. W. (2025). Snow Interception Relationships With Meteorology and Canopy Density. *Hydrological Processes*, 39(4), e70135. <https://doi.org/10.1002/hyp.70135>

Role in thesis: This journal article addresses Research Question 2.

Author Contribution:

A. Cebulski: Initial idea, data collection, analysis, manuscript preparation J. Pomeroy: Idea refinement, analysis refinement, manuscript revision

#### 3.1 Abstract

Snow accumulation models differ in how snow interception and ablation processes are represented and thus their application to diverse climates and forest types is uncertain. Existing parameterisations of initial snow interception before unloading include inherently coupled canopy snow accumulation and ablation processes. This leads to difficulty in diagnosing processes and adding possible errors to simulations when incorporated as canopy interception routines in models that already account for canopy snow ablation. This study evaluates the theory underpinning parameterisations of initial snow interception using high-temporal resolution and fine-scale measurements of throughfall for events with minimal snow ablation and redistribution in both the canopy and on the ground. Relationships between these throughfall measurements, event meteorology, and a novel lidar-based canopy density measurement were assessed in two subalpine forest plots in the Canadian Rockies. Contrary to existing theories, no association of canopy snow load or air temperature with interception efficiency was observed. Instead, snow-leaf contact area emerged as the primary factor governing snow accumulation. A wind-driven snowfall event demonstrated that non-vertical hydrometeor trajectories can significantly increase snow-leaf contact area, thereby enhancing initial interception before ablation. Prediction of interception efficiency for this event was improved when adjusted for hydrometeor trajectory angle based on the wind speed at one-third of the canopy height. Snow-leaf contact area showed a

high sensitivity to wind speed, increasing by up to 95% with a  $1 \text{ m s}^{-1}$  wind speed. The study proposes a new parameterisation that calculates throughfall, independent of processes that ablate snow from the canopy, as a function of snowfall, canopy cover, wind speed, and hydrometeor fall velocity. This new parameterisation successfully estimated subcanopy snow accumulation for a snowfall event at two forest plots of differing canopy density and structure. By separating canopy snow ablation from snow interception processes, this new model offers potentially improved prediction of subcanopy snow accumulation when combined with canopy snow ablation parameterisations.

**Keywords:** snow interception, throughfall, ablation, forest, snowpack, lidar, process-based modelling

## 3.2 Introduction

Over half of North America's snow-covered zone is covered by forests (Kim et al., 2017), significantly impacting the accumulation and redistribution of snowpacks and subsequent snowmelt runoff. Essery et al. (2003) estimated that 25–45% of annual snowfall may be lost to the atmosphere due to sublimation of snow intercepted in forest canopies globally. Snow intercepted in the canopy can sublimate and melt at much higher rates than the subcanopy snowpack (Katsushima et al., 2023; Lundberg & Halldin, 1994; Pomeroy et al., 1998b), reducing the amount of snow available for runoff. Canopy density is one of the primary factors controlling the partitioning of snowfall into throughfall and interception (Hedstrom & Pomeroy, 1998; Staines & Pomeroy, 2023) and thus governs the quantity of snow subject to sublimation from the canopy. Canopy structure metrics such as distance to canopy edge and total gap area have also shown strong correlations to throughfall measurements at the event-based (Moeser et al., 2015a) and seasonal (Mazzotti et al., 2019) timescales. Despite these relationships, forest thinning efforts aimed at limiting sublimation losses to increase snowmelt runoff do not always lead to a corresponding increase in spring streamflow (Golding & Swanson, 1978; Harpold et al., 2020; Pomeroy et al., 2012; Troendle, 1983). This may be due to increased ablation rates when forest cover is reduced, desynchronization of snowmelt timing, and sub-surface hydrology interactions (Ellis et al., 2013; Musselman et al., 2015; Pomeroy et al., 1997; Safa et al., 2021; Varhola et al., 2010). Given the significant impact of forest cover on snowpacks, along with the limited or absent monitoring networks for subcanopy snow accumulation (Rittger et al., 2020; Vionnet et al., 2021), land management, ecological conservation, and water resource decisions depend on reliable models of snow redistribution.

Hedstrom & Pomeroy (1998), working in the cold continental boreal forest, proposed that initial snow interception efficiency was controlled by the maximum canopy load which itself was a function of leaf area index and fresh snow density. Andreadis et al. (2009), incorporating measurements from several studies (Kobayashi, 1987; Pfister & Schneebeli, 1999; Storck et al., 2002), emphasized the role of leaf area index and air temperature in controlling the maximum canopy snow load. Although these two parameterisations incorporate different processes and relationships with air temperature, the Hedstrom & Pomeroy (1998) initial

snow interception parameterisation has shown strong performance at sites across Canada, Russia, Switzerland, and Spain (Ellis et al., 2010; Gelfan et al., 2004; Pomeroy et al., 2022; Sanmiguel-Vallelado et al., 2022a), while the Andreadis et al. (2009) parameterisation has produced accurate results in coastal environments (Andreadis et al., 2009; Clark et al., 2015b). Subsequent research by Lundquist et al. (2021) and Lumbrago et al. (2022) has revealed overestimation of subcanopy snow accumulation when combining the Hedstrom & Pomeroy (1998) routine with ablation parameterisations from different studies (i.e., Roesch et al., 2001). The coupling of ablation processes within existing snow interception parameterisations (Andreadis et al., 2009; Hedstrom & Pomeroy, 1998) may contribute to overestimates of throughfall, canopy snow unloading, and canopy snowmelt when combined with other canopy snow ablation parameterisations (Cebulski & Pomeroy, 2025a). Additional observations that separate initial snow interception from ablation processes could help determine the applicability of the interception theories proposed by Hedstrom & Pomeroy (1998) and Andreadis et al. (2009). Hedstrom & Pomeroy's (1998) theory also suggests that moderate wind speeds, which can result in more horizontal hydrometeor trajectories, increasing snow-leaf contact area and interception efficiency at the plot scale. This association has also been shown in rainfall interception studies to decrease throughfall of rain (Herwitz & Slye, 1995; Van Stan et al., 2011). However, the relationship proposed by Hedstrom & Pomeroy (1998), is typically not included in snow accumulation models as empirical testing of this relationship is lacking.

The objective of this paper is to evaluate the theories underlying existing snow interception models using high spatial and temporal resolution measurements of subcanopy snow accumulation for events with minimal canopy snow ablation. These new observations are investigated to address the following research questions:

1. Are the existing theories regarding the relationships between meteorology and canopy density and initial snow interception supported by in-situ observations collected in the Canadian Rockies?
2. How is initial snow interception influenced by non-vertical hydrometeor trajectory angles over a wind-driven snowfall event?
3. To what extent can these findings inform the development of a new parameterisation for initial snow interception?

### 3.3 Theory

#### 3.3.1 Canopy snow mass balance

The change in canopy snow load over time,  $\frac{dL}{dt}$  ( $\text{mm s}^{-1}$ ), can be estimated from the mass balance:

$$\frac{dL}{dt} = [q_{sf} - q_{tf} + q_{ros}] - q_{unld} - q_{drip} - q_{wind}^{veg} - q_{sub}^{veg} \quad (3.1)$$

where  $q_{sf}$  is the snowfall rate ( $\text{mm s}^{-1}$ ),  $q_{tf}$  ( $\text{mm s}^{-1}$ ) is the throughfall rate ( $\text{mm s}^{-1}$ ),  $q_{ros}$  ( $\text{mm s}^{-1}$ ) is the rate of rainfall falling on snow intercepted in the canopy,  $q_{unld}$  is the canopy snow unloading rate ( $\text{mm s}^{-1}$ ),  $q_{drip}$  is the canopy snow drip rate due to canopy snowmelt ( $\text{mm s}^{-1}$ ),  $q_{wind}^{veg}$  is the wind transport rate in or out of the control volume ( $\text{mm s}^{-1}$ ), and  $q_{sub}^{veg}$  is the intercepted snow sublimation rate ( $\text{mm s}^{-1}$ ). Figure 1 in Cebulski & Pomeroy (2025a) presents a visual representation of this mass balance.

Interception efficiency,  $\frac{I}{P}$  (-), which is the fraction of snowfall intercepted over  $\Delta t$  before ablation, can be calculated as:

$$\frac{I}{P} = \frac{\Delta L}{\bar{q}_{sf}\Delta t} \quad (3.2)$$

During periods with low air temperatures and low wind speeds,  $q_{ros}$ ,  $q_{unld}$ ,  $q_{drip}$ ,  $q_{wind}^{veg}$ , and  $q_{sub}^{veg}$  can be assumed negligible and thus the right side of Equation 4.1 can be simplified and used as an approximation of  $\Delta L$  to calculate  $\frac{I}{P}$  as:

$$\frac{I}{P} = \frac{(q_{sf} - q_{tf})\Delta t}{q_{sf}\Delta t} \quad (3.3)$$

### 3.3.2 Hydrometeor trajectory angle

Herwitz & Slye (1995) calculate the trajectory angle of a hydrometeor,  $\theta_h$ , as the departure in degrees ( $^\circ$ ) from a vertical plane as:

$$\theta_h = \arctan \left( \frac{x_h(u_z)}{v_h(D_h)} \right) * \frac{180}{\pi} \quad (3.4)$$

where  $v_h(D_h)$  is the terminal fall velocity of the hydrometeor ( $\text{m s}^{-1}$ ), which is a function of the hydrometeor diameter,  $D_h$  and  $x_h(u_z)$  is the horizontal velocity of the hydrometeor ( $\text{m s}^{-1}$ ) which is a function of the within canopy wind speed,  $u_z$  at height above ground,  $z$ . In the absence of hydrometeor velocity observations,  $v_h(D_h)$  may be approximated from values in the literature (e.g.,  $0.8 \text{ m s}^{-1}$  in Isyumov, 1971) and  $x_h(u_z)$  can be approximated by the horizontal wind speed. This assumes the hydrometeors are following fluid points in the atmosphere.

### 3.3.3 Within-canopy wind flow

Cionco (1965) showed that,  $u_z$  may be approximated using the exponential formula:

$$u_z = u \cdot \exp \left[ a \cdot \left( \frac{z}{h_c} - 1 \right) \right] \quad (3.5)$$

where  $u$  is the horizontal wind speed at the top of the canopy ( $\text{m s}^{-1}$ ),  $a$  is an attenuation coefficient,  $z$  is the height above ground (m), and  $h_c$  is the average height of the canopy elements. Parviainen & Pomeroy (2000) provided a method to calculate  $a$  using observations from two boreal forest jack pine stands, which was applied in this study.

## 3.4 Data and methods

### 3.4.1 Study site

This study was conducted at Fortress Mountain Research Basin (FMRB), Alberta, Canada,  $-115^\circ$  W,  $51^\circ$  N, a continental headwater basin in the Canadian Rockies (Figure 4.3). Data from this study was collected between October 2021 and July 2023 within and surrounding two forest plots adjacent to the FMRB Powerline Station (PWL) and Forest Tower Station (FT) at  $\sim 2100$  m above sea level as shown in Figure 4.3. The average annual precipitation at PWL Station from 2013 to 2023 was 1045 mm, with the average peak annual snow water equivalent (SWE) reaching 465 mm, typically in late April. The PWL plot is adjacent to PWL station and the FT plot surrounds FT station and both include discontinuous stands of 70% subalpine fir (*Abies lasiocarpa*) and 30% Engelmann spruce (*Picea engelmannii*) (Langs et al., 2020). The canopy closures are 0.51 and 0.29 and the winter leaf area indices are 2.07 and 1.66 for PWL and FT respectively. The average height of the canopy within the PWL plot is 10.5 m and within the FT plot is 7.1 m. In August of 1936, most vegetation in FMRB burned during a large forest fire that affected most of the Kananaskis Valley (Fryer et al., 1988). Following the fire, the forest within the PWL and FT forest plots has naturally regenerated, though some trees have been removed for a powerline clearing and creation of a snow study plot.

### 3.4.2 Meteorological measurements

Measurements of air temperature and relative humidity (Vaisala model HMP155A), wind speed and direction (RM Young model 86000 2-D ultrasonic anemometer) were made 4.3 m above the ground at FT station (Figure 4.3). Wind speed measurements from a 3-cup anemometer (Met One model 014A), installed adjacent to the 2-D ultrasonic anemometer at 4.3 m, were used to fill data gaps in the 2-D ultrasonic anemometer records.

At PWL station, the snowfall rate was measured by an Alter-shielded OTT Pluvio weighing precipitation gauge 2.6 m above ground, corrected for undercatch following phase correction by Harder & Pomeroy (2013) using the catch efficiency equation of Smith (2007). The instrument accuracy of the OTT Pluvio specified in the instrument manual is  $\pm 0.1$  mm or 0.2% (whichever is larger). Wind speed for undercatch correction

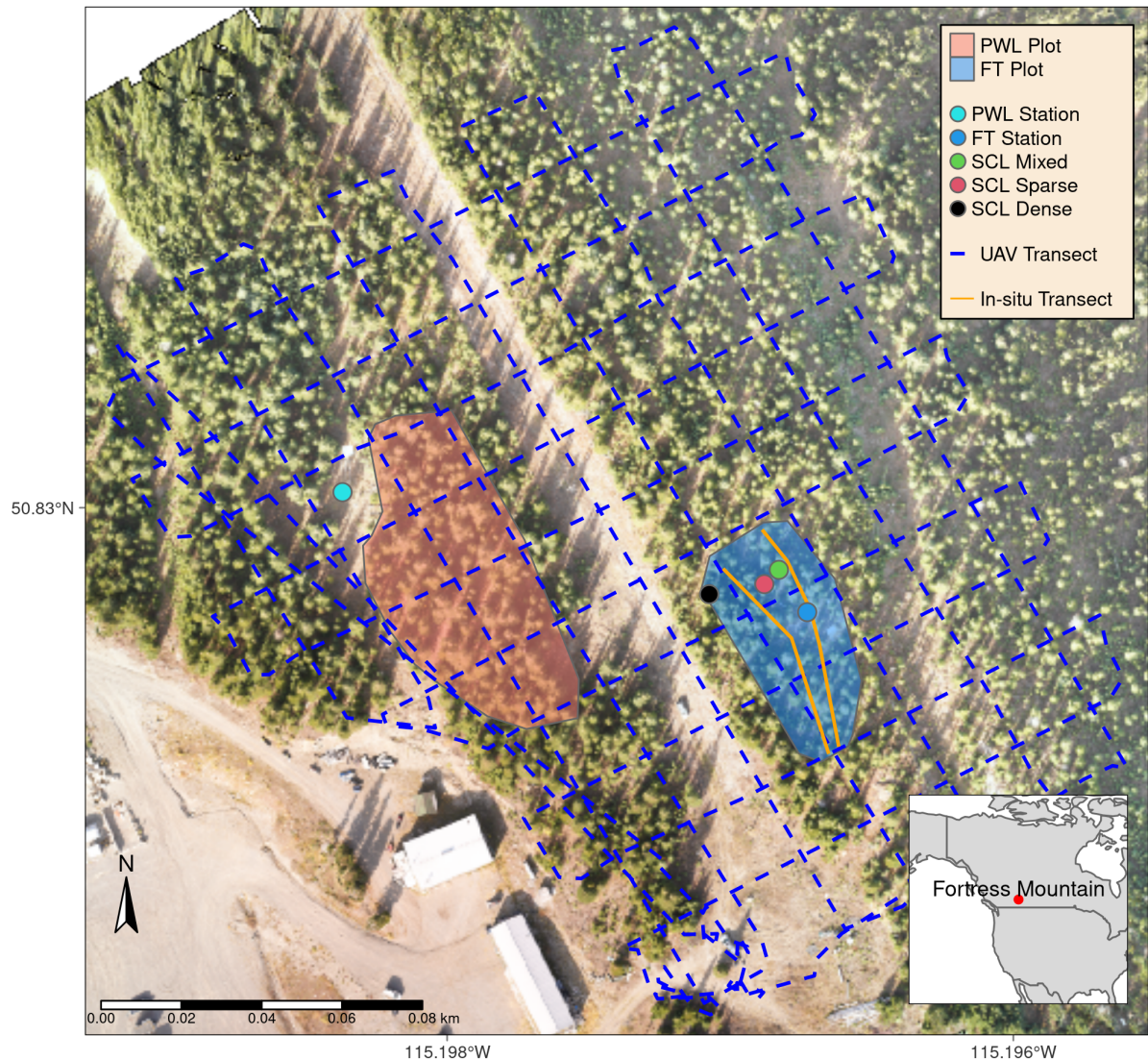


**Figure 3.1:** Map showing the location of forest plots, flux towers, subcanopy lysimeter instruments, and survey transects. The inset map on the lower right shows the regional location of Fortress Mountain Research basin.

was measured by a 3-cup anemometer (Met One model 014A) at a height of 2.6 m at PWL station. An optical disdrometer (OTT Parsivel2) provided measurements of hydrometeor particle size and vertical velocity. All measurements were recorded at 15-min intervals using Campbell Scientific dataloggers, except the Parsivel2 which was recorded at 1-minute intervals by an onsite computer.

### 3.4.3 Lysimeter measurements

Three subcanopy lysimeters were installed surrounding the FT Station (Figure 4.3) to provide measurements of throughfall for 26 distinct snowfall events, where canopy snow ablation rates were deemed negligible. The subcanopy lysimeter instrument design was adapted from MacDonald (2010) and consisted of a plastic horse-watering trough with an opening of 0.9 m<sup>2</sup> and depth of 20 cm suspended from a load cell (Intertechnology 9363-D3-75-20T1) attached to an aluminum pipe connected between two trees (Figure 3.2). The manufacturer-specified combined error of full-scale output for the load cells is +/- 0.02% with a temperature sensitivity of +/- 0.001%/5°C. The throughfall rate was calculated by dividing the weight of snow in the subcanopy lysimeter by the cross-sectional area of the opening and determining the rate of change at hourly intervals. Canopy snow load was estimated using Equation 4.1, incorporating cumulative throughfall measurements from the subcanopy lysimeters and cumulative snowfall measurements from the PWL gauge for each of the 26 events. Interception efficiency was calculated using Equation 3.3 and accumulated measurements of snowfall and throughfall at both hourly intervals and within bins of air temperature, wind speed, and initial canopy snow load measured from the weighed tree. The hourly interval measurements resulted in lower accumulations of snowfall and throughfall within each interval and thus had higher relative error compared to the binned measurements. To evaluate the association of hourly interception efficiency with air temperature, wind speed, and initial canopy snow load, linear models were fitted using ordinary least squares regression. The non-parametric Wilcoxon signed-rank test was also applied to compare the distribution of hourly interception efficiency measurements across differing groups of air temperature, wind speed, and initial canopy snow load. Timelapse imagery, mass change on a weighed tree lysimeter (Pomeroy & Schmidt, 1993), and in-situ observations were used to ensure unloading, melt, and wind redistribution of canopy snow was minimal over each interval. Additionally, the throughfall measurements were filtered to include observations that coincided with a snowfall rate  $> 0 \text{ mm hr}^{-1}$  and a snowfall rate that exceeded the subcanopy lysimeter measured throughfall rate. While these careful manual mitigation and automated filtering strategies substantially reduced the contribution of unloading in the subcanopy lysimeter throughfall measurements, a small contribution is still possible.

The subcanopy lysimeters were installed to limit preferential throughfall and unloading by choosing locations with relatively uniform distribution of canopy elements and away from large branches which could preferentially unload snow. The canopy surrounding the subcanopy lysimeters led to reduced wind speeds and reduced the potential for gauge undercatch by these instruments. Photographs of the three subcanopy

lysimeters and surrounding canopy are shown in Figure 3.2. Canopy density measurements, including leaf area index and canopy closure, are summarized in Table 3.1. A viewing angle from zenith to  $60^\circ$  was selected to describe the surrounding canopy, as a range in hydrometeor trajectory angles was expected to influence the measurements at these locations. The canopy density metrics were measured using hemispherical photography (Nikon Coolpix 4500 and EC-F8 hemispherical lens) for a snow free canopy and analyzed with the hemispheR R package Chianucci & Macek (2023).

The weighed tree lysimeter, a live subalpine fir (*Abies lasiocarpa*) tree suspended from a load cell (Artech S-Type 20210-100) measured the weight of canopy snow load (kg). This weight was scaled to an areal estimate of canopy snow load ( $L$ , mm) using measurements of areal throughfall (mm) from in-situ snow surveys and snowfall from the PWL Station snowfall gauge, following the method described in Pomeroy & Schmidt (1993). Three sets of in-situ snow survey locations were selected for scaling, each with a mean canopy closure corresponding to one of the subcanopy lysimeters. This resulted in three datasets of canopy snow load from the weighed tree, each reflecting the canopy density of a respective subcanopy lysimeter. Variations in the weighed tree mass were attributed to intercepted snowfall, canopy snow sublimation, unloading, and melt. Since the subcanopy lysimeter estimates of canopy snow load are not influenced by sublimation, they provided a measurement of interception efficiency with less uncertainty and thus were used for the interception efficiency analyses.

**Table 3.1:** Leaf area index (LAI) and canopy closure of the three subcanopy lysimeters located proximal to the FT Station.

Name	LAI (-)	Canopy Closure (-)
Sparse	1.56	0.64
Mixed	2.10	0.75
Closed	2.40	0.79

### 3.4.4 UAV-Lidar data collection and processing

The UAV (FreeFly Alta X) payload included a REIGL miniVUX-2 airborne laser scanner, an Applanix APX-20 inertial measurement unit (IMU) and global navigation satellite system (GNSS). The UAV was flown 90 m above the ground at a speed of  $3 \text{ m s}^{-1}$  following the path shown in Figure 4.3. The methods outlined by Harder et al. (2020) and Staines & Pomeroy (2023) were incorporated to reconcile survey lidar, IMU, and GNSS data. A systematic vertical bias of up to 6 cm between UAV-lidar flight lines was observed in the resulting point clouds on March 13<sup>th</sup> and 14<sup>th</sup>, 2024 and was attributed to IMU position drift. After strip alignment, the mean elevation bias in the point clouds compared to the GNSS data was 0.000 m and the RMS error declined from 0.055 m to 0.038 m on March 13<sup>th</sup> and from 0.033 m to 0.029 m on March 14<sup>th</sup>. The point cloud density ranged from  $\sim 1200$  returns  $\text{m}^2$  in sparse forest to  $\sim 2200$  returns  $\text{m}^2$  in open

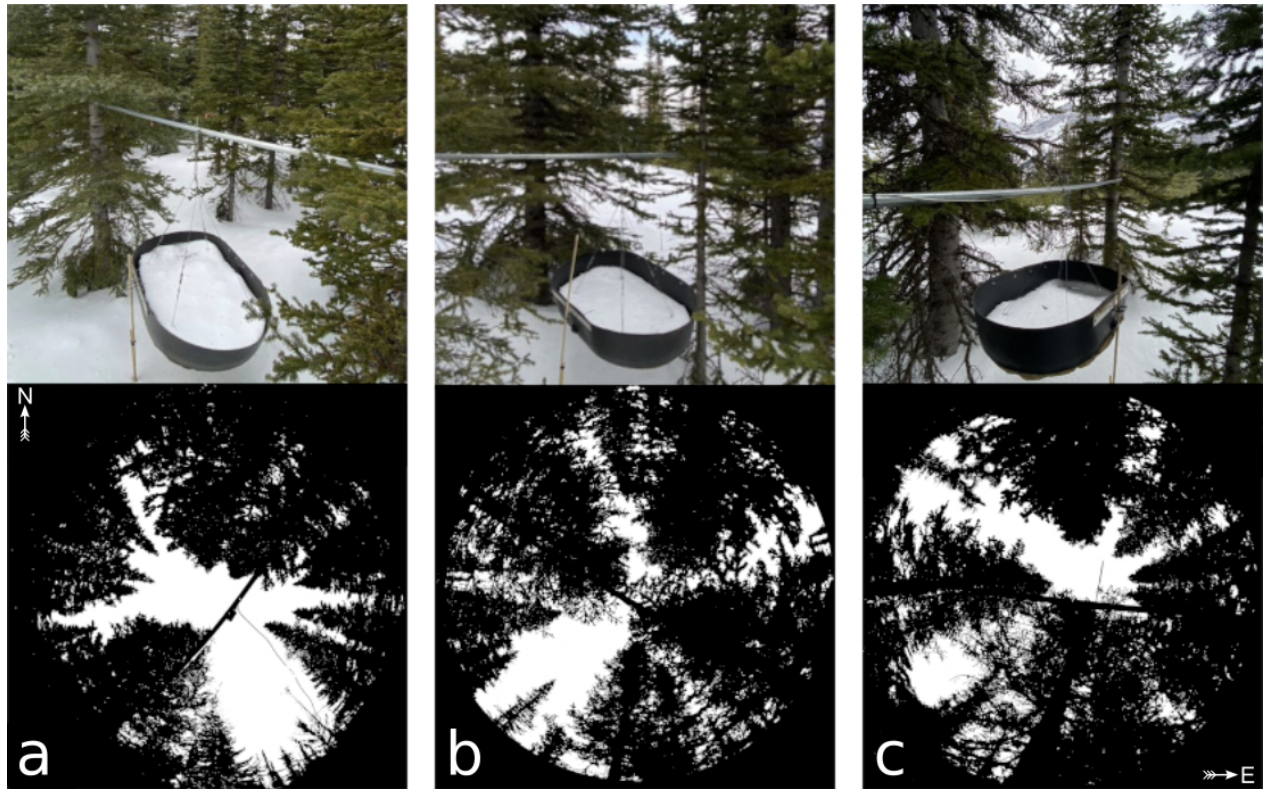


**Figure 3.2:** Images of the three subcanopy lysimeter instruments and surrounding canopy located in sparse (a), mixed (b), and dense (c) canopy. The top row presents a side view of each instrument and the bottom row shows hemispherical photographs. These hemispherical images are oriented with north at the top and have been mirrored to provide a view from above (e.g., east is on the right side of each image). See Table 3.1 for the corresponding canopy density measurement.

clearings. Quality control, ground classification, calculation of surface elevation change was conducted on the point cloud data and then converted to 0.05 m resolution rasters. Further quality control was conducted on the 0.05 m raster data to remove values that exceeded the .999th quantile and then resampled to 0.25 m grid cell resolution by taking the median. A detailed description of the UAV, payload, flight settings, and software packages used is provided in the Supporting Information.

### 3.4.5 Snow surveys

#### 3.4.5.1 In-situ snow depth and density

Event-based snow surveys provided measurements of subcanopy throughfall depth and density at 30 locations following the transects shown in Figure 4.3. These measurements were used to upscale the weighed tree from weight to weight per unit area, assess the accuracy of lidar derived snow depth measurements, and provide a fresh snow density for the calculation of SWE (mm) from the snow depth measurements. Minimal ablation and redistribution of both the surface snowpack and/or snow intercepted in the canopy was crucial to ensure the snow survey measurements were attributed to throughfall. Therefore, only snowfall events with minimal canopy snow ablation as determined through in-situ observations, analysis of timelapse imagery, and mass change on the weighed tree lysimeter were selected. A 1000 cm<sup>3</sup> Perla snow density wedge sampler (RIP Cutter, <https://snowmetrics.com/shop/rip-1-cutter-1000-cc/>) was used to measure the density of the fresh snow layer,  $\bar{\rho}_{tf}$  (kg m<sup>-3</sup>) from snow pits. Throughfall depth measurements,  $\Delta HS$  were converted to SWE using the following equation:

$$\Delta SWE_{tf} = \Delta HS \cdot \bar{\rho}_{tf} \quad (3.6)$$

If a pre-event crust layer was present, the depth of post event fresh snow accumulation above the crust layer was interpreted as throughfall over the event. In the absence of a defined crust layer, the difference in pre- and post-event snow depth to ground was interpreted as event throughfall. Interception efficiency, used in scaling the weighed tree, was calculated using Equation 3.3 and the  $\Delta SWE_{tf}$  and cumulative snowfall measurements.

#### 3.4.5.2 UAV-Lidar snow depth

Two uncrewed aerial vehicle (UAV) lidar surveys were conducted before and after a 24-hour snowfall event that occurred between March 13–14<sup>th</sup>, 2023 to facilitate the measurement of snow accumulation and canopy density within the FT and PWL forest plots. This period was selected based on two criteria: 1) it provided sufficient cumulative snowfall to result in a low relative error in UAV-lidar measured throughfall, and 2) minimal snow redistribution and ablation was observed, as confirmed by the subcanopy lysimeters, weighed tree, and timelapse imagery. The change in surface elevation between the two UAV-lidar point clouds was interpreted as the

increase in snow accumulation,  $\Delta HS$ , over the snowfall event.  $\Delta SWE_{tf}$  was calculated using Equation 3.6 together with in-situ measurements of  $\overline{\rho_{tf}}$ . The measurement error of the UAV-lidar derived  $\Delta HS$  was assessed using the in-situ snow depth observations which is shown in the Supporting Information. Spatially distributed measurements of  $\frac{I}{P}$ , were then determined using Equation 3.3 with  $\Delta SWE_{tf}$  as the throughfall component and cumulative snowfall to the PWL clearing.

### 3.4.6 UAV-Lidar canopy metrics

The canopy of the study site was characterized from two UAV-lidar point clouds (March 13<sup>th</sup> and March 14<sup>th</sup>) using the voxel ray sampling (VoxRS) methodology for lidar data analysis, as developed by Staines & Pomeroy (2023). This method was chosen for its ability to provide canopy metrics that are less sensitive to the inherent non-uniform nature of lidar sampling data resulting from beam occlusion in vegetation. Using this method radiation transmittance,  $\tau$  (-), was measured across the hemisphere at a 1° step, e.g., azimuth angles (0°, 1°, ..., 359°) and zenith angles (0°, 1°, ..., 90°) for each 0.25 m grid cell within the FT and PWL forest plots. The fraction of snow-leaf contact area per unit area of ground proposed by Hedstrom & Pomeroy (1998), and hereafter called leaf contact area ( $C_p$ ), was then calculated as:

$$C_p(C_c, \theta_h) = 1 - \tau \quad (3.7)$$

$$C_p(C_c, \theta_h) = \begin{cases} 1 - \tau, & \text{if } \theta_h > 0^\circ \\ 1 - \tau \approx C_c, & \theta_h = 0^\circ \end{cases} \quad (3.8)$$

where  $C_p$  is a function of the canopy cover ( $C_c$ ) and hydrometeor trajectory angle ( $\theta_h$ ).  $C_c$  is the fraction of canopy area to total ground area when viewed from above, which differs from canopy closure, an angular-derived metric usually measured from the ground perspective.

To determine how  $C_p$  was associated with interception efficiency at different azimuth and zenith angles over the March 13–14<sup>th</sup> snowfall event, the entire hemisphere at each grid location was considered. The relationship between interception efficiency and  $C_p$  was found to be linear and thus the Pearson Correlation Coefficient was used. The Pearson Correlation Coefficient was computed between a single raster of interception efficiency and each of the 32,760 rasters of  $C_p$  measured on March 13<sup>th</sup>, representing locations across the hemisphere (azimuth [0°, 1°, ..., 359°], zenith angle [0°, 1°, ..., 90°]) at 0.25 m grid cells spanning the FT and PWL forest plots.

The pair of azimuth and zenith angles corresponding to the  $C_p$  that had the highest correlation with interception efficiency was selected for further analysis. This involved aggregating the interception efficiency and selected  $C_p$  rasters from a 0.25 m resolution to 5 m, followed by fitting an ordinary least squares regression

between these two variables. The regression was constrained to pass through the origin based on the theoretical principle that the dependent variable must equal zero when the independent variable is zero. To appropriately account for this constraint, the  $R^2$  values were adjusted according to Equation 10 presented in Kozak & Kozak (1995). The relationship between leaf contact area and simulated trajectory angle was investigated by fitting non-linear models using a non-linear least squares regression. All statistical analyses were performed using the R ‘stats’ package (R Core Team, 2024).

## 3.5 Results

### 3.5.1 The influence of meteorology on snow interception

Measurements of canopy snow load derived from the subcanopy lysimeters and weighed tree increased linearly with cumulative event snowfall for 26 snowfall events, without evidence of reaching a maximum (Figure 3.3). Over these events, air temperature ranged from -24.5°C to 1°C, wind speeds at 4.3 m height ranged from calm to 4.6 m s<sup>-1</sup> (Table 3.2), and wind direction was predominately from the southwest during snowfall (Figure 3.4). Missing canopy snow load measurements, as shown in Figure 3.3 for certain events, were caused by wiring damage from animals and heavy snow loads. Some of the variability in interception rates within and between different events may be attributed to small amounts of canopy snow unloading and melt, which could not be fully accounted for through the manual and automated filtering mitigation strategies in both the subcanopy lysimeter and weighed tree measurements.

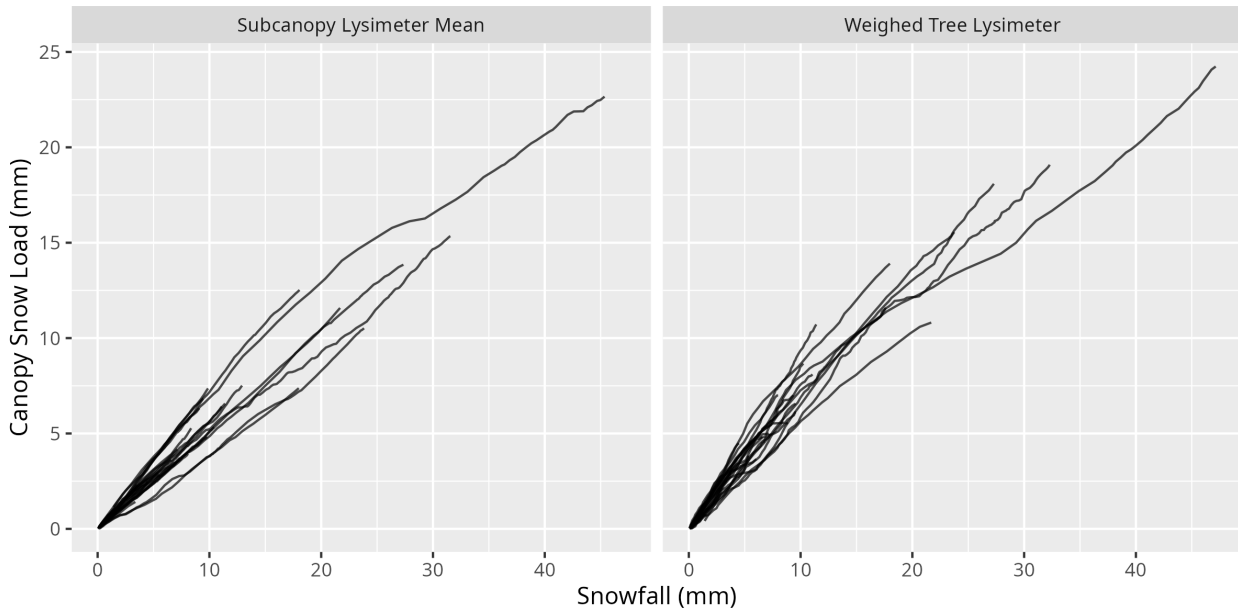


**Figure 3.3:** Plot showing the cumulative event snowfall versus canopy snow load calculated using the mean of the three subcanopy lysimeters (left) and weighed tree lysimeter (right) for each of the 26 snowfall events. Both datasets represent canopy snow load for a canopy closure of 0.73 corresponding to the mean of the three subcanopy lysimeter canopies.

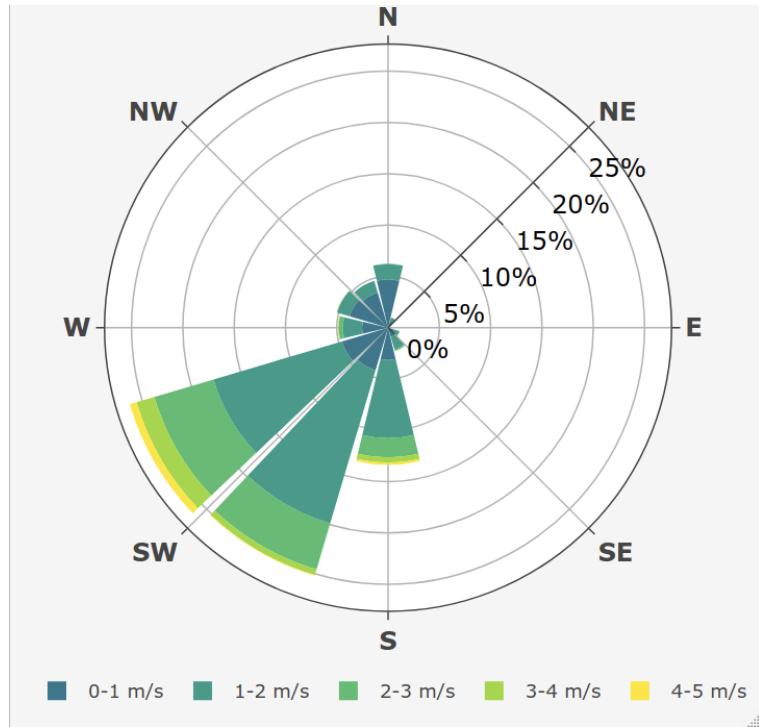


**Figure 3.4:** Wind rose showing the frequency of wind speed and direction over the 26 snowfall periods for the ultrasonic anemometer 4.3 m above ground at FT station.

Linear regression analysis revealed no relationship between hourly interception efficiency (from the subcanopy lysimeters) and air temperature, wind speed or canopy snow load, either due to non-significant relationships ( $p < 0.05$ ) and/or weak predictive power ( $R^2 < 0.05$ ) (Table 3.3). The Wilcoxon test indicated that the difference in hourly interception efficiencies for air temperatures above and below  $-5^\circ\text{C}$  was not significant ( $p > 0.05$ , Table 3.4). Additionally, the interception efficiency across differing bins of air temperature did not show any systematic pattern (Figure 3.5). Although Figure 3.5 indicates potentially higher interception efficiency in sparse and mixed canopies at air temperatures below  $-10^\circ\text{C}$ , these measurements have substantial uncertainty due to heightened instrument error associated with the small accumulations of snowfall and throughfall within these temperature ranges.

When examining wind speed effects, hourly interception efficiencies were found to be significantly higher ( $p < 0.05$ , Table 3.4) during periods when wind speeds exceeded  $1 \text{ m s}^{-1}$  compared to calmer conditions in the sparse and closed canopies using the Wilcoxon test. The binned data also show an increase in interception efficiency with increasing wind speed for these two canopy types (Figure 3.5). In contrast, the mixed canopy, which had a canopy opening towards the prevailing wind direction (Figure 3.2), exhibited no significant difference ( $p > 0.05$ , Table 3.4). Binned measurements of interception efficiencies corresponding to wind speed bins above  $2 \text{ m s}^{-1}$  (Figure 3.5) contained considerable uncertainty resulting from lower snowfall and throughfall accumulation, reducing confidence in these particular findings across all three canopy environments.

**Table 3.2:** Meteorology of the 26 snowfall events. Air temperature and wind speed were measured at FT station. Interception efficiency is estimated from cumulative snowfall measured at PWL station and the average cumulative throughfall of all three subcanopy lysimeters located within the FT forest plot.

Start Date	Air Temperature (°C)			Wind Speed (m/s)			Interception Efficiency (-)			Snowfall (mm)
	Min	Mean	Max	Min	Mean	Max	Min	Mean	Max	
2021-12-23	-6.2	-5.3	-4.6	0.6	3.1	4.6	0.1	0.5	0.9	21.7
2022-01-02	-15.9	-10.8	-5.8	0.2	1.8	4.2	0.0	0.5	1.0	31.6
2022-01-17	-14.8	-7.8	-0.8	0.2	1.1	1.8	0.0	0.6	1.0	12.9
2022-01-31	-24.5	-12.1	-6.4	0.1	1.0	1.7	0.2	0.7	1.0	9.1
2022-02-14	-9.9	-9.0	-8.5	0.4	0.8	1.2	0.2	0.5	0.8	1.7
2022-02-19	-4.7	-3.2	-2.5	1.3	2.3	3.6	0.3	0.6	0.9	11.1
2022-03-01	-8.3	-5.4	-1.0	0.1	1.0	3.1	0.4	0.8	1.0	9.9
2022-03-07	-12.5	-8.6	-4.4	0.3	0.8	1.7	0.3	0.7	1.0	9.5
2022-03-14	-2.7	-2.1	-0.8	1.0	1.6	2.9	0.2	0.6	0.9	8.4
2022-03-19	-3.1	-2.8	-2.5	0.0	0.7	1.3	0.3	0.5	0.6	6.6
2022-03-23	-7.9	-5.3	-0.9	0.8	1.2	1.8	0.4	0.6	0.9	1.6
2022-04-04	-3.5	-2.9	-2.1	0.6	1.0	1.9	0.0	0.4	0.6	3.4
2022-04-18	-5.2	-4.0	-2.7	0.4	1.1	1.9	0.1	0.5	0.9	7.4
2022-04-22	-2.8	-1.8	-0.5	0.4	0.8	1.2	0.1	0.5	1.0	9.8
2022-05-09	-4.9	-4.3	-3.2	0.1	0.4	0.9	0.2	0.5	0.9	8.1
2022-05-19	-4.9	-2.1	0.3	0.1	0.4	0.9	0.2	0.6	0.9	7.1
2022-06-13	-1.1	-0.3	0.6	0.1	0.1	0.4	0.0	0.5	0.9	45.4
2022-12-27	-3.0	-2.7	-1.9	0.6	1.1	1.8	0.2	0.5	0.9	4.5
2023-01-27	-11.5	-7.3	-4.5	0.6	0.9	1.2	0.1	0.5	0.8	10.4
2023-02-19	-14.3	-9.5	-6.3	0.2	0.8	1.4	0.2	0.7	1.0	18.1
2023-02-26	-9.2	-8.4	-6.6	0.2	1.0	2.1	0.3	0.5	1.0	5.4
2023-03-13	-8.9	-3.6	-0.1	0.3	1.3	2.2	0.0	0.5	1.0	27.4
2023-03-24	-7.9	-5.7	-3.5	0.1	0.5	1.2	0.1	0.4	0.7	23.8
2023-04-01	-8.9	-7.7	-4.7	0.1	0.6	1.4	0.4	0.6	0.8	11.4
2023-04-10	-1.1	-0.5	0.3	0.1	0.3	1.0	0.2	0.4	0.6	18.0
2023-05-08	0.2	0.6	1.0	0.4	0.6	0.8	0.6	0.6	0.7	3.5

Significantly higher hourly interception efficiencies ( $p < 0.05$ , Table 3.4) were found for initial canopy snow loads below 10 mm compared to heavier snow loads across all three canopy types using the Wilcoxon test. Additionally, the sparse and mixed canopies exhibited significantly lower interception efficiencies ( $p < 0.05$ ) for snow loads below 5 mm compared to those between 5–10 mm. The closed canopy displayed a similar initial increase for the binned data visible in Figure 3.5, but this was not statistically significant for the hourly data ( $p > 0.05$ , Table 3.4). For the sparse and closed canopies, a slight increase in binned interception efficiency was observed as snow load increased up to 10 mm, followed by a decline when snow loads exceeded 10 mm (Figure 3.5). For snow loads exceeding 15 mm, interception efficiency decreased in the sparse and closed canopies, while the mixed canopy showed an increase; however, these measurements carried high uncertainties due to lower accumulated snowfall and throughfall in these higher snow load bins. The differences between the relationships observed in the hourly-interval and binned interception efficiency measurements can be attributed to two factors: greater instrument uncertainty in the hourly measurements and the potential for the dependent and independent variables to be non-stationary over the hourly interval.

**Table 3.3:** Statistics corresponding to the ordinary least squares linear regression test between hourly interval measurements of independent variables: mean air temperature, mean wind speed, and initial canopy snow load and the dependent variable mean interception efficiency. The test was run separately for three levels of canopy coverage ( $C_c$ ) corresponding to each subcanopy lysimeter (SCL).

Dependent Variable	SCL Name	$C_c$	Adjusted $R^2$	$p$ -value	$n$
Air Temperature (°C)	closed	0.79	0.002	0.239	191
Air Temperature (°C)	mixed	0.75	0.024	0.005	298
Air Temperature (°C)	sparse	0.64	0.003	0.208	190
Initial Canopy Snow Load (mm)	closed	0.79	0.029	0.011	188
Initial Canopy Snow Load (mm)	mixed	0.75	0.010	0.049	294
Initial Canopy Snow Load (mm)	sparse	0.64	0.031	0.009	187
Wind Speed (m/s)	closed	0.79	0.025	0.017	191
Wind Speed (m/s)	mixed	0.75	0.034	0.001	298
Wind Speed (m/s)	sparse	0.64	0.046	0.002	190

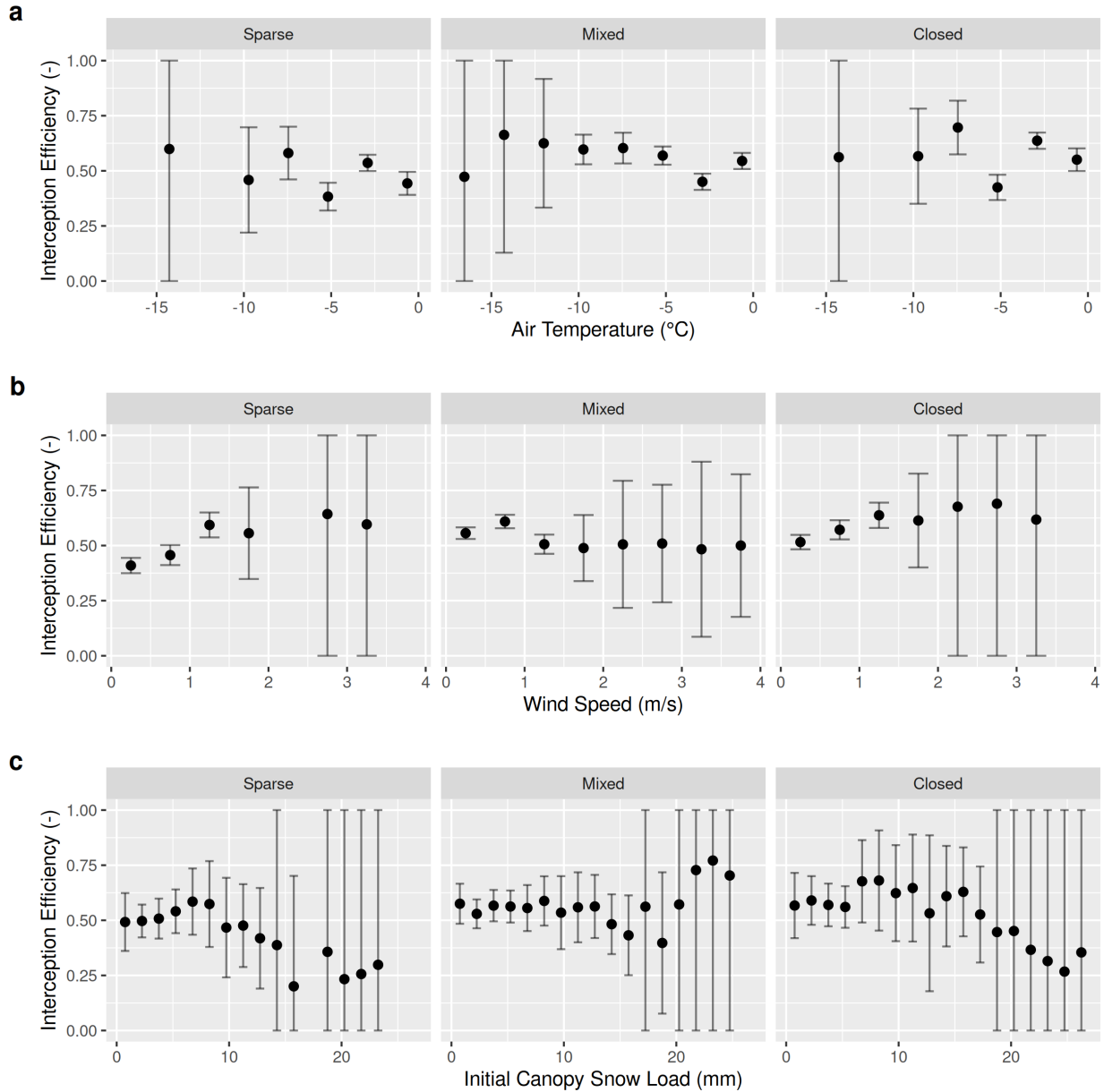


**Figure 3.5:** Scatter plots showing the interception efficiency calculated from accumulated snowfall (Pluvio) and throughfall (subcanopy lysimeter) measurements for bins of air temperature, wind speed, and initial canopy snow load (the snow load observed by the weighed tree at the beginning of the timestep) over the 26 snowfall events. The error bars represent the estimated combined instrument error of the snowfall gauge and subcanopy lysimeters.

**Table 3.4:** Results of the Wilcoxon signed-rank tests comparing the distributions of hourly interception efficiency (IP) measured by the subcanopy lysimeters for differing groups of air temperatures (Ta), wind speeds (u), and initial canopy snow loads (L). The table reports the canopy corresponding to the subcanopy lysimeter (Canopy), null hypothesis ( $H_0$ ),  $p$ -value, and sample size ( $n$ ) and median IP for the ‘low’ group (e.g.,  $Ta < -5^{\circ}\text{C}$ ) and ‘high’ group (e.g.,  $Ta = -5^{\circ}\text{C}$ ).

Canopy	Null Hypothesis ( $H_0$ )	$p$ -value	$n$ (low / high)	median I/P	
				(low / high)	Reject $H_0$
closed	Median IP ( $Ta < -5^{\circ}\text{C}$ )	0.282	76 / 115	0.56 / 0.62	no
	Median IP ( $Ta = -5^{\circ}\text{C}$ )				
mixed	Median IP ( $Ta < -5^{\circ}\text{C}$ )	0.990	165 / 133	0.57 / 0.53	no
	Median IP ( $Ta = -5^{\circ}\text{C}$ )				
sparse	Median IP ( $Ta < -5^{\circ}\text{C}$ )	0.864	72 / 118	0.54 / 0.5	no
	Median IP ( $Ta = -5^{\circ}\text{C}$ )				
closed	Median IP ( $u < 1 \text{ m/s}$ )	0.004	116 / 75	0.53 / 0.65	yes
	Median IP ( $u = 1 \text{ m/s}$ )				
mixed	Median IP ( $u < 1 \text{ m/s}$ )	1.000	165 / 133	0.6 / 0.5	no
	Median IP ( $u = 1 \text{ m/s}$ )				
sparse	Median IP ( $u < 1 \text{ m/s}$ )	< 0.001	110 / 80	0.43 / 0.59	yes
	Median IP ( $u = 1 \text{ m/s}$ )				
closed	Median IP ( $L < 10 \text{ mm}$ )	0.048	129 / 59	0.62 / 0.57	yes
	Median IP ( $L = 10 \text{ mm}$ )				
mixed	Median IP ( $L < 10 \text{ mm}$ )	< 0.001	218 / 76	0.57 / 0.49	yes
	Median IP ( $L = 10 \text{ mm}$ )				
sparse	Median IP ( $L < 10 \text{ mm}$ )	< 0.001	157 / 30	0.53 / 0.34	yes
	Median IP ( $L = 10 \text{ mm}$ )				
closed	Median IP ( $L < 5 \text{ mm}$ )	0.333	62 / 67	0.62 / 0.62	no
	Median IP ( $5 \text{ mm} < L < 10 \text{ mm}$ )				
mixed	Median IP ( $L < 5 \text{ mm}$ )	0.019	117 / 101	0.57 / 0.61	yes
	Median IP ( $5 \text{ mm} < L < 10 \text{ mm}$ )				
sparse	Median IP ( $L < 5 \text{ mm}$ )	0.043	90 / 67	0.49 / 0.6	yes
	Median IP ( $5 \text{ mm} < L < 10 \text{ mm}$ )				

### 3.5.2 The influence of canopy density on snow interception

UAV-lidar measurements of throughfall and canopy density provide insights on how the forest canopy influenced subcanopy snow accumulation during a wind-driven snowfall event between March 13–14<sup>th</sup>. This event totaled 28.7 mm of snowfall at PWL station and was characterized by a transition from low rates of snowfall and air temperatures near 0°C to higher rates of snowfall by late afternoon on March 13<sup>th</sup> coinciding with air temperatures around -2.5 °C. An average wind speed of 1.3 m s<sup>-1</sup> and direction of 188° was observed 4.3 m above the ground at FT Station. The mean observed hydrometeor terminal fall velocity observed over the event was 0.9 m s<sup>-1</sup>.

The throughfall depth measured by UAV-lidar aligned with the in-situ manual measurements resulting in a mean bias of -0.001 m and RMSE of 0.024 m. More details on the accuracy of UAV-lidar snow depth measurements are provided in the Supporting Information section. Figure 3.6 shows the spatial distribution of throughfall and interception efficiency at the PWL and FT forest plots. Reduced throughfall and greater interception efficiency was observed on the north (lee) side of individual trees, which may be due to non-vertical hydrometeor trajectories caused by the steady southerly winds observed over this event. Transparent areas within the forest plots in Figure 3.6 represent grid cells that did not have any lidar ground returns (e.g., under dense canopy proximal to tree trunks) or were masked due to disturbance (e.g., walking paths in clearings). Visual observations on March 13<sup>th</sup> and 14<sup>th</sup> confirmed non-vertical hydrometeor trajectories and increased canopy snow loads were observed on the windward side of individual trees. This effect is more apparent in the PWL forest plot than the FT forest plot and may be attributed to the taller trees and higher canopy cover of the PWL forest plot compared to the FT forest plot (Figure 3.6).

The VoxRS measurements of  $C_p$  on March 13<sup>th</sup> were selected for analysis and represent the canopy of both forest plots without snow. Little difference in  $C_p$  was observed between the March 13<sup>th</sup> and March 14<sup>th</sup> measurements. A strong linear correlation between  $C_p$  measured on March 13<sup>th</sup> and interception efficiency was observed towards the southern portion of the hemisphere, aligning with the average event wind direction (Figure 3.7). For the PWL forest plot, the upper 97.5<sup>th</sup> percentile of the Pearson Correlation Coefficient ( $\rho_p$ ) values were found between azimuth angles of 167°–217°. Similarly, for the FT forest plot, the upper 97.5<sup>th</sup> percentile of  $\rho_p$  was found between azimuth angles of 171°–223°. The zenith angle found to have the highest correlation over this azimuth range was 22° ( $\rho_p = 0.7$ ) and 21° ( $\rho_p = 0.83$ ) for PWL and FT respectively. The high correlation coefficients found for non-vertical zenith angles for both PWL and FT are hypothesized to result from non-vertical hydrometeor trajectories.

The spatial distribution of  $C_p$  measurements, selected based on the vector corresponding to the azimuth and zenith angles observed to have the highest correlation with interception efficiency in Figure 3.7, is shown in Figure 3.8. These  $C_p$  measurements generally align with the spatial distribution of interception efficiency and throughfall (Figure 3.6).

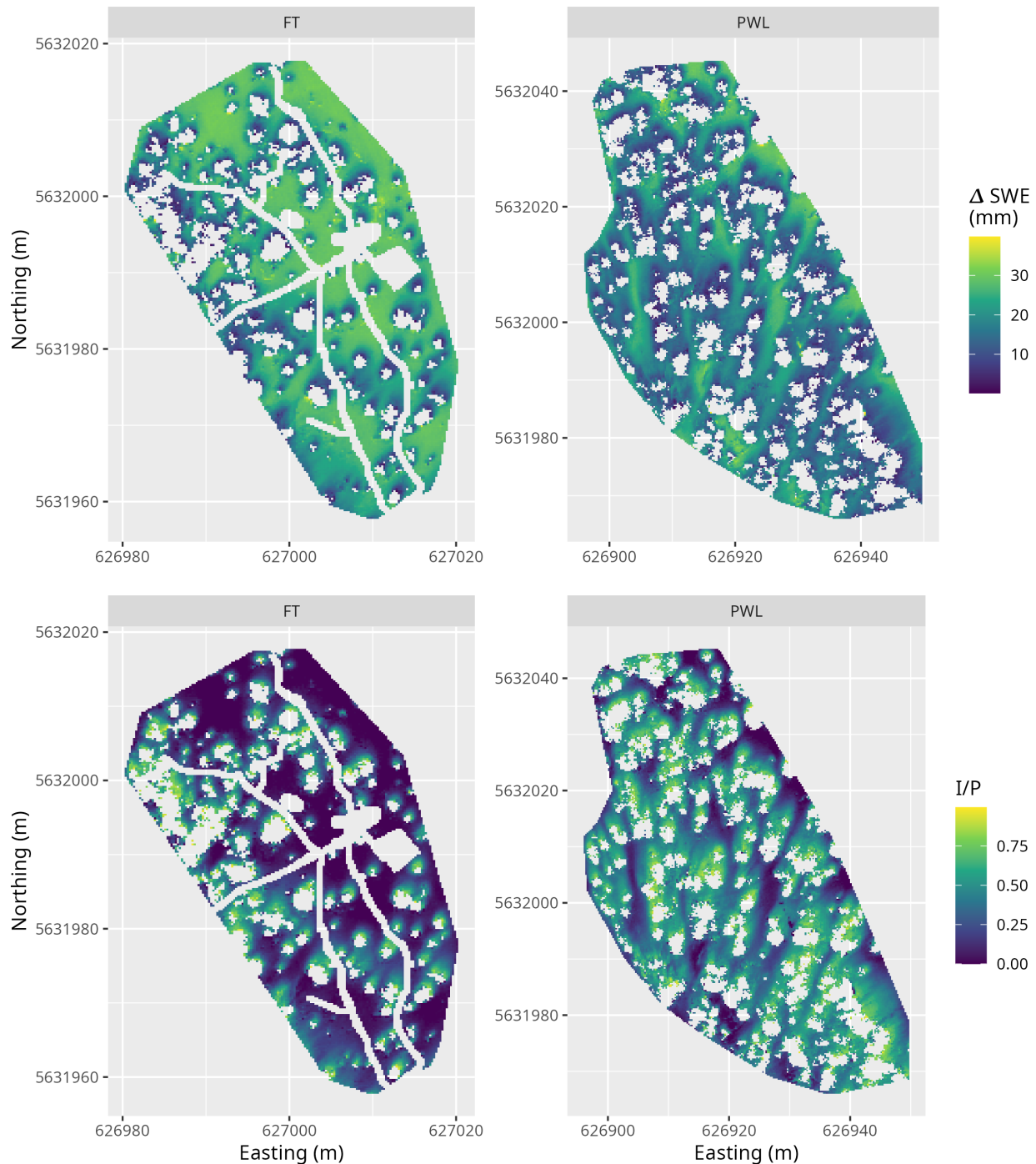


**Figure 3.6:** UAV-lidar measurements of the change in snow water equivalent, SWE (mm) and interception efficiency, I/P (-), over the March 13–14<sup>th</sup> 24-hour snowfall event for the FT and PWL forest plots at a 0.25 m resolution. See the location of the two forest plots in Figure 4.3.

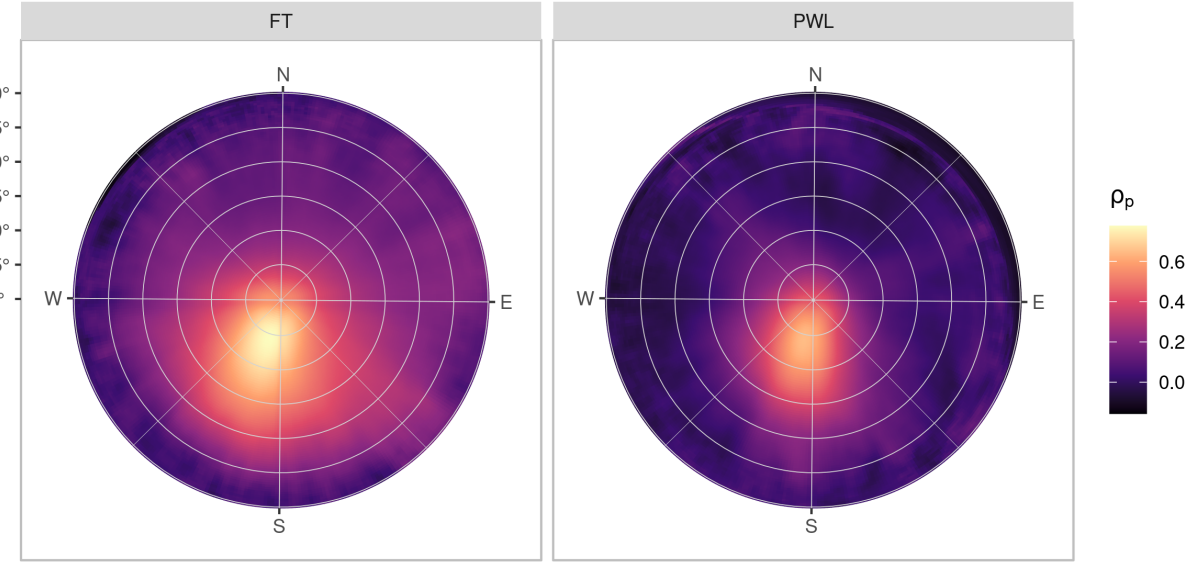


**Figure 3.7:** The Pearson Correlation Coefficient between rasters (0.25 m resolution) of interception efficiency and leaf contact area (measured on March 13th) for each grid cell across the study site for each azimuth angles ( $0^\circ, 1^\circ, \dots, 359^\circ$ ) and zenith angles ( $0^\circ, 1^\circ, \dots, 90^\circ$ ) for the FT (left) and PWL (right) forest plots.

The correlation between interception efficiency (Figure 3.6) and  $C_p$  (Figure 3.8), resampled to a 5 m grid resolution, was higher compared to the association with leaf contact angle measured at a zenith angle of  $0^\circ$  (Figure 3.9). The stronger association for the vector-based calculation is hypothesized to stem from a more accurate representation of the snowfall contact area and suggests that adjusted  $C_p$  is a useful predictor of interception efficiency before ablation. An ordinary least squares linear regression forced through the origin was fit to the observed data points using the following equation:

$$\frac{I}{P} = C_p(C_c, \theta_h) \cdot \alpha \quad (3.9)$$

where  $\alpha$  is an efficiency constant which determines the fraction of snowflakes that contact the  $C_p$  elements and are stored in the canopy (i.e., intercepted) before canopy snow unloading or ablation processes begin.

For the vector-based model, the relationship between interception efficiency and  $C_p$  resulted in  $R^2$  values of 0.45 and 0.8 for PWL and FT respectively. Model error statistics show the vector-based model provided a better prediction of interception efficiency compared to the nadir canopy coverage measurements (Table 3.5). The increase in interception efficiency with  $C_p$  follows a reduced slope compared to the nadir models with  $\alpha$  values of 0.72 and 0.69 for the PWL and FT vector-based models respectively. The reduced slope for the vector-based models may be due to snowflakes that weaved through and/or bounced off branch elements in addition to UAV-lidar throughfall measurement uncertainty which may have been slightly affected by

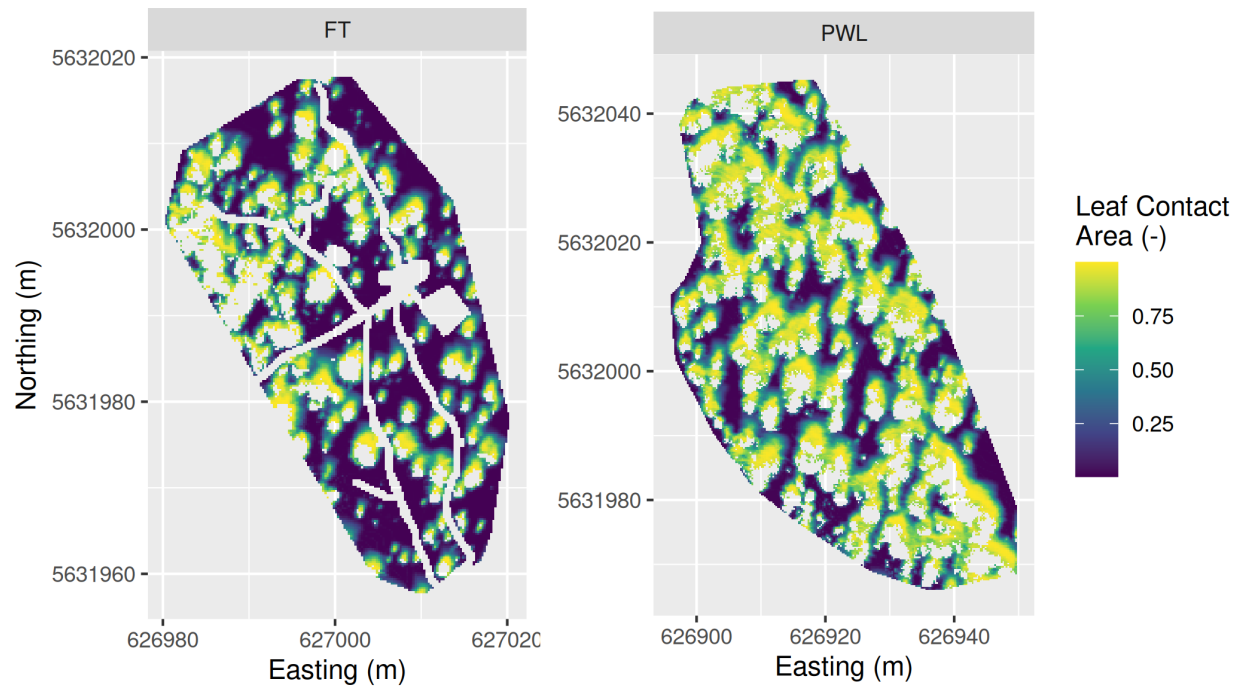


**Figure 3.8:** UAV-lidar VoxRS measurements of leaf contact area measured on March 13<sup>th</sup> for the PWL and FT forest plots for zenith angles (PWL = 22°, FT = 21°) and azimuth angles (PWL = 167°, 178°, ... 217°; FT = 171°, 172°, ... 223°).

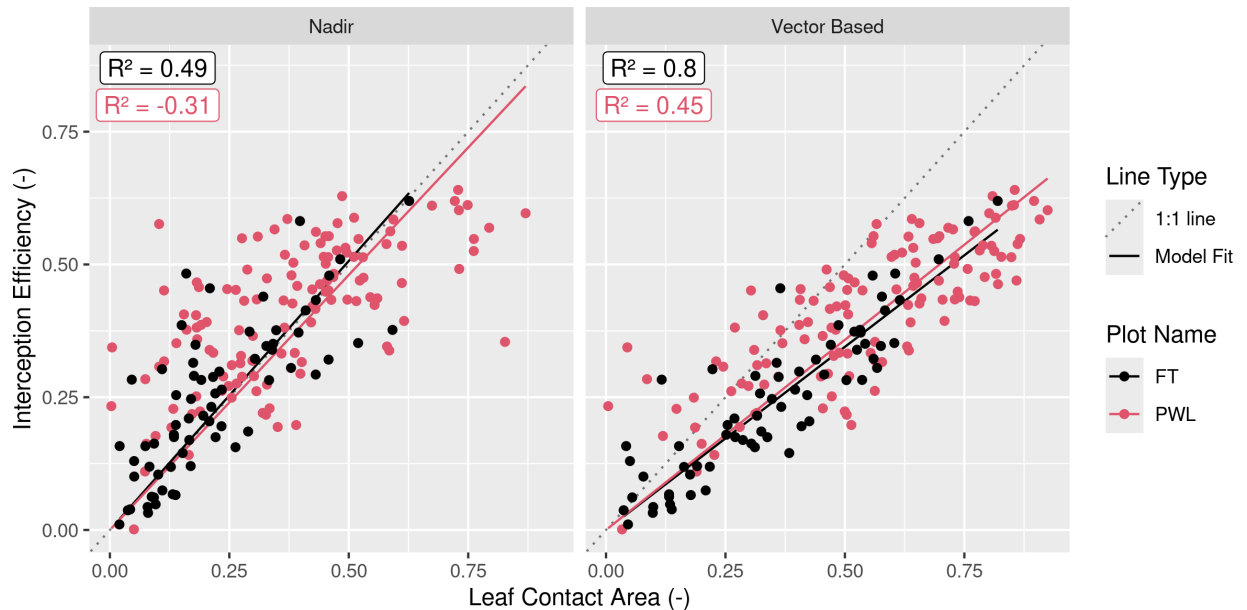


**Figure 3.9:** Scatter plots showing the relationship between leaf contact area and interception efficiency rasters resampled to a 5 m grid cell resolution. The left plot (nadir) shows canopy coverage and the right plot (Vector Based) shows the leaf contact area averaged over rasters with zenith angles (PWL = 22°, FT = 21°) and azimuth angles (PWL = 167°, 178°, ... 217°; FT = 171°, 172°, ... 223°). The solid lines (Model fit) show an ordinary least squares linear regression forced through the origin and fitted to the PWL (red) and FT (black) data and the light grey dotted line shows a 1:1 line. The  $R^2$  values for the four different models are shown in the upper left of each panel calculated following the methods outlined in Kozak & Kozak (1995).

unloading and redistribution. These processes would have reduced the fraction of snowfall that was stored in the canopy. Some of the scatter observed in the nadir model shown in Figure 3.9 may be explained by grid cells within canopy gaps which observed a greater interception efficiency compared to the corresponding canopy cover. Conversely, grid cells where interception efficiency is less than the canopy cover, may be affected by non-vertical trajectory hydrometeors making their way underneath the canopy as observed by the reduced interception efficiency on the windward edges of individual trees in Figure 3.6.

**Table 3.5:** Summary of error statistics for the linear regression models relating leaf contact area to interception efficiency, presented in Figure 3.9. The Mean bias is the difference in the model and observed values, MAE is the mean of the absolute error, RMS Error is the root mean squared error,  $R^2$  is the coefficient of determination adjusted using Equation 10 in Kozak & Kozak (1995).

Plot Name	Canopy Calculation	Model Slope			RMS	
		(-)	Mean Bias (-)	MAE (-)	Error (-)	$R^2$
FT	Nadir	1.01	0.024	0.072	0.101	0.49
FT	Vector Based	0.69	0.003	0.047	0.063	0.80
PWL	Nadir	0.96	0.049	0.115	0.148	-0.31
PWL	Vector Based	0.72	0.020	0.079	0.096	0.45

### 3.5.3 The combined influence of trajectory angle and canopy density on snow interception

VoxRS measurements of  $C_p$  prior to snowfall on March 13<sup>th</sup>, increased substantially with simulated hydrometeor trajectory angle and corresponding simulated wind speed (Figure 3.10). The standard deviation in VoxRS measured  $C_p$ , illustrated by the shaded area in Figure 3.10, exhibits the broad range in values for individual grid cells across each forest plot. Despite this large scatter, a systematic increase in the mean  $C_p$  across both forest plots results from a rise in the number of canopy elements for more horizontal angles, when averaged across each forest plot, over all azimuth angles (see top left panel Figure 3.10). This results in a large rise in  $C_p$  over relatively common wind speeds. For example, with a wind speed of 1 m s<sup>-1</sup> and estimated trajectory angle of 48°,  $C_p$  would increase by 0.31 and 0.28 for the PWL and FT forest plots respectively (Figure 3.10). The increase in  $C_p$  from nadir measured canopy coverage with increasing trajectory angle exhibits a similar relationship for both forest plots FT and PWL until trajectory angles reach approximately 60° (see bottom row of Figure 3.10). Beyond 60°, the PWL rate of increase slows as the  $C_p$  approaches 1.0, while the FT plot, which has lower canopy coverage, continues to rise until around 75° as a  $C_p$  of 1.0 is approached.  $C_p$  was also quantified across trajectory angles for both PWL and FT on March 14<sup>th</sup>, post snowfall, and showed a negligible increase in  $C_p$  compared to  $C_p$  measured on March 13<sup>th</sup> without snow in the canopy.

A function is proposed here to calculate plot-scale leaf contact area,  $C_p$  (-):

$$C_p = C_c + C_{inc}(\theta_h, C_c) \quad (3.10)$$

where  $C_{inc}$  represents the increase in leaf contact area from nadir measured canopy coverage ( $C_c$ ), and is a function of  $\theta_h$  and  $C_c$ . To estimate  $C_{inc}$  in the absence of detailed canopy measurements, the following

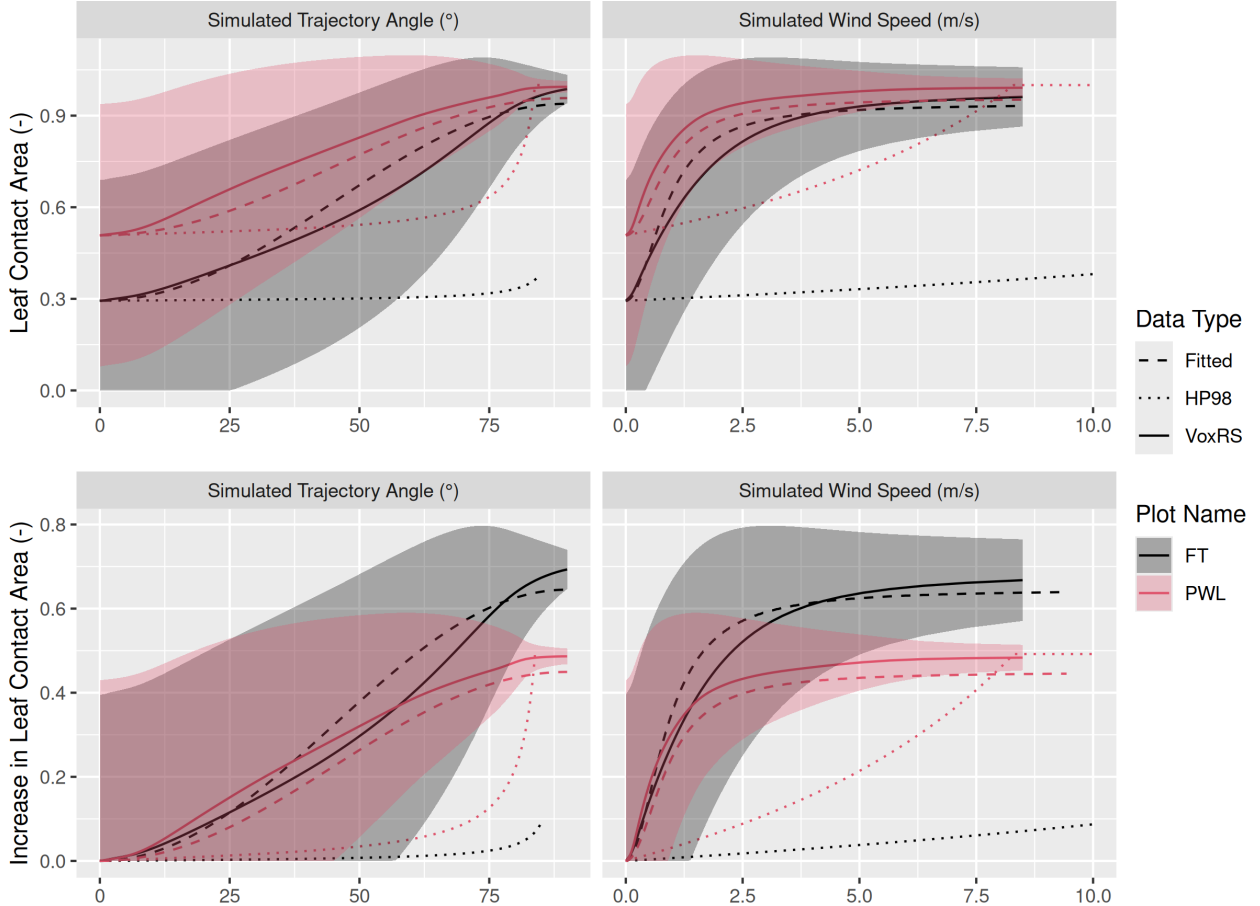


**Figure 3.10:** Plots showing the relationship between hydrometeor trajectory angle (left column) and wind speed (right column) with mean plot-wide snow-leaf contact area,  $C_p$  (top row) and the increase in mean plot-wide  $C_p$ , i.e.,  $C_p - C_c$  (bottom row). The simulated hydrometeor trajectory angle is measured as degrees from zenith. Simulated wind speed was calculated as a function of hydrometeor trajectory angle by rearranging Equation 3.4 and an observed event hydrometeor fall velocity of 0.9 m s<sup>-1</sup>. The solid lines (VoxRS) represent the mean  $C_p$  (top row) or increase in mean  $C_p$  (bottom row) for a single zenith angle observed from VoxRS across all grid cells for each forest plot and across all azimuth angles. The shaded area represents one standard deviation above and below the observed VoxRS mean. The dashed lines (Fitted) represent predictions from Equation 3.10 (top row) and Equation 3.11 (bottom row). The dotted lines (HP98) represent the predictions from Equation 10 in Hedstrom & Pomeroy (1998). A forested downwind distance of 100 m was assumed for the HP98 calculation.

function is proposed:

$$C_{inc} = (1 - C_c) \cdot f(\theta_h) \quad (3.11)$$

where  $1 - C_C$  quantifies the available void space within the canopy and  $f(\theta_h)$  represents the fraction of that space contributing to increased leaf contact area. Here,  $f(\theta_h)$  is approximated as:

$$f(\theta_h) = b \cdot \sin(\theta_h)^2 \quad (3.12)$$

where  $b$  is a fitting coefficient, estimated to be  $\sim 0.91$  through a non-linear least squares regression fit to the VoxRS measurements at both FT and PWL. The term  $\sin(\theta_h)^2$  reflects the relative increase in snow-leaf contact area, which in turn leads to a proportional decrease in the canopy void space  $(1 - C_c)$ . Thus, for  $\theta_h$  of  $0^\circ$ ,  $C_p$  is equal to the canopy cover. In contrast, for  $\theta_h$  close to  $90^\circ$ ,  $C_p$  approaches a value of 1.0. The assumptions of Equation 3.12 include that  $C_c$  represents a measurement of continuous canopy cover without large open areas many times greater than the mean canopy height and that snowfall trajectories are linear.

Simulated  $C_p$  using Equation 3.10 is shown in the dashed lines in the top row of Figure 3.10 and follows the VoxRS-measured mean  $C_p$  closely. Model error statistics demonstrate that Equation 3.11 performed well, with a mean bias and RMSE of  $-0.05$  (-) and  $0.05$  (-) for PWL, and  $0.03$  (-) and  $0.05$  (-) for FT respectively (Table 3.6). In contrast, the Hedstrom & Pomeroy (1998) method produced significantly less accurate estimates of  $C_p$ , with a mean bias and RMSE of  $-0.2$  (-) and  $0.23$  (-) for PWL, and  $-0.26$  (-) and  $0.32$  (-) for FT respectively (Table 3.6).

**Table 3.6:** Model error statistics calculated for the prediction of leaf contact area from trajectory angle using Equation 3.11 and Equation 10 from Hedstrom & Pomeroy (1998) (HP98) for the PWL and FT forest plots. Mean bias is the difference in the model and observed values, MAE is the mean of the absolute error, RMS Error is the root mean squared error and  $R^2$  is the coefficient of determination. The units for all metrics are dimensionless. A forested downwind distance of 100 m was used for the HP98 calculation.

Model	Plot Name	Mean Bias (-)	MAE (-)	RMS Error (-)	$R^2$
HP98	FT	-0.26	0.26	0.32	-0.97
HP98	PWL	-0.20	0.20	0.23	-0.96
Eq. 10	FT	0.03	0.04	0.05	0.95
Eq. 10	PWL	-0.05	0.05	0.05	0.90

### 3.5.4 Throughfall model performance

The performance of the interception efficiency (Equation 3.9) and leaf contact area (Equation 3.10) parameterisations in estimating event throughfall was assessed against UAV-lidar measurements of throughfall at the plot scale for the March 13–14<sup>th</sup> snowfall event. In this assessment, the hydrometeor trajectory angle was approximated using Equation 3.4 combined with the mean event wind speed at one-third the mean canopy height (estimated from Equation 3.5 and the observed wind speed at FT station) and hydrometeor terminal velocity (measured at PWL station). Leaf contact area was then estimated using Equation 3.10 for the PWL and FT plots, incorporating the approximated hydrometeor trajectory angle and observed canopy cover ( $C_c$ ) from the VoxRS dataset. Interception efficiency was calculated using Equation 3.9 with the estimated leaf contact area from Equation 3.10 and accumulated snowfall measured at PWL station for the event. An  $\alpha$  value, used in Equation 3.9, of 0.978 (-) was found through calibration which provided the best fit between observed and simulated interception efficiency at the plot scale for both FT and PWL.

The new vector-based parameterisation closely matched the UAV-lidar measurements of throughfall (Figure 3.11). Modelled throughfall from the vector-based model was 17.2 mm compared to the measured throughfall of 16.6 mm for PWL. For FT, the vector-based modelled throughfall was 21.5 mm, while the measured values were 22.1 mm. The vector-based model shows a lower mean bias of -0.6 mm for PWL and 0.6 mm for FT, in contrast to the nadir-based model, which overestimated throughfall for both plots (Table 3.7). This overestimation arose from the nadir-based model's approximation of leaf contact area from canopy coverage measurements (without adjustment via Equation 3.10), which yielded a reduced estimated contact area and consequently underestimated canopy snow interception.

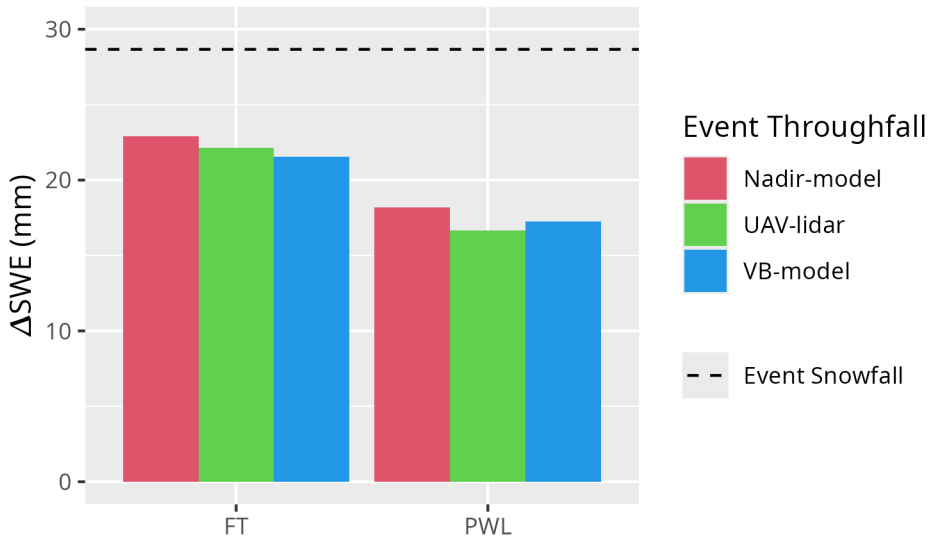


**Figure 3.11:** Bar chart comparing the observed and modelled mean change in throughfall ( $\Delta\text{SWE}$ , mm) over the March 13-14<sup>th</sup> snowfall event averaged over forest plots FT and PWL. The ‘Nadir-model’ calculated interception efficiency as a function of canopy coverage and the Vector-based ‘VB-model’ used Equation 3.9 with  $C_p$  adjusted for trajectory angle. ‘UAV-lidar’ corresponds to throughfall calculated using Equation 3.6 incorporating UAV-lidar snow depth and snow density from in-situ snow pits. The black horizontal dashed line shows the accumulated SWE (mm) over the snowfall event to the PWL station open clearing.

**Table 3.7:** Model error statistics for model estimates of snow interception efficiency (I/P) and throughfall (TF) compared to measurements of I/P and TF using UAV-lidar averaged over the FT and PWL forest plots. Units for I/P are (-) and TF are (mm). The vector-based model utilized Equation 3.9 with  $C_p$  adjusted for trajectory angle. The nadir model also utilized Equation 3.9 but was not adjusted for trajectory angle and thus  $C_c$  was used instead of  $C_p$ . The ‘Obs. Value’ column contains measurements from UAV-lidar while the ‘Mod. Value’ column contains the modelled values. The mean bias was calculated as observed minus modelled and percent error is the percent error between predicted and observed values.

	Model	Value		Obs.	Mod.	Mean	Perc.
Plot	Type	Name	Units	Value	Value	Bias	Error
FT	VB-model	I/P	-	0.23	0.25	-0.02	-9.01
FT	Nadir-model	I/P	-	0.23	0.20	0.03	12.10
FT	VB-model	TF	mm	22.12	21.53	0.59	2.67
FT	Nadir-model	TF	mm	22.12	22.91	-0.79	-3.58
PWL	VB-model	I/P	-	0.42	0.40	0.02	4.91
PWL	Nadir-model	I/P	-	0.42	0.37	0.05	12.95

**Table 3.7:** Model error statistics for model estimates of snow interception efficiency (I/P) and through-fall (TF) compared to measurements of I/P and TF using UAV-lidar averaged over the FT and PWL forest plots. Units for I/P are (-) and TF are (mm). The vector-based model utilized Equation 3.9 with  $C_p$  adjusted for trajectory angle. The nadir model also utilized Equation 3.9 but was not adjusted for trajectory angle and thus  $C_c$  was used instead of  $C_p$ . The ‘Obs. Value’ column contains measurements from UAV-lidar while the ‘Mod. Value’ column contains the modelled values. The mean bias was calculated as observed minus modelled and percent error is the percent error between predicted and observed values.

	Model	Value		Obs.	Mod.	Mean	Perc.
Plot	Type	Name	Units	Value	Value	Bias	Error
PWL	VB-model	TF	mm	16.64	17.24	-0.59	-3.55
PWL	Nadir-model	TF	mm	16.64	18.20	-1.56	-9.35

## 3.6 Discussion

The point scale observations presented in Figure 3.5 indicate that air temperature had little influence on initial interception efficiency during periods where melt and unloading of snow were less likely. This finding aligns with Storck et al. (2002), who observed that variations in air temperature did not significantly affect initial interception efficiency. While other studies have reported both positive (Andreadis et al., 2009; Katsushima et al., 2023; Roth & Nolin, 2019) and negative (Hedstrom & Pomeroy, 1998; Schmidt & Gluns, 1991) relationships between air temperature and snow interception, the limited association observed here may be explained by competing temperature-dependent processes. Warmer temperatures simultaneously increase branch flexibility, reducing  $C_p$  (Schmidt & Gluns, 1991; Schmidt & Pomeroy, 1990) and enhance snow cohesion and adhesion, increasing interception efficiency (Katsushima et al., 2023; Kobayashi, 1987; Pfister & Schneebeli, 1999).

Initial interception efficiency was found to increase with wind speed at two locations which were sheltered from the predominant wind direction (Figure 3.5). This is hypothesized to be due to an increase in  $C_p$  associated with non-vertical hydrometeor trajectories, as demonstrated by observations during a wind-driven snowfall event (Figure 3.6) and analysis of canopy density data (Figure 3.10). These findings are also consistent with observations by Schmidt & Troendle (1989) who observed a slight increase in snowfall interception with increasing wind speeds up to  $6 \text{ m s}^{-1}$ , Staines & Pomeroy (2023) who observed reduced canopy transmittance with increasing angle from zenith, and studies of rainfall interception by Herwitz & Slye (1995) and Van Stan et al. (2011).

The slight increase in interception efficiency for smaller canopy snow loads and decline for larger canopy snow loads is attributed to the influence of canopy snow load on  $C_p$  (Figure 3.5). Whilst small, this effect is

consistent with the theory proposed by Satterlund & Haupt (1967) that interception efficiency increases as the canopy fills with snow bridging gaps in the canopy, while later declining due to branch bending and decreased canopy cover. However, at the plot-scale, Staines & Pomeroy (2023) showed that these two processes may partially compensate for each other as  $C_p$  increases for closed canopies, as new snow bridges form in the canopy, but decreases in partially open canopy due to branch bending (i.e., Fig. 2 in Schmidt & Gluns, 1991). Still, the increase in  $C_p$  resulting from snow load in Staines & Pomeroy (2023) was small compared to the substantial rise in  $C_p$  due to trajectory angle presented in their study; which corroborates with the plot-scale observations of  $C_p$  in this study (Figure 3.10). Additional observations by Watanabe & Ozeki (1964), Calder (1990), and Storck et al. (2002) support the findings in Figure 3.3 showing a linear increase in canopy snow load with increasing snowfall. Further evidence in support of the relatively small influence of canopy snow load on  $C_p$ , is provided by Lundquist et al. (2021) who reported improved simulation of subcanopy snow accumulation without the use of a maximum canopy snow load, when linked with a comprehensive canopy snow ablation routine. The low sensitivity to canopy snow load found here may result from reduced inclusion of ablation processes in our measurements, limited influence of snow load on  $C_p$  at this site, and/or the compensatory effects described by Satterlund & Haupt (1967).

The limited influence of air temperature and canopy snow load on initial interception reported here differs from the theories underpinning existing snow interception parameterisations (Andreadis et al., 2009; Hedstrom & Pomeroy, 1998; Moeser et al., 2015b; Satterlund & Haupt, 1967). Cebulski & Pomeroy (2025a) note studies that have identified a relationship between air temperature and/or snow load and interception efficiency (Katsushima et al., 2023; Roth & Nolin, 2019; Schmidt & Gluns, 1991) did not specifically examine initial interception prior to canopy snow ablation. In addition, since a maximum canopy snow load was not observed in this study, the air temperature dependent canopy snow load capacities included in the Hedstrom & Pomeroy (1998) and Andreadis et al. (2009) models were not applicable. Since canopy snow ablation is strongly correlated with air temperature and snow load (Ellis et al., 2010; Floyd, 2012; Hedstrom & Pomeroy, 1998; Roesch et al., 2001) some of the previously observed relationships related to these variables may be explained by changes in ablation rather than initial interception. The coupling of ablation processes within existing models may contribute to overestimates of throughfall and canopy snow unloading when combined with other canopy snow ablation parameterisations due to ‘double counting’ (Cebulski & Pomeroy, 2025a).

To address these issues, a new vector-based snow interception parameterisation is presented (Equation 3.9) which calculates initial interception efficiency as a function of  $C_p$  and an efficiency constant,  $\alpha$ . This new parameterisation allows for canopy snow loading processes to be isolated from canopy snow ablation processes and is consistent with current rainfall interception theory (Valante et al., 1997; Zhong et al., 2022). Equation 3.9 differs only slightly from the original Hedstrom & Pomeroy (1998) parameterisation (see Equation 6 in Hedstrom & Pomeroy 1998), in that it does not calculate interception efficiency as a function of canopy snow load and from the Storck et al. (2002) parameterisation who found interception efficiency to be constant.

Further research is needed to explore how processes such as the increased cohesion and adhesion of snowfall to the canopy at warm temperatures, as observed by Kobayashi (1987), Pfister & Schneebeli (1999), as well as hydrometeor velocity, particle size, and shape suggested by (Katsushima et al., 2023), may influence the  $\alpha$  parameter, although these effects were not observed in this study. Since Equation 3.9 intentionally excludes processes attributed to canopy snow ablation that were previously included in earlier snow interception models, these ablation processes must be incorporated in canopy snow ablation parameterisations to fully represent the canopy snow mass balance.

The exponential relationship proposed by Hedstrom & Pomeroy (1998) to scale  $C_p$  with wind speed failed to reproduce the observations presented in Figure 3.10. Instead, plot-wide  $C_p$  was found to increase as function of hydrometeor trajectory angle and canopy cover. However, the large scatter in  $C_p$  measurements shown in Figure 3.10 suggests Equation 3.11 is only applicable at the forest stand scale, or larger, where the sub-metre variability in  $C_p$  resulting from directional differences averages out. Canopy cover measurements at larger scales may lack sufficient resolution to identify large open area components of forests, where the assumptions of Equation 3.10 would not be valid, and  $C_p$  should be estimated using horizontal canopy cover without adjusting for snowfall trajectory angle. If fine-scale canopy observations are available, canopy structure metrics such as the gap area indices described in Moeser et al. (2015a) could be helpful for identifying large gaps in the canopy. Moreover, our measurements show the hydrometeor trajectory angle required for Equation 3.11, can be approximated from Equation 3.4 incorporating the hydrometeor fall velocity and the mean horizontal wind speed selected at one-third of the canopy height. This is consistent with Katsushima et al. (2023), who also proposed using a wind speed at one-third the canopy height for modelling unloading of canopy snow. The transferability of the snow-leaf contact area equation (Equation 3.11) remains uncertain, as it has only been tested at a single site with two tree species, and the relationship of  $C_p$  with environmental factors is expected to vary across different climate conditions, canopy structures, densities, species, and ages. Additionally, Equation 3.4 assumes a linear hydrometeor trajectory, and does not consider non-linear patterns such as wind flow directions around tree elements, turbulent flow, or differences in wind speed with height. Staines & Pomeroy (2023) showed, at a proximal montane spruce-fir forest, that backflows and large eddies that occur within the canopy can contribute to mixed responses. Therefore, further testing and modification of Equation 3.11 is needed in diverse forest environments.

Although the vector-based model showed relatively modest improvement over the nadir model, it is preferred due to its lower error compared to the UAV-lidar measurements and better representation of physical processes. Developed and tested at the forest plot scale (hectares), the vector-based model is suitable for hydrological models discretized by forest density at this scale, though the relationship between snow interception and snow-leaf contact area should be applicable at larger scales. Previous subcanopy snow accumulation models were developed based on process understanding at varying scales: Hedstrom & Pomeroy (1998) used snow survey transects at the forest plot scale with observations at intervals ranging from days to weeks, whilst

Storck et al. (2002) relied on point-scale lysimetry observations at 30-minute intervals. Recent evidence from Staines & Pomeroy (2023) and the results presented here suggest that some of the process understanding developed in previous studies may not be applicable at larger extents or finer temporal resolutions. The theoretical basis of the vector-based model is supported by observations across a broad range of meteorological conditions and forest densities and aligns with globally tested rainfall interception models (e.g., Valante et al., 1997; Zhong et al., 2022), suggesting potential broader applicability, though further validation is required.

### 3.7 Conclusions

New observations of initial snow interception, collected over a wide range of meteorological conditions and canopy densities indicate that leaf contact area is the primary factor influencing subcanopy snow accumulation. At the point scale, measurements revealed no evidence of a maximum canopy snow load, even for event snowfalls up to 45 mm, nor was there any indication of air temperature influencing the cohesion and adhesion of snowfall to the canopy. Instead, wind speed was found to influence interception efficiency by changing the hydrometeor trajectory angle, which led to a substantial increase in snow-leaf contact area.

At the forest plot scale, UAV-lidar measurements of throughfall aligned with the point-scale observations demonstrating that leaf contact area was strongly associated with interception efficiency at a particular site. Leaf contact area, which incorporates changes in canopy density with hydrometeor trajectory angle, proved to be a better predictor of interception efficiency compared to nadir-calculated canopy cover. When averaged across each forest plot, leaf contact area was shown to be highly sensitive to hydrometeor trajectory angle, increasing by 61–95% for trajectory angles associated with a  $1 \text{ m s}^{-1}$  wind speed. An existing theoretical relationship failed to adequately represent the measured increase in leaf contact area with simulated trajectory angles. As a result, a new relationship is proposed as a function of canopy cover and hydrometeor trajectory angle, approximated from wind speed and hydrometeor terminal fall velocity, demonstrated accurate performance at this study site.

The weak association between air temperature and canopy snow load with initial interception efficiency, as presented here and in earlier studies, coupled with novel insights on the influence of wind speed on leaf contact area, suggests the potential benefits of a new snow interception parameterisation. A new parameterisation is proposed that calculates initial interception as a function of snowfall and leaf contact area. This parameterisation is consistent with rainfall interception studies, which also separate canopy loading and ablation processes, and calculate interception as a function of canopy cover. Additionally, a second equation is proposed to estimate leaf contact area as a function of hydrometeor trajectory angle and nadir canopy cover. This updated snow interception parameterisation performed well in the subalpine forest studied here at the forest plot scale. However, further validation is necessary in a range of climates, forests, and spatial extents.

## **3.8 Acknowledgments**

We acknowledge financial support from the University of Saskatchewan Dean’s Scholarship, the Natural Sciences and Engineering Research Council of Canada’s Discovery Grants, the Canada First Research Excellence Fund’s Global Water Futures Programme, Environment and Climate Change Canada, Alberta Innovates Water Innovation Program, the Canada Foundation for Innovation’s Global Water Futures Observatories facility, and the Canada Research Chairs Programme. We thank Madison Harasyn, Hannah Koslowsky, Kieran Lehan, Lindsey Langs and Fortress Mountain Resort for their help in the field. Jacob Staines, Madison Harasyn, Alistair Wallace, and Rob White contributed to developing the UAV-lidar processing workflow.

## **3.9 Data Availability**

The data that support the findings in this study are available at <https://doi.org/10.5281/zenodo.14018893>.

# 4 PROCESSES GOVERNING THE ABLATION OF INTERCEPTED SNOW

Manuscript status: This chapter has been submitted as a research article to the journal *Water Resources Research* on August 19, 2025 and is currently under review.

Citation: Cebulski, A. C., & Pomeroy, J. W. (under review). Processes Governing the Ablation of Intercepted Snow. *Water Resources Research*.

Role in thesis: This journal article answers research question 1.3 of the thesis. It will present analysis of canopy snow ablation observations from Fortress Mountain Research basin collected over the 2022 and 2023 water years and contrast these against existing theories.

Author Contribution:

A. Cebulski: Conceptualization (lead), data collection (equal), analysis (lead), visualization (lead), writing – original draft (lead), writing review and editing (equal) J. Pomeroy: Conceptualization (supporting), data collection (supporting), funding acquisition (lead), analysis (equal), project administration (lead), resources (lead), supervision (lead), writing review and editing (equal).

## 4.1 Abstract

Interception and ablation of snow in forest canopies significantly influence the quantity, timing, and phase of precipitation that reaches the ground in cold regions forests. Yet current modelling approaches have uncertain transferability across differing climate and forest types, often omit key processes, and typically couple interception and ablation processes in ways that limit both process representation and evaluation. Here, in-situ observations from a needleleaf forest in the Canadian Rockies are utilised to evaluate the theories underpinning existing canopy snow ablation models and develop novel understanding to support the development of a new canopy snow ablation model. The observations revealed that canopy snow load, wind shear stress, and canopy snowmelt were strongly associated with unloading; however, air temperature and sublimation were not. A new canopy snow ablation model was developed based on these associations and their impact on the canopy snow energy and mass balance. This model demonstrated improved performance in simulating canopy snow load relative to previous approaches, especially for melt- and wind-dominated

ablation events. The improved performance in representing canopy snow load compared to existing models results from including energy balance-based melt and dry snow unloading relationships with snow load and wind shear stress. The inclusion of both melt and dry snow unloading processes in the new model also led to more consistent partitioning of snowfall to the atmosphere versus the ground compared to existing approaches across a wide range of meteorologies.

## 4.2 Introduction

The seasonal snowpack is an essential component of global water resources (Immerzeel et al., 2020; Vivioli et al., 2020) and is increasingly threatened by rapid climate and land cover change (Aubry-Wake & Pomeroy, 2023; Fang & Pomeroy, 2023; López-Moreno et al., 2014; Szczypta et al., 2015). Vegetation cover can significantly alter the quantity (Essery et al., 2003; Pomeroy & Gray, 1995; Sanmiguel-Vallelado et al., 2020) and timing (Ellis et al., 2010; Safa et al., 2021) of snow that reaches the ground. Forest canopies cover more than half of the snow-covered area in the Northern Hemisphere (Kim et al., 2017), making forest-snow interactions crucial to understand for informed ecological, land management, and water resource decision-making. Needleleaf canopies are particularly effective at intercepting snowfall (Cebulski & Pomeroy, 2025b; Hedstrom & Pomeroy, 1998; Pomeroy & Schmidt, 1993; Storck et al., 2002), where intercepted snow is subject to increased energy inputs relative to the subcanopy snowpacks, leading to increased rates of melt, unloading, and/or sublimation (Parviainen & Pomeroy, 2000; Pomeroy et al., 1998b; Roesch et al., 2001; Storck et al., 2002). The partitioning of snow to the atmosphere via sublimation (Parviainen & Pomeroy, 2000; Pomeroy et al., 1998b) or to the ground through unloading and meltwater drip (Lumbrazo et al., 2022; Roesch et al., 2001; Storck et al., 2002) is highly sensitive to meteorological conditions and forest structure contributing to substantial variability in subcanopy snowpacks across regions and snowfall events. Coastal humid environments typically exhibit small sublimation losses and a larger influence of unloading and melt (Floyd, 2012; Storck et al., 2002). Here, enhanced canopy energy inputs combined with high humidity increases both solid snow unloading and melt of snow intercepted in the canopy (Lumbrazo et al., 2022; Lundquist et al., 2021; Roesch et al., 2001). Conversely, the colder and drier winters in continental climates typical of the boreal forests can induce substantial canopy sublimation losses (e.g., 25–45% of annual snowfall in Essery et al., 2003) in addition to unloading (Essery et al., 2003; Gelfan et al., 2004; Parviainen & Pomeroy, 2000; Pomeroy et al., 1998b, 2002). As a result, reliable models of snow accumulation and streamflow in forested basins rely on a comprehensive understanding of interception processes (Clark et al., 2015b; Essery et al., 2003; Pomeroy et al., 1998a; Versegheghy, 2017; Wheater et al., 2022).

Canopy snow models have demonstrated variable transferability across different climates and forest types (Essery et al., 2003; Gelfan et al., 2004; Lumbrazo et al., 2022; Lundquist et al., 2021), and uncertainty in transferability has been attributed as a key area limiting the performance in predicting forest snowpacks in hydrological model intercomparisons (Kriinner et al., 2018; Rutter et al., 2009). Recent studies have empha-

sized the importance of distinguishing between initial snow interception and subsequent ablation processes (Cebulski & Pomeroy, 2025a; Cebulski & Pomeroy, 2025b). This separation allows for individual parameterisations for distinct processes, improving both process representation and the modular design of contemporary models, thereby supporting broader applicability across diverse environments and model structures (Clark et al., 2015b; Pomeroy et al., 2022). In addition, Lundquist et al. (2021) and Cebulski & Pomeroy (2025b) demonstrated that canopy snow processes can be more accurately represented without the concept of a maximum canopy snow load, which is included in initial accumulation parameterisations (Andreadis et al., 2009; Hedstrom & Pomeroy, 1998). Existing ablation routines were integrated in canopy snow accumulation parameterisations, likely as a result of some ablation included in measurements of interception efficiency (Cebulski & Pomeroy, 2025a). For example, Hedstrom & Pomeroy (1998) found that interception efficiency declined as the canopy is loaded with snow, while Storck et al. (2002) found a constant interception efficiency of 0.6 and is also typically combined with a maximum canopy snow load. Consequently, both the Hedstrom & Pomeroy (1998) and Storck et al. (2002) parameterisations have significantly lower interception efficiencies—prior to canopy snow ablation—compared to the observations by Cebulski & Pomeroy (2025b). Staines & Pomeroy (2023) and Cebulski & Pomeroy (2025b) show that interception efficiency is best predicted by canopy density alone—consistent with some rainfall interception parameterisations (e.g., Valante et al., 1997; Zhong et al., 2022)—and that snow load has a small influence on canopy density, challenging the Hedstrom & Pomeroy (1998) and Storck et al. (2002) initial snow interception theories. Together these studies (Cebulski & Pomeroy, 2025a; Cebulski & Pomeroy, 2025b; Lundquist et al., 2021) emphasize the need to revisit canopy snow ablation parameterisations.

Ablation of intercepted snow due to snow unloading to the ground has previously been shown to be associated air temperature (Katsushima et al., 2023; Roesch et al., 2001; Schmidt & Pomeroy, 1990), ice-bulb temperature—which more accurately represents the cooling effect of sublimation compared to air temperature—(Ellis et al., 2010; Floyd, 2012), canopy snowmelt rate (Storck et al., 2002), and wind speed as shown in Figure 4.1 for (Bartlett & Verseghy, 2015; Katsushima et al., 2023; Roesch et al.; 2001, 2001). Each of these factors were also found to be dependent on canopy snow load and time (Figure 4.1). While Hedstrom & Pomeroy (1998) did not make direct observations of canopy snow unloading, they proposed a parameterisation based on canopy snow load and time. In addition to the empirical observations by the aforementioned studies, physical reasoning also supports the inclusion of these processes. For example, melt promotes unloading through loss of structural integrity, particle bond weakening, and lubrication of intercepted snow. Wind drag promotes unloading through shear stress applied to intercepted snow, wind erosion through direct entrainment in the atmosphere of intercepted snow, and branch movement. Branch elasticity increases with temperature (Schmidt & Pomeroy, 1990) which can increase the likelihood of unloading due to increasing branch angle under a snow load and decreased stiffness to resist swaying in a turbulent wind.

Melt of snow intercepted in the canopy is typically represented by either an energy balance approach (An-

dreadis et al., 2009; Clark et al., 2015b; e.g., Parviaainen & Pomeroy, 2000), as a function of air temperature (Roesch et al., 2001), or a function of ice-bulb temperature (Ellis et al., 2010; Floyd, 2012) (Figure 4.2). Sublimation is generally represented using a coupled energy and mass balance approach (e.g., Essery et al., 2003; Pomeroy et al., 1998b; Verseghy, 2017). The Essery et al. (2003) and Pomeroy et al. (1998b) approaches differ in that Pomeroy et al. (1998b) does not include longwave radiation in the canopy snow energy balance. Both the Essery et al. (2003) and Pomeroy et al. (1998b) parameterisations decrease the latent heat flux from snow intercepted in the canopy as the canopy fills up with snow and its specific surface area decreases. However, these parameterisations are based on estimates of maximum canopy snow load which may underestimate true maxima (Cebulski & Pomeroy, 2025b; Lundquist et al., 2021; Storck et al., 2002) and should be reconsidered using a larger maximum load or an approach that avoids prescribing a maximum load. The merits of including more physically based energy balance methods compared to more empirically based functions for calculating snowmelt and sublimation have not been directly assessed using an event-based process investigation.

Quantifying individual canopy snow ablation processes including unloading, wind redistribution, melt, drip, and sublimation remains challenging, even with sophisticated lysimetry (Storck et al., 2002) and eddy-covariance systems (Conway et al., 2018; Harding & Pomeroy, 1996; Harvey et al., 2025). Consequently, some canopy snow ablation parameterisations have been developed using methods, such as above canopy albedo, which do not distinguish individual processes (Bartlett & Verseghy, 2015; Roesch et al., 2001). While these approaches offer useful indices of model performance, they provide limited insight into the accuracy of individual process representations. Lysimeter-based measurements offer more direct process-level observations, but interpretation of their observations is made uncertain by freeze-thaw cycles and concurrent processes (Floyd, 2012; MacDonald, 2010; Storck et al., 2002). A hybrid diagnostic approach that combines individual process measurements with simulations and employs observations such as canopy snow load from a weighed tree has yet to be applied but is explored in this study.

The objective of this study is to better understand and predict the influences of meteorology and snow load on intercepted snow ablation. This study specifically looks at canopy snow ablation after snowfall and initial interception. Cebulski & Pomeroy (2025b) has addressed processes governing the initial accumulation of snow in the canopy.

The specific research questions this research aims to address include:

1. How do air temperature, humidity, wind exposure, canopy snow sublimation, and snowmelt influence the rate of canopy snow unloading?
2. To what extent do current theoretical models of canopy snow ablation align with detailed in-situ observations?

3. What modifications to existing models, are necessary to accurately represent ablation of snow intercepted in the canopy and what is the improvement in performance from these modifications?

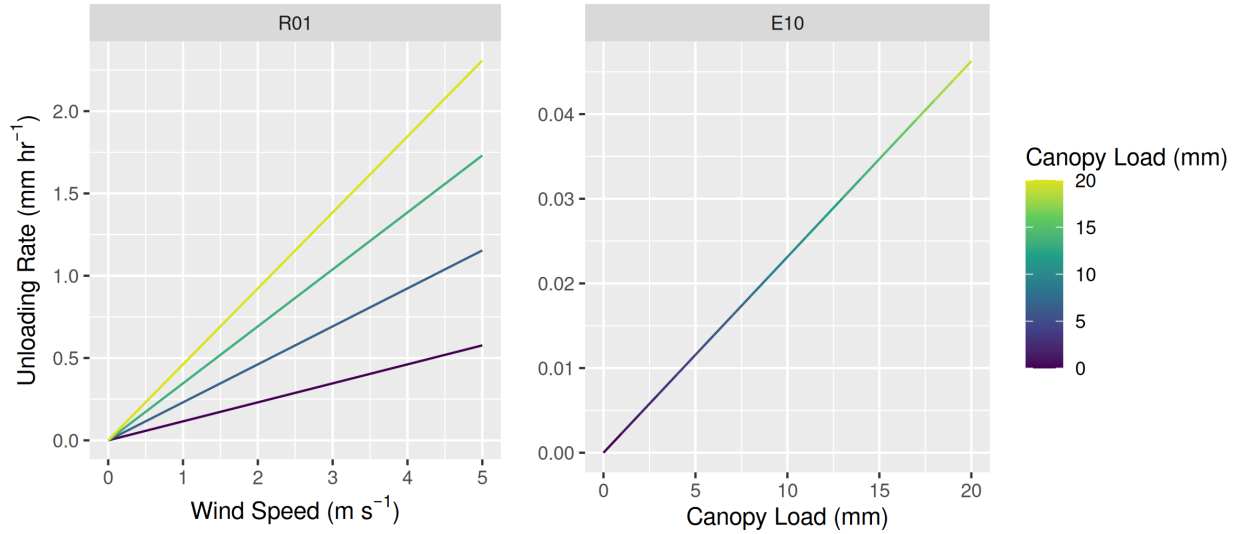


**Figure 4.1:** The Roesch et al. (2001) model of unloading rate with increasing wind speed and canopy snow load (left, R01) and the Hedstrom & Pomeroy (1998) model of unloading rate with increasing snow load (right, E10). Both examples have a constant air temperature of -10°C to disable the influence of warming on unloading and drip.

## 4.3 Methods

### 4.3.1 Study Site

The observations presented in this study were collected at Fortress Mountain Research Basin (FMRB), Alberta, Canada, -115° W, 51° N, a continental headwater basin in the Canadian Rockies. The site is located 2100 m above sea level on a ridge covered by mature fir and spruce forest. Air temperature, humidity, and wind speed were measured at a height of 4.3 m at Forest Tower (FT) Station (Figure 4.3). Shear stress was calculated using the EddyPro software (LI-COR Biosciences) based on high-frequency wind measurements from a CSAT3 three-dimensional sonic anemometer (Campbell Scientific) installed at 3.0 m at FT station. The CSAT3 was occasionally covered in snow during the analysis period, and thus to provide a complete record of shear stress, a linear relationship was established between shear stress derived from the CSAT3 and the square of wind speed measured at 4.3 m at the FT station ( $R^2 = 0.71$ ,  $p < 0.05$ ). This relationship was then used to gap-fill shear stress during periods when the CSAT3 was snow-covered. The precipitation rate was measured by an Alter-shielded OTT Pluvio weighing precipitation gauge installed 2.6 m above ground at the adjacent Powerline (PWL) Station (Figure 4.3). Incoming and outgoing solar radiation was measured by a Kipp & Zonen CNR4 4-Component Net Radiometer installed 3.27 m above the ground at Fortress Ridge Station (FRS) 2.0 km to the northwest of FT station (-115.2° W, 50.8° N). This windy exposed site

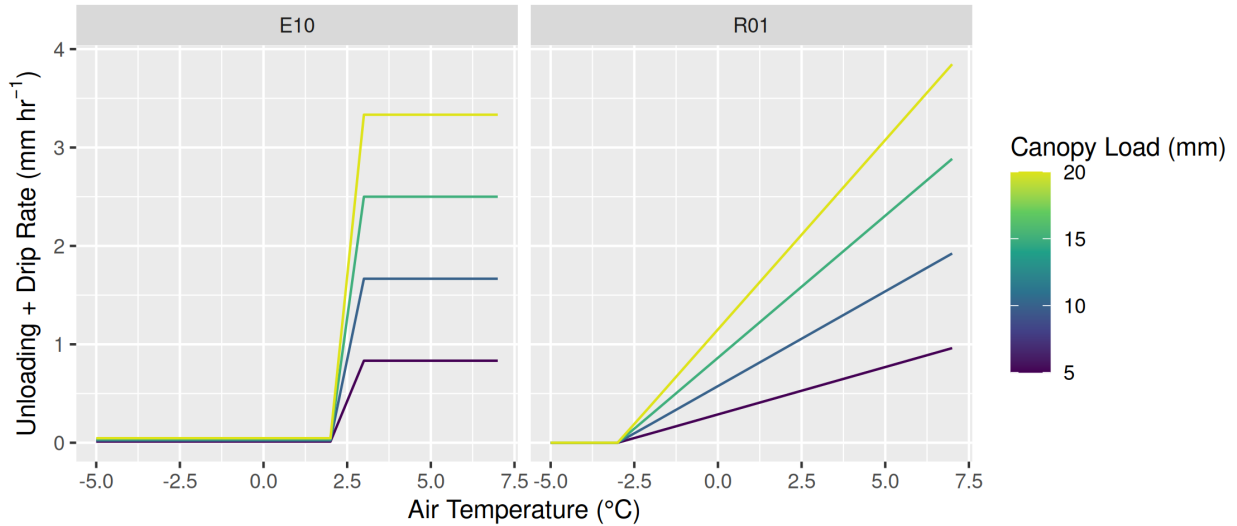


**Figure 4.2:** The Ellis et al. (2010) and Floyd (2012) (E10) model of unloading and drip rate (left) and the Roesch et al. (2001) (R01) model of unloading rate (right) with increasing air temperature. Wind speed for the R01 parameterisation was set to zero.

was selected to reduce snow accumulation on the radiometers, in addition to the CNR4's built-in heating element. Three subcanopy lysimeters, consisting of plastic horse-watering troughs with an opening of 0.9 m<sup>2</sup> and depth of 20 cm suspended from a load cell, were installed to measure subcanopy snow accumulation. A weighed tree lysimeter (subalpine fir) suspended from a load cell (Artech S-Type 20210-100) measured the weight of canopy snow load (kg) and was scaled to an areal estimate of snow load (mm) using snow surveys as in Pomeroy & Schmidt (1993). To isolate the subcanopy lysimeter measurements of canopy snow unloading from throughfall, 15-min intervals were selected that had no atmospheric precipitation based on the precipitation gauge at PWL. The weighed tree and timelapse imagery also were used to confirm there was no atmospheric precipitation and to identify periods where snow was intercepted in the canopy and ablation was possible. Four tipping bucket rain gauges—3 Texas Electronics TR-525M and 1 Hyquest Solutions TB4MM—were installed along a 15 m transect adjacent to the dense canopy subcanopy lysimeter to quantify sub-canopy drip from melting intercepted snow. Additional details on this study site and the meteorological and lysimeter measurements have been described in Cebulski & Pomeroy (2025b).

### 4.3.2 The Cold Regions Hydrological Model Platform

The Cold Regions Hydrological Model Platform (CRHM) was used to implement calculations of the canopy snow energy and mass budget. A full description of the CRHM platform is described in Pomeroy et al. (2022) and the source code is available at <https://github.com/srlabUsask/crhmcode>. The climate forcing data used to run CRHM was from station-based fifteen-minute interval measurements of air temperature, relative humidity, wind speed, precipitation, and incoming solar radiation from the FT, PWL, and FRS stations. CRHM incorporates a flexible modular design allowing the user to select various modules (parameterisations)

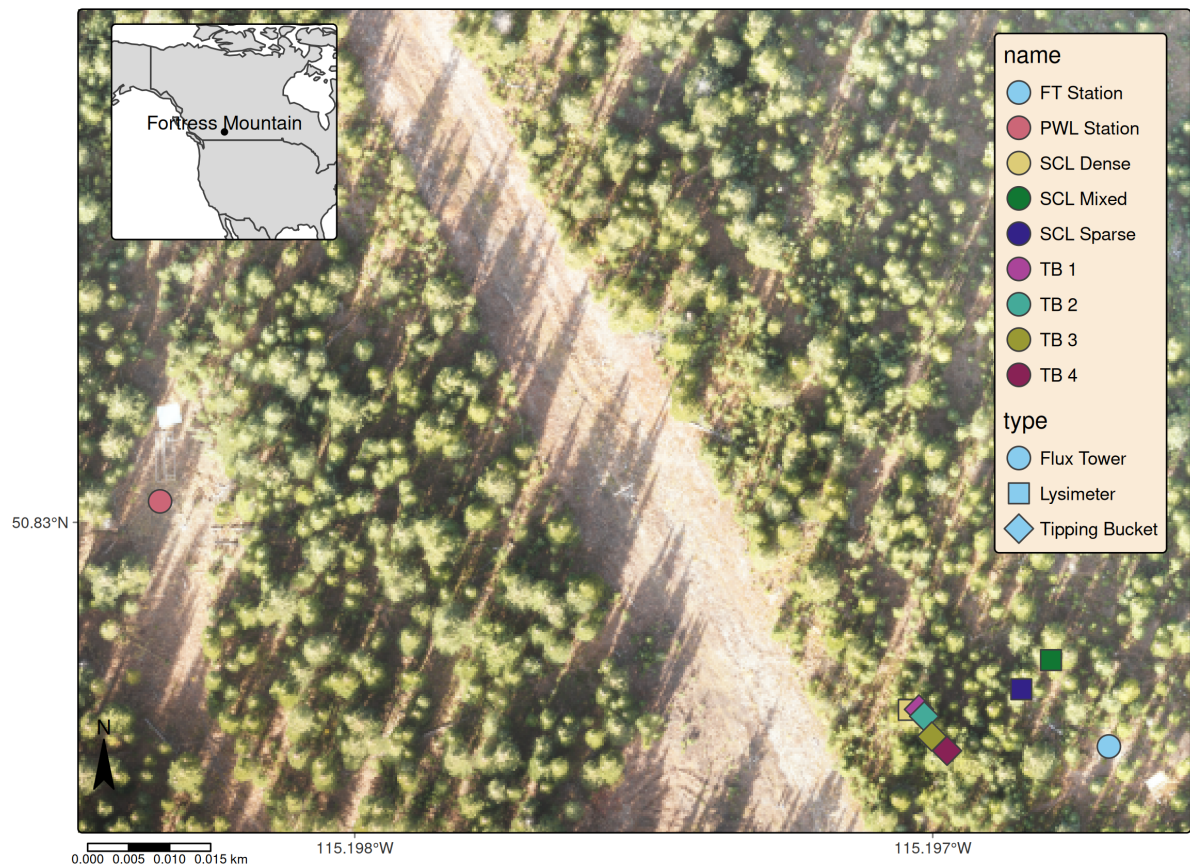


**Figure 4.3:** Map showing the location of flux towers and lysimeter instruments. The inset map on the upper left shows the regional location of Fortress Mountain Research basin. Flux towers are denoted by a circle, lysimeters by a square, and tipping bucket rain gauges (TB) by diamonds.

that represent hydrological processes. The phase of atmospheric precipitation was determined from the energy balance of falling hydrometeors (Harder & Pomeroy, 2013). A new CRHM module was created here to simulate the coupled mass and energy balance of snow intercepted in the canopy. The energy balance is described in detail in Section 4.3.5 and the updates to the mass balance through revisions to the canopy snow unloading empirical functions are presented in Section 4.4.1.1 and Section 4.4.1.2.

### 4.3.3 Canopy Snow Mass Balance

The following mass balance as described in Cebulski & Pomeroy (2025a) was implemented in CRHM to track the state of canopy snow load ( $L$ , mm) over time:

$$\frac{dL}{dt} = [q_{sf} - q_{tf} + q_{ros}] - [q_{unld}^{melt} + q_{unld}^{dry}] - q_{drip} - q_{wind}^{veg} - q_{sub}^{veg} \quad (4.1)$$

where  $\frac{dL}{dt}$  is the change in canopy snow load over time, (mm s<sup>-1</sup>),  $q_{sf}$  is the snowfall rate (mm s<sup>-1</sup>),  $q_{tf}$  is the throughfall rate (mm s<sup>-1</sup>),  $q_{ros}$  is the rate of rainfall falling on snow intercepted in the canopy (mm s<sup>-1</sup>),  $q_{unld}^{melt}$  is the unloading rate due to melt (mm s<sup>-1</sup>),  $q_{unld}^{dry}$  is the dry snow unloading rate due to shear stress on snow, wind erosion, branch movement, structural degradation, bond weakening and increased elasticity of branches and other non-melt related processes (mm s<sup>-1</sup>),  $q_{drip}$  is the canopy snow drip rate (mm s<sup>-1</sup>) resulting from canopy snowmelt ( $q_{melt}$ , mm s<sup>-1</sup>),  $q_{wind}^{veg}$  is the wind transport rate in or out of the control volume (mm s<sup>-1</sup>), and  $q_{sub}^{veg}$  is the intercepted snow sublimation rate (mm s<sup>-1</sup>) which includes any evaporation of liquid water in the canopy. Figure 1 in Cebulski & Pomeroy (2025a) presents a visual representation of this mass balance.

### 4.3.4 Mass Balance Parameterisations

In addition to the updated canopy snow model presented in this study, hereafter referred to as CP25 (described in Section 4.4.1.1 and Section 4.4.1.2), three other canopy snow models were implemented in CRHM following previous studies by Ellis et al. (2010) and Floyd (2012) (E10), Roesch et al. (2001) (R01), and Andreadis et al. (2009) who built on observations by Storck et al. (2002) (SA09). The E10 model includes canopy snow sublimation as described in Pomeroy et al. (1998b), dry snow unloading as a function of canopy snow load from Hedstrom & Pomeroy (1998) with modifications described in Ellis et al. (2010) and Floyd (2012) to handle canopy snow melt and drip processes using an ice-bulb temperature threshold. The R01 model represents dry snow unloading, melt, and drip using linear functions of wind speed and air temperature, while sublimation is simulated using the parameterisation from Pomeroy et al. (1998b). The SA09 model unloads snow as a ratio of the canopy snowmelt rate, following observations by Storck et al. (2002) and does not include dry snow unloading. The snowmelt rate from Equation 4.3 was used to calculate the unloading rate for the Andreadis et al. (2009) unloading and thus differs from the energy balance routine described in their study. Canopy snow sublimation in SA09 was represented based on the Essery et al. (2003) parameterisation

(Equation 4.10) as implemented in CP25.

The retention of canopy snow meltwater differs between the four canopy snow models implemented in CRHM. For E10, liquid meltwater is not retained in the canopy and immediately drips before it can evaporate. The R01 model also does not represent evaporation of liquid meltwater as canopy snow is not explicitly separated between solid snow unloading and melt/drip. The canopy liquid water storage capacity ( $L_{max}^{liq}$ , mm) from SA09 and CP25 was calculated as:

$$L_{max}^{liq} = Lh + nLAI \quad (4.2)$$

where  $h$  is the liquid meltwater holding capacity that canopy can retain against gravity and  $n$  is a storage constant of the vegetation elements. Andreadis et al. (2009) estimated  $h$  as 0.035 (-) and  $n$  as  $e^{-4}$ . In this study,  $h$  was set to 0.01 (-), and  $n$  was defined as  $C_c \cdot 0.2$ . A one-sided effective plant (leaf) area index (LAI) was used, including the clumping factor to account for needleleaf canopy structures, following the approach of Ellis et al. (2010) for rainfall interception.

#### 4.3.5 Canopy Snow Energy Balance

The CP25 and SA09 canopy snow models implemented the following energy balance approach to calculate the energy available for melting snow intercepted in the canopy ( $Q_{melt}$ , W m<sup>-2</sup>) and to track the canopy snow temperature over time ( $\frac{\Delta T_{vs}}{\Delta t}$ , K s<sup>-1</sup>). The energy balance is expressed as:

$$Q_{melt} = Q_{sw} + Q_{lw} + Q_p + Q_h + Q_l - [C_p^{ice} L \frac{\Delta T_{vs}}{\Delta t}] \quad (4.3)$$

where  $Q_{sw}$  and  $Q_{lw}$  (W m<sup>-2</sup>) are the net shortwave and longwave radiation heat fluxes to the canopy snow,  $Q_p$  (W m<sup>-2</sup>), is the advective energy rate, and  $Q_l$  and  $Q_h$  (W m<sup>-2</sup>), are the turbulent fluxes of latent heat and sensible heat respectively (positive towards canopy snow), and  $C_p^{ice}$  (J kg<sup>-1</sup> K<sup>-1</sup>) is the specific heat capacity of ice. Figure 2 in Cebulski & Pomeroy (2025a) shows a visual representation of this energy balance.

#### 4.3.6 Energy Balance Parameterisations

The E10 and R01 parameterisations relied on physically guided empirical relationships to simulate sublimation and melt and are described in full detail in their respective articles and are also summarised in Cebulski & Pomeroy (2025a). The following section describes the energy balance parameterisations implemented in the CP25 and SA09 models.

$Q_{sw}$  was determined as:

$$Q_{sw} = Q_{sw}^{in} \cdot (1 - \alpha_s) \cdot \tau_{50}^{veg} \quad (4.4)$$

where  $Q_{sw}^{in}$  is the downwelling shortwave radiation ( $\text{W m}^{-2}$ ),  $\alpha_s$  is the albedo of snow intercepted in the canopy (-),  $\tau_{50}^{veg}$  (-) is the canopy transmittance to  $Q_{sw}^{in}$ . Equation 10 from Pomeroy et al. (2009) was used to determine  $\tau_{50}^{veg}$ , using half of the leaf area index (LAI) based on studies Weiskittel et al. (2009) and Kesselring et al. (2024) that approximately 50% of the total leaf area is concentrated in the upper half of coniferous canopies.  $Q_{sw}$  provides an approximation of the net shortwave radiation to all snow intercepted in the canopy and is a simplification from using a partial differential equation to determine the radiation incident to individual height layers within the canopy. Upwelling shortwave radiation reflected off the surface snowpack is considered negligible contribution to the snow intercepted in the canopy as it is primarily blocked by vegetation elements underlying the canopy snow (Pomeroy et al., 2009).

$Q_{lw}$  was approximated as:

$$Q_{lw} = \downarrow Q_{lw}^{atm} + \uparrow Q_{lw}^{veg} - Q_{lw}^{vs} \quad (4.5)$$

where  $Q_{lw}^{atm}$  is the downwelling longwave radiation from the atmosphere ( $\text{W m}^{-2}$ ),  $Q_{lw}^{veg}$  is the longwave radiation upwelling from vegetation elements underlying snow intercepted in the canopy ( $\text{W m}^{-2}$ ), and  $Q_{lw}^{vs}$  ( $\text{W m}^{-2}$ ) is the outgoing longwave radiation from the top and bottom of the canopy snow layer calculated as:

$$Q_{lw}^{vs} = 2\epsilon_s \sigma T_{vs}^4 \quad (4.6)$$

where  $\epsilon_s$  is the emissivity (-) of snow taken as 0.99 and  $\sigma$  is the Stefan–Boltzmann ( $5.67e^{-10} \text{ W m}^{-1} \text{ K}^{-4}$ ).  $Q_{lw}^{atm}$  was approximated in this study as in Sicart et al. (2006) to represent the influence of atmospheric moisture and clouds on emissivity.  $Q_{lw}^{veg}$  was calculated with the assumption that canopy elements are in equilibrium with the air temperature plus any increase in vegetation temperature from the extinction of  $Q_{sw}^{in}$  in the canopy (Pomeroy et al., 2009, Eq. 4).

$Q_p$  was calculated as:

$$Q_p = [C_p^{liq} m_r (T_r - T_{vs}) + C_p^{ice} m_s (T_s - T_{vs})] / \Delta t \quad (4.7)$$

where  $C_p^{liq}$  is the specific heat capacity of liquid water ( $\text{J kg}^{-1} \text{ K}^{-1}$ ),  $m_r$  is the specific mass of liquid water in precipitation (mm),  $T_r$  is the rainfall temperature (K),  $m_s$  is the specific mass of snow in precipitation (mm), and  $T_s$  is the snowfall temperature (K).

$Q_h$  was calculated as:

$$Q_h = \frac{\rho_a}{r_a} C_p^{air} (T_a - T_{vs}) \quad (4.8)$$

where  $\rho_a$  is the air density ( $\text{kg m}^{-3}$ ),  $C_p^{air}$  is the specific heat capacity of air ( $\text{J kg}^{-1} \text{ K}^{-1}$ ),  $T_a$  is the air temperature, and  $r_a$  is the aerodynamic resistance ( $\text{s m}^{-1}$ ) which was approximated from Equation 4 in Allan et al. (1998) as:

$$r_a = \frac{\log(\frac{z_T-d_0}{z_0})\log(\frac{z_u-d_0}{z_0})}{\kappa^2 u_z} \quad (4.9)$$

where  $z_T$  is the height of temperature measurement (m),  $d_0$  is the displacement height (m) which was approximated as  $2/3^{\text{rd}}$  the mean canopy height,  $z_0$  is the roughness length (m) which was approximated as  $1/10^{\text{th}}$  of the mean canopy height,  $z_u$  is the wind speed measurement height (m),  $\kappa$  is von Kármán's constant, 0.41 (-), and  $u_z$  is the wind speed measurement at  $z_u$  ( $\text{m s}^{-1}$ ).

$Q_l$  was calculated as:

$$Q_l = \frac{\rho_a}{r_i + r_a} (q_a(T_a) - q_{vs}(T_{vs})) \quad (4.10)$$

where  $r_i$  is a resistance for transport of moisture from intercepted snow to the canopy air space (Eq. 28 in Essery et al., 2003),  $q_a(T_a)$  and  $q_{vs}(T_{vs})$  are the specific humidity (-) at the air temperature and canopy snow temperature, respectively.  $r_i$  was calculated following the concept of how full the canopy is with snow as introduced by Pomeroy & Schmidt (1993) with modifications to incorporate a larger maximum canopy snow load capacity of 50 mm based on observations by Storck et al. (2002), Floyd (2012), and Cebulski & Pomeroy (2025b).

The above sensible and latent heat flux equations assume neutral atmospheric stability conditions, which is supported by the uncertainty of stability correction in forest canopies (Conway et al., 2018) and mountain environments in winter (Helgason & Pomeroy, 2012a). Solving Equation 4.3 requires an iterative solution to determine  $\Delta T_{vs}$  and the remaining terms which are also a function of  $T_{vs}$ .

### 4.3.7 Influence of Predictive Variables on Unloading

The effects of air temperature, wind speed, snow load, melt, and sublimation on the unloading process were assessed using a multivariate ordinary least squares regression. The following hypotheses were tested:

- a. Melt promotes unloading through loss of structural integrity, particle bond weakening, and lubrication

- of intercepted snow.
- b. Sublimation promotes unloading via structural degradation and bond weakening of intercepted snow.
  - c. Wind drag promotes unloading through shear stress applied to intercepted snow, wind erosion through direct entrainment in the atmosphere of intercepted snow, and branch movement.
  - d. Increasing air temperature promotes unloading by increasing the elasticity of branches and its association with melt and/or sublimation.

Since these processes occur simultaneously and could not be isolated experimentally, different combinations of the independent variables were included in the regression to identify which sets of processes significantly influenced unloading. The subcanopy lysimeter unloading measurements had a high relative instrument error due to the relatively small accumulation of unloaded snow over the 15-min intervals. To improve instrument accuracy, whilst maintaining consistency of the unloading measurements with the independent variables, the 15-min interval measurements of unloading were aggregated over differing predictive variable bins. Independent variable bins that had less than 0.1 mm of accumulated snow were removed, resulting in a mean instrument error of +/- 2% for the remaining bins. Air temperature and wind speed were measured at the FT station, canopy snow load from the weighed tree lysimeter (scaled to the canopy of each respective subcanopy lysimeter), and canopy snowmelt and sublimation simulated using CRHM with the CP25 model as described in the previous section. The individual processes found to be significant predictors of unloading in the multivariate regression (i.e., shear stress and canopy snow melt) were isolated to parameterise a model of their effects that was implemented in the CP25 model.

#### **4.3.7.1 Dry Snow Unloading**

Wind, shear stress, and canopy snow load were assessed as predictors of dry snow unloading during intervals without canopy snowmelt. These periods were defined using simulated canopy snowmelt in CRHM as well as visual analysis of time-lapse imagery for canopy snow drip and/or icicle formation. The relationships between wind speed, shear stress, canopy snow load, and unloading were analyzed using linear and non-linear least squares regressions, linearly with shear stress and exponentially with wind speed. The linear relationship between shear stress, canopy load, and unloading did not include an intercept term and was thus the coefficient of determination ( $R^2$ ) was adjusted following (Kozak & Kozak, 1995).

#### **4.3.7.2 Canopy Snowmelt Induced Unloading**

A mass balance approach was incorporated to determine the unloading rate resulting from canopy snowmelt ( $q_{unld}^{melt}$ ,  $\text{mm s}^{-1}$ ). The effect of the canopy snowmelt rate ( $q_{melt}$ ) on unloading was then assessed by fitting a linear model using an ordinary least squares regression. Since direct measurements of canopy snow unloading are challenging to obtain independently from canopy snowmelt drainage (Storck et al., 2002), the mass balance introduced in Equation 4.1 was incorporated to determine  $q_{unld}^{melt}$  as a residual. During intervals without  $[q_{sf} - q_{tf} + q_{ros}]$  or  $q_{wind}^{veg}$  Equation 4.1 was simplified and rearranged to:

$$q_{unld}^{melt} = -\frac{dL}{dt} - q_{drip} - q_{unld}^{dry} - q_{sub}^{veg} \quad (4.11)$$

While some components of the canopy snow mass balance can be measured directly, such as  $\frac{\Delta L}{\Delta t}$  with the weighed tree, sublimation of canopy snow is more difficult to quantify directly especially in forested mountain environments (Conway et al., 2018; Harding & Pomeroy, 1996; Helgason & Pomeroy, 2012b; Parviaainen & Pomeroy, 2000) and thus  $q_{sub}^{veg}$  was simulated in this study in CRHM using Equation 4.10 as described in Essery et al. (2003).  $q_{drip}$  was measured where possible using the rain gauges, however problems with freezing of liquid water in the tipping bucket mechanisms limited the ability to measure  $q_{drip}$  reliably. Thus,  $q_{drip}$  was also estimated using simulations of canopy snowmelt ( $q_{melt}$ ) in CRHM as in Equation 4.3, with storage limited by the canopy liquid water holding capacity and drainage of excess water. Canopy snow ablation periods that were dominated by melt were selected for calculating  $q_{unld}^{melt}$  where the contribution of  $q_{unld}^{dry}$  and  $q_{sub}^{veg}$  to canopy snow ablation was less than 5%.

## 4.4 Results

### 4.4.1 Unloading Relationships

Amongst the models evaluated, a multivariate linear regression incorporating canopy snow load, canopy snowmelt, and wind speed provided the highest explanatory power for predicting canopy snow unloading measured by subcanopy lysimeters ( $R^2 = 0.79$ ,  $p < 0.05$ ; Table 4.1). Shear stress was found to explain less variability compared to wind speed, when both were combined with canopy snow load and snowmelt ( $R^2 = 0.71$ ,  $p < 0.05$ ). Air temperature and canopy snow sublimation were not significant predictors in any model ( $p > 0.05$ ; Table 4.1). A model including only canopy load, air temperature, and wind speed produced an  $R^2$  of 0.11 however, only canopy load and wind speed were statistically significant ( $p < 0.05$ ). As shown in Figure 4.4, unloading rates varied more with snowmelt and sublimation (0–2 mm hr<sup>-1</sup>) than with air temperature and wind speed (0–0.5 mm hr<sup>-1</sup>).

The mean unloading rate was observed to increase with increasing canopy load, air temperature, ice-bulb temperature depression, shear stress, and wind speed (Figure 4.4). An increase in unloading was found with sublimation rates between 0–0.3 mm hr<sup>-1</sup> (Figure 4.4). For sublimation rates higher than 0.3 mm hr<sup>-1</sup>, unloading declined with sublimation. The decline in unloading with wind speed  $>3$  m s<sup>-1</sup> might have been contributed to by wind transport and entrainment into the atmosphere, and/or increased sublimation rates at higher wind speeds.

**Table 4.1:** Summary of multivariate linear regression results evaluating all combinations of predictor variables for canopy snow unloading including: canopy load ( $L$ ), wind speed ( $u$ ), canopy snowmelt rate ( $q_{melt}$ ), canopy snow sublimation rate ( $q_{subl}$ ), and air temperature ( $T_a$ ). Columns  $L$  to  $T_a$  show the coefficient estimate for each respective term, and the significance of each term is shown in brackets. Significance codes: \* =  $p < 0.05$ ; ns = not significant ( $p > 0.05$ ). The models are ranked by their corresponding AIC value.

Model									
Name	Intercept	$L$	$u$	$q_{melt}$	$q_{subl}$	$\tau$	$T_a$	$R^2$	AIC
M1	-0.11 (ns)	0.02 (*)	0.08 (*)	0.40 (*)	—	—	—	0.79	-12.8
M4	-0.08 (ns)	0.04 (*)	—	0.39 (*)	—	0.75 (*)	—	0.71	5.5
M7	0.13 (ns)	0.02 (*)	—	0.32 (*)	-0.22 (ns)	—	—	0.54	10.0
M10	-0.06 (ns)	0.02 (*)	0.08 (*)	0.38 (*)	—	—	0.00 (ns)	0.52	-4.4
M24	-0.00 (ns)	0.02 (*)	0.05 (*)	0.36 (*)	0.13 (ns)	—	—	0.37	-2.0
M40	0.07 (ns)	0.01 (*)	0.06 (*)	—	—	—	0.01 (ns)	0.11	2.4
M63	0.22 (*)	0.00 (ns)	-0.01	—	0.07 (ns)	—	—	-0.02	39.8
			(ns)						

#### 4.4.1.1 The Influence of Wind on Dry Snow Unloading

Canopy snow unloading measured from the subcanopy lysimeters—filtered to include intervals without canopy snowmelt—were positively associated in a linear relationship with shear stress and an exponential relationship with wind speed (Figure 4.5). The following equations were fitted to these relationships and tested.

The dry unloading rate,  $q_{unld}^{dry}$ , was represented as a linear function of shear stress:

$$q_{unld}^{dry} = L \cdot \tau_{mid} \cdot a \quad (4.12)$$

where  $\tau_{mid}$  is the shear stress at mid canopy height and  $a$  is a fitting constant.

An exponential function of wind speed was defined as:

$$q_{unld}^{dry} = L \cdot u_{mid} \cdot a \cdot e^{b \cdot u_{mid}} \quad (4.13)$$

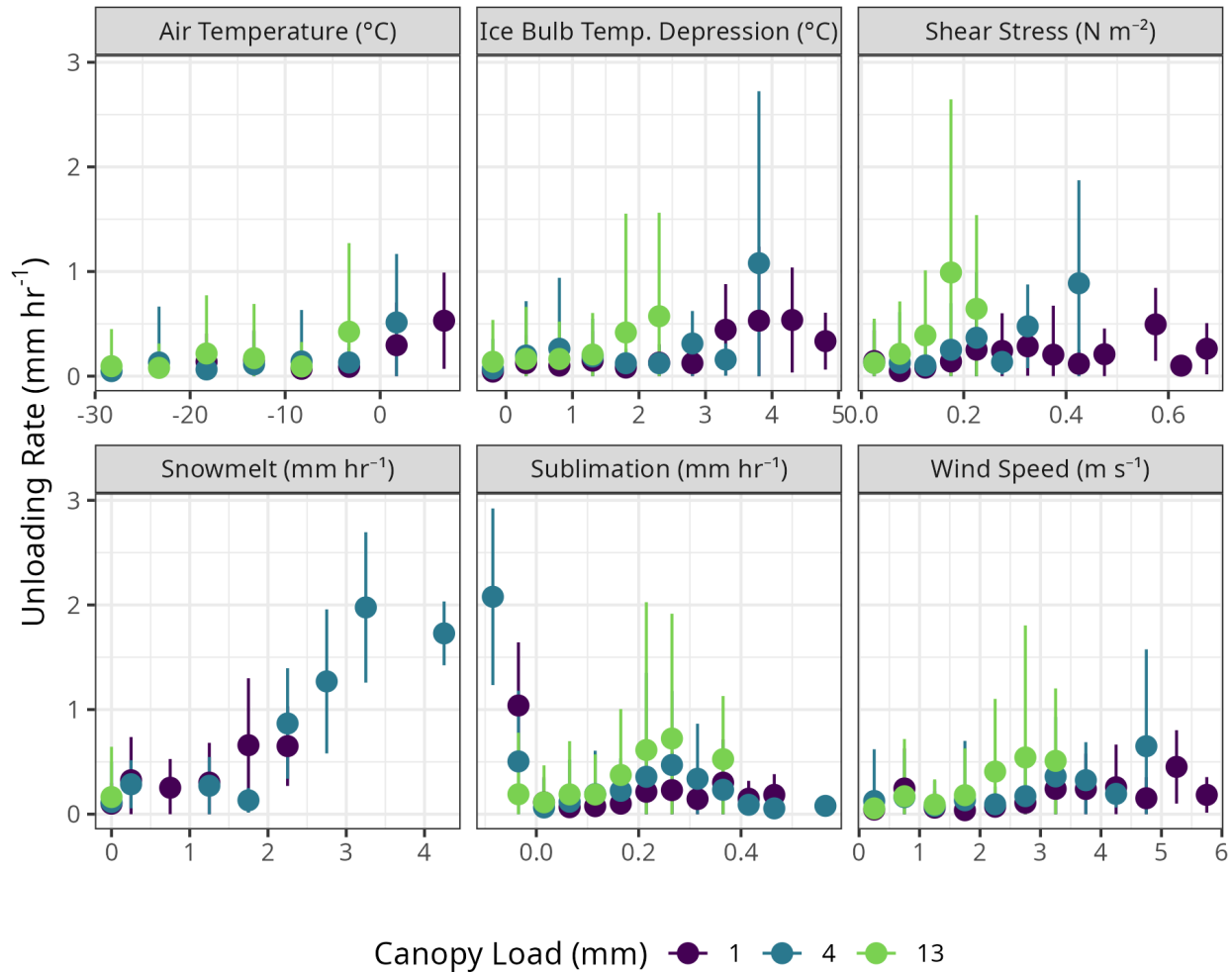


**Figure 4.4:** Scatter plots showing the mean unloading rate ( $\text{mm hr}^{-1}$ ) for differing bins of air temperature ( $^{\circ}\text{C}$ ), ice-bulb temperature depression ( $^{\circ}\text{C}$ ), shear stress ( $\text{N m}^{-2}$ ), canopy snowmelt ( $\text{mm hr}^{-1}$ ), canopy snow sublimation ( $\text{mm hr}^{-1}$ ), and wind speed ( $\text{m s}^{-1}$ ). Note: unloading was measured by the subcanopy lysimeters, air temperature and wind speed were measured at FT station, canopy snowmelt and sublimation were calculated using CRHM.

where  $u_{mid}$  is the wind speed at mid canopy height, and  $a$  and  $b$  are fitting constants.

The shear stress relationship (Equation 4.12) accounted for slightly more variability in unloading ( $p < 0.05$ ,  $R^2 = 0.61$ ) compared to wind speed ( $p < 0.05$ ,  $R^2 = 0.54$ ) (Table 4.2). The mean bias of the shear stress model of  $0.037 \text{ mm hr}^{-1}$  was also lower compared to the wind speed model of  $0.048 \text{ mm hr}^{-1}$ , additional model error statistics and fitting coefficients are provided in Table 4.2. Both models exhibited considerable scatter, with notable uncertainty resulting from instrument error and processes other than wind contributing to unloading (Figure 4.5). The wind-induced unloading rate was observed to be higher for greater canopy snow loads (Figure 4.5). The  $R^2$  of both the shear stress and wind speed relationships was much higher than the variance explained by wind speed when including intervals with melting snow (Table 4.1). The higher  $R^2$  of the shear stress model compared to wind speed, coupled with the better physical representation of kinetic energy, suggests that shear stress be selected as the independent variable to predict dry snow unloading in the model evaluation.

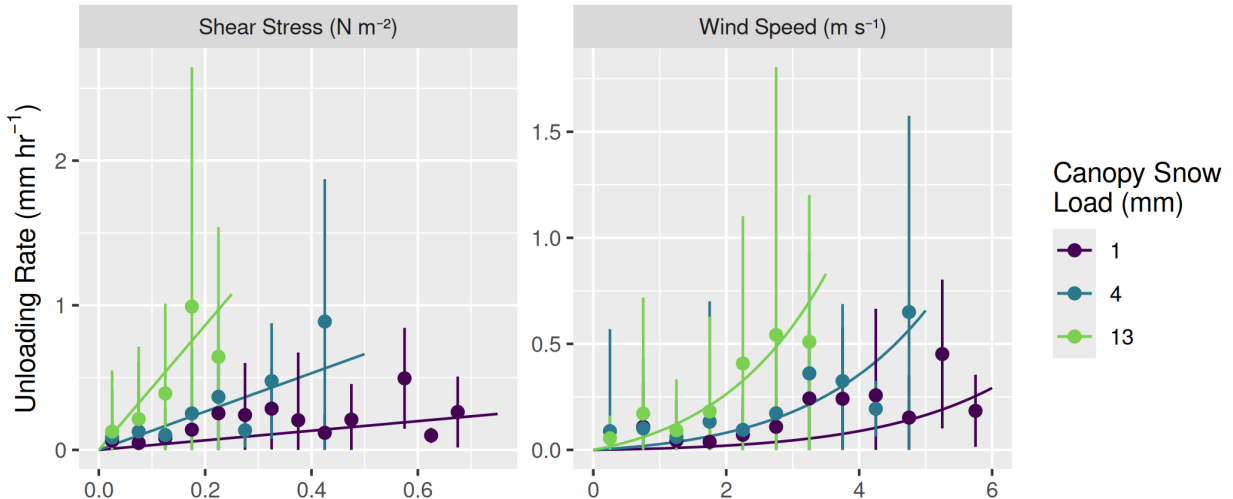


**Figure 4.5:** Canopy snow unloading rate measured by the subcanopy lysimeters versus shear stress (left) and wind speed (right) during periods without canopy snowmelt. The dots represent mean unloading rates within bins of shear stress and wind speed for three canopy snow load levels; error bars indicate  $\pm 1$  standard deviation. The fitted lines show predictions from Equation 4.12 (left) and Equation 4.13 (right).

**Table 4.2:** Summary of regression error statistics and coefficients for the relationship between canopy snow unloading with wind speed (Equation 4.12) and shear stress (Equation 4.13), as shown in Figure 4.5. Coefficients are shown for hourly unloading.

Metric	Wind	Shear Stress
Mean Bias (mm/hr)	0.048	0.037
Mean Absolute Error (mm/hr)	0.087	0.115
Root Mean Square Error (mm/hr)	0.11	0.15

**Table 4.2:** Summary of regression error statistics and coefficients for the relationship between canopy snow unloading with wind speed (Equation 4.12) and shear stress (Equation 4.13), as shown in Figure 4.5. Coefficients are shown for hourly unloading.

Metric	Wind	Shear Stress
Coefficient of Determination ( $R^2$ )	0.54	0.61
Coefficient a	$4.62 \times 10^{-03}$	$3.31 \times 10^{-01}$
Significance of a	$p < 0.05$	$p < 0.05$
Coefficient b	$3.93 \times 10^{-01}$	NA
Significance of b	$p < 0.05$	NA

#### 4.4.1.2 The Influence of Melt on Unloading

Five warm & humid events were selected, in which the median air temperature was above 0°C and relative humidity was above 65%, resulting in less than 5% contribution of dry snow unloading and sublimation to ablation as determined by the CP25 model. For these events, unloading was calculated using Equation 4.11 and canopy snowmelt rates were calculated using CRHM with Equation 4.3. These unloading estimates were found to be positively correlated with canopy snowmelt (Figure 4.6).

When canopy snow loads remained between 0 and 5 mm, the unloading-to-melt ratio varied from approximately 0 to 0.5. As snow loads increased, this ratio increased linearly, reaching its peak value of 5.0 for a canopy snow load of 30 mm (Figure 4.6). This relationship can be expressed through a linear function:

$$q_{unld}^{melt} = R \cdot q_{melt}(L) \quad (4.14)$$

where  $R$  represents the unloading-to-snowmelt ratio and  $q_{melt}$  is the canopy snowmelt rate ( $\text{mm hr}^{-1}$ ). Equation 4.14 is similar to Equation 33 in Andreadis et al. (2009); however, instead of a constant value of 0.4 for  $R$ , it was determined as:

$$R = m \cdot L + b \quad (4.15)$$

where  $m$  and  $b$  were determined as 0.16 and -0.5, respectively, using an ordinary least squares regression. Equation 4.14 using these fitted parameters resulted in a statistically significant relationship ( $p < 0.05$ ,  $R^2 = 0.73$ ) (Figure 4.6). Additional observations of canopy snowmelt from the subcanopy rain gauges were also used to estimate  $R$  (Figure 4.6). The number of usable observations was limited to three events (out of the 5 warm & humid events) due to freeze-thaw events that seized up the tipping bucket mechanisms in the rain gauges, however, these measurements are still useful in providing some validation of the CRHM

canopy snowmelt/drip calculations (Figure 4.7). The CRHM-estimated cumulative drip was higher than the subcanopy rain gauges for two out of the three melt events. Differences in the timing and magnitude of the observed and simulated values were expected due to both instrument uncertainties in the rain gauges from freezing of rain gauges and thawing of snow in the collection funnels, and in the canopy snow energy balance simulation.

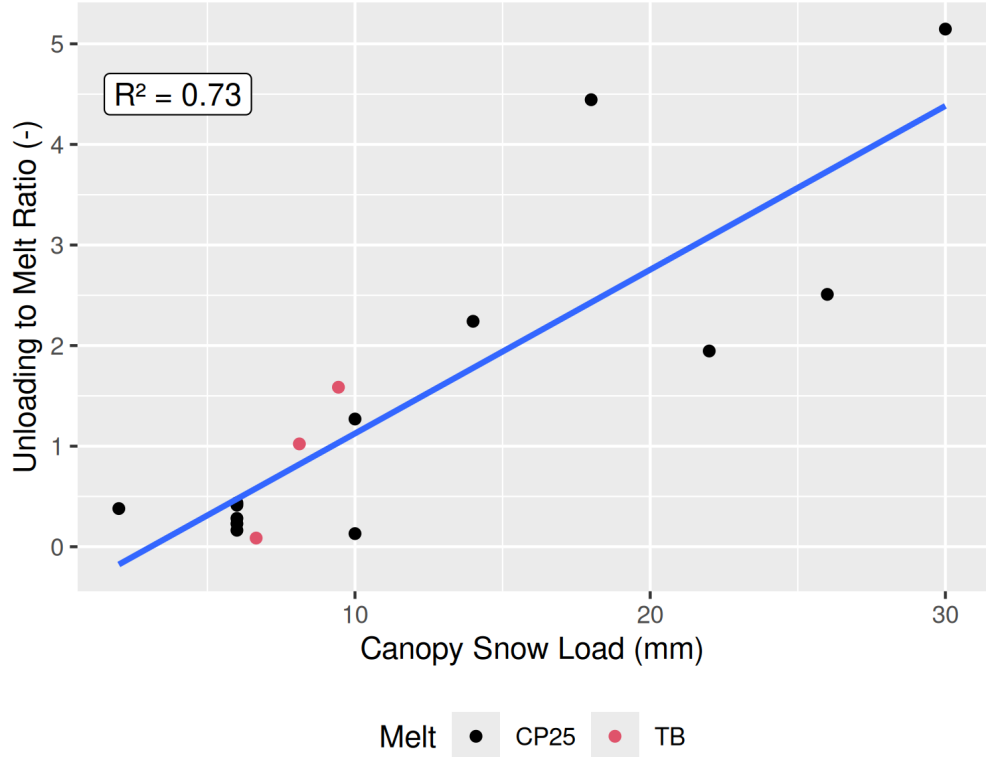


**Figure 4.6:** The ratio of canopy snow unloading (weighed tree residual) to snowmelt across different canopy snow load bins and events. Black dots represent the observed cumulative unloading divided by the cumulative simulated snowmelt from the updated CP25 canopy snow routine in CRHM for each of the five warm & humid events. Red dots show the cumulative observed unloading divided by snowmelt measured by the rain gauges. Multiple dots within a bin correspond to different events. The blue line represents the best-fit line derived from ordinary least squares regression.

#### 4.4.2 New Canopy Snow Model

The CP25 model is based on the canopy snow mass balance formulation (Equation 4.1), where  $q_{tf}$  was represented as:

$$q_{tf} = [(1 - C_p)\alpha]q_{sf} \quad (4.16)$$

where  $C_p$  is the leaf contact area calculated using Equation 10 in Cebulski & Pomeroy (2025b) and  $\alpha$  is

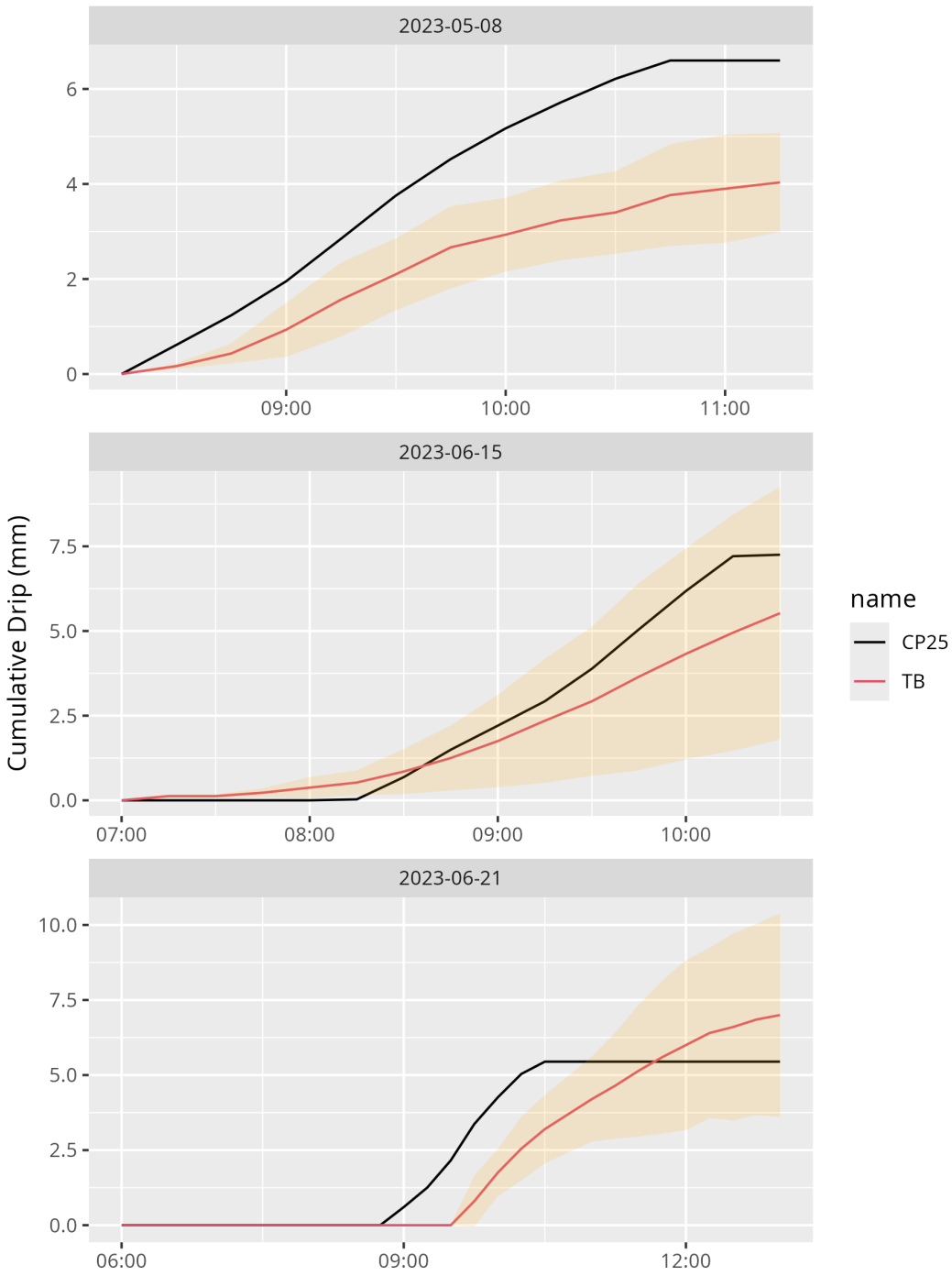


**Figure 4.7:** Cumulative canopy snow drip measured by the average of four subcanopy tipping bucket rain gauges (TB) and simulated using the CRHM CP25 model (Equation 4.3). Yellow shading indicates the range of  $\pm 1$  standard deviation amongst the individual rain gauge measurements.

an efficiency constant. Melt-driven unloading ( $q_{unld}^{melt}$ ) was modelled using Equation 4.14, while dry snow unloading ( $q_{unld}^{dry}$ ) was represented using Equation 4.12. Canopy snow drip ( $q_{drip}$ ) is derived from calculations of canopy snowmelt from Equation 4.3, with storage limited by the canopy liquid water holding capacity computed from Equation 4.2; any excess was assumed to immediately drain. Wind transport of canopy snow ( $q_{wind}^{veg}$ ) is incorporated in the Equation 4.12 calculation. Sublimation of intercepted snow ( $q_{veg}^{sub}$ ) was represented using Equation 4.10.

#### 4.4.3 Event-based Evaluation of Canopy Snow Ablation Models

The updated canopy snow model (CP25), as well as the existing models R01, SA09, and E10 were evaluated using weighed tree lysimeter measurements of canopy load during seventeen canopy snow ablation events. The seventeen ablation events had air temperatures ranging from -30.5°C to +6.9°C and wind speeds from calm to 5.3 m s<sup>-1</sup> (Figure 4.8). This range of meteorological conditions is particularly wide and spans conditions typical of the cold boreal to temperate maritime needleleaf forests. Events were classified as cold & dry, cold & humid, warm & dry, and warm & humid based on the median event air temperature (above or below 0°C) and relative humidity (above or below 65%) (Figure 4.8).

Simulated canopy snow load by the CP25 model closely matched the observations for all 17 events, demonstrating the most consistent agreement amongst the models evaluated (Figure 4.9). The large declines in canopy snow load for E10 (Figure 4.9) are due to the maximum canopy snow load used in this model which ranged from 7 to 12 mm depending on the fresh snow density (a function of air temperature in Hedstrom & Pomeroy, 1998).

The energy balance-based snowmelt modelling approaches (CP25 & SA09) yielded the most accurate representation of canopy snowmelt over the warm & humid events. The CP25 mean bias of 0.02 mm hr<sup>-1</sup>, which was smaller than the -0.11 mm hr<sup>-1</sup> bias associated with SA09 (Figure 4.10). The improvement for CP25 over SA09 comes from its representation of the increase in unloading at higher canopy snow loads (Figure 4.6), as observed for the 2022-06-14 event (Figure 4.9). The air temperature (R01) and ice-bulb temperature (E10) models produced a wider range of mean biases (Figure 4.10) and larger mean bias of over 0.42 mm hr<sup>-1</sup> during the warm & humid events, compared to CP25 and SA09. The rate of ablation was slower for canopy snow loads below ~1.5 mm and ~0.3 mm for CP25 and SA09 respectively; due to their differing liquid water storage capacities (Figure 4.9). For the warm events other than 2022-04-23, the observed decline in ablation rate occurs around 2 to 3 mm, exceeding the threshold predicted by all models.

The warm & dry events had consistent performance with mean biases of 0.02 mm hr<sup>-1</sup> for each of the four models (Figure 4.10). Initiation of ablation was delayed compared to observations from the weighed tree for the CP25 and SA09 models for all three of the warm & dry events (Figure 4.9). The temperature threshold methods (E10 & R01) achieved better timing on the onset of ablation for two events (2022-03-29 and 2022-

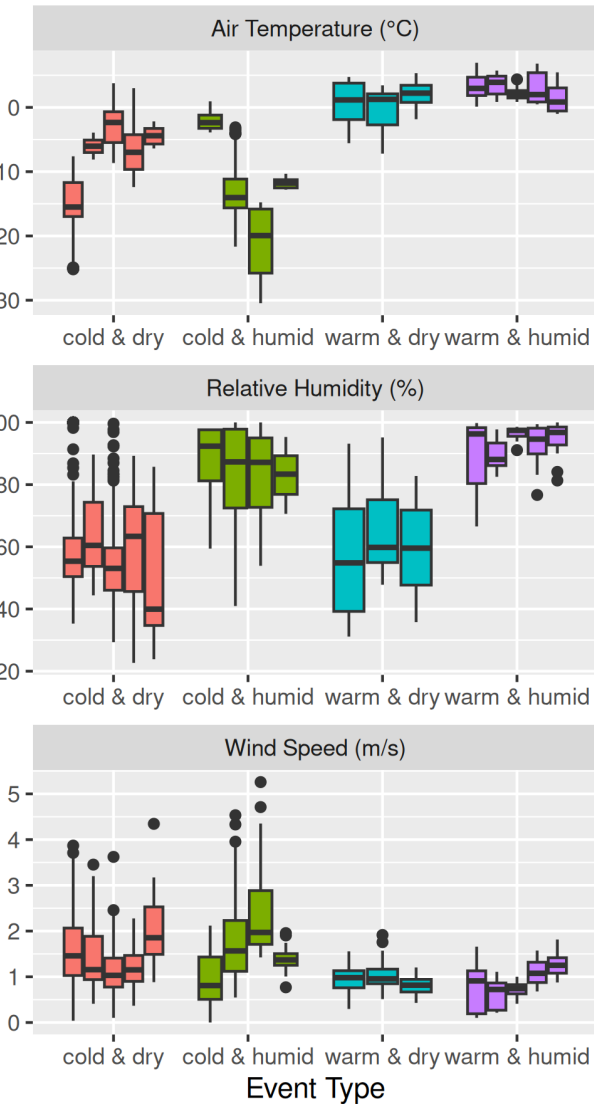


**Figure 4.8:** Boxplots showing the distribution of meteorological measurements of air temperature, relative humidity, and wind speed over each of the seventeen select ablation events. Air temperature, relative humidity, and wind speed were measured at FT station. Note: the rectangle vertical extent represents the interquartile range (25<sup>th</sup> to 75<sup>th</sup> percentile), the horizontal line within each box indicates the median, and the whiskers extend to 1.5 times the interquartile range. Circular points beyond the whiskers represent outliers.

04-21) compared to CP25. However, E10 initiated the onset of ablation slightly earlier for 2022-04-23 and the rate of ablation was also lower than observed for this event.

For the cold & dry events, all models had accurate performance with mean biases ranging from -0.01 to 0.01 mm hr<sup>-1</sup>, with a slight improvement in the mean bias for CP25 of -0.009 mm hr<sup>-1</sup> (Figure 4.10). Canopy snowmelt was overestimated by the E10 model and caused the steep initial decline in canopy snow load on 2022-03-02 which is not registered by the weighed tree or other models. However, underestimates of ablation compensated for this overestimate over the remaining cold & dry events—which had moderate wind speeds—as wind-driven unloading is not included in the E10 model (Figure 4.8). For events 2022-03-02 and 2023-03-14 the R01 model overestimated canopy snow ablation due to an overestimation of wind-driven unloading (Figure 4.9).

The importance of representing wind-driven unloading was clear during the cold & humid events, where the mean bias of models including this mechanism was reduced compared to other approaches; for example, 0.04 mm hr<sup>-1</sup> for R01 and 0.15 mm hr<sup>-1</sup> for CP25. In contrast, simulations that did not explicitly account for wind-driven unloading exhibited higher biases, exceeding 0.32 mm hr<sup>-1</sup> (Figure 4.10). Although the E10 model does not include wind-driven unloading, it performed best for the 2023-02-26 event due to its relatively slow time-based unloading rate compared to CP25 and R01 which overestimate ablation for this event (Figure 4.9). The R01 model overestimated unloading over most of the cold & humid events and had a higher median bias for the cold & humid events compared to CP25 (Figure 4.10). The CP25 model had consistently lower bias across the three cold & humid events, but still underestimated ablation for the 2023-02-24 event which had peak wind speeds of over 5 m s<sup>-1</sup>. Over this event, 1.3 mm of snow was measured at a shielded precipitation gauge in a nearby clearing and was likely derived from wind transport of snow from the canopy, as clear skies with no precipitation were observed. The amount of snow observed to unload from the canopy into the subcanopy lysimeters during this event was consistent with simulated unloading in CRHM suggesting that the remaining unaccounted-for snow was likely entrained into the atmosphere and sublimated and/or transported to distant sites.

#### 4.4.4 Canopy Snow Partitioning

During warm & humid events, all four parameterisations showed relatively consistent partitioning of canopy snow, with only a small fraction returned to the atmosphere (Figure 4.11). The warm & dry events had greater variability in the partitioning of intercepted snow—when compared to the warm & humid events—with a larger contribution from sublimation and evaporation processes. Increased unloading from the E10 model resulted in a greater fraction of intercepted snow reaching the ground compared to the CP25 model over the warm & dry events.

For the cold & dry and cold & humid events, the two parameterisations that include wind-driven unloading

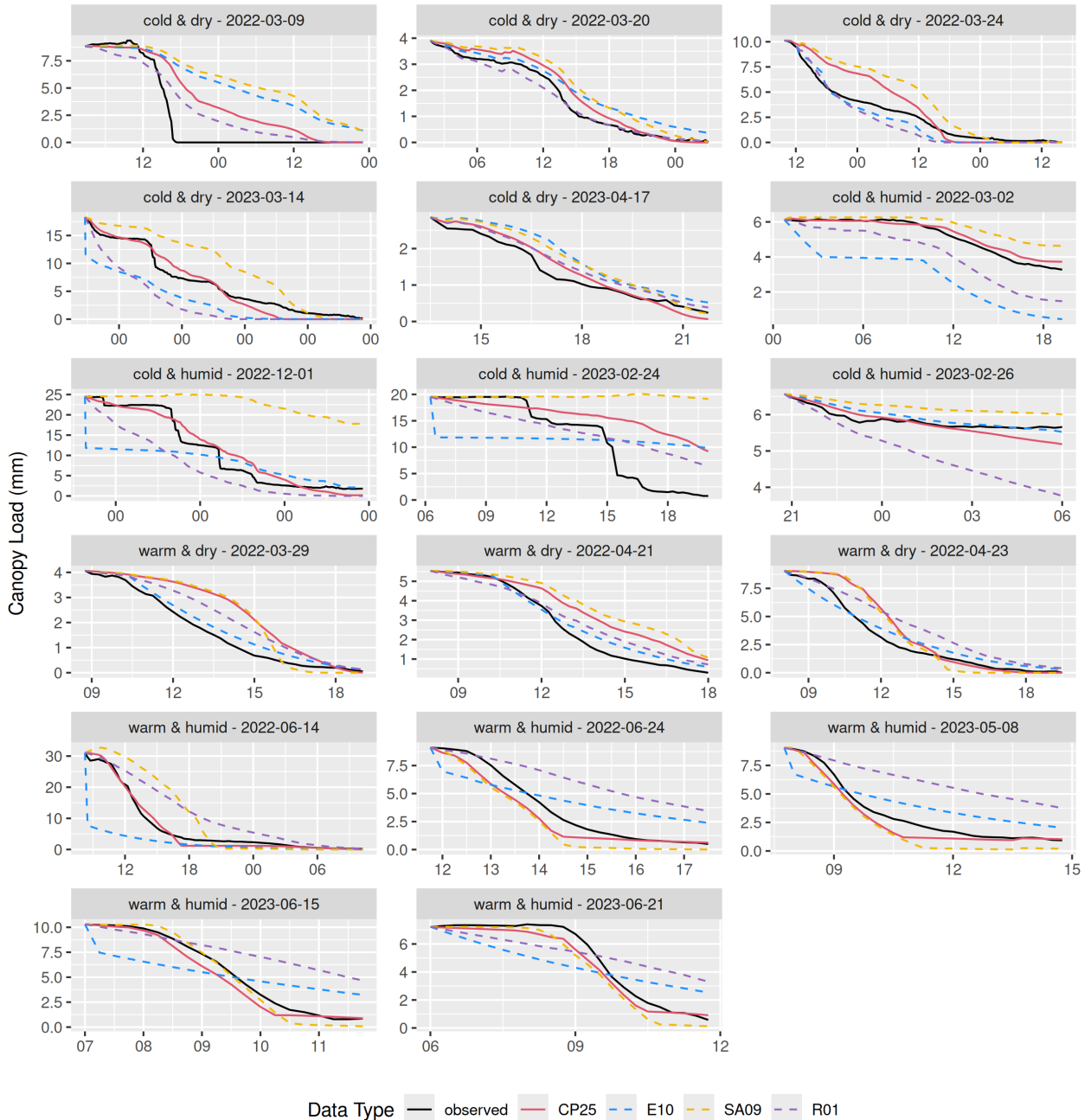


**Figure 4.9:** Time series of canopy snow load for individual events measured by the weighed tree (observed) and simulated using the four canopy snow models.

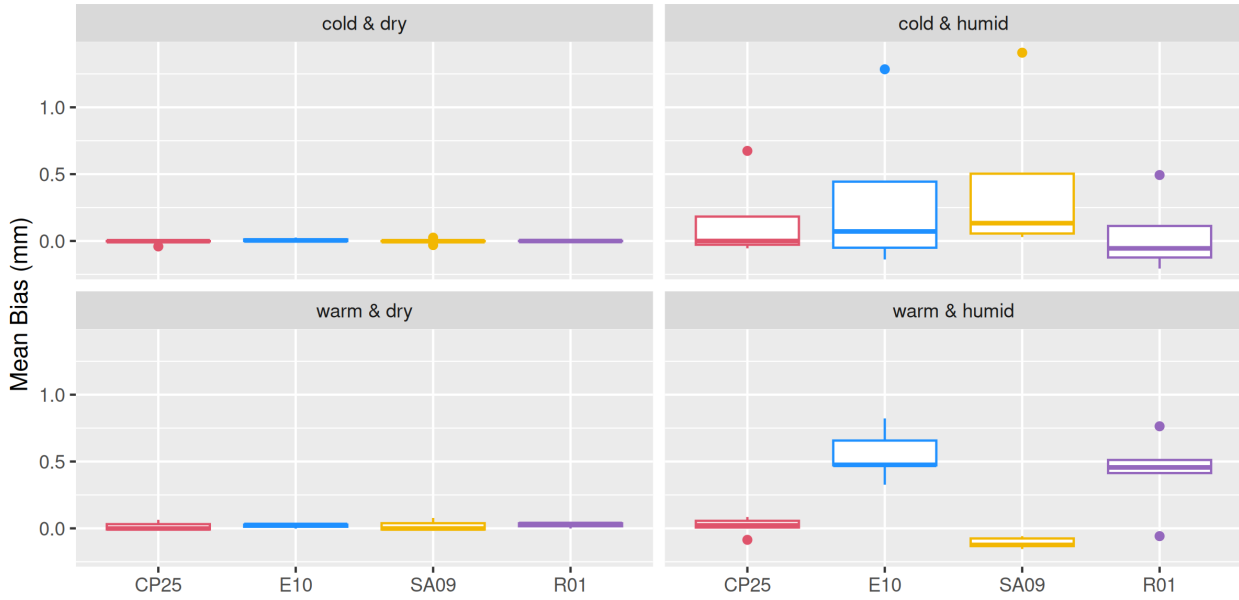


**Figure 4.10:** Boxplots illustrating the distribution of event mean biases calculated between simulations of canopy snowload and observations from the weighed tree. The vertical extent of each rectangle represents the interquartile range (25<sup>th</sup> to 75<sup>th</sup> percentile), the horizontal line within each box indicates the median, and the whiskers extend to 1.5 times the interquartile range. Circular points beyond the whiskers represent outliers. The diamonds represent the mean of the event biases.

(R01 and CP25) had differing fractions of snow partitioned to the ground via unloading. A higher fraction of intercepted snow reached the ground for R01 due to the higher dry snow unloading rate compared to CP25 over all of the cold events. For both the cold & dry and cold & humid events SA09 partitioned all snow back to the atmosphere via sublimation as dry snow unloading is not included in this parameterisation. Although CP25 and E10 include differing unloading processes, when averaged over all events, both had a similar fraction of snow reaching the ground (70%) versus the atmosphere (30%) (Table 4.3). SA09 has the largest discrepancy which returned 40% of intercepted snow back to the atmosphere and the R01 with the least amount of snow reaching the atmosphere with 24%.

**Table 4.3:** Fraction of canopy-intercepted snow returned to the atmosphere as sublimation and evaporation of melted snow or input to the ground as unloading or drip of melted snow for each parameterisation over the 17 select ablation events.

Model	Atmosphere (-)	Ground (-)
CP25	0.29	0.71
E10	0.31	0.69
R01	0.24	0.76
SA09	0.40	0.60

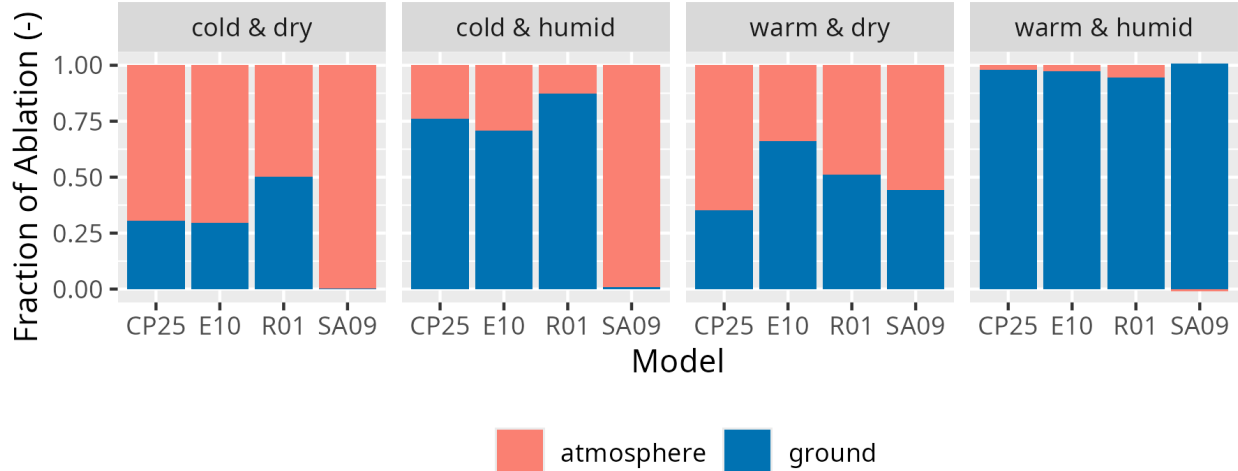


**Figure 4.11:** Bar chart illustrating the proportion of intercepted snow that was either lost to the atmosphere as sublimation and/or evaporation of melted snow or transferred to the ground through unloading or drip of melted snow by each event type for all 17 events.

## 4.5 Discussion

### 4.5.1 Processes Governing Canopy Snow Unloading

Observations of canopy snow unloading support the hypothesis that unloading is primarily controlled by snowmelt and dry-snow related processes, both of which are also influenced by the amount of snow intercepted in the canopy (Table 4.1). The ratio of unloading to canopy snowmelt was found to increase linearly with increasing canopy snow load (Figure 4.6), which differs from Storck et al. (2002) who originally found the ratio of canopy snow unloading to melt to be constant at 0.4. The measurement difficulties noted by Storck et al. (2002) limited their estimate of this ratio to a single mid-December event, preventing any association with canopy snow load. Similar instrument difficulties here in measuring canopy snowmelt drainage limited direct measurements to three events and hybrid measurements (from Equation 4.11) to 5 events (Figure 4.6). The reasonable correspondence between observed and modelled canopy snow drip for these events supports the linear increase hypothesis (Figure 4.7). Previous studies have identified relationships between melt-induced unloading and various meteorological parameters, including empirical functions of air temperature (Katsushima et al., 2023; Roesch et al., 2001), ice-bulb temperature (Ellis et al., 2010; Floyd, 2012), and solar radiation (Katsushima et al., 2023). Although branch bending and subsequent unloading has been shown to be associated with air temperature (Schmidt & Gluns, 1991; Schmidt & Pomeroy, 1990), observations here indicate that temperature-related unloading increases occur primarily near the freezing point (Figure 4.4), eliminating the need for a separate temperature parameterisation beyond snowmelt-associated unloading processes.

Dry snow unloading was found to increase exponentially with wind speed and linearly with shear stress (Table 4.2). These results differ from earlier research that has represented this process as a linear function of wind speed and canopy load (Bartlett & Verseghy, 2015; Katsushima et al., 2023; Roesch et al., 2001), as shown in Figure 4.1. The higher  $R^2$  found for shear stress compared to wind speed for predicting unloading—when excluding melt events—is likely due to the physical relationship between shear stress force and kinetic energy transfer to the canopy, wind transport from the canopy, and movement of branches in the canopy induced by drag (shear) forces. The differing relationship presented here, compared to the R01 model (Figure 4.1), may be attributed to the development of that parameterisation using above canopy albedo as a proxy for canopy snow unloading (Bartlett & Verseghy, 2015; Roesch et al., 2001). This approach would have included both unloading and sublimation processes, in addition to greater measurement uncertainties (Cebulski & Pomeroy, 2025a). Conversely, the subcanopy lysimeter measurements employed here provided a more direct quantification of canopy snow unloading rates. Simulated unloading over events classified as cold & humid—which had the largest contribution of wind-driven unloading—resulted in the highest overall mean biases compared to the warm & dry, warm & humid, and cold & dry events (Figure 4.10). Additional factors that may influence dry snow unloading that are not considered in the new parameterisation (Equation 4.13) include wind erosion, branch movement, structural degradation, bond weakening, increased elasticity of branches, snow density, and liquid water content. The addition of liquid water content in the canopy snow due to phase change can increase cohesion and adhesion of snow clumps within the canopy (Pomeroy & Gray, 1995). However, high liquid water contents during rapid melt can lubricate the snow attachment to the canopy and weaken cohesive bonds, inducing unloading, much as for wet snow avalanches (Baggi & Schweizer, 2008).

The density of snow intercepted in the canopy is expected to influence both dry snow and melt-induced unloading processes—and is incorporated in the E10 parameterisation for the initial accumulation component based on the findings of Schmidt & Gluns (1991)—but is not explicitly represented in any of the ablation calculations included in this study. Fresh, low-density snow typically exhibits lower cohesion and adhesion compared to older snow, which may have undergone freeze-thaw cycles or equitemperature metamorphism, processes that increase snow density and bond strength hence, increasing the mechanical resistance to unloading. While vapour deposition and rime-ice accumulation are simulated in some models (e.g., Clark et al., 2015b; Ellis et al., 2010) via the latent heat flux parameterisation, they are usually treated as additions to the canopy snow reservoir. However, in humid or maritime regions rime can form dense, ice-like structures (e.g., Berndt & Fowler, 1969) with high resistance to unloading by either melt or wind (Lumbrazo et al., 2022). Although canopy snow density is expected to influence ablation processes, it was not observed in this study due to its continental location and remains a research gap for maritime climates.

The relationship between unloading and canopy snow sublimation was not statistically significant (Figure 4.4). This differs from earlier work by MacDonald (2010) who found an association between these two variables

and attributed this to the reduction in structural integrity and bond weakening of the canopy snow clumps as snow particles are removed through sublimation. It is possible that the association identified by MacDonald (2010) arose from the concurrent increase in canopy energy inputs that promote both sublimation and other ablation mechanisms such as melt and other dry snow unloading processes which were not directly accounted for.

#### 4.5.2 Performance Comparison of Ablation Models

The improved performance of the new CP25 model across a wide range of meteorological conditions demonstrates the advantages of incorporating comprehensive snow unloading processes coupled with physically based representations of the energy balance to simulate ablation (Figure 4.9). In contrast, existing models were limited by missing processes such as wind-driven unloading (SA09 and E10) or relied on temperature-dependent parameterisations of melt and drip processes which had limited transferability across differing events (R01 and E10). Although the SA09 model—originally developed in a relatively warm maritime climate with limited wind influence (Storck et al., 2002)—performed similarly well to CP25 during most of the melt-dominated events, its exclusion of wind-induced unloading led to poor performance for the cold & dry and cold & humid events. This process omission caused SA09 to overestimate sublimation when averaged over all events (Table 4.3). Moreover, the constant canopy snow unloading to melt ratio of 0.4 in the SA09 model led to reduced performance for one melt event with canopy snow loads up to 30 mm, whereas the CP25 model more accurately predicted ablation over this event. The low liquid water retention capacity implemented in SA09 also contributed to an underestimation of canopy loads during the end of most melt events (Figure 4.9).

Models utilising temperature-based canopy snowmelt parameterisations (E10 and R01) exhibited inconsistent performance, particularly during warm & humid events where they underestimated ablation. This was due to their reliance on air temperature or ice-bulb temperature as proxies for energy input into the canopy, which failed to represent the energy availability over these events. In contrast, all four models performed similarly during warm & dry events, where air temperatures were closer to 0°C. The superior performance of the energy balance-based canopy snowmelt models (CP25 and SA09) during warm & humid events likely reflects their ability to represent the elevated energy inputs which were present over the warmer events.

While E10 omitted any explicit representation of wind-driven unloading, its exponential time decay parameterisation indirectly addressed this process, though it still underestimated overall ablation for the cold events which had higher wind speeds (Figure 4.9). The maximum canopy snow load threshold implemented in the E10 model was lower than observations from the weighed tree. This limitation offset its tendency to underestimate unloading processes as was also observed by Lundquist et al. (2021) and Lumbrago et al. (2022). In this study, the CP25, SA09, and R01 models did not include a maximum snow load, and their performance aligns with the hypothesis of Lundquist et al. (2021) that this limit may be unnecessary—or

much higher than previously though—when combined with a comprehensive canopy snow ablation routine. In contrast, R01 consistently overestimated wind-driven unloading during both the cold & dry and cold & humid events, potentially due to the differing methodology used to develop this parameterisation (Figure 4.9). CP25 provided a better representation of wind-driven unloading compared to R01 aside from one event with high wind speeds ( $>5 \text{ m s}^{-1}$ )—that cause wind redistribution/entrainment of snow into the atmosphere. Wind unloading parameters also may be influenced by tree species, forest structure, and snow characteristics (Lumbrazo et al., 2022), necessitating further field-based research on canopy snow unloading in diverse environments to assess their broader applicability.

The infrequent occurrence of wind-transport from the canopy in our observations may account for underestimation of ablation during one strongly wind-dominated events by CP25 (2023-02-24, Figure 4.9). Wind transport of canopy snow to the nearby Powerline snowfall gauge occurred during this event, but was a small fraction of canopy snow ablation, 1.3 mm of a total of 20 mm of canopy snow ablation. Since unloading measured by the subcanopy lysimeters corresponded well with CP25 predictions for this event, the approximately 9 mm of unaccounted canopy snow ablation may be attributed to uncertainties within the wind-driven unloading parameterisation (Figure 4.5) and possible atmospheric entrainment of canopy snow that was either transported to distant locations and/or sublimated. These findings align with observations by Troendle (1983) but contrast with Hoover & Leaf (1967), who proposed that most wind-transported snow relocates to nearby sites with minimal sublimation effects.

### 4.5.3 Canopy Snow Partitioning

Substantial variability was found in the fraction of snow that sublimated and/or evaporated as liquid meltwater versus unloading and drip depending on the canopy snow ablation model selected (Figure 4.11). For example, the exclusion of wind-driven unloading processes in the SA09 model resulted in 100% of intercepted snow reaching the atmosphere for both the cold & dry and cold & humid events. This differed considerably from the CP25 model which returned 70% and 24% of snow back to the atmosphere for the cold & dry and cold & humid events, respectively. Although E10 and CP25 include differing process representations, they predicted comparable fractions of snow reaching the ground versus returning to the atmosphere. The agreement between CP25 and E10 is notable, since the E10 has been tested and found to perform well in predicting subcanopy snowpacks around the world (Ellis et al., 2010; Gelfan et al., 2004; Pomeroy et al., 2022; Sanmiguel-Vallelado et al., 2022b). However, the results shown here reveal that E10's individual process representations can be in error, particularly under warm and windy conditions, potentially explaining the difficulties when applying E10 at locations where parameterisation errors fail to offset one another (Lumbrazo et al., 2022; Lundquist et al., 2021). For example, at locations which intercept a larger amount of snow, the E10 maximum canopy snow load would overestimate the amount of unloading, and a greater deviation between the E10 and CP25 model is expected.

#### 4.5.4 Future Directions

Physically based approaches such as CP25 are particularly relevant for predictions of snow hydrology under a changing climate, where warming may reduce the reliability of empirically derived canopy snowmelt models like E10 and R01. The improved representation of melt events by CP25 and SA09 demonstrates the reliability of more physically based methods across a range of meteorological conditions, compared to temperature-based canopy snowmelt routines (E10 and R01) which had reduced performance over these events. Amongst all canopy snow ablation processes, dry snow unloading introduced the most uncertainty. Although the revised model performed best for this dataset, further validation is required across a wider range of climates and forest structures. Since unloading, melt, and sublimation are competitive ablation processes, they strongly influence whether snow is returned to the atmosphere or reaches the ground.

Key limitations remain in measuring canopy snow sublimation using eddy correlation systems (Conway et al., 2018; Harding & Pomeroy, 1996; Harvey et al., 2025; Helgason & Pomeroy, 2012b; Parviainen & Pomeroy, 2000) and separating snow unloading from meltwater drip (Floyd, 2012; Storck et al., 2002), which limit the development and testing of canopy snow ablation parameterisations. Whilst separating initial interception and ablation processes (Cebulski & Pomeroy, 2025a; Cebulski & Pomeroy, 2025b), will improve process representations, these routines still need to be evaluated together against additional field observations. Incorporating the updated unloading schemes developed here could improve the representation of canopy snow ablation and, by extension, the partitioning of precipitation and canopy albedo in hydrological and land surface models. Nonetheless, further testing is needed across different sites, climates, forest types, and spatial scales to assess model transferability and performance.

### 4.6 Conclusions

Canopy snow ablation processes govern the timing and partitioning of snowfall to the ground versus the atmosphere in forested environments, yet their representation in modelling frameworks remains uncertain due to insufficient process-level validation. This study evaluates existing canopy snow ablation theories using in-situ measurements of canopy snow load, unloading, and drip combined with a novel canopy snow energy and mass balance model. These observations revealed that canopy snow load, wind shear stress, and canopy snowmelt were statistically significant predictors of snow unloading, collectively explaining 80% of its variability. In addition to this empirical evidence, physical processes such as structural degradation, snow particle bond weakening, lubrication of wet canopy snow during melt, and the shear force exerted on canopy snow by wind further support representing these processes. Although some studies use air temperature as an index of unloading resulting from canopy snowmelt and potential branch bending, here energy balance methodologies show improved performance in simulating canopy load during melt events.

Previous studies have demonstrated relationships between unloading and snow load, wind speed, and canopy

snowmelt rate, but these processes have not been evaluated collectively. This study represents the first development and validation of an unloading model addressing both energy balance-based melt and dry snow unloading processes together. Novel parameterisations for dry snow and melt-induced unloading were introduced, with key differences from previously established approaches. Shear stress was found to be a stronger predictor of dry snow unloading ( $R^2 = 0.61$ ) than wind speed ( $R^2 = 0.54$ ) for non-melt periods. The canopy melt rate exerted the strongest control on snow unloading during melt events, consistent with one existing model. A new finding was that the ratio of unloading to canopy snowmelt increased with canopy snow load. Additionally, an existing approach which used the concept of a maximum intercepted snow load greatly underestimated the canopy snow storage capacity when compared to observed snow loads from weighed tree measurements. Throughout the two-years of observations presented here, a maximum canopy snow load was not observed, likely as unloading rates increased with higher snow loads. Wind transport events were relatively rare in this wind-exposed subalpine forest, but resulted in a considerable underestimation of the amount of snow returned to the atmosphere or surrounding sites during one event.

A new canopy snow ablation model that integrates an updated canopy snow mass and energy balance demonstrated improved accuracy across varied meteorological conditions compared to existing approaches. Existing models failed to maintain accuracy across events with a wide range of meteorology due to neglect of key processes and/or empirical representations of melt processes. The greatest inter-model discrepancies in canopy snow load occurred during warm and humid events, where temperature-based canopy snowmelt parameterisations showed substantially higher mean biases relative to energy balance-based models.

Amongst the models tested, the largest errors were found during cold & dry unloading events—though performance was improved when incorporating a site-specific shear stress-based parameterisation. Partitioning of intercepted snow disposition between the ground and atmosphere varied most amongst cold events, where neglecting the dry snow unloading process resulted in considerable overestimates of canopy snow sublimation losses. All canopy snow models had greater consistency in partitioning canopy snow during warm & humid events, where all canopy snow was typically unloaded or melted as drip towards the ground surface. However, the rate of unloading was best represented by energy balance-based canopy snowmelt routines compared to empirical relationships. Although improved performance was found for the updated canopy snow ablation model compared to existing methods, across a wide range of meteorological conditions, additional testing across various climate and forest compositions is required to assess model transferability.

## 4.7 Acknowledgements

We acknowledge financial support from the University of Saskatchewan Dean's Scholarship, the Natural Sciences and Engineering Research Council of Canada's Discovery Grants, the Canada First Research Excellence Fund's Global Water Futures Programme, Environment and Climate Change Canada, Alberta Innovates Wa-

ter Innovation Program, the Canada Foundation for Innovation’s Global Water Futures Observatories facility, and the Canada Research Chairs Programme. We thank Madison Harasyn, Hannah Koslowsky, Kieran Lehan, Lindsey Langs and Fortress Mountain Resort for their help in the field and Tom Brown and Logan Fang for support of the CRHM platform.

## 4.8 Data & Software Availability Statement

The Cold Regions Hydrological Model Platform (CRHM) source code is available at <https://github.com/srlabUsask/crhmcode>. Model forcing data, model outputs, validation data, processed data, and scripts are available at <https://doi.org/10.5281/zenodo.16898881>.

# 5 EVALUATION OF A NEW NEEDLELEAF FOREST SNOWPACK MODEL FOR DIAGNOSING SNOW ACCUMULATION REGIMES IN WESTERN AND NORTHERN CANADA

Manuscript status: Analysis is complete and manuscript is currently in progress. Anticipated submission is to the journal *Hydrological Processes* Fall, 2025.

Citation: Cebulski, A. C., Pomeroy, J. W., Floyd, W. C. (in prep.). Evaluation of a New Needleleaf Forest Snowpack Model for Diagnosing Snow Accumulation Regimes in Western and Northern Canada. *Hydrological Processes*, 12, e70010. <https://doi.org/10.1002/wat2.70010>

Role in thesis: This journal article corresponds to research question 2.1 of the thesis, the model implementation and testing phase. New parameterisations and process understanding of snow interception and ablation processes from chapters 1, 2 and 3 will incorporated into the Cold Regions Hydrological Model (CRHM) platform to model forest snow accumulation at four research basins in western Canada. The updated parameterisations will be evaluated by including them in an updated CRHM canopy module. Simulated SWE using this updated module will be compared to observed SWE at a point within the forest of each research basin.

## 5.1 Abstract

## 5.2 Introduction

Snow is an important water resource, directly supporting over two billion people globally (Immerzeel et al., 2020; Vivioli et al., 2020), while also affecting earths energy balance via surface albedo (Thackeray et al., 2014; Wang et al., 2016) and stream temperatures (e.g., Leach & Moore, 2014). However, snowpacks are increasingly threatened due to changes in both climate and vegetation cover worldwide (Immerzeel et al., 2020; López-Moreno et al., 2014; Vivioli et al., 2020). In cold-dry climates, sublimation of snow intercepted by forest canopies can return up to 45% of seasonal snowfall back to the atmosphere (Essery et al., 2003; Sanmiguel-Vallelado et al., 2017), whereas in temperate-maritime climates sublimation is less prevalent and a large fraction of snowfall melts in the canopy (Storck et al., 2002). Hydrological models are essential tools

for understanding how climate and vegetation influence snow processes and downstream water resources, and their accuracy depends on accurate representations of forest-snow processes. Yet, uncertainties in forest-snow process representation lead to variable transferability across climates and forest types when simulating subcanopy snow water equivalent (SWE) (Essery et al., 2003; Gelfan et al., 2004; Krinner et al., 2018; Rutter et al., 2009) and diagnosing snow processes (Lumbrazo et al., 2022; Lundquist et al., 2021). This variability is compounded by the strong dependence of snow partitioning by vegetation on meteorology and canopy density which has challenged earlier canopy snow parameterisations that have been tested and developed on sparse observations (Lundquist et al., 2021). Over half of the Northern Hemisphere experiences snowfall in forested areas (Kim et al., 2017) and over 23% of land mass globally (Deschamps-Berger et al., 2025), spanning diverse climates and forest structures, highlighting the need for robust models, transferable models. While simulation of SWE in forests remains challenging it is a crucial aspect to understand the impacts of climate and land cover changes on water resources in many cold regions across the globe.

Recent studies have advanced understanding of the canopy snow energy and mass balance (Cebulski & Pomeroy, 2025b; Cebulski & Pomeroy, 2025c; Lumbrazo et al., 2022; Lundquist et al., 2021), with potential to improve SWE simulations in forested basins. For example, Lundquist et al. (2021) demonstrated that calculating throughfall as a function of antecedent snow load can overestimate snow reaching the ground—when also combined with a comprehensive canopy snow unloading routine. Building on this, Staines & Pomeroy (2023) and Cebulski & Pomeroy (2025b) showed that initial interception can predicted as a function of canopy density without assuming maximum canopy snow load. Moreover, Roesch et al. (2001) and Lumbrazo et al. (2022) show the importance of representing both wind and melt-induced unloading for representing canopy snow ablation. A new physically-based canopy snow mass and energy balance presented in Cebulski & Pomeroy (2025c) provided improved representation of canopy snow ablation compared to previous approaches that were either missing key processes (i.e., dry snow unloading in Andreadis et al., 2009) or based on empirical relationships (i.e., ice-bulb temperature induced melt unloading and drip in Ellis et al., 2010). These advances have been implemented as new parameterisations in the Cold Regions Hydrological Modelling Platform to answer the following research questions:

1. What is the performance of a novel hydrological model in simulating the accumulation of subcanopy SWE in forested environments characterized by varying tree species, canopy structures, and meteorological conditions?
2. How does the performance of the new model in simulating SWE compare to that of a conventional modelling approach across differing environments?
3. What are the canopy snow processes that account for the differences in SWE between the modelling approaches and how do these differ with climate and forest structural differences?

The objective of this research is to evaluate new snow interception and ablation parameterizations for simulating subcanopy SWE and diagnosing causative processes in needleleaf forests. Evaluation of the new model

in simulating initial accumulation of snow in the canopy has been addressed in Cebulski & Pomeroy (2025b) and canopy snow ablation in Cebulski & Pomeroy (2025c).

## 5.3 Methods

### 5.3.1 Study Sites

The needleleaf snowpack models were evaluated at four locations in western Canada spanning a range of climate and forest types (Figure 5.1; Table 5.1). The model simulation years for each site are shown in Table 5.1 and were selected based on the availability of bi-weekly to monthly subcanopy SWE measurements and hourly station-based observations of air temperature, relative humidity, wind speed, total precipitation, and net solar radiation adjacent to the snow survey transects. At each site, snow surveys consisted of snow depth measurements at all locations and snow density measurements at one out of every five locations. SWE was calculated from snow depth and snow density following the methods outlined in Pomeroy & Gray (1995). The four study sites include:

Wolf Creek Research Basin - Forest Site (60.60, -134.96, 750 m asl.) is located 16 km south of Whitehorse, Yukon Territory in a level dense forest with a sub-arctic climate (see basin scale location in Fig. 1 in Rasouli et al., 2019a). Snow surveys were conducted along a transect that traverses through mature forest consisting of primarily White spruce and Lodgepole pine. Additional details on the snow survey and meteorological measurements is described in Rasouli et al. (2019a) and Pomeroy et al. (2025).

Russell Creek Experimental Watershed - Upper Stephanie Old Growth Site (50.32, -126.35, 700 m asl.) is located on northern Vancouver Island, British Columbia with a temperate-maritime climate that receives substantial winter precipitation. Snow survey transects were conducted in cardinal directions within a mature old growth forest that consists of Amabilis fir and Western hemlock (Floyd, 2012). Additional details on the snow survey and meteorological instrumentation are provided in Floyd (2012). Total precipitation data were unavailable at the Russell site for the 2008 water year. For this period, records from the Tsitika Summit station (50.28°N, 126.36°W; 450 m asl.), operated by the British Columbia Ministry of Transport and located 5 km from Russell, were used instead.

Fortress Mountain Research Basin - Powerline site (50.83, -115.20, 2100 m asl., Kananaskis, Alberta) is located on a wind-exposed subalpine ridge top covered with sparse forest with a continental climate (see basin scale location in Fig. X in Pomeroy et al., 2025). The vegetation at this site consists of coexisting Subalpine fir and Engelmann spruce tree species (Langs et al., 2020). Snow survey measurements of snow depth and density were collected following a transect through mature forest east of the Powerline meteorological tower (see Fig. 1 in Cebulski & Pomeroy, 2025b) and described in further detail in Pomeroy et al. (2025). The meteorological forcing data used in this study is described in detail in Cebulski & Pomeroy (2025c).

Marmot Creek Research Basin - Upper Forest site (50.93, -115.16, 1848 m asl., Kananaskis, Alberta) is located on a dense forested plateau with a continental climate 14 km north of Fortress but receives much less precipitation (see basin scale location in Fig. 1 in Fang et al., 2019). Vegetation consisted primarily of Engelmann spruce, subalpine fir, and lodgepole pine (Fang et al., 2019; Staines & Pomeroy, 2023). Snow surveys were conducted following a cardinal transect through mature forest surrounding the “Upper Clearing” meteorological tower (see Fig. 1b in Staines & Pomeroy, 2023) and described in further detail in Pomeroy et al. (2025). The meteorological forcing data and corresponding instrumentation used from this site is described in Fang et al. (2019) and Pomeroy et al. (2025).

**Table 5.1:** Simulation period (Years), location, and vegetation characteristics, including canopy cover ( $C_c$ ), leaf area index (LAI), and mean tree height ( $\bar{h}_t$ ), for the four study sites.

Site		Ele.						Dominant
Name	Years	(m)	Lon.	Lat.	$C_c$	LAI	$\bar{h}_t$ (m)	Species
Wolf Creek	2015—2022	750	-134.96	60.60	0.81	3.82	15.0	White Spruce and interior lodgepole pine
Marmot Creek	2007—2023	1848	-115.16	50.93	0.80	3.00	15.0	Engelmann spruce, subalpine fir, and lodgepole pine
Fortress Moun-tain	2013—2023	2100	-115.20	50.83	0.65	1.44	10.5	Subalpine fir and engelmann spruce
Russell Creek	2006—2008	700	-126.35	50.32	0.86	1.93	44.9	Amabilis fir and western hemlock

### 5.3.2 Simulation of Subcanopy Snowpack

The Cold Regions Hydrological Modelling Platform (CRHM) was implemented to simulate SWE at each of the four forest plots. The CRHM platform is described in detail in Pomeroy et al. (2022); and the up-to-date source code is available at <https://github.com/srlabUsask/crhmcodes>. Hourly climate forcing data from station-based measurements of air temperature, relative humidity, wind speed, total precipitation, and above canopy incoming solar radiation were used to run the CRHM models. Incoming solar radiation observations were not available for Wolf Creek and were simulated following theoretical clear-sky radiation by Garnier & Ohmura (1970) and atmospheric transmittance by Annandale et al. (2002) and Shook & Pomeroy (2011).

Atmospheric precipitation was partitioned into snow and/or rain phases following the psychometric energy

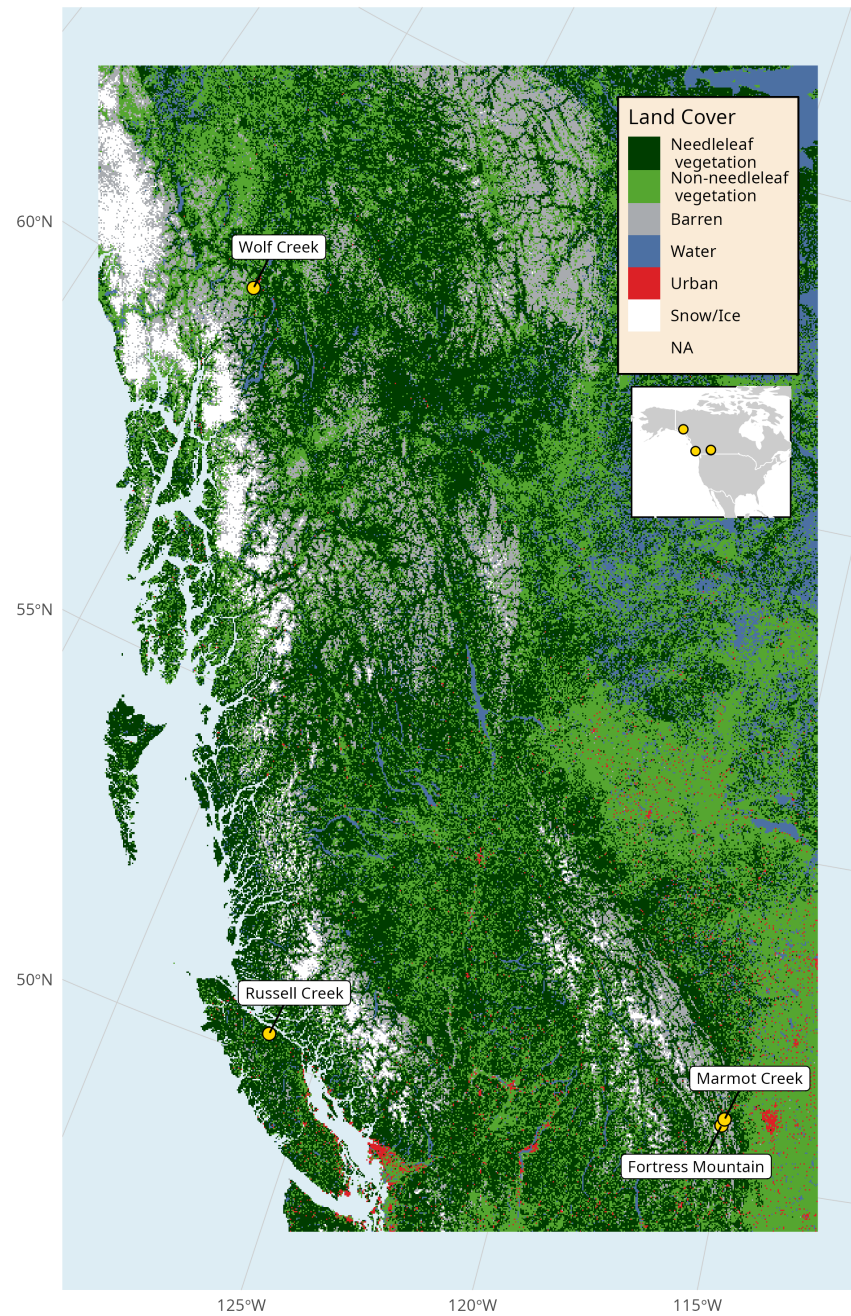


**Figure 5.1:** Map showing the regional scale location of the four research basins and land cover data from the Canada Centre for Remote Sensing et al. (2020) North American Land Change Monitoring 30-meter dataset.

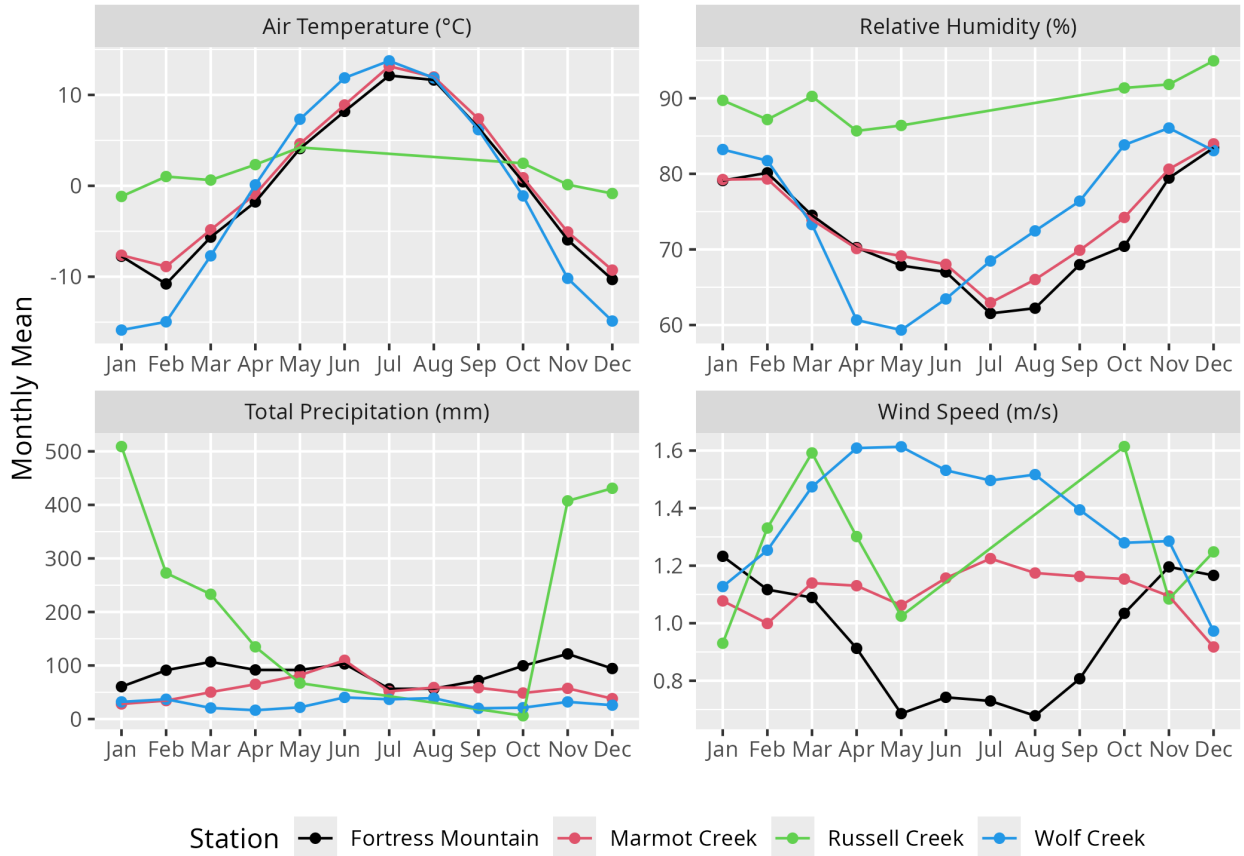


**Figure 5.2:** Graph showing mean monthly relative humidity, air temperature, total precipitation, and wind speed over the simulation period for each station. See Table 5.1 for the corresponding date ranges of each site. Observations were not available during the snow free period for Russell Creek (Jun—Sept).

balance approach of Harder & Pomeroy (2013) which accounts for the influence of temperature and humidity on precipitation phase. The interaction of incoming precipitation with the forest canopy was treated using two different approaches. An updated approach following new relationships presented in Cebulski & Pomeroy (2025b) and Cebulski & Pomeroy (2025c) (CP25) to represent the canopy snow energy and mass balance were integrated within CRHM. This new approach simulates initial interception of snow in the canopy as a function of canopy density (Cebulski & Pomeroy, 2025b) and subsequent ablation of snow intercepted in the canopy by melt and dry-snow unloading (Cebulski & Pomeroy, 2025c), energy balance-based snowmelt (Cebulski & Pomeroy, 2025c), and energy balance-based sublimation (Essery et al., 2003). A second approach (E10) which is based on observations by Hedstrom & Pomeroy (1998), Pomeroy et al. (1998b), and Floyd (2012); and implemented as described in Ellis et al. (2010). E10 calculates initial interception of snow in the canopy as a function of canopy density, antecedent snow load, and a species dependent storage capacity following Hedstrom & Pomeroy (1998). Ablation of snow intercepted in the canopy is determined by dry snow unloading (function of canopy snow load as in Hedstrom & Pomeroy, 1998), unloading due to melt (Ellis et al., 2010), canopy snowmelt drainage (threshold function of ice-bulb temperature as in Ellis et al., 2010), and sublimation by an analytical energy balance-based parameterisation (Pomeroy et al., 1998b). See Cebulski & Pomeroy (2025a) for a complete description of the E10 parameterisation. While neither the E10 nor CP25 model was calibrated for this study, their parameterisations were originally developed using data from Marmot and Fortress, respectively.

A two-layer energy and mass balance snowmelt model (Snobal, Marks et al., 1998) was used to calculate subcanopy snowpack processes. Net shortwave radiation to the subcanopy snowpack was simulated by calculating the transmittance of irradiance through the canopy, less the amount reflected from the snow surface (Ellis et al., 2010; Pomeroy et al., 2009). Incoming longwave radiation to subcanopy snow was simulated by thermal emissions from the atmosphere and vegetation elements, weighted by sky-view-factor (Ellis et al., 2010; Pomeroy et al., 2009). Sensible and latent heat fluxes to the subcanopy snowpack were determined using an approach adopted from Brutsaert (1982) and Marks & Dozier (1992) and is described in the CRHM source code. Only two water years were simulated at Russell due to limited model forcing and validation data.

### 5.3.3 Model Evaluation

Simulated subcanopy SWE by the two models (E10 and CP25) was evaluated using snow survey observations collected from transects at the four forest plots. The performance of the two models was evaluated based on the differences in simulated ( $S_i$ ) and observed ( $O_i$ ) values of SWE using mean bias (MB) and root mean squared error (RMSE) as:

$$MB = \frac{1}{n} \sum_{i=1}^n (S_i - O_i) \quad (5.1)$$

and

$$\text{RMSE} = \sqrt{\frac{\sum_{i=1}^n (S_i - O_i)^2}{n}} \quad (5.2)$$

Values for  $S_i$  were selected for each site from the E10 and CP25 CRHM simulated SWE state for the timestamp that matched each of the snow survey observations ( $O_i$ ). The MB and RMSE statistics represent the model performance over all simulation years for each site.

## 5.4 Results

### 5.4.1 Snowpack Observations

Amongst the sites and years included in the study, accumulation of snowfall below the canopy was less than cumulative snowfall, as observed in open clearings adjacent to each forest transect (Figure 5.3). At peak seasonal subcanopy SWE, Fortress had the highest fraction of seasonal snowfall stored in the subcanopy snowpack at 0.6, followed by Marmot and Wolf Creek which both had similar fractions at 0.4, and Russell had the smallest fraction at 0.3 when averaged over all years. Variations in the prevalence of canopy snow unloading, melt/drip, and sublimation contributed to the observed differences in subcanopy snow accumulation relative to the open clearings at each site. At the temperate-maritime Russell site mid-winter melt events also contributed to these observed differences. Following validation of the new CP25 model in representing subcanopy SWE, a diagnosis on the contribution of each canopy snow processes in influencing subcanopy snowfall accumulation will be conducted in Section 5.4.3 for each site.

Observed subcanopy SWE varied from a seasonal mean of 14.6 to 366.8 kg m<sup>-2</sup> (Figure 5.4) and seasonal peak SWE varied from 27.1 to 498.4 kg m<sup>-2</sup> (Figure 5.5) across all sites and years. The CP25 model tended to underestimate both mean and peak SWE at these three colder sites while E10 overestimated SWE at all four sites.

### 5.4.2 Evaluation of Snowpack Models

Over all years and sites, the CP25 model had a lower mean bias of -0.63 kg m<sup>-2</sup> compared to E10's mean bias of -26.23 kg m<sup>-2</sup> in representing the individual subcanopy SWE measurements shown in Figure 5.6. Across the three colder climate sites (i.e., Fortress, Marmot, and Wolf Creek) CP25 underestimated SWE (MB = 3.38 kg m<sup>-2</sup>) and E10 overestimated SWE (MB = -11.5 kg m<sup>-2</sup>). CP25 had its smallest mean bias at Fortress of 2.53 kg m<sup>-2</sup>—where the canopy snow energy and mass balance parameterisations were developed—followed by Marmot, Wolf Creek, and Russell. E10 had its lowest mean bias at Marmot—where this canopy snow model had previously been tested and developed—followed by Wolf Creek, Fortress, and Russell (Table 5.2).

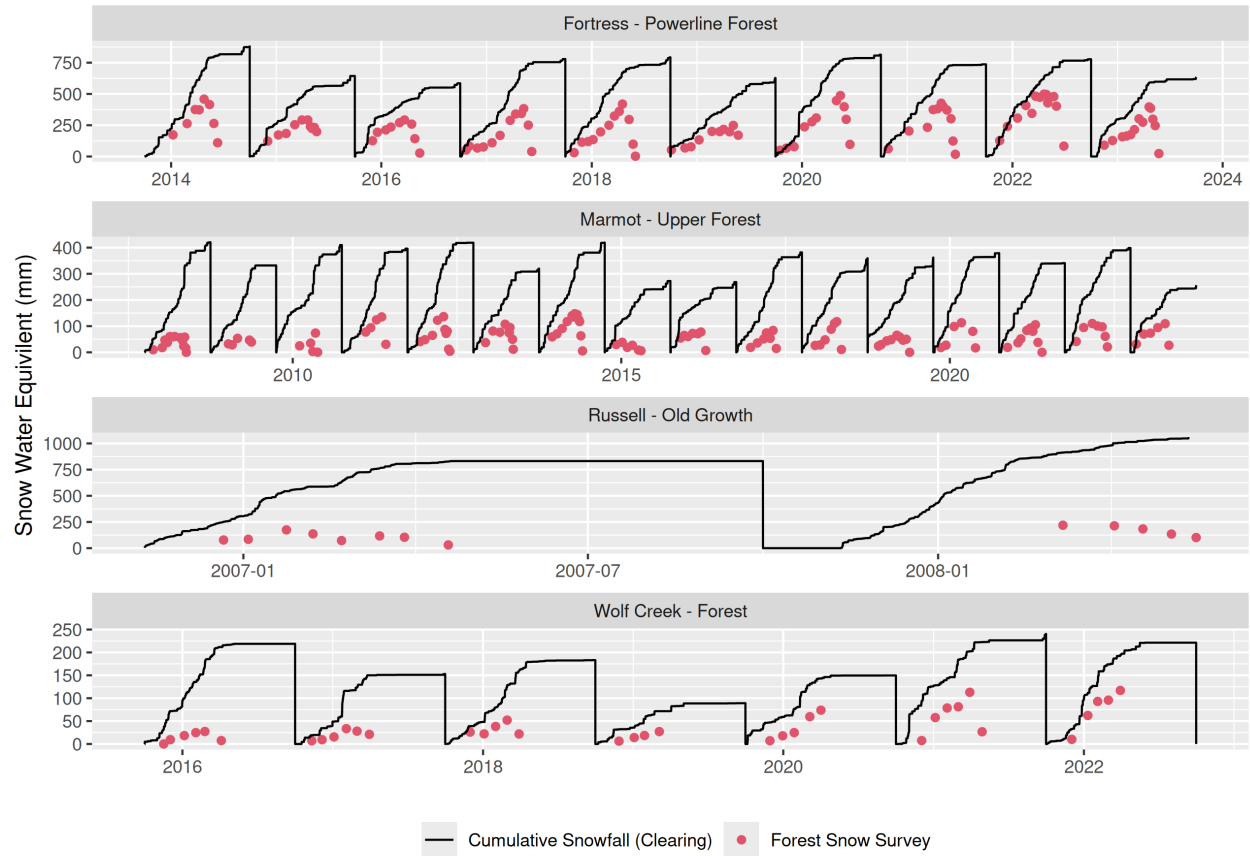


**Figure 5.3:** Time series showing seasonal cumulative snowfall (black lines) and subcanopy snow water equivalent from in situ snow surveys (red dots). Note: snowfall was determined from observed total precipitation for each site using the snowfall fraction simulated in CRHM following Harder & Pomeroy (2013).

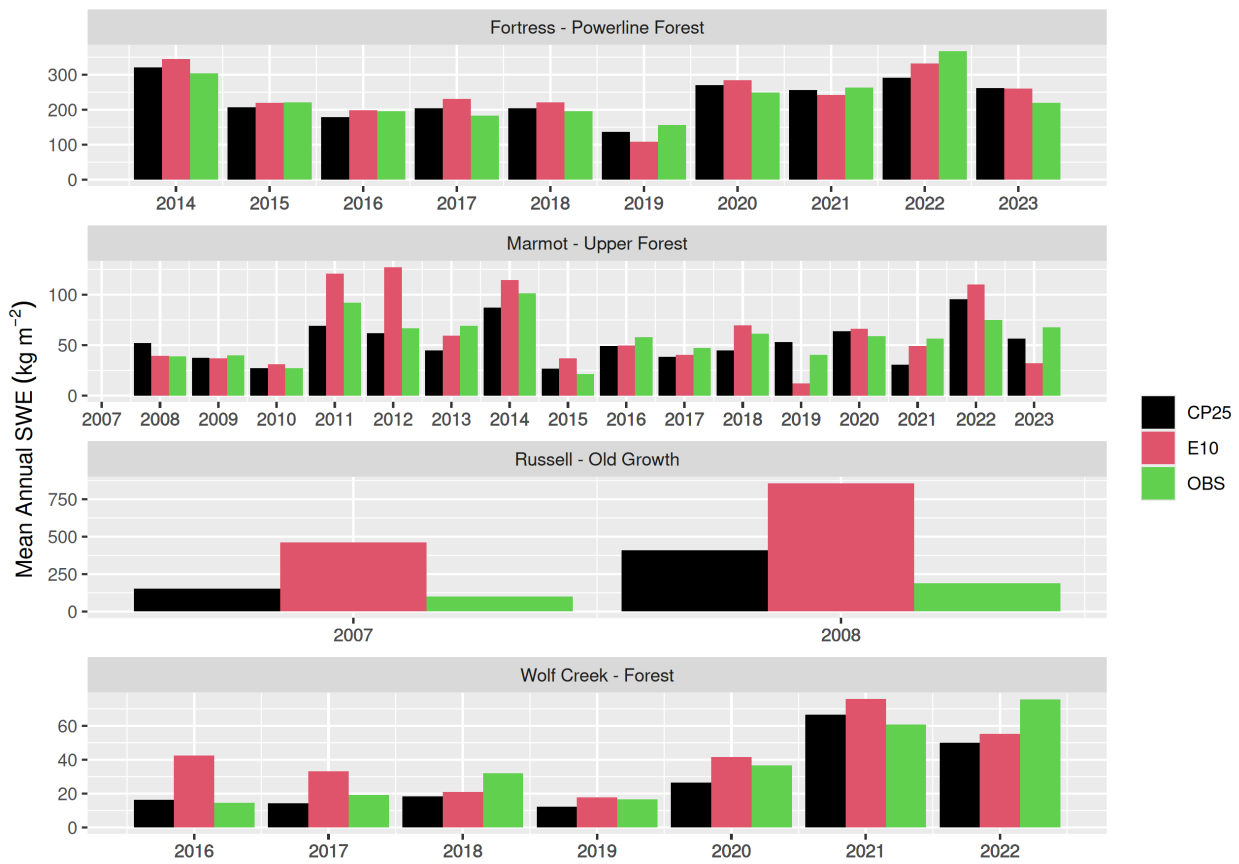


**Figure 5.4:** Bar chart comparing mean water year snow water equivalent between snow survey observations (OBS) and the two models (CP25 and E10).

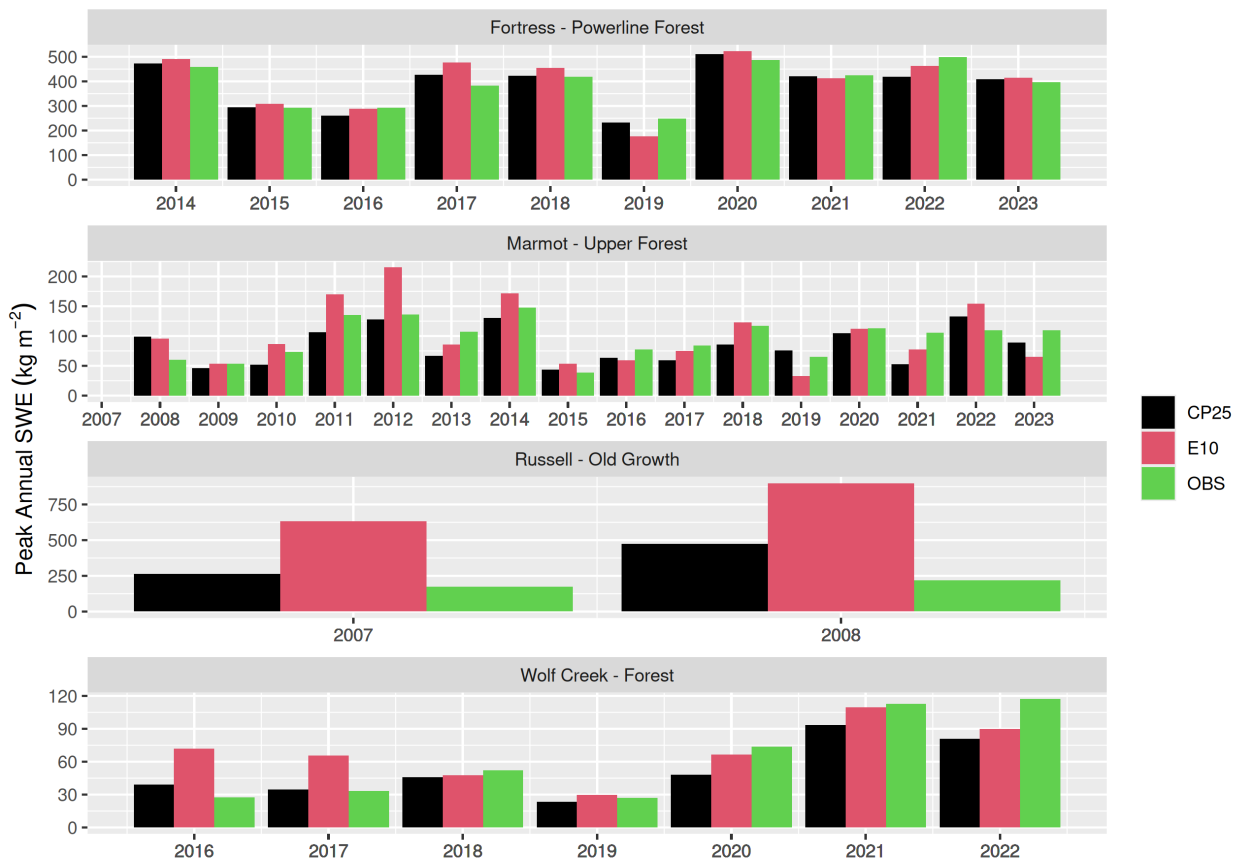


**Figure 5.5:** Bar chart comparing peak water year snow water equivalent between snow survey observations (OBS) and the two models (CP25 and E10).

Both the CP25 and E10 models had relatively similar performance at Marmot and Wolf Creek based on their mean biases which had absolute values which differed by less than 1 kg m<sup>-2</sup> (Table 5.2). Although E10 had a marginally reduced mean bias at Wolf Creek of -5.81 kg m<sup>-2</sup> compared to 6.72 kg m<sup>-2</sup> for CP25 the RMSE across all sites was lower for CP25 (Table 5.2). The lower RMSE for CP25 compared to E10 is also reflected in CP25's closer estimates to mean and peak seasonal SWE across all water years across all four sites compared to E10 (Figure 5.4; Figure 5.5). Three years contributed to the higher RMSE at Marmot where E10 simulated SWE was greatly overestimated based on a mean and peak value by over 50 kg m<sup>-2</sup> (nearly 100% of observed SWE) for the water years 2011 and 2012 (Figure 5.4; Figure 5.5). In contrast, E10 had a very large underestimation in subcanopy SWE at Marmot for the water year 2019. At Wolf Creek, E10 also had deviations of ~30 kg m<sup>-2</sup> (~100% greater than observed SWE) from observed mean and peak seasonal SWE for 2016 and 2017. Both models had their worst overall performance for the temperate-maritime Russell site; however, CP25 did show a substantial improvement compared to the E10 model with mean biases of -108.87 kg m<sup>-2</sup> and -465.37 kg m<sup>-2</sup> respectively. Although the intent of this evaluation is to assess the performance of each model in simulating subcanopy SWE, uncertainties in model forcing and physical parameters (i.e., canopy coverage, LAI) may also contribute to systematic biases in the evaluation. Some of the increased model error at Russell during the 2008 water year may reflect the use of total precipitation data from a nearby highway station rather than on-site measurements.

**Table 5.2:** Mean bias (MB) and root mean squared error (RMSE) determined from time-series simulations of snow water equivalent for the two canopy snow models at each of the four sites.

Model	Station	MB	RMSE
CP25	Fortress - Powerline Forest	2.53	46.10
CP25	Marmot - Upper Forest	4.88	20.92
CP25	Russell - Old Growth	-108.87	141.79
CP25	Wolf Creek - Forest	6.72	17.62
CP25	All Station Mean	-0.63	43.70
E10	Fortress - Powerline Forest	-8.94	53.84
E10	Marmot - Upper Forest	-5.02	30.62
E10	Russell - Old Growth	-465.37	499.99
E10	Wolf Creek - Forest	-5.81	21.93
E10	All Station Mean	-26.23	110.61

Seasonal subcanopy SWE accumulation and ablation was generally well represented by both models at Fortress, Marmot, and Wolf Creek (Figure 5.6). However, E10 failed to simulate the timing of SWE accumulation and ablation well for 2011, 2012, and 2019 at Marmot. The largest deviation in simulated seasonal SWE occurred at Russell for E10 where subcanopy snow accumulation was simulated at a much

higher rate compared to the observed and CP25 over the two years that were simulated. At Wolf Creek CP25 had a delay in simulating the initial accumulation of subcanopy SWE for water years 2017, 2018, and 2019. The lower snowfall rate at Wolf Creek and higher interception rate for CP25 compared to E10 led to throughfall and unloading rates that were smaller than the snowpack initiation threshold employed in Snobal, which Snobal then melts SWE accumulations below this threshold completely. In contrast, E10 intercepted less snow and had higher unloading rates than CP25 leading to higher initial accumulation for these three years at Wolf Creek.

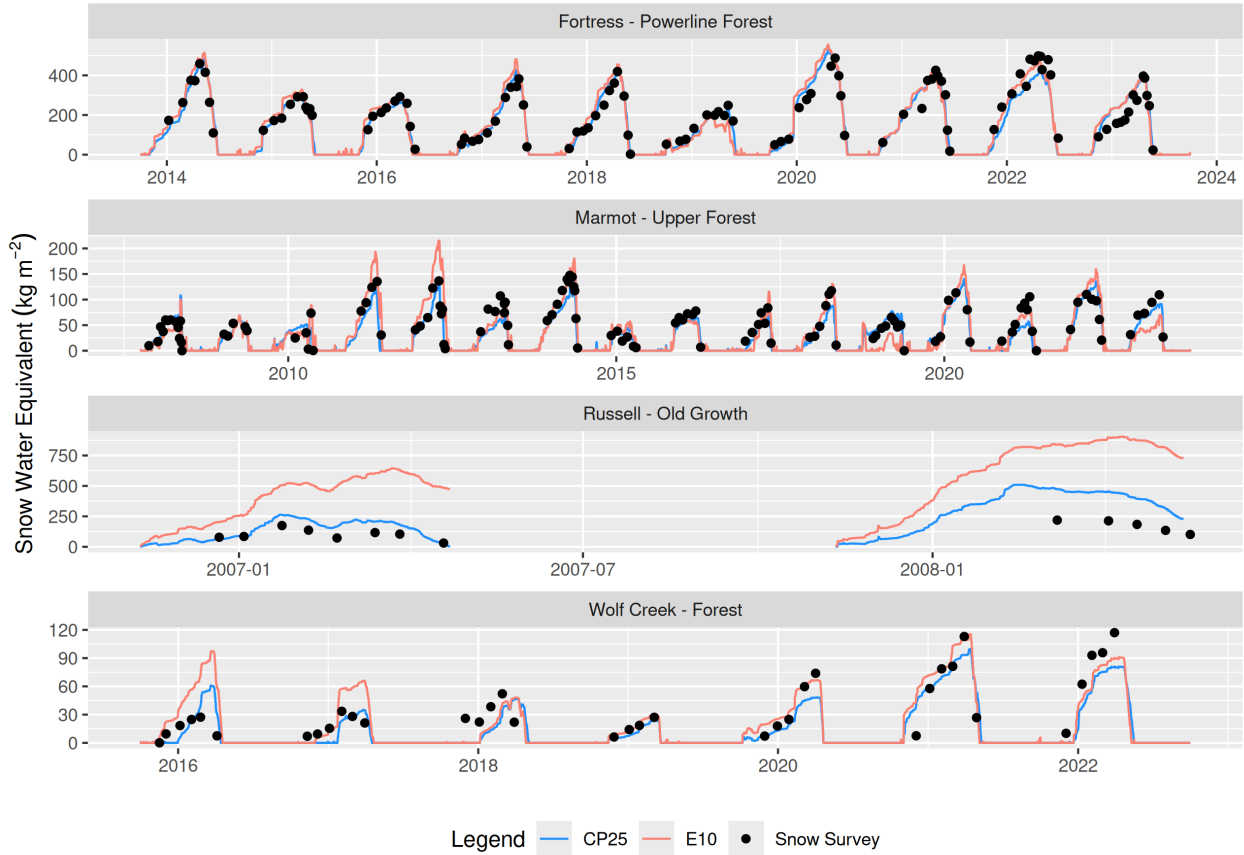


**Figure 5.6:** Timeseries of observed and simulated (CP25 and E10) forest snow water equivalent at each station.

### 5.4.3 Snowfall Partitioning

A greater fraction of annual snowfall was sublimated by CP25 compared to E10 for all four sites across all years (Figure 5.7). Lower interception efficiency combined with higher average rates of unloading for the E10 model led to more snowfall being partitioned towards the ground compared to the CP25 model (Figure 5.8) leading to reduced sublimation of canopy snow and thus overprediction of subcanopy SWE accumulation (Table 5.2). The underprediction of subcanopy SWE by the CP25 model at Fortress, Marmot, and Wolf Creek (Table 5.2) may have been due to an overestimate of sublimation and/or canopy snowmelt

rates leading to less snowfall being partitioned to the ground as solid snow. The difference in the annual fraction of snowfall that was sublimated between the CP25 and E10 models was most prevalent at Marmot (Figure 5.7). Factors that may contribute to this large deviation include the lower unloading rates observed for CP25 at this site (Figure 5.8) compared to E10 resulting from the lower wind speed and air temperatures at this site (Figure 5.2), reducing the unloading and canopy snowmelt rates thus increasing the amount of canopy snow subject to sublimation for CP25. For E10, the April–June monthly air temperature normals at Marmot—months when this site receives most of its snowfall (Figure 5.2)—are also largely within the E10 ice-bulb temperature unloading range (-3°C to 6°C) which are ideal conditions for initiating unloading due to warming for the E10 model. Relatively similar fractions of annual snowfall was sublimated by the two models at Fortress and Wolf Creek (Figure 5.7) due to the similar sublimation parameterisation used by the two models combined with the similar fraction of snow partitioned towards the ground (Figure 5.8). Although CP25 had higher drip/melt rates than E10, increased throughfall by E10 coupled with the constant unloading rate as a function of snow load likely made up for E10’s lower melt/drip rate (Figure 5.9). Process observations of unloading, melt, and sublimation were not available and thus the simulations of snowfall partitioning could not be directly evaluated.

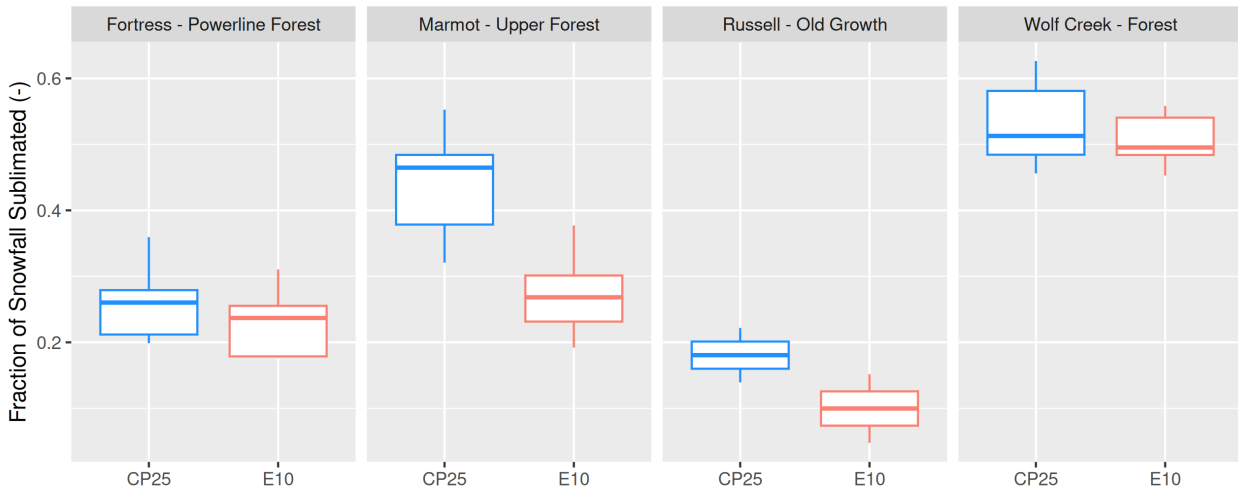


**Figure 5.7:** Boxplots showing the distribution of the fraction of total atmospheric snowfall that was sublimated out of the canopy at each station. Note: the rectangle vertical extent represents the interquartile range (25<sup>th</sup> to 75<sup>th</sup> percentile), the horizontal line within each box indicates the median, and the whiskers extend to 1.5 times the interquartile range. Circular points beyond the whiskers represent outliers.

#### 5.4.4 Simulated Canopy Snow Load

Over all years and sites, CP25 predicted consistently higher canopy snow loads compared to the E10 model (Figure 5.10). This results from E10’s increase in throughfall with increasing antecedent snow load as well as the constant unloading rate as a function of snow load and ice-bulb temperature and led to more snowfall partitioned to the ground as solid snow compared to CP25 (Figure 5.8). Some snowfall events had similar

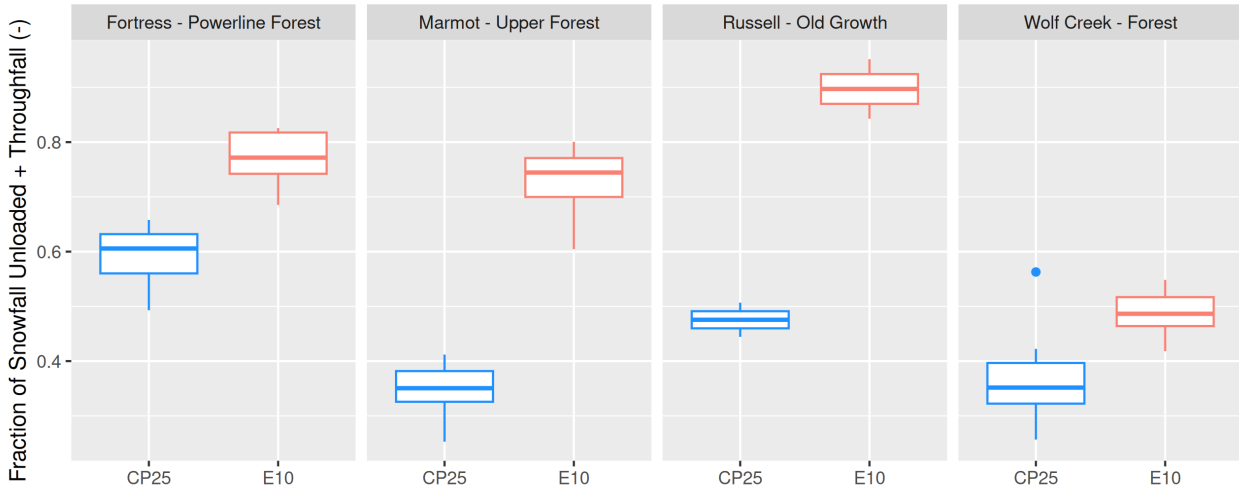


**Figure 5.8:** Boxplots showing the distribution of the fraction of total atmospheric snowfall that reached the subcanopy via unloading and/or throughfall. Note: the rectangle vertical extent represents the interquartile range (25<sup>th</sup> to 75<sup>th</sup> percentile), the horizontal line within each box indicates the median, and the whiskers extend to 1.5 times the interquartile range. Circular points beyond the whiskers represent outliers.

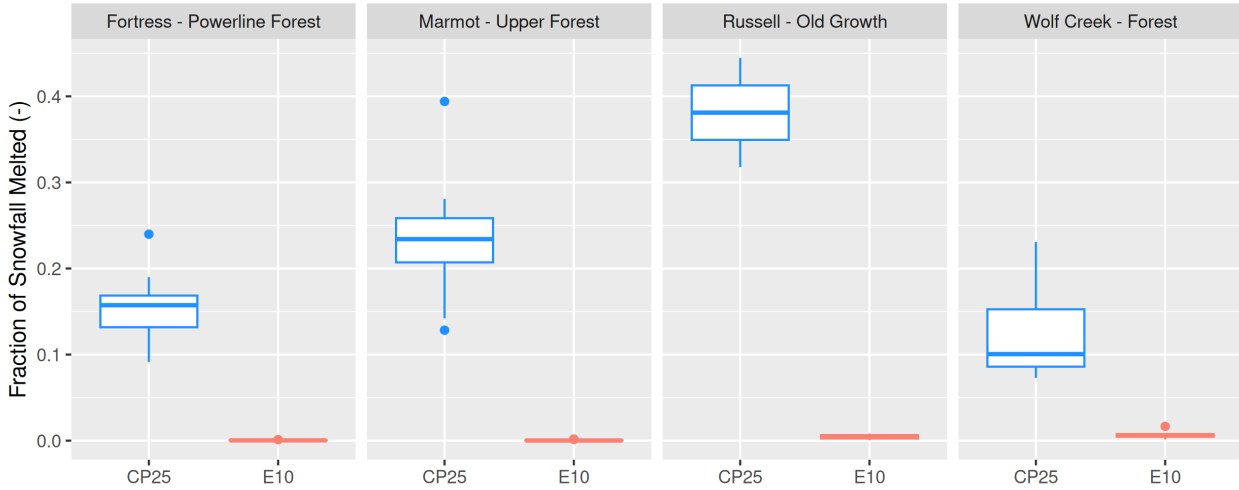


**Figure 5.9:** Boxplots showing the distribution of the fraction of total atmospheric snowfall that was melted out of the canopy at each station. Note: the rectangle vertical extent represents the interquartile range (25<sup>th</sup> to 75<sup>th</sup> percentile), the horizontal line within each box indicates the median, and the whiskers extend to 1.5 times the interquartile range. Circular points beyond the whiskers represent outliers.

initial accumulation of snow in the canopy between the two models up until the E10 species snow load capacity was reached (see colder events in Jan and Feb at Fortress, Marmot, and Wolf Creek in Figure 5.11). Canopy snow load infrequently reached the CP25 maximum load of  $50 \text{ kg m}^{-2}$  at all four sites (Figure 5.10). At Russell, while annual snowfall amounts were similar to Fortress (Figure 5.3), increased canopy snow ablation rates due to warmer temperatures at Russell limited the accumulation of snow in the canopy in spring (Figure 5.10; Figure 5.11).

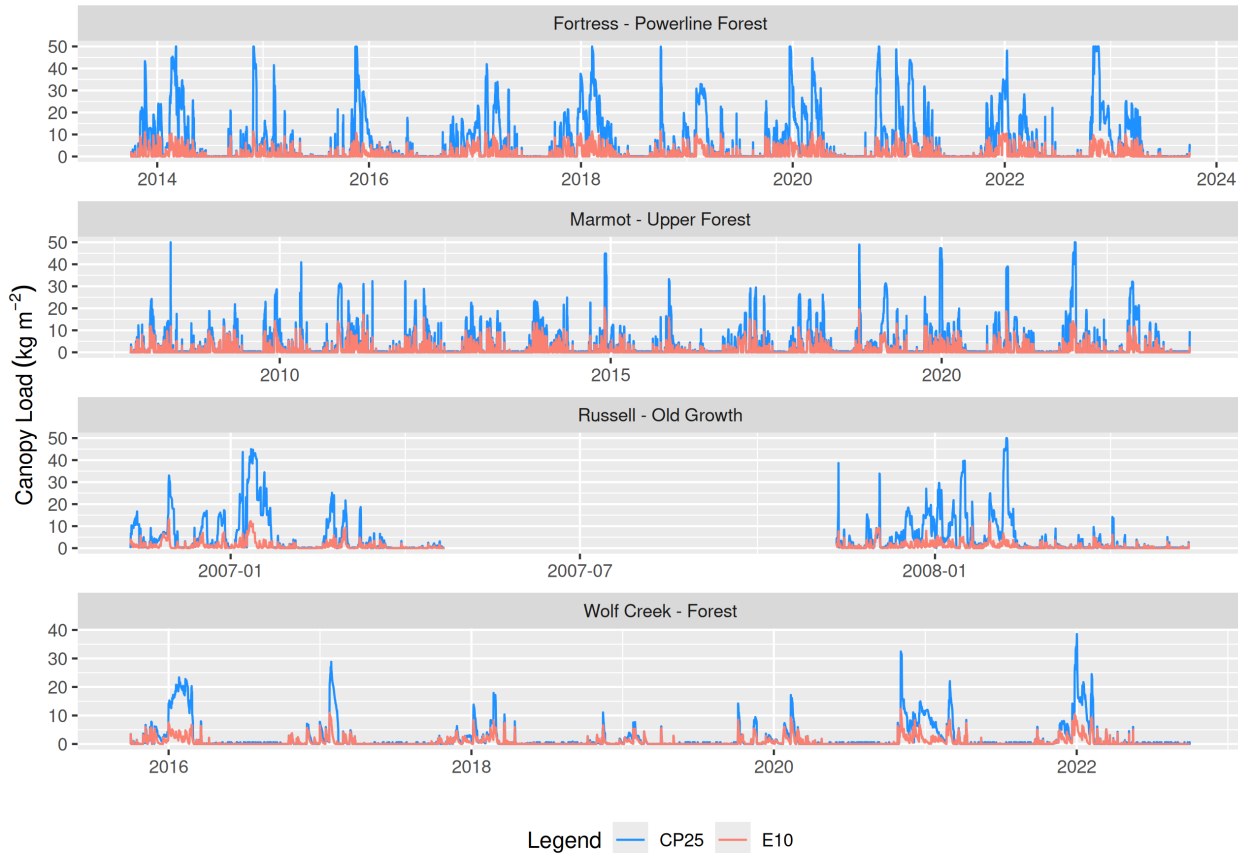


**Figure 5.10:** Timeseries of simulated canopy load for CP25 and E10 at each station for the full simulation period.

In addition to the large difference in canopy load simulated between CP25 and E10 across all four sites, the duration that the canopies of each site were simulated to have more than  $2 \text{ kg m}^{-2}$  of snow varied between the four sites and two models (Figure 5.12). A threshold of  $2 \text{ kg m}^{-2}$  was selected based on observations by Pomeroy & Dion (1996) who found minimal influence of canopy snow load on above canopy albedo for loads less than  $1.6 \text{ kg m}^{-2}$ . Across all four sites, canopy loads greater than  $2 \text{ kg m}^{-2}$  were observed to persist longer for CP25 compared to E10 (Figure 5.12). At Fortress and Russell snow loads above this threshold persisted up to two times longer for CP25 compared to E10. The difference at Marmot and Wolf Creek between the two models were found to be less due to the lower snowfall of these sites which lowered event canopy snow loads thus yielding higher interception inefficiencies for the E10 model.

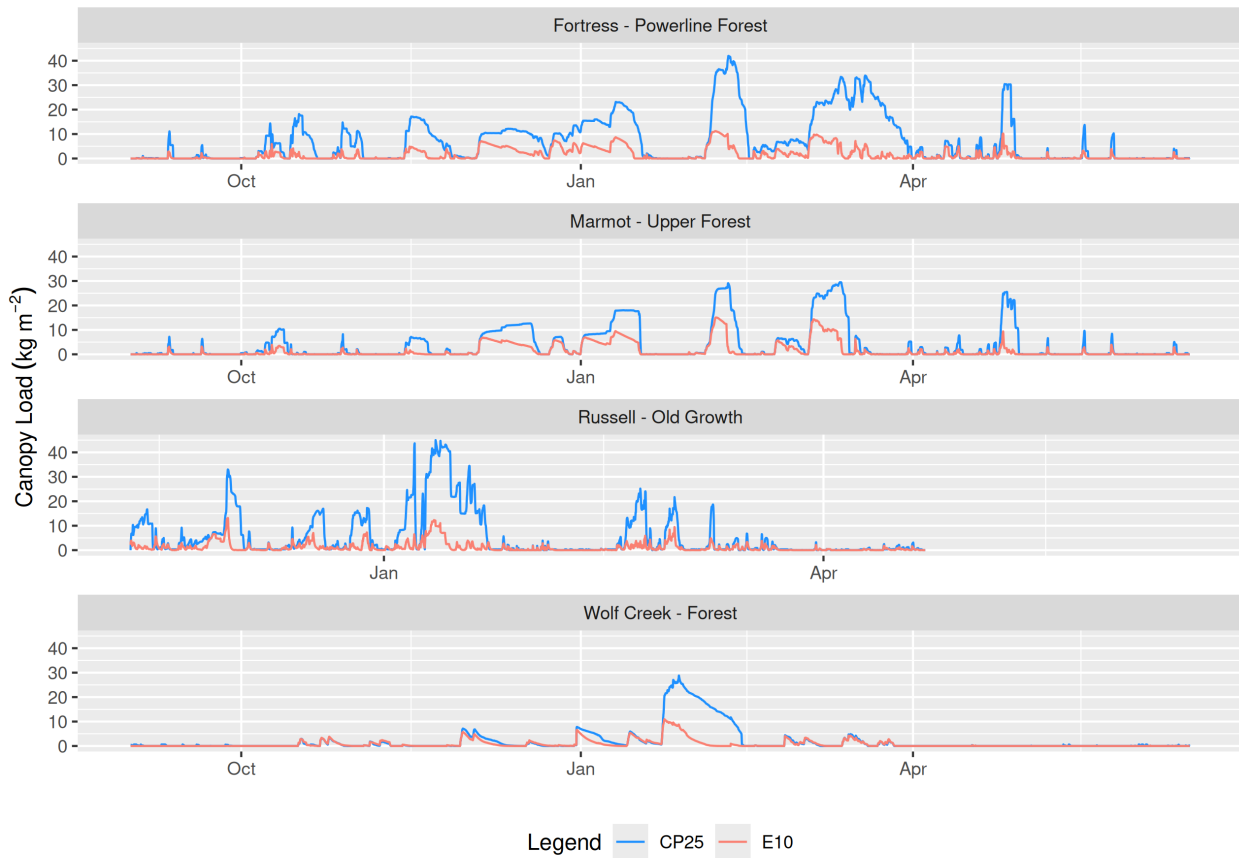


**Figure 5.11:** Timeseries of simulated canopy load for CP25 and E10 at each station for select water years. The water year 2017 was selected for Fortress, Marmot, and Wolf Creek, while 2007 was selected for Russell.

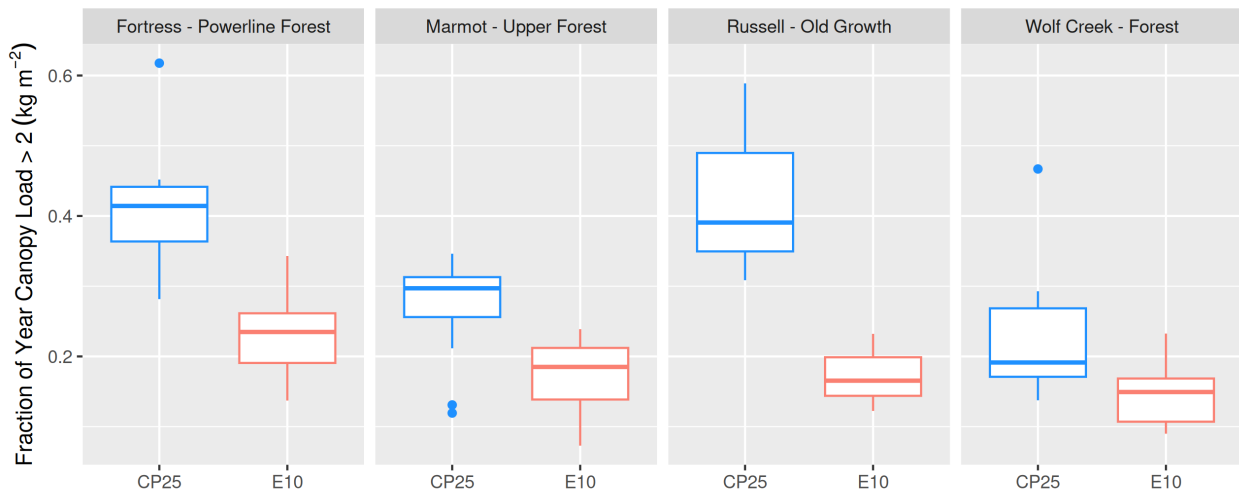


**Figure 5.12:** Boxplots showing the annual fraction of time where simulated canopy snow load is greater than  $2 \text{ kg m}^{-2}$  by the CP25 and E10 models.

## 5.5 Discussion

### 5.5.1 Model Performance in Simulating Subcanopy Snow Accumulation

New parameterisations of the canopy snow energy and mass balance—supported by advances in process understanding (Cebulski & Pomeroy, 2025b; Cebulski & Pomeroy, 2025c; Lumbrazo et al., 2022; Lundquist et al., 2021; Staines & Pomeroy, 2023)—were evaluated for their ability to simulate subcanopy SWE across a broad range of climate and forest types. The higher canopy snow loads simulated by CP25 are consistent with empirical observations (Calder, 1990; Cebulski & Pomeroy, 2025b; Hedstrom & Pomeroy, 1998; Storck et al., 2002; Watanabe & Ozeki, 1964), which demonstrate a linear increase in interception with snowfall without evidence of reaching a maximum capacity. By calculating throughfall as a function of canopy density (Cebulski & Pomeroy, 2025b; Staines & Pomeroy, 2023) and combining this with a comprehensive canopy snow ablation routine (Cebulski & Pomeroy, 2025c; Lundquist et al., 2021), CP25 resulted in much larger intercepted snow loads compared to E10. Consequently, E10 underestimated subcanopy SWE, as less intercepted snow was exposed to sublimation or melt (Table 5.2).

Inclusion of both dry- and melt-induced unloading of canopy snow is supported by observations (Cebulski & Pomeroy, 2025c; Ellis et al., 2010; Floyd, 2012; Lumbrazo et al., 2022; Roesch et al., 2001), with mechanisms such as bond weakening, lubrication during melt, and wind shear reinforcing their physical basis. An energy balance-based canopy melt routine—recommended by many studies (Andreadis et al., 2009; Cebulski & Pomeroy, 2025c; Lumbrazo et al., 2022; Lundquist et al., 2021; Storck et al., 2002)—improved representation of ablation under warm conditions (Cebulski & Pomeroy, 2025c) and likely contributed to reduced error in subcanopy SWE simulations in this study at the temperate-maritime Russell site. In contrast, the ice-bulb temperature-based melt threshold ( $> 6^{\circ}\text{C}$ ) was infrequently reached and caused unloading to occur mainly as solid snow. While accounting for wind-driven unloading reduced errors slightly in colder sites, the largest improvements were at Russell, where CP25 better captured canopy melt and drip.

Both models performed best at the sites where they were originally developed (CP25 at Fortress and E10 at Marmot), which aligns with observations by Lumbrazo et al. (2022) that parameters for unloading are site specific and may suggest the initial interception parameters are as well. Low error at the cold sites suggests that the dry snow unloading parameterisation is transferable across sites and is consistent with observations by Lumbrazo et al. (2022)—where a wind-driven unloading parameterisation had good accuracy across a cold-climate sites. The CP25 model performed worst at the temperate-maritime Russell site, where melt/drip and melt-induced unloading processes dominated, despite showing improvements over E10 in this study and showing strong performance over warm melt-driven events in Cebulski & Pomeroy (2025c). Remaining error at Russell may reflect unrepresented processes, such as rime-ice accumulation observed in other maritime forests (Lumbrazo et al., 2022), which increases canopy loads and alters partitioning into liquid water. Additional

uncertainties stem from simplifications in the canopy energy balance (e.g., radiation transmittance, longwave emission, and turbulent fluxes), as well as parameterisations of interception and unloading (Cebulski & Pomeroy, 2025b; Cebulski & Pomeroy, 2025c). These issues are likely amplified at Russell, where frequent air temperatures near the melting point increase sensitivity to energy balance formulations, compared to the colder sites with more stable conditions.

Across the three colder sites, mean bias differed by less than  $10 \text{ kg m}^{-2}$  between models, yet CP25 simulated longer periods of canopy snow loads greater than  $2 \text{ kg m}^{-2}$ . This has implications for improving the representation of above-canopy albedo in land surface models which have previously shown poor performance with existing canopy snow ablation models (Thackeray et al., 2014; Wang et al., 2016). Moreover, E10's performance varied substantially between years; it overestimated SWE over most years, but underestimated SWE in low-snowfall years when reduced unloading rates allowed more sublimation (e.g., Marmot in 2019; Figure 5.4).

These results show that recent process-based parameterisations—particularly the treatment of canopy load, ablation, and unloading—yield measurable improvements in simulating subcanopy SWE across diverse climates and forest types, and have direct implications for representation of surface albedo in land-surface schemes.

### 5.5.2 Influence of Climate on Snowfall Partitioning

Although Russell and Fortress received similar amounts of snowfall (Figure 5.3), subcanopy accumulation was lower at Russell due to enhanced canopy ablation: ~40% of annual snowfall melted and 20% sublimated in the canopy, compared to ~35% combined losses at Fortress. The low cold content of the maritime snowpack at Russell led to canopy snow drip rarely refreezing, and warmer air temperatures (Figure 5.2) further promoted melt throughout the season (Figure 5.6). The prevalence of snowmelt both in the canopy and on the ground at Russell led to the lowest fraction of seasonal snowfall stored in the subcanopy (0.3) at peak SWE.

At Fortress, colder conditions, higher snowfall, and greater wind exposure increased unloading rates, limited sublimation despite the meteorological conditions favourable for it (Figure 5.7). Combined with low canopy melt (Figure 5.9), these processes yielded the highest subcanopy storage fraction (0.6) across all four sites.

Marmot and Wolf Creek experienced cooler, drier conditions and lower snowfall, leading to reduced unloading and a greater role of sublimation in canopy losses (Figure 5.7). Canopy melt played only a minor role, but high sublimation fractions meant that only ~0.4 of snowfall remained in the subcanopy snowpack at peak SWE. Simulated sublimation for these two sites (~50% of seasonal snowfall; Figure 5.7) exceeded the upper range of global estimates (25–45%) reported by Essery et al. (2003) but is consistent with observations by Pomeroy & Gray (1995) and Ellis et al. (2010).

Despite storing the smallest fraction of snowfall, Russell delivered the greatest amount of water to the soil because most canopy ablation occurred as melt and solid snow unloading rather than sublimation. Relatively consistent mid winter melt of snow in the canopy provided a steady year-round input of liquid water, which could contribute to the longer vegetation growing season and may enhance groundwater recharge. Previous studies (Barnhart et al., 2016; Hayashi, 2020) highlight that slow, sustained melt increases infiltration opportunity, whereas rapid melt promotes runoff. In contrast, colder sites with fewer mid-winter melt events may partition a greater fraction of precipitation into runoff.

### 5.5.3 Influence of Tree Species on Snowfall Partitioning

The species of needleleaf forest overlying each site also influenced subcanopy SWE accumulation. However, limited research has been conducted on how branches elasticity, needle composition, and crown structure affect both the interception and ablation of snow in the canopy. The Marmot and Wolf Creek sites both were primarily composed of spruce trees (Table 5.1) and exposed to similarly cool climates (Figure 5.2), showed comparable fractions of snowfall stored in the subcanopy and similar canopy melt and sublimation losses (Figure 5.9; Figure 5.7).

In contrast, Fortress and Russell were both primarily fir-dominated forests, yet diverged strongly due to climate differences (Figure 5.2) and vegetation structure. Despite only ~20% greater canopy cover, Russell stored about half the fraction of snowfall in the subcanopy compared to Fortress. Tree size is a likely factor: large 50 m tall fir trees at Russell can intercept far more snow than the smaller 10 m fir trees at Fortress. Coupled with low winds, this increased exposure of intercepted snow to canopy energy fluxes favored melt and drip at Russell. The larger, more supportive branches may also have slowed unloading, contributing to CP25's overestimate of subcanopy SWE at Russell.

These results support earlier theory by Satterlund & Haupt (1970) that vegetation structure, density, and climate exert stronger control on forest–snow partitioning than needleleaf species alone. However, other forest types, such as broadleaf deciduous or cedar stands, have less supportive branches and different needle or leaf structures, and are therefore expected to exert a stronger influence on canopy–snow processes than the relatively subtle species differences observed among needleleaf sites in this study.

## 5.6 Conclusions

This study shows that advances in the representation of canopy snow energy and mass balance can substantially improve the snowpack simulations across forests spanning a range of climates and canopy structures. The new physically based canopy snow model reduced errors in simulating subcanopy snowpacks and provided new opportunities to diagnose the processes that govern how snowfall is partitioned between the atmosphere, canopy, and forest floor. Building on recent developments, the new approach replaced earlier theories on the

assumption of a maximum canopy snow load with an interception calculation based on canopy density, and represented ablation more explicitly through melt- and wind-driven unloading, energy balance-based melt and drip, and sublimation processes that vary with canopy snow load. Compared with an existing model, the revised approach more accurately represented the melt of intercepted snow, particularly in the coastal-maritime environment, where errors in subcanopy SWE were an order of magnitude lower. These results highlight the robustness of physically based parameterisations under warm conditions, which is particularly important given that continued warming may reduce the applicability of empirically derived routines.

Process diagnosis conducted using the new approach highlighted the role of vegetation in controlling snowfall partitioning. The greatest influence was observed in the temperate–maritime forest, where high energy input to intercepted snow caused nearly half of seasonal snowfall to melt within the canopy, producing the lowest subcanopy SWE fraction and a steady contribution of meltwater throughout the winter. Despite the large influence of vegetation on the subcanopy snowpack, sublimation losses were relatively small (~20% of seasonal snowfall) due to high humidity. At two cold continental sites with lower annual snowfall, reduced unloading allowed a larger proportion of intercepted snow to be lost to sublimation (~50%). In contrast, the cold wind-exposed site with higher snowfall exhibited greater unloading, which limited sublimation losses relative to the other cold sites. Overall, climate and canopy density exerted stronger controls on seasonal snowfall partitioning than species-level differences among fir- and spruce-dominated forests.

Although the new model simulated subcanopy SWE well, uncertainties remain in partitioning of snowfall between sublimation losses and liquid water inputs to the forest floor, as direct flux measurements have only been validated at one site in a previous study. Measurements of snow interception, unloading, drip, and sublimation are rarely made at hydrometeorological stations but would provide important data to evaluate and refine process-level representations across differing environments. Further research is also needed to determine how unloading depends on intercepted snow load, as this relationship is likely to vary with both climate and tree characteristics. Greater cohesion and adhesion in humid climates and more supportive branch and needle structures in certain species may influence how snow is retained or shed from canopies. Improved process-level measurements, combined with continued model development, will help to identify these uncertainties and support the transferability of canopy snow models across the wide range of conditions found in cold-region forests.

## 5.7 Acknowledgements

We acknowledge financial support from the University of Saskatchewan Dean’s Scholarship, the Natural Sciences and Engineering Research Council of Canada’s Discovery Grants, the Canada First Research Excellence Fund’s Global Water Futures Programme, Environment and Climate Change Canada, Alberta Innovates Water Innovation Program, the Canada Foundation for Innovation’s Global Water Futures Observatories facility,

and the Canada Research Chairs Programme. We thank Hannah Koslowsky, Kieran Lehan, Lindsey Langs, Rosy Tutton, David Barrett, and Tyler De Jong for their help in the field and Tom Brown and Logan Fang for support of the CRHM platform.

## 5.8 Data and Sofware Availability Statement

The Cold Regions Hydrological Model Platform (CRHM) source code is available at <https://github.com/srlabUsask/crhmcode>. Model forcing data, model outputs, validation data, processed data, and scripts to run the processing are available at \_\_\_\_\_ .

## REFERENCES

- Allan, R., Pereira, L., Raes, D., & Smith, M. (1998). *Crop evapotranspiration Guidelines for computing crop water requirements*. Food and Agriculture Organization of the United Nations.
- Andreadis, K. M., Storck, P., & Lettenmaier, D. P. (2009). Modeling snow accumulation and ablation processes in forested environments. *Water Resources Research*, 45(5), 1–33. <https://doi.org/10.1029/2008WR007042>
- Annandale, J., Jovanovic, N., Benadé, N., & Allen, R. (2002). Software for missing data error analysis of Penman-Monteith reference evapotranspiration. *Irrigation Science*, 21(2), 57–67. <https://doi.org/10.1007/s002710100047>
- Aston, A. R. (1979). Rainfall interception by eight small trees. *Journal of Hydrology*, 42(3-4), 383–396. [https://doi.org/10.1016/0022-1694\(79\)90057-X](https://doi.org/10.1016/0022-1694(79)90057-X)
- Aubry-Wake, C., & Pomeroy, J. W. (2023). Predicting hydrological change in an alpine glacierized basin and its sensitivity to landscape evolution and meteorological forcings. *Water Resources Research*, 59(9). <https://doi.org/10.1029/2022WR033363>
- Baggi, S., & Schweizer, J. (2008). Characteristics of wet-snow avalanche activity: 20 years of observations from a high alpine valley (Dischma, Switzerland). *Natural Hazards*, 50(1), 97–108. <https://doi.org/10.1007/s11069-008-9322-7>
- Barnhart, T. B., Molotch, N. P., Livneh, B., Harpold, A. A., Knowles, J. F., & Schneider, D. (2016). Snowmelt rate dictates streamflow. *Geophysical Research Letters*, 43(15), 8006–8016. <https://doi.org/10.1002/2016gl069690>
- Bartlett, P. A., & Verseghy, D. L. (2015). Modified treatment of intercepted snow improves the simulated forest albedo in the Canadian Land Surface Scheme. *Hydrological Processes*, 29(14), 3208–3226. <https://doi.org/10.1002/HYP.10431>
- Beria, H., Larsen, J. R., Ceperley, N. C., Michelon, A., Vennemann, T., & Schaeafi, B. (2018). Understanding snow hydrological processes through the lens of stable water isotopes. *Wiley Interdisciplinary Reviews: Water*, 5(6), 1–23. <https://doi.org/10.1002/wat2.1311>
- Berndt, H. W., & Fowler, W. B. (1969). Rime and hoarfrost in upper-slope forests of eastern Washington. *Journal of Forestry*, 67(2), 92–95. <https://doi.org/10.1093/jof/67.2.92>
- Best, M. J., Pryor, M., Clark, D. B., Rooney, G. G., Essery, R. L. H., Ménard, C. B., Edwards, J. M., Hendry, M. A., Porson, A., Gedney, N., Mercado, L. M., Sitch, S., Blyth, E., Boucher, O., Cox, P. M., Grimmond, C. S. B., & Harding, R. J. (2011). The Joint UK Land Environment Simulator (JULES),

- model description – Part 1: Energy and water fluxes. *Geoscientific Model Development*, 4(3), 677–699. <https://doi.org/10.5194/gmd-4-677-2011>
- Betts, A. K., & Ball, J. H. (1997). Albedo over the boreal forest. *Journal of Geophysical Research: Atmospheres*, 102(D24), 28901–28909. <https://doi.org/10.1029/96JD03876>
- Brutsaert, W. (1982). *Evaporation into the atmosphere: Theory, history, and applications*. Dordrecht, Holland: Reidel.
- Bush, E., & Lemmen, D. S. (2019). *Canada's changing climate report* (p. 444). Government of Canada.
- Calder, I. R. (1990). *Evaporation in the uplands* (p. 148). Wiley.
- Canada Centre for Remote Sensing, Canada Centre for Mapping and Earth Observation, & Canada, N. R. (2020). *Land Cover of North America at 30 meters* [Raster Digital Data].
- Cebulski, A. C., & Pomeroy, J. W. (2025a). Theoretical Underpinnings of Snow Interception and Canopy Snow Ablation Parameterisations. *WIREs Water*, 12, e70010. <https://doi.org/10.1002/wat2.70010>
- Cebulski, A. C., & Pomeroy, J. W. (2025b). Snow Interception Relationships With Meteorology and Canopy Density. *Hydrological Processes*, 39(4), e70135. <https://doi.org/10.1002/hyp.70135>
- Cebulski, A. C., & Pomeroy, J. W. (2025c). Processes Governing the Ablation of Intercepted Snow. *Water Resources Research, in review*.
- Chianucci, F., & Macek, M. (2023). hemispheR: An R package for fisheye canopy image analysis. *Agricultural and Forest Meteorology*.
- Cionco, R. M. (1965). A mathematical model for air flow in a vegetative canopy. *Journal of Applied Meteorology* (1962), 4(4), 517–522. [https://doi.org/10.1175/1520-0450\(1965\)004%3C0517:AMMFAF%3E2.0.CO;2](https://doi.org/10.1175/1520-0450(1965)004%3C0517:AMMFAF%3E2.0.CO;2)
- Claassen, H. C., & Downey, J. S. (1995). A Model for Deuterium and Oxygen 18 Isotope Changes During Evergreen Interception of Snowfall. *Water Resources Research*, 31(3), 601–618. <https://doi.org/10.1029/94WR01995>
- Clark, M. P., & Kavetski, D. (2010). Ancient numerical daemons of conceptual hydrological modeling: 1. Fidelity and efficiency of time stepping schemes. *Water Resources Research*, 46(10), 1–23. <https://doi.org/10.1029/2009WR008894>
- Clark, M. P., Nijssen, B., Lundquist, J. D., Kavetski, D., Rupp, D. E., Woods, R. A., Freer, J. E., Gutmann, E. D., Wood, A. W., Brekke, L. D., Arnold, J. R., Gochis, D. J., & Rasmussen, R. M. (2015a). A unified approach for process-based hydrologic modeling: 1. Modeling concept. *Water Resources Research*, 51(4), 2498–2514. <https://doi.org/10.1002/2015WR017198>
- Clark, M. P., Nijssen, B., Lundquist, J. D., Kavetski, D., Rupp, D. E., Woods, R. A., Freer, J. E., Gutmann, E. D., Wood, A. W., Gochis, D. J., Rasmussen, R. M., Tarboton, D. G., Mahat, V., Flerchinger, G. N., & Marks, D. G. (2015b). A unified approach for process-based hydrologic modeling: 2. Model implementation and case studies. *Water Resources Research*, 51(4), 2515–2542. <https://doi.org/10.1002/2015WR017200>

- Clark, M. P., Wood, A., Nijssen, B., Bennett, A., Knoben, W., & Lumbrazo, C. (2020). *SUMMA v3.0.3*. Zenodo. <https://doi.org/10.5281/zenodo.4558054>
- Conway, J. P., Pomeroy, J. W., Helgason, W. D., & Kinar, N. J. (2018). Challenges in modeling turbulent heat fluxes to snowpacks in forest clearings. *Journal of Hydrometeorology*, 19(10), 1599–1616. <https://doi.org/10.1175/JHM-D-18-0050.1>
- Dai, A. (2013). Erratum: Increasing drought under global warming in observations and models. *Nature Climate Change*, 3(2), 171. <https://doi.org/10.1038/nclimate1811>
- Deschamps-Berger, C., López-Moreno, J. I., Gascoin, S., Mazzotti, G., & Boone, A. (2025). Where Snow and Forest Meet: A Global Atlas. *Geophysical Research Letters*, 52(10), e2024GL113684. <https://doi.org/10.1029/2024GL113684>
- Dettinger, M. (2014). Climate change: Impacts in the third dimension. *Nature Geoscience*, 7(3), 166–167. <https://doi.org/10.1038/ngeo2096>
- Dickerson-Lange, S. E., Gersonde, R. F., Hubbart, J. A., Link, T. E., Nolin, A. W., Perry, G. H., Roth, T. R., Wayand, N. E., & Lundquist, J. D. (2017). Snow disappearance timing is dominated by forest effects on snow accumulation in warm winter climates of the Pacific Northwest, United States. *Hydrological Processes*, 31(10), 1846–1862. <https://doi.org/10.1002/hyp.11144>
- Dingman, S. L. (2015). *Physical hydrology* (Third ed.). Waveland Press Inc.
- Dong, C., & Menzel, L. (2017). Snow process monitoring in montane forests with time-lapse photography. *Hydrological Processes*, 31(16), 2872–2886. <https://doi.org/10.1002/hyp.11229>
- Ellis, C. R., Pomeroy, J. W., Brown, T., & MacDonald, J. (2010). Simulation of snow accumulation and melt in needleleaf forest environments. *Hydrology and Earth System Sciences*, 14(6), 925–940. <https://doi.org/10.5194/hess-14-925-2010>
- Ellis, C. R., Pomeroy, J. W., & Link, T. E. (2013). Modeling increases in snowmelt yield and desynchronization resulting from forest gap-thinning treatments in a northern mountain headwater basin. *Water Resources Research*, 49(2), 936–949. <https://doi.org/10.1002/wrcr.20089>
- Essery, R., & Pomeroy, J. W. (2004). Vegetation and topographic control of wind-blown snow distributions in distributed and aggregated simulations for an arctic tundra basin. *Journal of Hydrometeorology*, 5(5), 735–744. [https://doi.org/10.1175/1525-7541\(2004\)005%3C0735:VATCOW%3E2.0.CO;2](https://doi.org/10.1175/1525-7541(2004)005%3C0735:VATCOW%3E2.0.CO;2)
- Essery, R., Pomeroy, J. W., Parviainen, J., & Storck, P. (2003). Sublimation of snow from coniferous forests in a climate model. *Journal of Climate*, 16(11), 1855–1864. [https://doi.org/10.1175/1520-0442\(2003\)016%3C1855:SOSFCF%3E2.0.CO;2](https://doi.org/10.1175/1520-0442(2003)016%3C1855:SOSFCF%3E2.0.CO;2)
- Fang, X., & Pomeroy, J. W. (2020). Diagnosis of future changes in hydrology for a Canadian Rocky Mountain headwater basin. *Hydrology and Earth System Sciences Discussions*, 1–40. <https://doi.org/10.5194/hess-2019-640>
- Fang, X., & Pomeroy, J. W. (2023). Simulation of the impact of future changes in climate on the hydrology of Bow River headwater basins in the Canadian Rockies. *Journal of Hydrology*, 620, 129566. <https://doi.org/10.1016/j.jhydrol.2023.129566>

//doi.org/10.1016/j.jhydrol.2023.129566

- Fang, X., Pomeroy, J. W., Debeer, C. M., Harder, P., & Siemens, E. (2019). Hydrometeorological data from marmot creek research basin, canadian rockies. *Earth System Science Data*, 11(2), 455–471. <https://doi.org/10.5194/essd-11-455-2019>
- Floyd, W. C. (2012). *Snowmelt energy flux recovery during rain-on-snow in regenerating forests* (p. 180) [PhD thesis, University of British Columbia]. <https://doi.org/https://dx.doi.org/10.14288/1.0073024>
- Floyd, W., & Weiler, M. (2008). Measuring snow accumulation and ablation dynamics during rain-on-snow events: Innovative measurement techniques. *Hydrological Processes*, 22(24), 4805–4812.
- Friesen, J., Lundquist, J., & Van Stan, J. T. (2015). Evolution of forest precipitation water storage measurement methods. *Hydrological Processes*, 29(11), 2504–2520. <https://doi.org/10.1002/hyp.10376>
- Friesen, J., Van Beek, C., Selker, J., Savenije, H. H. G., & Van De Giesen, N. (2008). Tree rainfall interception measured by stem compression. *Water Resources Research*, 44(12), 1–5. <https://doi.org/10.1029/2008WR007074>
- Fryer, B. Y. G. I., Johnson, E. A., Fryer, G. I., & Johnson, E. A. (1988). Reconstructing fire behaviour and effects in a subalpine forest. *The Journal of Applied Ecology*, 25(3), 1063–1072. <https://doi.org/10.2307/2403766>
- Galewsky, J., Steen-Larsen, H. C., Field, R. D., Worden, J., Risi, C., & Schneider, M. (2016). Stable isotopes in atmospheric water vapor and applications to the hydrologic cycle. *Reviews of Geophysics*, 54(4), 809–865. <https://doi.org/10.1002/2015RG000512>
- Garnier, B. J., & Ohmura, A. (1970). The evaluation of surface variations in solar radiation income. *Solar Energy*, 13(1), 21–34. [https://doi.org/10.1016/0038-092X\(70\)90004-6](https://doi.org/10.1016/0038-092X(70)90004-6)
- Garvelmann, J., Pohl, S., & Weiler, M. (2013). From observation to the quantification of snow processes with a time-lapse camera network. *Hydrology and Earth System Sciences*, 17(4), 1415–1429. <https://doi.org/10.5194/hess-17-1415-2013>
- Gelfan, A. N., Pomeroy, J. W., & Kuchment, L. S. (2004). Modeling forest cover influences on snow accumulation, sublimation, and melt. *Journal of Hydrometeorology*, 5(5), 785–803. [https://doi.org/10.1175/1525-7541\(2004\)005%3C0785:MFCIOS%3E2.0.CO;2](https://doi.org/10.1175/1525-7541(2004)005%3C0785:MFCIOS%3E2.0.CO;2)
- Golding, D. L., & Swanson, R. H. (1978). Snow accumulation and melt in small forest openings in Alberta. *Canadian Journal of Forest Research*, 8(4), 380–388. <https://doi.org/10.1139/x78-057>
- Gottfried, M., Pauli, H., Futschik, A., Akhalkatsi, M., Barančok, P., Benito Alonso, J. L., Coldea, G., Dick, J., Erschbamer, B., Fernández Calzado, M. R., Kazakis, G., Krajčí, J., Larsson, P., Mallaun, M., Michelsen, O., Moiseev, D., Moiseev, P., Molau, U., Merzouki, A., ... Grabherr, G. (2012). Continent-wide response of mountain vegetation to climate change. *Nature Climate Change*, 2(2), 111–115. <https://doi.org/10.1038/nclimate1329>
- Gouttevin, I., Lehning, M., Jonas, T., Gustafsson, D., & Mölder, M. (2015). A two-layer canopy model with thermal inertia for an improved snowpack energy balance below needleleaf forest (model SNOWPACK,

- version 3.2.1, revision 741). *Geoscientific Model Development*, 8(8), 2379–2398. <https://doi.org/10.5194/gmd-8-2379-2015>
- Gray, D. M., & Landine, P. G. (1988). An energy-budget snowmelt model for the Canadian Prairies. *Canadian Journal of Earth Sciences*, 25(8), 1292–1303. <https://doi.org/10.1139/e88-124>
- Gutmann, E. D., Van Stan, J. T., Friesen, J., Aubrey, D. P., & Lundquist, J. (2017). Observed compression of in situ tree stems during freezing. *Agricultural and Forest Meteorology*, 243, 19–24. <https://doi.org/10.1016/j.agrformet.2017.05.004>
- Harder, P., & Pomeroy, J. W. (2013). Estimating precipitation phase using a psychrometric energy balance method. *Hydrological Processes*, 27(13), 1901–1914. <https://doi.org/10.1002/hyp.9799>
- Harder, P., Pomeroy, J. W., & Helgason, W. D. (2020). Improving sub-canopy snow depth mapping with unmanned aerial vehicles: Lidar versus structure-from-motion techniques. *The Cryosphere*, 14(6), 1919–1935. <https://doi.org/10.5194/tc-14-1919-2020>
- Harding, R. J., & Pomeroy, J. W. (1996). The Energy Balance of the Winter Boreal Landscape. *Journal of Climate*, 9(11), 2778–2787. <https://www.jstor.org/stable/26201420>
- Harpold, A. A., Krogh, S. A., Kohler, M., Eckberg, D., Greenberg, J., Sterle, G., & Broxton, P. D. (2020). Increasing the efficacy of forest thinning for snow using high-resolution modeling: A proof of concept in the Lake Tahoe Basin, California, USA. *Ecohydrology : Ecosystems, Land and Water Process Interactions, Ecohydrogeomorphology*, 13(4). <https://doi.org/10.1002/eco.2203>
- Harvey, N., Burns, S. P., Musselman, K. N., Barnard, H., & Blanken, P. D. (2025). Identifying Canopy Snow in Subalpine Forests: A Comparative Study of Methods. *Water Resources Research*, 61(1), e2023WR036996. <https://doi.org/10.1029/2023WR036996>
- Hayashi, M. (2020). Alpine hydrogeology: The critical role of groundwater in sourcing the headwaters of the world. *Groundwater*, 58(4), 498–510. <https://doi.org/10.1111/gwat.12965>
- He, Z., Pomeroy, J. W., Fang, X., & Peterson, A. (2021). Sensitivity analysis of hydrological processes to perturbed climate in a southern boreal forest basin. *Journal of Hydrology*, 601(July), 126706. <https://doi.org/10.1016/j.jhydrol.2021.126706>
- Hedstrom, N. R., & Pomeroy, J. W. (1998). Measurements and modelling of snow interception in the boreal forest. *Hydrological Processes*, 12(10-11), 1611–1625. [https://doi.org/10.1002/\(SICI\)1099-1085\(199808/09\)12:10/11%3C1611::AID-HYP684%3E3.0.CO;2-4](https://doi.org/10.1002/(SICI)1099-1085(199808/09)12:10/11%3C1611::AID-HYP684%3E3.0.CO;2-4)
- Helgason, W., & Pomeroy, J. W. (2012a). Characteristics of the near-surface boundary layer within a mountain valley during winter. *Journal of Applied Meteorology and Climatology*, 51(3), 583–597. <https://doi.org/10.1175/JAMC-D-11-058.1>
- Helgason, W., & Pomeroy, J. W. (2012b). Problems closing the energy balance over a homogeneous snow cover during midwinter. *Journal of Hydrometeorology*, 13(2), 557–572. <https://doi.org/10.1175/JHM-D-11-0135.1>
- Henderson, G. R., Peings, Y., Furtado, J. C., & Kushner, P. J. (2018). Snow–atmosphere coupling in the

northern hemisphere. *Nature Climate Change*, 8(11), 954–963. <https://doi.org/10.1038/s41558-018-0295>

6

- Herwitz, S. R., & Slye, R. E. (1995). Three-dimensional modeling of canopy tree interception of wind-driven rainfall. *Journal of Hydrology*, 168(1-4), 205–226. [https://doi.org/10.1016/0022-1694\(94\)02643-P](https://doi.org/10.1016/0022-1694(94)02643-P)
- Hoover, M. D., & Leaf, C. F. (1967). Processss and Significance of Interception in Colorado Subalpine Forest. *Proceeding of a National Science Foundation Advanced Science Seminar*.
- Hu, J. M., & Nolin, A. W. (2020). Widespread warming trends in storm temperatures and snowpack fate across the Western United States. *Environmental Research Letters*, 15(3), 034059. <https://doi.org/10.1088/1748-9326/ab763f>
- Huerta, M. L., Molotch, N. P., & McPhee, J. (2019). Snowfall interception in a deciduous Nothofagus forest and implications for spatial snowpack distribution. *Hydrological Processes*, 33(13), 1818–1834.
- Immerzeel, W. W., Lutz, A. F., Andrade, M., Bahl, A., Biemans, H., Bolch, T., Hyde, S., Brumby, S., Davies, B. J., Elmore, A. C., Emmer, A., Feng, M., Fernández, A., Haritashya, U., Kargel, J. S., Koppes, M., Kraaijenbrink, P. D. A., Kulkarni, A. V., Mayewski, P. A., ... Baillie, J. E. M. (2020). Importance and vulnerability of the world's water towers. *Nature*, 577(7790), 364–369. <https://doi.org/10.1038/s41586-019-1822-y>
- Isyumov, N. (1971). *An approach to the prediction of snow loads* [PhD thesis]. The University of Western Ontario (Canada).
- Kasischke, E. S., & Turetsky, M. R. (2006). Recent changes in the fire regime across the North American boreal region - Spatial and temporal patterns of burning across Canada and Alaska. *Geophysical Research Letters*, 33(9). <https://doi.org/10.1029/2006GL025677>
- Kasischke, E. S., Verbyla, D. L., Rupp, T. S., McGuire, A. D., Murphy, K. A., Jandt, R., Barnes, J. L., Hoy, E. E., Duffy, P. A., Calef, M., & Turetsky, M. R. (2010). Alaska's changing fire regime – implications for the vulnerability of its boreal forests. *Canadian Journal of Forest Research*, 40(7), 1313–1324.
- Katsushima, T., Kato, A., Aiura, H., Nanko, K., Suzuki, S., Takeuchi, Y., & Murakami, S. (2023). Modelling of snow interception on a Japanese cedar canopy based on weighing tree experiment in a warm winter region. *Hydrological Processes*, 37(6), 1–16. <https://doi.org/10.1002/hyp.14922>
- Kesselring, J., Morsdorf, F., Kükenbrink, D., Gastellu-Etchegorry, J.-P., & Damm, A. (2024). Diversity of 3D APAR and LAI dynamics in broadleaf and coniferous forests: Implications for the interpretation of remote sensing-based products. *Remote Sensing of Environment*, 306, 114116. <https://doi.org/10.1016/j.rse.2024.114116>
- Kim, E., Gatebe, C., Hall, D., Newlin, J., Misakonis, A., Elder, K., Marshall, H. P., Hiemstra, C., Brucker, L., De Marco, E., Crawford, C., Kang, D. H., & Entin, J. (2017). NASA's snowex campaign: Observing seasonal snow in a forested environment. *2017 IEEE International Geoscience and Remote Sensing Symposium (IGARSS)*, 1388–1390. <https://doi.org/10.1109/IGARSS.2017.8127222>
- King, J. C., Pomeroy, J. W., Gray, D. M., Fierz, C., Föhn, P. M. B., Harding, R. J., Jordan, R. E.,

- Martin, E., & Plüss, C. (2008). Snow-atmosphere energy and mass balance. In *Snow and climate: Physical processes, surface energy exchange and modelling* (pp. 70–123). Cambridge University Press. <https://doi.org/10.1017/S0954102008001612>
- Kobayashi, D. (1987). Snow accumulation on a narrow board. *Cold Regions Science and Technology*, 13(3), 239–245. [https://doi.org/10.1016/0165-232X\(87\)90005-X](https://doi.org/10.1016/0165-232X(87)90005-X)
- Koeniger, P., Hubbart, J. A., Link, T., & Marshall, J. D. (2008). Isotopic variation of snow cover and streamflow in response to changes in canopy structure in a snow-dominated mountain catchment. *Hydrological Processes*, 22(4), 557–566. <https://doi.org/10.1002/hyp.6967>
- Kozak, A., & Kozak, R. A. (1995). Notes on regression through the origin. *Forestry Chronicle*, 71(3), 326–330. <https://doi.org/10.5558/tfc71326-3>
- Krinner, G., Derksen, C., Essery, R., Flanner, M., Hagemann, S., Clark, M. P., Hall, A., Rott, H., Brutel-Vuilmet, C., Kim, H., Ménard, C. B., Mudryk, L., Thackeray, C., Wang, L., Arduini, G., Balsamo, G., Bartlett, P., Boike, J., Boone, A., ... Zhu, D. (2018). ESM-SnowMIP: Assessing snow models and quantifying snow-related climate feedbacks. *Geoscientific Model Development*, 11(12), 5027–5049. <https://doi.org/10.5194/gmd-11-5027-2018>
- Kurz, W. A., Dymond, C. C., Stinson, G., Rampley, G. J., Neilson, E. T., Carroll, A. L., Ebata, T., & Safranyik, L. (2008). Mountain pine beetle and forest carbon feedback to climate change. *Nature*, 452(7190), 987–990.
- Langs, L. E., Petrone, R. M., & Pomeroy, J. W. (2020). A  $\delta^{18}\text{O}$  and  $\delta^2\text{H}$  stable water isotope analysis of subalpine forest water sources under seasonal and hydrological stress in the Canadian Rocky Mountains. *Hydrological Processes*, 34(26), 5642–5658. <https://doi.org/10.1002/hyp.13986>
- Leach, J. A., & Moore, R. D. (2014). Winter stream temperature in the rain-on-snow zone of the Pacific Northwest: Influences of hillslope runoff and transient snow cover. *Hydrology and Earth System Sciences*, 18(2), 819–838. <https://doi.org/10.5194/hess-18-819-2014>
- Lehtonen, I., Kämäräinen, M., Gregow, H., Venäläinen, A., & Peltola, H. (2016). Heavy snow loads in Finnish forests respond regionally asymmetrically to projected climate change. *Natural Hazards and Earth System Sciences*, 16(10), 2259–2271. <https://doi.org/10.5194/nhess-16-2259-2016>
- LeMone, M. A., Angevine, W. M., Bretherton, C. S., Chen, F., Dudhia, J., Fedorovich, E., Katsaros, K. B., Lenschow, D. H., Mahrt, L., Patton, E. G., & Others. (2019). 100 years of progress in boundary layer meteorology. *Meteorological Monographs*, 59, 9.1–9.85. <https://doi.org/10.1175/AMSMONOGRAPHS-D-18-0013.1>
- López-Moreno, J. I., & Latron, J. (2007). Influence of canopy density on snow distribution in a temperate mountain range. *Hydrological Processes*, 22(1), 117–126. <https://doi.org/10.1002/hyp.6572>
- López-Moreno, J. I., Zabalza, J., Vicente-Serrano, S. M., Revuelto, J., Gilaberte, M., Azorin-Molina, C., Morán-Tejeda, E., García-Ruiz, J. M., & Tague, C. (2014). Impact of climate and land use change on water availability and reservoir management: Scenarios in the Upper Aragón River, Spanish Pyrenees.

- Science of The Total Environment*, 493, 1222–1231. <https://doi.org/10.1016/j.scitotenv.2013.09.031>
- Lumbrazo, C., Bennett, A., Currier, W. R., Nijssen, B., & Lundquist, J. (2022). Evaluating multiple canopy-snow unloading parameterizations in SUMMA with time-lapse photography characterized by citizen scientists. *Water Resources Research*, 58(6), 1–22. <https://doi.org/10.1029/2021WR030852>
- Lundberg, A., & Halldin, S. (1994). Evaporation of intercepted snow: Analysis of governing factors. *Water Resources Research*, 30(9), 2587–2598.
- Lundberg, A., & Halldin, S. (2001). Snow interception evaporation. Review of measurement techniques, processes, and models. *Theoretical and Applied Climatology*, 70(1-4), 117–133. <https://doi.org/10.1007/s007040170010>
- Lundquist, J. D., Dickerson-Lange, S., Gutmann, E., Jonas, T., Lumbrazo, C., & Reynolds, D. (2021). Snow interception modelling: Isolated observations have led to many land surface models lacking appropriate temperature sensitivities. *Hydrological Processes*, 35(7), 1–20. <https://doi.org/10.1002/hyp.14274>
- Lv, Z., & Pomeroy, J. W. (2019). Detecting intercepted snow on mountain needleleaf forest canopies using satellite remote sensing. *Remote Sensing of Environment*, 231(March), 111222. <https://doi.org/10.1016/j.rse.2019.111222>
- Lv, Z., & Pomeroy, J. W. (2020). Assimilating snow observations to snow interception process simulations. *Hydrological Processes*, 34(10), 2229–2246. <https://doi.org/10.1002/hyp.13720>
- MacDonald, J. P. (2010). *Unloading of intercepted snow in conifer forests* (p. 93) [M.{Sc}]. Thesis]. Department of Geography, University of Saskatchewan.
- Marks, D., & Dozier, J. (1992). Climate and energy exchange at the snow surface in the Alpine Region of the Sierra Nevada: 2. Snow cover energy balance. *Water Resources Research*, 28(11), 3043–3054. <https://doi.org/10.1029/92WR01483>
- Marks, D., Kimball, J., Tingey, D., & Link, T. (1998). The sensitivity of snowmelt processes to climate conditions and forest cover during rain-on-snow: A case study of the 1996 Pacific Northwest flood. *Hydrological Processes*, 12(10-11), 1569–1587. [https://doi.org/10.1002/\(SICI\)1099-1085\(199808/09\)12:10/11%3C1569::AID-HYP682%3E3.0.CO;2-L](https://doi.org/10.1002/(SICI)1099-1085(199808/09)12:10/11%3C1569::AID-HYP682%3E3.0.CO;2-L)
- Martin, K. A., Van Stan, J. T., Dickerson-Lange, S. E., Lutz, J. A., Berman, J. W., Gersonde, R., & Lundquist, J. D. (2013). Development and testing of a snow interceptometer to quantify canopy water storage and interception processes in the rain/snow transition zone of the North Cascades, Washington, USA. *Water Resources Research*, 49(6), 3243–3256. <https://doi.org/10.1002/wrcr.20271>
- Mazzotti, G., Currier, W. R., Deems, J. S., Pflug, J. M., Lundquist, J. D., & Jonas, T. (2019). Revisiting snow cover variability and canopy structure within forest stands: Insights from airborne lidar data. *Water Resources Research*, 55(7), 6198–6216. <https://doi.org/10.1029/2019WR024898>
- Merriam, R. A. (1960). A note on the interception loss equation. *JOURNAL OF GEOPHYSICAL RESEARCH*, 65(11), 3850–3851.
- Miller, D. H. (1962). Snow in the trees: Where does it go. *Proceedings of the Western Snow Conference*, 30,

21–27.

- Moeser, D., Morsdorf, F., & Jonas, T. (2015a). Novel forest structure metrics from airborne LiDAR data for improved snow interception estimation. *Agricultural and Forest Meteorology*, 208, 40–49. <https://doi.org/10.1016/j.agrformet.2015.04.013>
- Moeser, D., Stähli, M., & Jonas, T. (2015b). Improved snow interception modeling using canopy parameters derived from airborne LiDAR data. *Water Resources Research*, 51(7), 5041–5059. <https://doi.org/10.1002/2014WR016724>
- Molotch, N. P., Blanken, P. D., Williams, M. W., Turnipseed, A. A., Monson, R. K., & Margulis, S. A. (2007). Estimating sublimation of intercepted and sub-canopy snow using eddy covariance systems. *Hydrological Processes*, 21(12), 1567–1575. <https://doi.org/10.1002/hyp>
- Musselman, K. N., & Pomeroy, J. W. (2017). Estimation of needleleaf canopy and trunk temperatures and longwave contribution to melting snow. *Journal of Hydrometeorology*, 18(2), 555–572. <https://doi.org/10.1175/JHM-D-16-0111.1>
- Musselman, K. N., Pomeroy, J. W., & Link, T. E. (2015). Variability in shortwave irradiance caused by forest gaps: Measurements, modelling, and implications for snow energetics. *Agricultural and Forest Meteorology*, 207, 69–82. <https://doi.org/10.1016/j.agrformet.2015.03.014>
- Nakai, Y., Sakamoto, T., Terajima, T., Kitamura, K., & Shirai, T. (1999). Energy balance above a boreal coniferous forest: A difference in turbulent fluxes between snow-covered and snow-free canopies. *Hydrological Processes*, 13(4), 515–529. [https://doi.org/10.1002/\(SICI\)1099-1085\(199903\)13:4%3C515::AID-HYP712%3E3.0.CO;2-J](https://doi.org/10.1002/(SICI)1099-1085(199903)13:4%3C515::AID-HYP712%3E3.0.CO;2-J)
- of Engineers, U. States. Army. C. (1956). *Snow hydrology: Summary report of the snow investigations*. North Pacific Division, Corps of Engineers, U.S. Army.
- Papesch, A. J. G. (1984). *Wind and its effects on (Canterbury) forests* [PhD thesis]. University of Canterbury.
- Parajka, J., Haas, P., Kirnbauer, R., Jansa, J., & Blöschl, G. (2012). Potential of time-lapse photography of snow for hydrological purposes at the small catchment scale. *Hydrological Processes*, 26(22), 3327–3337. <https://doi.org/10.1002/hyp.8389>
- Parviainen, J., & Pomeroy, J. W. (2000). Multiple-scale modelling of forest snow sublimation: Initial findings. *Hydrological Processes*, 14(15), 2669–2681. [https://doi.org/10.1002/1099-1085\(20001030\)14:15%3C2669::AID-HYP85%3E3.0.CO;2-Q](https://doi.org/10.1002/1099-1085(20001030)14:15%3C2669::AID-HYP85%3E3.0.CO;2-Q)
- Pfister, R., & Schneebeli, M. (1999). Snow accumulation on boards of different sizes and shapes. *Hydrological Processes*, 13(14–15), 2345–2355. [https://doi.org/10.1002/\(SICI\)1099-1085\(199910\)13:14/15%3C2345::AID-HYP873%3E3.0.CO;2-N](https://doi.org/10.1002/(SICI)1099-1085(199910)13:14/15%3C2345::AID-HYP873%3E3.0.CO;2-N)
- Pomeroy, J. W., Brown, T., Fang, X., Shook, K. R., Pradhananga, D., Armstrong, R., Harder, P., Marsh, C., Costa, D., Krogh, S. A., Aubry-Wake, C., Annand, H., Lawford, P., He, Z., Kompanizare, M., & Moreno, J. I. L. (2022). The cold regions hydrological modelling platform for hydrological diagnosis and prediction based on process understanding. *Journal of Hydrology*, 615(128711), 1–25. <https://doi.org/10.1016/j.jhydrol.2022.128711>

1016/j.jhydrol.2022.128711

- Pomeroy, J. W., Davies, T. D., Jones, H. G., Marsh, P., Peters, N. E., & Tranter, M. (1999). Transformations of snow chemistry in the boreal forest: Accumulation and volatilization. *Hydrological Processes*, 13(14-15), 2257–2273. [https://doi.org/10.1002/\(SICI\)1099-1085\(199910\)13:14/15%3C2257::AID-HYP874%3E3.0.CO;2-G](https://doi.org/10.1002/(SICI)1099-1085(199910)13:14/15%3C2257::AID-HYP874%3E3.0.CO;2-G)
- Pomeroy, J. W., & Dion, K. (1996). Winter radiation extinction and reflection in a boreal pine canopy: Measurements and modelling. *Hydrological Processes*, 10(12), 1591–1608. [https://doi.org/10.1002/\(sici\)1099-1085\(199612\)10:12%3C1591::aid-hyp503%3E3.0.co;2-8](https://doi.org/10.1002/(sici)1099-1085(199612)10:12%3C1591::aid-hyp503%3E3.0.co;2-8)
- Pomeroy, J. W., Fang, X., & Ellis, C. R. (2012). Sensitivity of snowmelt hydrology in Marmot Creek, Alberta, to forest cover disturbance. *Hydrological Processes*, 26(12), 1891–1904. <https://doi.org/10.1002/hyp.9248>
- Pomeroy, J. W., & Gray, D. M. (1995). *Snowcover Accumulation, Relocation and Management* (NHRI Science Report No. 7, p. 144). National Hydrology Research Institute, Environment Canada, Saskatoon, Canada.
- Pomeroy, J. W., Gray, D. M., Brown, T., Hedstrom, N. R., Quinton, W. L., Granger, R. J., & Carey, S. K. (2007). The cold regions hydrological model: A platform for basing process representation and model structure on physical evidence. *Hydrological Processes*, 21(19), 2650–2667. <https://doi.org/10.1002/hyp.6787>
- Pomeroy, J. W., Gray, D. M., Hedstrom, N. R., & Janowicz, J. R. (2002). Prediction of seasonal snow accumulation in cold climate forests. *Hydrological Processes*, 16(18), 3543–3558. <https://doi.org/10.1002/hyp.1228>
- Pomeroy, J. W., Gray, D. M., & Landine, P. G. (1993). The Prairie Blowing Snow Model: Characteristics, validation, operation. *Journal of Hydrology*, 144(1-4), 165–192. [https://doi.org/10.1016/0022-1694\(93\)90171-5](https://doi.org/10.1016/0022-1694(93)90171-5)
- Pomeroy, J. W., Gray, D. M., Shook, K. R., Toth, B., Essery, R. L. H. H., Pietroniro, A., & Hedstrom, N. (1998a). An evaluation of snow accumulation and ablation processes for land surface modelling. *Hydrological Processes*, 12(15), 2339–2367. [https://doi.org/10.1002/\(SICI\)1099-1085\(199812\)12:15%3C2339::AID-HYP800%3E3.0.CO;2-L](https://doi.org/10.1002/(SICI)1099-1085(199812)12:15%3C2339::AID-HYP800%3E3.0.CO;2-L)
- Pomeroy, J. W., Marks, D., Link, T., Ellis, C. R., Hardy, J., Rowlands, A., & Granger, R. (2009). The impact of coniferous forest temperature on incoming longwave radiation to melting snow. *Hydrological Processes*, 23, 2513–2525. <https://doi.org/10.1002/hyp.7325>
- Pomeroy, J. W., Marsh, P., & Gray, D. M. (1997). Application of a distributed blowing snow model to the arctic. *Hydrological Processes*, 11(11), 1451–1464. [https://doi.org/10.1002/\(sici\)1099-1085\(199709\)11:11%3C1451::aid-hyp449%3E3.0.co;2-q](https://doi.org/10.1002/(sici)1099-1085(199709)11:11%3C1451::aid-hyp449%3E3.0.co;2-q)
- Pomeroy, J. W., Parviainen, J., Hedstrom, N., & Gray, D. M. (1998b). Coupled modelling of forest snow interception and sublimation. *Hydrological Processes*, 12(15), 2317–2337. [https://doi.org/10.1002/\(SICI\)1099-1085\(199812\)12:15%3C2317::AID-HYP799%3E3.0.CO;2-X](https://doi.org/10.1002/(SICI)1099-1085(199812)12:15%3C2317::AID-HYP799%3E3.0.CO;2-X)

- Pomeroy, J. W., & Schmidt, R. A. (1993). The use of fractal geometry in modelling intercepted snow accumulation and sublimation. *Eastern Snow Conference*, 50, 231–239.
- Pomeroy, J. W., Westbrook, C. J., Petrone, R. M., Hayashi, M., Stadnyk, T. A., Thériault, J. M., Fang, X., & Langs, L. E. (2025). *The Canadian Rockies Hydrological Observatory: Long term observations from a high altitude observation network.* in prep.
- R Core Team. (2024). *R: A language and environment for statistical computing* [Manual]. R Foundation for Statistical Computing.
- Raleigh, M. S., Gutmann, E. D., Van Stan II, J. T., Burns, S. P., Blanken, P. D., & Small, E. E. (2022). Challenges and Capabilities in Estimating Snow Mass Intercepted in Conifer Canopies With Tree Sway Monitoring. *Water Resources Research*, 58(3). <https://doi.org/10.1029/2021WR030972>
- Rasouli, K., Pomeroy, J. W., Janowicz, J. R., Williams, T. J., & Carey, S. K. (2019a). A long-term hydrometeorological dataset (1993–2014) of a northern mountain basin: Wolf creek research basin, yukon territory, canada. *Earth System Science Data*, 11(1), 89–100. <https://doi.org/10.5194/essd-11-89-2019>
- Rasouli, K., Pomeroy, J. W., & Whitfield, P. H. (2019b). Are the effects of vegetation and soil changes as important as climate change impacts on hydrological processes? *Hydrology and Earth System Sciences*, 23(12), 4933–4954. <https://doi.org/10.5194/hess-23-4933-2019>
- Rittger, K., Raleigh, M. S., Dozier, J., Hill, A. F., Lutz, J. A., & Painter, T. H. (2020). Canopy adjustment and improved cloud detection for remotely sensed snow cover mapping. *Water Resources Research*, 56(6), n/a. <https://doi.org/10.1029/2019WR024914>
- Roesch, A., Wild, M., Gilgen, H., & Ohmura, A. (2001). A new snow cover fraction parameterization for the ECHAM4 GCM. *Climate Dynamics*, 17(12), 933–946. <https://doi.org/10.1007/s003820100153>
- Roth, T. R., & Nolin, A. W. (2019). Characterizing maritime snow canopy interception in forested mountains. *Water Resources Research*, 55(6), 4564–4581. <https://doi.org/10.1029/2018WR024089>
- Ruess, R. W., Winton, L. M., & Adams, G. C. (2021). Widespread mortality of trembling aspen (*Populus tremuloides*) throughout interior Alaskan boreal forests resulting from a novel canker disease. *PLoS ONE*, 16(4 April), 1–24. <https://doi.org/10.1371/journal.pone.0250078>
- Russell, M., Eitel, J. U. H., Maguire, A. J., & Link, T. E. (2020). Toward a novel laser-based approach for estimating snow interception. *Remote Sensing*, 12(7), 1–11. <https://doi.org/10.3390/rs12071146>
- Rutter, N., Essery, R., Pomeroy, J. W., Altimir, N., Andreadis, K. M., Baker, I., Barr, A., Bartlett, P., Boone, A., Deng, H., Douville, H., Dutra, E., Elder, K., Ellis, C. R., Feng, X., Gelfan, A., Goodbody, A., Gusev, Y., Gustafsson, D., ... Yamazaki, T. (2009). Evaluation of forest snow processes models (SnowMIP2). *Journal of Geophysical Research: Atmospheres*, 114(D6), 10–18. <https://doi.org/10.1029/2008JD011063>
- Safa, H., Krogh, S. A., Greenberg, J., Kostadinov, T. S., & Harpold, A. A. (2021). Unraveling the controls on snow disappearance in montane conifer forests using multi-site lidar. *Water Resources Research*, 57(12), 1–20. <https://doi.org/10.1029/2020WR027522>
- Sanmiguel-Vallelado, A., López-Moreno, J. I., Morán-Tejeda, E., Alonso-González, E., Navarro-Serrano, F.

- M., Rico, I., & Camarero, J. J. (2020). Variable effects of forest canopies on snow processes in a valley of the central Spanish Pyrenees. *Hydrological Processes*, 34(10), 2247–2262. <https://doi.org/10.1002/hyp.13721>
- Sanmiguel-Vallelado, A., McPhee, J., Esmeralda Ojeda Carreño, P., Morán-Tejeda, E., Julio Camarero, J., & López-Moreno, J. I. (2022b). Sensitivity of forest–snow interactions to climate forcing: Local variability in a Pyrenean valley. *Journal of Hydrology*, 605. <https://doi.org/10.1016/j.jhydrol.2021.127311>
- Sanmiguel-Vallelado, A., McPhee, J., Esmeralda Ojeda Carreño, P., Morán-Tejeda, E., Julio Camarero, J., & López-Moreno, J. I. (2022a). Sensitivity of forest–snow interactions to climate forcing: Local variability in a Pyrenean valley. *Journal of Hydrology*, 605. <https://doi.org/10.1016/j.jhydrol.2021.127311>
- Sanmiguel-Vallelado, A., Morán-Tejeda, E., Alonso-González, E., & López-Moreno, J. I. (2017). Effect of snow on mountain river regimes: An example from the Pyrenees. *Frontiers of Earth Science*, 11(3), 515–530. <https://doi.org/10.1007/s11707-016-0630-z>
- Satterlund, D. R., & Haupt, H. F. (1967). Snow catch by conifer crowns. *Water Resources Research*, 3(4), 1035–1039. <https://doi.org/10.1029/WR003i004p01035>
- Satterlund, D. R., & Haupt, H. F. (1970). The disposition of snow caught by conifer crowns. *Water Resources Research*, 6(2), 649–652. <https://doi.org/10.1029/WR006i002p00649>
- Schlaepfer, D. R., Ewers, B. E., Shuman, B. N., Williams, D. G., Frank, J. M., Massman, W. J., & Lauenroth, W. K. (2014). Terrestrial water fluxes dominated by transpiration: Comment. *Ecosphere*, 5(5), 1–9. <https://doi.org/10.1890/ES13-00391.1>
- Schmidt, R. A. (1972). Sublimation of wind transported snow- a model. *USDA Forest Service Research Paper RM-90*, 0(Rocky Mountain Forest and Range Experiment Station, U.S. Department of Agriculture, Fort Collins), 24.
- Schmidt, R. A., & Gluns, D. R. (1991). Snowfall interception on branches of three conifer species. *Canadian Journal of Forest Research*, 21(8), 1262–1269. <https://doi.org/10.1139/x91-176>
- Schmidt, R. A., Jairell, R. L., & Pomeroy, J. W. (1988). Measuring Snow Interception and Loss From an Artificial Conifer. *Proceedings of the Western Snow Conference*, 56, 166–169.
- Schmidt, R. A., & Pomeroy, J. W. (1990). Bending of a conifer branch at subfreezing temperatures: Implications for snow interception. *Canadian Journal of Forest Research*, 20(8), 1251–1253. <https://doi.org/10.1139/x90-165>
- Schmidt, R. A., & Troendle, C. A. (1989). Snowfall into a forest and clearing. *Journal of Hydrology*, 110(3-4), 335–348. [https://doi.org/10.1016/0022-1694\(89\)90196-0](https://doi.org/10.1016/0022-1694(89)90196-0)
- Sexstone, G. A., Clow, D. W., Fassnacht, S. R., Liston, G. E., Hiemstra, C. A., Knowles, J. F., & Penn, C. A. (2018). Snow sublimation in mountain environments and its sensitivity to forest disturbance and climate warming. *Water Resources Research*, 54(2), 1191–1211. <https://doi.org/10.1002/2017WR021172>
- Sexstone, G. A., Clow, D. W., Stannard, D. I., & Fassnacht, S. R. (2016). Comparison of methods for quantifying surface sublimation over seasonally snow-covered terrain. *Hydrological Processes*, 30(19),

- 3373–3389. <https://doi.org/10.1002/hyp.10864>
- Shook, K., & Pomeroy, J. (2011). Synthesis of incoming shortwave radiation for hydrological simulation. *Hydrology Research*, 42(6), 433–446. <https://doi.org/10.2166/nh.2011.074>
- Sicart, J. E., Pomeroy, J. W., Essery, R. L. H., & Bewley, D. (2006). Incoming longwave radiation to melting snow: Observations, sensitivity and estimation in Northern environments. *Hydrological Processes*, 20(17), 3697–3708.
- Smith, C. D. (2007). Correcting the wind bias in snowfall measurements made with a Geonor T-200B precipitation gauge and alter wind shield. *87th AMS Annual Meeting*.
- Staines, J., & Pomeroy, J. W. (2023). Influence of forest canopy structure and wind flow on patterns of sub-canopy snow accumulation in montane needleleaf forests. *Hydrological Processes*, 37(10), 1–19. <https://doi.org/10.1002/hyp.15005>
- Stillinger, T., Rittger, K., Raleigh, M. S., Michell, A., Davis, R. E., & Bair, E. H. (2023). Landsat, MODIS, and VIIRS snow cover mapping algorithm performance as validated by airborne lidar datasets. *The Cryosphere*, 17(2), 567–590. <https://doi.org/10.5194/tc-17-567-2023>
- Storck, P., Lettenmaier, D. P., & Bolton, S. M. (2002). Measurement of snow interception and canopy effects on snow accumulation and melt in a mountainous maritime climate, Oregon, United States. *Water Resources Research*, 38(11), 1–16. <https://doi.org/10.1029/2002wr001281>
- Stull, R. B. (2017). *Practical meteorology: An algebra-based survey of atmospheric science*. (1.02b ed., pp. 1–944). University of British Columbia.
- Szczypta, C., Gascoin, S., Houet, T., Hagolle, O., Dejoux, J.-F., Vigneau, C., & Fanise, P. (2015). Impact of climate and land cover changes on snow cover in a small Pyrenean catchment. *Journal of Hydrology*, 521, 84–99. <https://doi.org/10.1016/j.jhydrol.2014.11.060>
- Thackeray, C. W., Fletcher, C. G., & Derksen, C. (2014). The influence of canopy snow parameterizations on snow albedo feedback in boreal forest regions. *Journal of Geophysical Research: Atmospheres*, 119(16), 9810–9821. <https://doi.org/10.1002/2014JD021858>
- Thériault, J. M., Stewart, R. E., & Henson, W. (2012). Impacts of terminal velocity on the trajectory of winter precipitation types. *Atmospheric Research*, 116, 116–129. <https://doi.org/10.1016/j.atmosres.2012.03.008>
- Thorpe, A. D., & Mason, B. J. (1966). The evaporation of ice spheres and ice crystals. *British Journal of Applied Physics*, 17(4), 541–548. <https://doi.org/10.1088/0508-3443/17/4/316>
- Troendle, C. A. (1983). The potential for water yield augmentation from forest management in the Rocky Mountain region. *Journal of the American Water Resources Association*, 19(3), 359–373. <https://doi.org/10.1111/j.1752-1688.1983.tb04593.x>
- Valante, F., David, J. S., & Gash, J. H. C. (1997). Modelling interception loss for two sparse eucalypt and pine forests in central Portugal using reformulated Rutter and Gash analytical models. *Journal of Hydrology*, 190(1-2), 141–162. [https://doi.org/10.1016/S0022-1694\(96\)03066-1](https://doi.org/10.1016/S0022-1694(96)03066-1)
- Van Stan, J. T., Gutmann, E., & Friesen, J. (2020). *Precipitation partitioning by vegetation: A global*

*synthesis.*

- Van Stan, J. T., Siegert, C. M., Levia, D. F., & Scheick, C. E. (2011). Effects of wind-driven rainfall on stemflow generation between codominant tree species with differing crown characteristics. *Agricultural and Forest Meteorology*, 151(9), 1277–1286. <https://doi.org/10.1016/j.agrformet.2011.05.008>
- Varhola, A., Coops, N. C., Weiler, M., & Moore, R. D. (2010). Forest canopy effects on snow accumulation and ablation: An integrative review of empirical results. *Journal of Hydrology*, 392(3-4), 219–233. <https://doi.org/10.1016/j.jhydrol.2010.08.009>
- Verseghy, D. L. (2017). *Class – the Canadian Land Surface Scheme (version 3.6.1) technical documentation*. (January; p. 174). Environment and Climate Change Canada Internal Rep.
- Verseghy, D. L., McFarlane, N. A., & Lazare, M. (1993). Class—A Canadian land surface scheme for GCMS, II. Vegetation model and coupled runs. *International Journal of Climatology*, 13(4), 347–370.
- Vionnet, V., Mortimer, C., Brady, M., Arnal, L., & Brown, R. (2021). Canadian historical snow water equivalent dataset (CanSWE, 1928–2020). *Earth System Science Data*, 13(9), 4603–4619. <https://doi.org/10.5194/essd-13-4603-2021>
- Viviroli, D., Archer, D. R., Buytaert, W., Fowler, H. J., Greenwood, G. B., Hamlet, A. F., Huang, Y., Koboltschnig, G., Litaor, M. I., López-Moreno, J. I., Lorentz, S., Schädler, B., Schreier, H., Schwaiger, K., Vuille, M., & Woods, R. (2011). Climate change and mountain water resources: Overview and recommendations for research, management and policy. *Hydrology and Earth System Sciences*, 15(2), 471–504. <https://doi.org/10.5194/hess-15-471-2011>
- Viviroli, D., Dürr, H. H., Messerli, B., Meybeck, M., & Weingartner, R. (2007). Mountains of the world, water towers for humanity: Typology, mapping, and global significance. *Water Resources Research*, 43(7), 1–13. <https://doi.org/10.1029/2006WR005653>
- Viviroli, D., Kummu, M., Meybeck, M., Kallio, M., & Wada, Y. (2020). Increasing dependence of lowland populations on mountain water resources. *Nature Sustainability*, 3(11), 917–928. <https://doi.org/10.1038/s41893-020-0559-9>
- Wang, L., Cole, J. N. S., Bartlett, P., Verseghy, D., Derksen, C., Brown, R., & von Salzen, K. (2016). Investigating the spread in surface albedo for snow-covered forests in CMIP5 models. *Journal of Geophysical Research: Atmospheres*, 121(3), 1104–1119. <https://doi.org/10.1002/2015JD023824>
- Watanabe, S., & Ozeki, J. (1964). Study of fallen snow on forest trees (II). Experiment on the snow crown of the Japanese cedar. *Jap. Govt. Forest Exp. Sta. Bull*, 169, 121–140.
- Weiskittel, A. R., Kershaw, J. A., Hofmeyer, P. V., & Seymour, R. S. (2009). Species differences in total and vertical distribution of branch- and tree-level leaf area for the five primary conifer species in Maine, USA. *Forest Ecology and Management*, 258(7), 1695–1703. <https://doi.org/10.1016/j.foreco.2009.07.035>
- Wheater, H. S., Pomeroy, J. W., Pietroniro, A., Davison, B., Elshamy, M., Yassin, F., Rokaya, P., Fayad, A., Tesemma, Z., Princz, D., Loukili, Y., DeBeer, C. M., Ireson, A. M., Razavi, S., Lindenschmidt, K.-E., Elshorbagy, A., MacDonald, M., Abdelhamed, M., Haghnegahdar, A., & Bahrami, A. (2022). Advances in

- modelling large river basins in cold regions with Modélisation Environmentale Communautaire—Surface and Hydrology (MESH), the Canadian hydrological land surface scheme. *Hydrological Processes*, 36(4), 1–24. <https://doi.org/10.1002/hyp.14557>
- Yamazaki, T., Fukabori, K., & Kondo, J. (1996). Albedo of forest with crown snow. *Journal of the Japanese Society of Snow and Ice*, 58(1), 11–18. <https://doi.org/10.5331/seppyo.58.11>
- Zhong, F., Jiang, S., van Dijk, A. I. J. M., Ren, L., Schellekens, J., & Miralles, D. G. (2022). Revisiting large-scale interception patterns constrained by a synthesis of global experimental data. *Hydrology and Earth System Sciences*, 26(21), 5647–5667. <https://doi.org/10.5194/hess-26-5647-2022>